**Department of Applied Chemistry**

# The Impact of Desilication Products on the Flocculation and Sedimentation Properties of Bauxite Residue

**Alexander Senaputra**

**This thesis is presented for the Degree of**
**Doctor of Philosophy**
**of**
**Curtin University**

**June 2014**

**Declaration**

To the best of my knowledge and belief this thesis contains no material previously published by any other person except where due acknowledgment has been made.

This thesis contains no material which has been accepted for the award of any other degree or diploma in any university.

Signature: 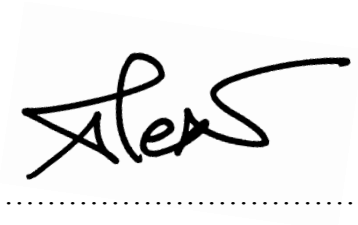

Date: 25.06.2014

## Acknowledgement

I would like to thank the following people and organisation for their contributions towards this PhD project:

| | |
|---|---|
| Dr Phillip Fawell | - primary supervisor at CSIRO Process Science & Engineering (CPSE), for initiating and directing the project and also with the thesis preparation |
| Dr Franca Jones | - primary supervisor at Curtin University, for her support with the experiments and also the thesis preparation |
| Dr Peter Smith | - co-supervisor at CPSE, for Bayer process non-flocculation experiments and information |
| Prof Kate Wright | - co-supervisor at Curtin University |
| Cytec Industries | - for reagents supply and technical discussions |
| Imerys Minerals | - for high purity kaolin supply |
| CPSE S/L Handling team | - for helping setting-up various flocculation tests |
| CPSE Bayer Red Side team | - for helping setting-up various non-flocculation tests |
| CPSE PAS | - for physicochemical characteristics of samples |
| Peter Chapman | - for support with equipment use at Curtin University |
| CSIRO | - for providing laboratory facilities and consumables |
| Curtin University, The Parker Centre for Integrated Hydrometallurgical solutions, MERIWA and PT. Geoservices (Indonesia) | - all for financial assistance |
| Nadine Smith | - for her support and efforts in relation to scholarship arrangements during her term as Education Program Manager for The Parker Centre |

# List of publications

## *Journal*

Senaputra, A. F. Jones, P.D. Fawell, and P.G. Smith. 2014.
"Focused beam reflectance measurement for monitoring the extent and efficiency of flocculation in mineral systems."
*AIChE Journal* 60: 251-265.

## *Conferences*

Jones, F., A. Senaputra, P. Fawell and P. Smith. 2014.
"The crystallization of desilication products in the Bayer process and its impact on hematite solid/liquid separation properties."
(*accepted for the International Symposium for Industrial Crystallization (ISIC) 19-2014*)

Senaputra, A., P. Fawell, F. Jones and P. Smith. 2013.
"Sodalite solids formation at the surface of iron oxide and its impact on flocculation."
*Light Metals 2013 - TMS 2013 Annual Meeting and Exhibition*, San Antonio, USA: TMS. 77-82.

Senaputra, A., P. Fawell, F. Jones and P. Smith. 2012.
"The impact of desilication product on bauxite residue flocculation."
*The 9th International Alumina Quality Workshop*, Perth, Australia: AQW Inc. 186-192.

# Abstract

The Bayer process has remained the dominant route of extracting alumina from aluminium bearing ores (bauxite) for over a century. It involves digestion of bauxite in sodium hydroxide liquor, followed by solid residue separation from the pregnant liquor and the subsequent precipitation of aluminium hydroxides.

Depletion of high grade ores has shifted attention to the processing of lower grade high-silica bauxites. Kaolin in such bauxite is converted to a sodium aluminosilicate phase through a desilication reaction prior to digestion, then separated from pregnant liquor with other insoluble residue phases. The presence of desilication product (DSP) is identified as a major problem in primary residue thickening, resulting in low settling rates, high overflow solids and low underflow density on flocculation.

This study sought to gain fundamental understanding of the impacts of DSP formation on flocculant adsorption and the characteristics of the aggregate subsequently formed. It focused on the formation of DSP in the presence of hematite as a model substrate for bauxite residue, under conditions as close as practical to those in the Bayer refineries. In a limited number of experiments, DSP was also added to hematite slurry as a distinct phase. By contrasting the physicochemical properties of the *in-situ* prepared DSP/hematite slurry and the physical mixture slurry, it was postulated that DSP formed a coating layer at the hematite surface.

The interaction between coated surfaces or pure DSP with polymeric flocculant was of special interest. The premise that DSP partially or completely coating the hematite surface may reduce the active sites for flocculant adsorption was proven incorrect. No evidence of flocculant adsorption being hindered was found, in either *in-situ* prepared DSP/hematite slurries or in pure DSP slurries.

The flocculated aggregate sizes reported by focused beam reflectance measurement (FBRM) for DSP-containing slurries could be comparable to those of pure hematite under the same shear regime. However, much higher flocculant dosages must be

added in the case of DSP-containing slurries. This clearly implied a lower degree of aggregate strength when DSP was present.

Flocculant chemistry and solids dilution were found to be key aspects in the flocculation of *in-situ* prepared DSP/hematite slurries. Cytec® HX PAM gave better flocculation response to increasing DSP content when compared to PAA. However, prohibitively high HX PAM dosage still could not effectively flocculate high DSP content slurries of high total solids concentration. Therefore, feedwells that provide solid dilution would be a requirement for high DSP content residue slurries.

Addition of a commercially available silane-containing polymer prior to the primary flocculant is claimed to improve flocculation of DSP-containing residues, although published results are conflicting. Its use did lead to enhanced flocculation of *in-situ* prepared DSP/hematite slurries, and while only minimally affecting settling rates, it could significantly improve clarity by coagulating fines before bridging flocculation took place. This was captured in the unweighted chord length distributions generated by the newly available G-series FBRM. Bimodal distributions were evident on flocculation of *in-situ* prepared DSP/hematite slurries and the magnitude of the peak at lower chord lengths (1-20 μm) decreased with silane-containing polymer pre-addition. A bimodal distribution was rarely seen with previous FBRM instruments, and with this enhanced sensitivity to particle number the new G-series FBRM represents a potential step-change in direct monitoring of mineral system flocculation, particularly when fines capture is a major process objective.

Better fines capture could also be achieved with higher shear or increasing primary flocculant dosage. However, aggregate break-up was more pronounced in higher shear conditions, whilst an excessive amount of primary flocculant magnified the risk of unadsorbed flocculant in the liquor. The latter was indicated by decreased supernatant liquor filtration rates following flocculation at high dosages. Combining silane-containing polymer and modest primary flocculant dosages is therefore preferable. Nonetheless, its effect in full-scale operation will be very much affected by the fluid flow and shear distribution within the feedwell.

# Contents

# 1 Introduction

## *1.1 Solid/liquid separation in hydrometallurgy*

Solid/liquid separation is a critical unit operation within every hydrometallurgical operation, with multiple stages often being required across the full flowsheet. The rate of the solid/liquid separation process can dictate plant throughput and may represent a bottleneck for production, while the efficiency of solids removal may strongly impact upon downstream operations, particularly when pregnant liquors are subject to treatments such as electrowinning, solvent extraction or precipitation.

Figure 1.1 shows the general approaches that can be applied to solid-liquid separation, based on the particle size. Note the high degree of overlap, particularly in the range from 1 to 100 µm ($10^{-6}$ to $10^{-4}$ m) which is of greatest interest for mineral systems. Although there are other equipment options for the same purpose (i.e. hydrocyclones or centrifuges), the continuous, high throughputs and low energy requirements offered by gravity thickeners make them the most commonly used for treating dilute suspensions. Thickeners become problematic at high solids, and are not appropriate for short-term batch operation. They also result in a lower degree of dewatering than filters or centrifuges.

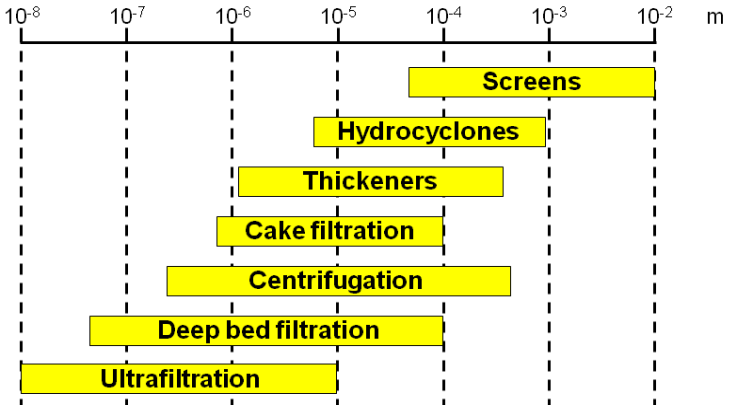


Figure 1.1. Typical size ranges for different dewatering techniques. Adapted from Klimpel (1998).

The main features of a thickener are represented in Figure 1.2. The feed stream is delivered through pipes or open launders with a high velocity to the feedwell, which

serves to dissipate much of the input stream's energy. The solids are then allowed to settle and consolidate in the main body of the thickener, while clarified liquor is removed at the overflow. Rakes may be present in the cone section to assist the movement of solids to the underflow and potentially provide additional consolidation. The underflow rate should be a minor fraction of the original volumetric feed rate.

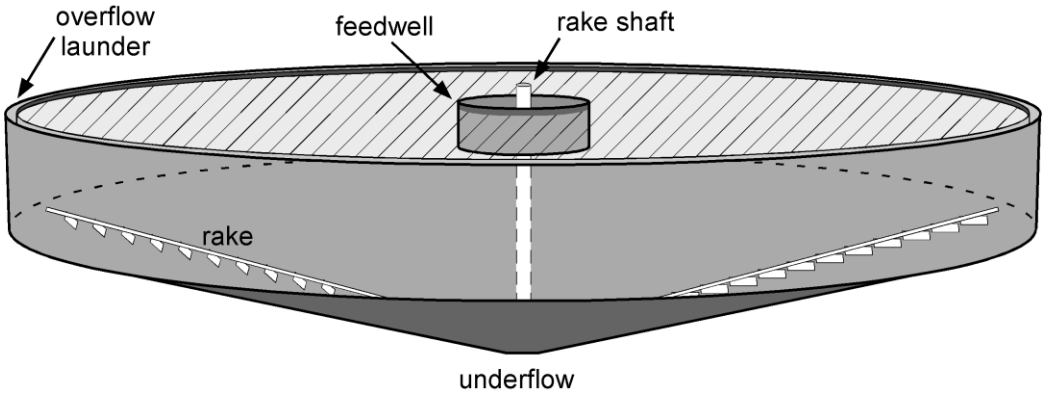


Figure 1.2. Schematic representation of a gravity thickener.

Fine particles have very low settling rates and thickening is often only practical through aggregation (generally by flocculation) to enhance their settling rates, particularly to give the volumetric flow of overflow liquor or underflow solids required by downstream processes. Considerable research has therefore been directed towards improving both the chemical and hydrodynamic aspects of achieving better flocculation and thickener performance. However, many aspects of these processes remain poorly understood, in part due to the complex interplay between the hydrodynamic and physical aspects of feedwell flocculation.

## *1.2 Bayer Process and its challenges for solid/liquid separation*

While the practical extraction routes for many mineral commodities may vary depending on the mineralogy and allow some flexibility in technology selection, alumina extraction from bauxite ores is dominated by the Bayer process, patented by Karl Josef Bayer in 1888. Approximately 90% of alumina production from bauxite is through the Bayer process (Authier-Martin et al. 2001) and this domination has hardly changed over time. Given that the aluminium produced from alumina has long

maintained its position as the second largest consumed metal after iron (USGS 2012), the Bayer process remains the most prominent example of hydrometallurgy across the world.

A simplified Bayer process flowsheet is shown in Figure 1.3. Digestion of the aluminium oxide phases is achieved at elevated temperatures (150-250°C) in caustic liquors. The "bauxite residue" left after digestion (also known as red mud) is mostly iron oxides but can be other insoluble or precipitated phases. The primary thickening process aims to provide (semi) clean pregnant liquor, super-saturated with aluminate, that typically goes to a filtration step for further residue solid removal prior to being fed to the precipitation circuit in which gibbsite ($Al(OH)_3$) is produced. The combination of thickening and filtration is referred to as clarification in the flowsheet.

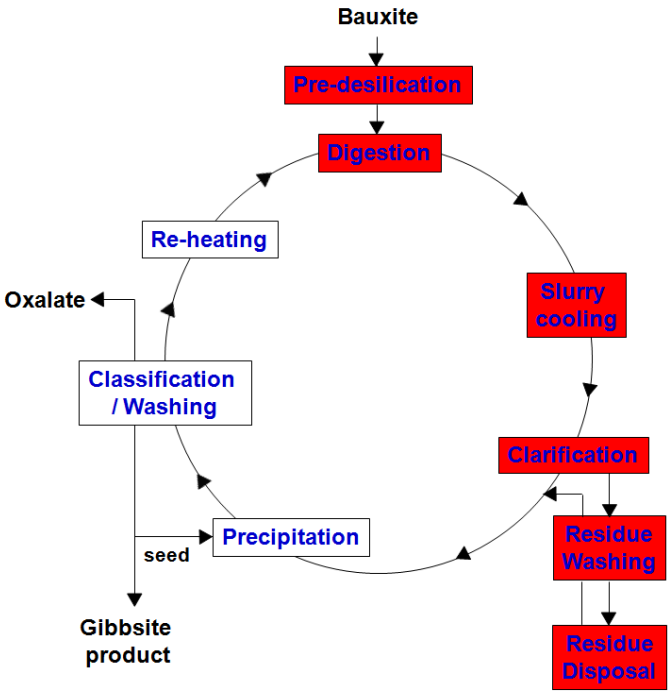


Figure 1.3. Simplified flowsheet of Bayer Process. Adapted from Smith (2009).

The primary thickener has to treat digested slurry that is highly caustic (≥ 4 M NaOH) immediately after being flashed (cooled) to near the liquor's boiling point. Such harsh conditions affect how polymer flocculants will adsorb on particle surfaces and have major implications for flocculant selection. In fact, bauxite residue

primary settling is one of few examples where alternative/novel flocculant functionalities (beyond conventional acrylamide/acrylate copolymers) have a major industrial impact.

The super-saturated aluminate solutions formed after digestion are unstable, and hence solid/liquid separation needs to be fairly rapid, usually at the expense of underflow density. However, the efficiency of solids removal also needs to be high, as any residual solids reporting to precipitation will negatively impact on product quality. While filtration is always used, overflow clarity still needs to be high to prevent filter blinding that may limit throughput. Considerable levels of aluminate report to the underflow liquors, and the recovery of this (along with caustic) is achieved in a counter-current decantation (washing) train of thickeners. The balancing of all these requirements is further complicated by the highly scaling environment that leads to the deterioration of thickener performance over time.

## *1.3 The impacts of reactive silica on bauxite residue flocculation*

Silica is typically present in bauxite in two forms. Quartz will only react under Bayer conditions at high temperatures and reports to the residue unchanged. Clays (usually as kaolin) within bauxite are termed "reactive silica" as they react with caustic (Equation 1.1) and reprecipitate as sodium aluminosilicates that are often referred to as sodalite (Equation 1.2). To minimise the risk of such a process occurring post-digestion, kaolin dissolution is encouraged before the digestion stage at a lower temperature (~90ºC) pre-desilication step, with the sodium aluminosilicates that then report to the residue referred to as desilication products (DSPs).

$$3Al_2Si_2O_5(OH)_4(s) + 18NaOH(aq) = 6Na_2SiO_3(aq) + 6NaAl(OH)_4(aq) + 3H_2O(aq) \quad 1.1$$

$$6Na_2SiO_3(aq) + 6NaAl(OH)_4(aq) + Na_2X(aq) = Na_6[Al_6Si_6O_{24}].Na_2X(s) + 12NaOH(aq) + 6H_2O(aq) \quad 1.2$$

$$X = SO_4^{2-}, CO_3^{2-}, 2Cl^-, 2Al(OH)_4^-, 2OH^-$$

Decline in ore quality is often marked by the increasing proportions of reactive silica. This increases the presence of DSP in residues, which is believed to have negative impacts on the solid/liquid separation process. Problems that DSP is believed to create are (i) lower settling rates, (ii) poor overflow clarity and (iii) low underflow density (Dai et al. 2008; Davis et al. 2010a, 2010b; Rousseaux et al. 2004).

The poor understanding of how the presence of DSP affects the flocculation of bauxite residue and the substantial practical benefits that would arise from enhancing such flocculation provide the main motivation for this present study. There are few published studies relevant to the flocculation of DSP-containing bauxite residue and none of them offer great insights into the processes involved. In recent years a new flocculant with silane functionality has been introduced that is claimed to improve the flocculation of DSP-containing residues (Dai et al. 2008; Davis et al. 2010a), although such improvements are sometimes marginal for reasons that remain unclear.

In seeking to advance the fundamental understanding of DSP impacts on bauxite residue flocculation, this thesis recognises that laboratory-scale investigations of the chemical and physical aspects of adsorption and aggregation cannot be considered in isolation from the hydrodynamic constraints of full-scale feedwell flocculation and the specific downstream requirements from bauxite residue thickening. The detailed review that follows sets out to provide the proper context for the experimental program that was developed and the interpretation of both the fundamental and practical implications of the results.

# 2 Background

## *2.1 Flocculation fundamentals*

During solid-liquid separation in a gravity thickener, the settling velocity of individual particles is governed by Stokes' Law (Stokes 1843):

$$V = \frac{2gr^2(d_1 - d_2)}{9\eta} \qquad 2.1$$

where $V$ is the settling velocity, $g$ is the gravitational constant, $r$ is the radius of the particle, $d_1$ and $d_2$ are the densities of the particle and media, respectively, and $\eta$ is the coefficient of viscosity of the media. The practical implication of this behaviour is that a particle 200 micron in diameter settles ~10,000 times faster than a 2 micron particle if both have identical specific gravity (Connelly et al. 1986).

In a hydrometallurgical context, the solid residues produced never consist of monodispersed particles and in fact, their particle size distribution (PSD) will typically be quite broad. A residue PSD will range from 0.1 to at least 100-200 microns, often to much larger sizes, and usually spanning a variety of mineralogies. The slower settling solids smaller than ~50 microns may represent as little as 20% of the total mass of residue, but will by far dominate their slurries in terms of the number of particles to be treated. Therefore, aggregation of particles is important to speed up and de-bottleneck the slow solid/liquid separation process in thickeners.

Aggregation of particles can be accomplished to different extents through either *coagulation* or *flocculation* (or in some instances, a combination of both). The former is achieved by manipulating the surface charge of particles to the point where particles can come together, whilst the latter is achieved by the formation of bridges between particles, generally by high molecular synthetic polyelectrolytes and with less substantial change of surface charge (e.g. Connelly et al. 1986; Fellows and Doherty 2006; Hocking et al. 1999).

The coagulation process is best understood through the well-known DLVO suspension stability concept (developed separately by Derjaguin and Landau (1941) and Verwey and Overbeek (1948)). Particles in an aqueous system experience electrical repulsive and van der Waals attractive forces that determine their actual potential energy (Figure 2.1). When the surfaces are very close (separation < 0.01 micron), the attractive London-van der Waals forces predominate and natural coagulation occurs (e.g. Gregory 1989; Moss 1978). However, the repulsive forces from water adsorption forming a solvation layer and from similarly charged surfaces hinder natural coagulation.

A reduction of the surface charge magnitude and accordingly the repulsive forces is possible, for example, through the addition of oppositely charged polymers that will be adsorbed to the active particle surface. Addition of salts can also promote coagulation through a slightly different mechanism that is discussed later in Section 5.2.1.

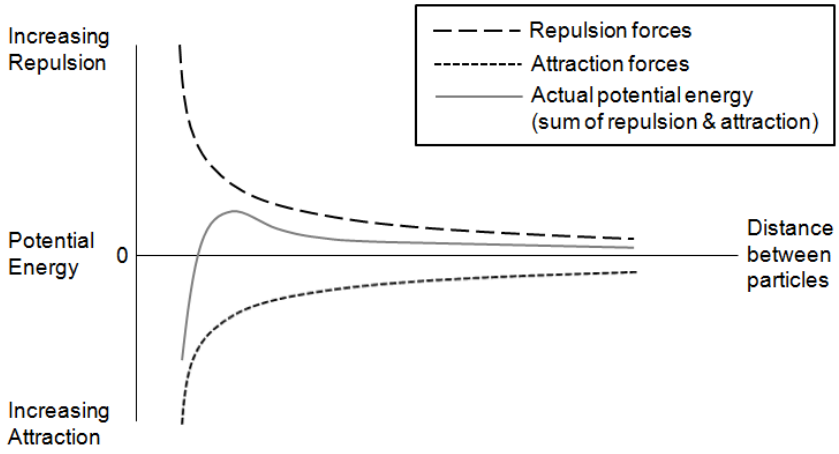


Figure 2.1. Schematic explanation of potential energy of particles as a function of inter-particle distance. Adapted from Moss (1978).

In contrast to coagulation, flocculation relies on the ability of a polymer (known as flocculant) to adsorb onto two or more particles, effectively behaving as a bridge that holds them together (e.g. Ayyala et al. 1993; Fellows and Doherty 2006; Hocking et al. 1999). High molecular weight polymers are preferred, as their more extended physical dimensions can potentially span many particles. Ayyala et al. (1993)

described that bridging flocculation in mineral processing systems occurs through the following steps (also represented schematically in Figure 2.2):

(i) mixing and adsorption of flocculant polymer molecules onto the surface of suspended particles,

(ii) reconformation of adsorbed flocculant towards an equilibrium configuration,

(iii) collisions among flocculants and particles,

(iv) aggregate growth as a result of collisions between barren surface and flocculant that is partly attached onto the surface of different particle(s), and

(v) aggregate rupture as a result of shear applied to the fragile aggregate structures.

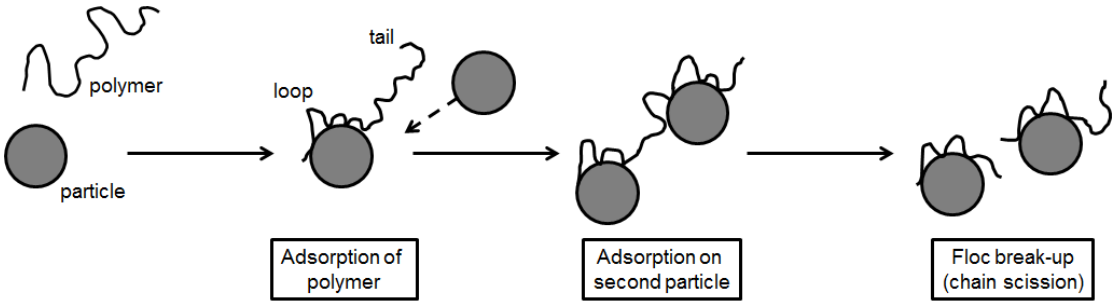


Figure 2.2. Schematic explanation of polymer bridging flocculation. Adapted from Hocking et al. (1999).

The distinct mechanisms of coagulation and bridging flocculation without a doubt affect the resulting aggregation process, in that:

(i) higher settling rates are typically observed from the flocculation process (5-50 m $h^{-1}$), compared to those from coagulation (1-5 m $h^{-1}$), because larger aggregates can be formed (e.g. Fawell 2013; Gregory 1989);

(ii) critically, aggregates formed by flocculation are more likely to survive shear during handling (e.g. Gregory 1997) although when breakage occurs, it becomes undesirably irreversible, unlike in the coagulation process where re-aggregation is possible if the magnitude of shear is reduced (e.g. Ayyala et al. 1993; Chen et al. 1990);

(iii) the weak forces associated with coagulation affects "smaller" colloidal-type particles ($\leq$ 2 μm) but their influence diminishes as the particles size increases (e.g. Fawell 2013);

(iv) statistical analysis by Hogg (1999) emphasized that adsorption of high molecular weight polymer (> $10^6$) has a low probability on "smaller" colloidal-

type particles and can only be enhanced by more intense agitation or by substantially increasing the polymer dosage;

(v) the coagulant dosages required are typically much higher than that of flocculant (e.g. Fellows and Doherty 2006; Hocking et al. 1999).

The advantages of flocculation outweigh its disadvantages for the feeds used in mineral processing, and therefore the use of high molecular weight synthetic polyelectrolyte flocculants dominates such applications.

### 2.1.1 Flocculants and surface adsorption

The tailings produced from the extraction stage of hydrometallurgical processes are generally metallic (*M*) oxides and/or silicates. Their surface chemistry can be explained by the simple oxide adsorption/dissociation reactions in Equations 2.2 and 2.3 (Drzymala and Fuerstenau 1987):

$$MOH^{+}_{2\,(surf)} \leftrightarrow MOH_{(surf)} + H^{+}_{(aq)} \qquad K_1 = a_{MOH}.a_{H^+} / a_{MOH^{+}_{2}} \qquad 2.2$$

$$MOH_{(surf)} \leftrightarrow MO^{-}{}_{(surf)} + H^{+}_{(aq)} \qquad K_1 = a_{MO^-}.a_{H^+} / a_{MOH^{+}_{2}} \qquad 2.3$$

The particular pH at which neutral hydroxyl sites (*MOH*) co-exist with equal numbers of positively charged ($MOH_2^+$) and negatively charged ($MO^-$) sites is known as the point of zero charge or pzc (e.g. Hunter 1993). The proportion of neutral, positively and negatively charged sites depends on the solution pH where at pH's:

(i) < pzc, positive sites are dominant – giving a net positive surface charge;

(ii) > pzc, negative sites are dominant – giving a net negative surface charge (Drzymala and Fuerstenau 1987).

It is worth noting that the pzc will vary due to several factors, such as mineralogy, solution composition and sample preparation (Johnson et al. 2000; Kosmulski 2002, 2004, 2006, 2009, 2011).

Flocculants can be tailored to accommodate different functionalities through the polymerisation of vinyl monomers that are cationic (dimethyl-aminoethyl acrylate or DMAEA), nonionic (acrylamide) and anionic (acrylate). The nonionic functionality

serves as a flexible backbone for copolymerisation with either cationic or anionic monomers to control the percentage of cationic/anionic character in a product (Pearse 2003). The chemical structures of DMAEA, acrylamide and acrylate copolymers can be found in Pearse (2003).

Cationic flocculants in the form of DMAEA/acrylamide copolymers were reported for ceramic applications with kaolin as giving low settling rates (2-7 m $h^{-1}$), limited by the relatively low flocculant molecular weights, ranging between $1\text{-}10\times10^{6}$ (Gill and Herrington 1987a, 1987b, 1987c, 1988, 1989). Such settling rates will rarely provide the high throughputs demanded by modern mineral processing plants. As a consequence, flocculant selection generally relies on the relative response of products with nonionic and anionic characters as a function of pH.

Taking hematite as an example of a metal oxide whose pzc lies at range of pH between 5 to 10 (Kosmulski 2011), at pH values below the pzc (e.g. under acidic conditions), the adsorption of flocculant will occur through the hydrogen bonding of nonionic amide functionality to the neutral sites (Connelly et al. 1986) and also through the chelating complexation of anionic carboxylate functionality to the positively charged sites (Kirwan et al. 2003). To date, there is no evidence that the protonated carboxylate functionality attaches to the hematite surface through the hydrogen bonding mechanism, at least within the investigated pH range of 2-14 (Jones, 1998; Kirwan 2003, 2004).

The importance of acrylate (anionic) content is practically seen when the pH rises to neutral and slightly basic condition (up to pH 10). Increasing the ionisation of carboxylate groups in the copolymers leads to these functionalities repelling each other, causing the polymer to uncoil and eventually improving its bridging capacity (Figure 2.3).

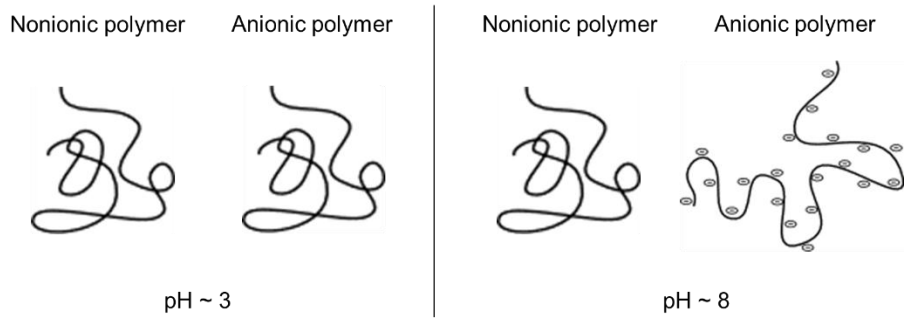


Figure 2.3. Schematic explanation of the effect of pH on polymer conformation. Adapted from Connelly et al. (1986).

The high pH condition is of greatest interest in the Bayer Process, especially when the pregnant liquor (highly caustic and supersaturated with alumina) has to be separated from the insoluble solid residue soon after digestion. Under primary settling conditions, anionic flocculants are exclusively used to flocculate bauxite residue, even though the surfaces would normally be expected to be negatively charged at high pHs and therefore to repel such flocculants. A key aspect contributing to adsorption being achieved is the high ionic strength of the liquors.

From work using iron oxide as a model substrate, sodium ions from the bulk solutions were found to adsorb strongly to the negatively charged surface, altering the net charge at the interface to a point where there is an excess of the sodium ions and the surface becomes positive (Kirwan et al. 2004). The positively charged surface from the screening effect given by sodium ions is then able to attract the anionic functionalities (carboxylate) from the polyacrylamide/acrylate (PAA) flocculants (Figure 2.4a).

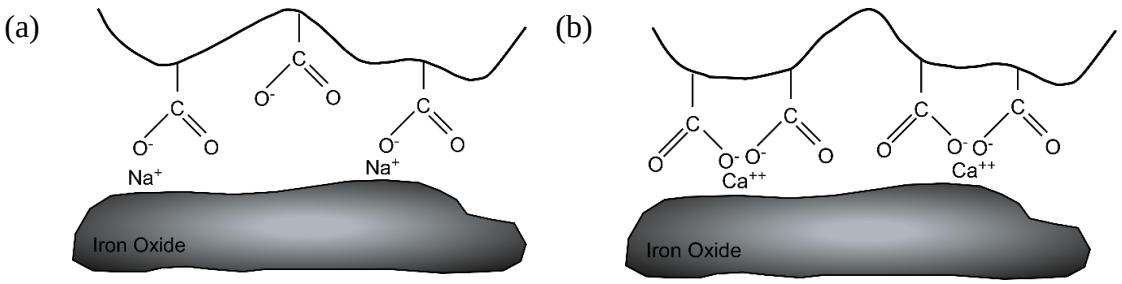


Figure 2.4. Schematic explanation of adsorption of PAA through: (a) sodium and (b) calcium bridging. Adapted from Chen et al. (2003).

Divalent cations in the form of calcium ions have been considered essential for bauxite residue flocculation through their adsorption to the surface providing extra sites for flocculant adsorption, as seen in Figure 2.4b (e.g. Rothenberg et al. 1989; Spitzer et al. 1991). However, it was later found that calcium at its solubility level , in the order of mg $L^{-1}$ (e.g. Rosenberg et al. 2001, The and Sivakumar 1985), helped reduce the supernatant turbidity of the post-flocculated hematite slurry without affecting flocculant adsorption density and the resultant settling rate (Jones 1998). This indicates that calcium ions may provide extra active sites for flocculant adsorption to a limited extent, but it certainly is not essential for flocculation to proceed. When adsorbed to the negatively charged sites, calcium ions could reduce the net surface charge of particles and then lead to partial coagulation, explaining why the supernatant turbidity of the post-flocculated slurry was improved when the settling rate remained largely unaffected.

The beneficial effect of calcium was more pronounced at much higher concentration (g $L^{-1}$ level) but this is likely due to the '*causticisation'* effect (Equation 2.4), precipitating some fraction of soluble carbonate impurities as calcite and thereby minimising adsorption of carbonate and blinding the active sites in bauxite residue (Hunter et al. 1991).

$$Na_2CO_3(aq) + Ca(OH)_2(s) = CaCO_3(s) + 2\ NaOH(aq) \qquad 2.4$$

In addition to PAA, there are also the hydroxamate/polyacrylate/acrylamide (HX PAM) terpolymer products that now dominate the market for bauxite residue flocculants in primary settling applications (Ballentine et al. 2011). The chemical compositions of HX PAM and PAA flocculants are given in Figure 2.5; note that significant acrylamide content is only desirable for the later stages of the residue circuit when the pH drops as a result of counter-current washing (CCW) and flocculant adsorption is then more effectively established through hydrogen bonding (Hunter et al. 1991; Pearse and Sartowski 1984; Sankey and Schwarz 1984).

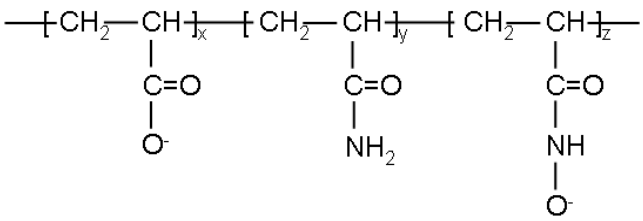

| Flocculant | Application | Composition | | |
|---|---|---|---|---|
| | | Acrylate (%X) | Acrylamide (%Y) | Hydroxamate (%Z) |
| HX PAM | Primary thickener & front washer | 85-55 | 5-15 | 10-30 |
| PAA | Primary thickener & front washer | 100-90 | 0-10 | 0 |
| | Middle & last washers | 60-100 | 40-0 | 0 |

Figure 2.5. The chemical composition of HX PAM and PAA flocculants. Adapted from Phillips (1999).

HX PAM development was originally based on the motivation to include functional groups that can directly interact with iron oxide, the major phase within bauxite residue, without cation bridging facilitation (Chen et al. 2003). Hydroxamic acid had shown such characteristics in the selective flocculation of iron oxide over kaolin during iron ore beneficiation and was chosen accordingly (RaviShankar et al. 1988).

The hydroxamate functionality adsorbs onto the surface of iron oxide through a chelating mechanism that forms a five-membered ring complex with Fe (Figure 2.6), and this is a stronger interaction than that achieved by cation bridging with PAA products (Chen et al. 2003). The distinct adsorption mechanism is postulated to give a different response when shear is applied and better fines capture efficiency (discussed later in Section 2.4). Adsorption itself is the first step in the bridging flocculation mechanism and it shares an equal role with shear in dictating the aggregate characteristics and resultant dewatering properties.

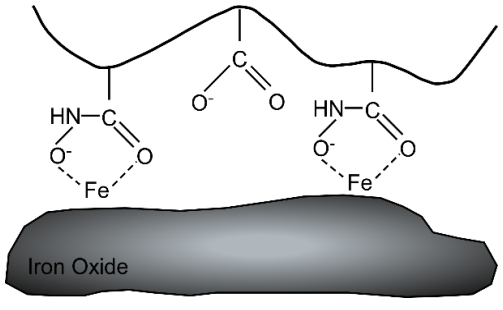


Figure 2.6. Chelating mechanism for HX PAM adsorption. Adapted from Chen et al. (2003).

### 2.1.2 Aggregate characteristics

Shear is required in bridging flocculation to create particle-particle, particle-aggregate or aggregate-aggregate collisions, resulting in aggregate growth. When the primary particles involved in flocculation are equal spheres, the aggregation of two such particles must be in the simple form of a dumbbell (Gregory 1997) and the complexity starts when the following particles attach to the doublet in many different random configurations.

In reality, there could be hundreds to thousands of particles that form a single aggregate, leading to the basic fractal concept that identifies an aggregate as an open structure whose mass is increased when the aggregate grows but its effective density decreases (e.g. Ayyala et al. 1993; Chakraborti et al. 2003; Gregory 1989; Gregory 1997; Klimpel and Hogg 1986; Meakin 1987).

For fractal structures, the mass increase as a function of diameter is illustrated in Figure 2.7 (Chakraborti et al. 2003) and the log-log plot of mass vs. size produces a straight line (Gregory 1989) that obeys the following relationship:

$$m \propto L^{D_f} \qquad 2.5$$

where $m$ is the mass, $L$ is the diameter or radius of the aggregate and $D_f$ is the mass-length fractal dimension. $D_f$ is therefore equal to three for a solid, non-porous spherical species, while a value of one would imply particles coming together in a linear fashion. Values in between these extremes describe porous aggregates, with most studies indicating values in the range 1.8-2.5. A lower $D_f$ value then indicates a more "open" aggregate structure.

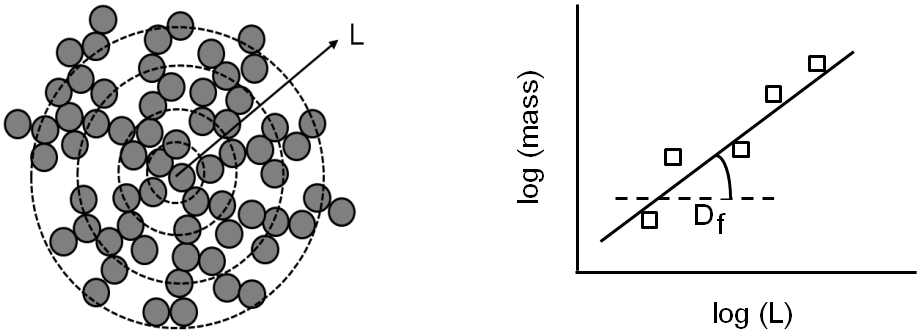


Figure 2.7. Schematic explanation of the mass increase as a function of diameter in fractal aggregates. Adapted from Chakraborti et al. (2003) and Gregory (1997).

The $D_f$ values vary depending on the aggregation mechanism, with particle-cluster interactions enabling single particles to penetrate and fill some voids in the fractal aggregate, while cluster-cluster interactions see the incorporation of two grown aggregates through single or multiple attachment points (Figure 2.8). It is immediately clear that particle-cluster interactions tend to exhibit higher $D_f$ values; in other words, lower porosity. As a rule-of-thumb, aggregates from a coagulation process generally have a lower $D_f$ because of the stabilisation effect given by the adsorbed polymer layers that are dehydrated and repel each other when they come too close (Gregory 1989). The risk of stabilisation is statistically lower in bridging flocculation when the polymer adsorbed onto the particle covers only a low fraction of the active surface.

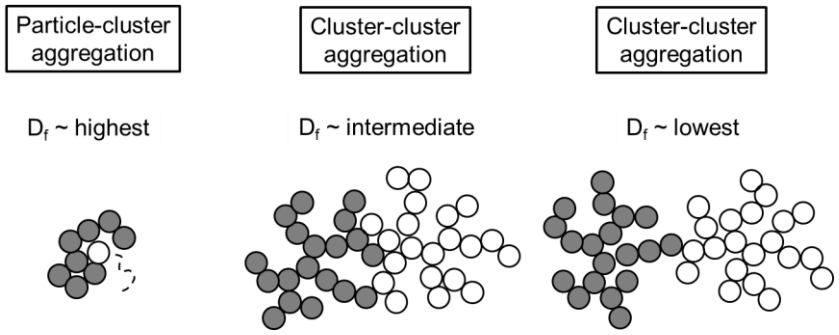


Figure 2.8. Schematic explanation of particle interactions giving different relative fractal dimensions. Adapted from Chakraborti et al. (2003) and Gregory (1997).

Gregory (1989) stated that for a given mass containing a fixed number of primary particles, the settling rate will be increased as the aggregate becomes more compact (higher $D_f$). Fractal properties were not accounted for in the original Stokes' Law,

which was developed for individual particle settling, and this has motivated refinements by many researchers by incorporating other contributing factors, such as solids concentration and $D_f$, to give more sensitive prediction for the settling rate. Some pertinent aspects of this are explained in the following discussion.

In polymer bridging flocculation as practised in mineral processing, the solids concentration of the slurry that is fed into a thickener is usually rather high. For example, feed concentrations of ~60 kg m$^{-3}$ were stated for a coal beneficiation plant (Sabah et al. 2004), 80-270 kg m$^{-3}$ for bauxite residue (Peloquin et al. 2002; Perrier et al. 1999), and up to 150 kg m$^{-3}$ for clay-type tailings (Fawell 2013). The impact of operating at such concentrations is that the settling regime shifts from the *free settling* to *hindered settling* condition, where interparticle interaction creates a hydrodynamic resistance for the fluid to flow past the particles and thereby reduces the settling rate (Buscall and White 1987, 1988; Landman et al. 1988). There are numerous refinements that incorporate the solids concentration, expressed as a solids volume fraction ($\phi_s$), into Stokes' Law to more accurately predict the settling rate of flocculated slurry (Dollimore and McBride 1968; Kynch 1952; Maude and Whitmore 1958; Richardson and Zaki 1954; Steinour 1944a, 1944b, 1944c). A more recent modification also involves $D_f$, as per the equation below (Heath et al. 2006c):

$$U_h = \frac{\bar{d}_{agg}^2 g(\rho_s - \rho_l)\left(\frac{\bar{d}_{agg}}{\bar{d}_p}\right)^{D_f-3}}{18\mu}\left(1 - \phi_s\left(\frac{\bar{d}_{agg}}{\bar{d}_p}\right)^{D_f-3}\right)^{4.65} \qquad 2.6$$

where $U_h$ is the hindered settling rate (m s$^{-1}$), $\rho_s$ and $\rho_l$ are the solid and liquid densities, respectively (kg m$^{-3}$), $g$ is the gravitational acceleration (m s$^{-2}$), $d_{agg}$ and $d_p$ are the aggregate and primary particle size, respectively (m), and $\mu$ is the dynamic viscosity (N s m$^{-2}$). The benefit gained from having more compact aggregates (higher $D_f$) or larger aggregates ($\bar{d}_{agg}$) is clear from Equation 2.6.

Flocculant selection would be expected to influence aggregate density, although there are few published examples of this with feeds of relevance to mineral processing. Grabsch et al. (2013) recently compared two commercial flocculants, and found that one containing an alternative functional group did give a higher aggregate

$D_f$. Scales and co-workers (Gladman et al. 2005; 2006; 2010) studied the effect of post-formation shear, finding that low shear rate (< 10 $s^{-1}$) helps aggregate densification (higher $D_f$) and improves the hindered settling, while high shear rate (> 100 $s^{-1}$) was detrimental to the hindered settling. The latter could be due to the limited mean aggregate size derived from increasing the breakage rate at high shear rate condition (e.g. Klimpel and Hogg 1986) and this is discussed in the following section.

### 2.1.3 Flocculation kinetics

As already stated, shear is crucial to aggregation by providing collisions, but not all collisions will lead into a growth in aggregate size. Only collisions between barren surfaces of a particle/aggregate with another that has active polymeric flocculant on its surface are effective for bridge formation. This condition is termed *collision efficiency*. Saffman and Turner (1956) refined the collision rate equation of particles of different size in laminar fluid flow that was originally introduced by Smoluchowski (1916, 1917) for modelling coagulation (described in Equation 2.7) into an aggregation kernel that accommodates collision efficiency (described in Equation 2.8):

$$\beta_{ij} = \frac{4}{3}\gamma(\alpha_i + \alpha_j)^3 \qquad 2.7$$

$$\beta_{ij} = 1.29\alpha G(\alpha_i + \alpha_j)^3 \qquad 2.8$$

$$G = \sqrt{\frac{\varepsilon}{\upsilon}} = \left(\frac{\varepsilon\,\rho_f}{\mu}\right)^{1/2} \qquad 2.9$$

where $\beta_{ij}$ is the rate of collision between i and j sized particles or aggregation kernel ($m^3$ $s^{-1}$), $\gamma$ is the laminar shear rate ($s^{-1}$), $a_i$ and $a_j$ are the particle radii (m), $G$ is the mean shear rate ($s^{-1}$), $\alpha$ is the collision efficiency [0,1], $\varepsilon$ is the energy dissipation rate ($m^2$ $s^{-3}$), $\rho_f$ is fluid density (kg $m^{-3}$) and $\upsilon$ is the kinematic viscosity ($m^2$ $s^{-1}$).

While shear is essential to promote collisions that induce aggregation, shear applied continuously in bridging flocculation can also contribute to the irreversible breakage

of the fragile aggregate structures that have been formed. The breakage rate ($S_i$) is given as the following function:

$$S_i = G^x = \left(\frac{\varepsilon \rho_f}{\mu}\right)^n \qquad 2.10$$

where *n* is an exponent higher than that in the aggregation kernel and typically takes a value between 0.5-1 (Chung et al. 1998; Curtis and Hocking 1970; Heath et al. 2006c; Oles 1992; Serra and Casamitjana 1998; Spicer and Pratsinis 1996). Hence, the mean aggregate size as a function of shearing time is usually reflected by an initial period of aggregate growth before it reaches an optimum value, beyond which irreversible breakage is the dominant process. A schematic representation of aggregate size as a function of reaction time under shear and its correlation to settling rate is provided in Figure 2.9.

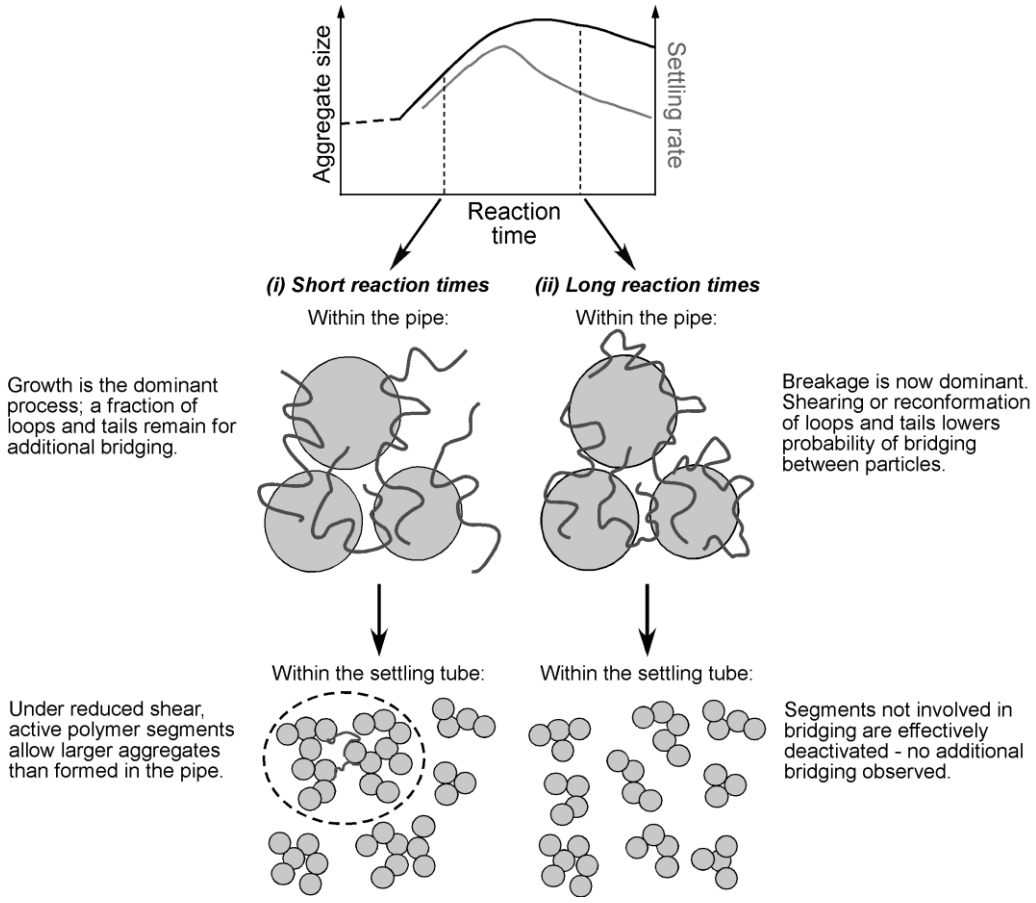


Figure 2.9. Schematic representation of post-sheared aggregate growth from turbulent pipe flow study connected to a settling column. Adapted from Owen et al. (2008).

From the kinetic point of view, higher shear rates result in a shorter induction time required to achieve the optimum mean aggregate size, however, its absolute value will be smaller than that achieved by a lower shear rate due to the fragility of large aggregates. The subsequent onset of size reduction will also be faster under higher shear (Heath et al. 2006c; Spicer et al. 1998; Swift et al. 2004).

The correlation of aggregate size and hindered settling rate provided in Equation 2.6 assumes that aggregates have stopped growing. Owen et al. (2008) were able to measure aggregate size *in-situ* for turbulent pipe flocculation, while also measuring settling rates on pipe outflow collected in cylinders. As shown in Figure 2.9, samples taken at short reaction times contained aggregates still in their growth phase, with further growth still possible under the milder shear within the cylinders, thereby greatly enhancing settling rates. Such enhancement was not observed at longer reaction times, when surface adsorbed flocculant was no longer active. This further emphasizes the need to avoid over-shearing during flocculation.

### 2.1.4 Flocculant dosage vs. collision efficiency

The amount of flocculant used to achieve aggregation can be expressed as the concentration across the slurry volume after addition, or perhaps more usefully, in terms of the mass of flocculant per tonne of substrate solids, termed the dosage. Higher flocculant dosages are assumed to enhance aggregation, but the relationship can be more complex. An important study in this area was conducted by La Mer and Healy (1963), who used filtration rate as an indicator of flocculation performance, with high rates resulting from openly packed beds formed by good flocculation. They found that filtration rate dropped when the flocculant concentration exceeded an optimum value (Figure 2.10).

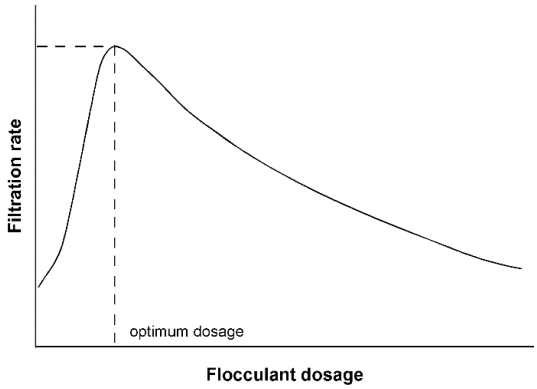


Figure 2.10. Schematic relationship between filtration rate vs. flocculant dosage. Adapted from La Mer and Healy (1963).

The authors proposed the concept of an optimum surface coverage ($\theta$) in correlating this to the collision efficiency in Equation 2.11:

$$\alpha = \theta(1 - \theta) \qquad 2.11$$

From this equation, optimum flocculation would be achieved when highest collision efficiency ($\alpha$ = 0.25) is given by half surface coverage ($\theta$ = 0.5), although this is now considered an oversimplification. Numerous more recent studies have attempted to derive a better estimate for $\theta$ and to understand its implications for the flocculation process. Hogg (1984) stated that Equation 2.11 is only valid for a first particle that has adsorbed polymer and a second particle that has bare surface. In reality, the reverse case has equal probability, making the maximum $\alpha$ equal to 0.5, or higher than in the La Mer and Healy model. Moudgil and co-workers (Moudgil and McCombs 1987; Moudgil et al. 1987) mentioned that Equation 2.11 is based on a homogenous surface while the particle surface is heterogeneous in their model, containing both active and inactive sites. If the proportion of inactive sites is higher than the active sites, the collision efficiency factor only increases to a very limited extent although more flocculant is added to achieve optimum surface coverage.

Regardless of which of these theories is applied, surface coverage is always a term that is hard to define without knowing exactly whether the flocculant is adsorbed in a coiled or flat conformation (Gregory and Barany 2011; Olsen et al. 2006; Swerin et al. 1996). However, dosing flocculant at a level that gives high surface coverage is

obviously detrimental for aggregation because it decreases the probability of successful collisions, thereby decreasing aggregation rates and aggregate sizes.

In a mineral processing context, it is important to recognise that the particle sizes being considered are often much larger than those within many of the fundamental studies used to develop relationships such as Equation 2.11. As a consequence, aggregate size often becomes visibly large at dosages representing less than 20% surface coverage. Owen et al. (2008) found that the dosages required to achieve settling rates of 10-20 m $h^{-1}$ (considered adequate in most thickening applications) were at least ten times lower than that required for reaching the plateau in the flocculant adsorption isotherm. For most mineral systems, the dosages required to give a reasonable settling rate can be very low (compared to that for maximum adsorption), and therefore the negative impact of higher flocculant dosages on performance may never be realised. However, this may not necessarily always be the case for feedwell flocculation, where the shear rate is not evenly distributed, and hence solid and flocculant may not be well dispersed, creating local overdosing or even significant proportions of unadsorbed flocculant.

### 2.1.5 The critical impact of solids concentration

Solids concentration is often expressed in different ways that can be confusing, e.g. as g $L^{-1}$, wt/wt% solid, wt/vol% solid or as solids volume fraction, the latter almost universally used in mathematical equations. While they all actually represent the same concept, the use of mass-based units can be misleading when comparing different feeds with quite different particle or liquor densities.

For mineral processing applications, flocculation takes place at high solids concentration, which affects the slurry viscosity through the following equation (e.g. Govier and Aziz 1972; Heath et al. 2006c; Liu and Masliyah 1996):

$$\mu_s = \mu_o \left(1 - \frac{\phi_s}{\phi_m}\right)^{-k} \qquad 2.12$$

Where $\mu_s$ is slurry viscosity (N s m$^{-2}$), $\mu_o$ is fluid viscosity in the absence of solid (N s m$^{-2}$), $\phi_m$ is maximum solids volume fraction and k ≈ 2. Values of $\phi_m$ are typically assumed between 0.6-0.7, reflecting the condition where particles are in close contact to form a continuous network that resists shear and makes viscosity rise exponentially (Bustos et al. 1999; Heath et al. 2006c; Schram 1996).

As the aggregates formed are porous with high enclosed volumes, the effective solids volume fraction ($\phi_{eff}$) is actually higher than $\phi_s$ in Equation 2.12 and can be represented as a function of aggregate size and fractal dimension (Flesch et al. 1999; Heath et al. 2006c; Kusters et al. 1996; Mills et al. 1991; Oles 1992; Potanin and Uriev 1991; Richardson and Zaki 1954):

$$\phi_{eff} = \phi_s \left( \frac{\bar{d}_{agg}}{\bar{d}_p} \right)^{3-D_f} \qquad 2.13$$

When $\phi_{eff}$ from Equation 2.13 is used as a substitute for the solids volume fraction, the slurry viscosity in Equation 2.12 can be rewritten as (Heath et al. 2006c):

$$\mu_s = \mu_o \left( 1 - \frac{\phi_{eff}}{\phi_m} \left( \frac{\bar{d}_{agg}}{\bar{d}_p} \right)^{3-D_f} \right)^{-k} \qquad 2.14$$

The implication of Equations 2.12-14 is that the slurry viscosity increases with increasing solids concentration (solids volume fraction). The actual increase is higher than that predicted without taking into account the effect of aggregation. The actual increase in slurry viscosity indeed creates more collisions or in other words, a higher probability of aggregation, as per Equation 2.8. However, it also increases the breakage rate expressed in Equation 2.10. This creates the optimum solids concentration concept, above which the maximum aggregate size formed will be lower in magnitude (e.g. Fawell et al. 2009a; Heath et al. 2006c; Owen et al. 2008).

An example of this behaviour is depicted in Figure 2.11 where the aggregate size of kaolin (measured in-stream as the mean square-weighted chord length in turbulent pipe flow at a constant flocculant dosage) increased from ~270 to ~300 μm when the

solids concentration was increased from 4.9 to 9.2 g $L^{-1}$ but further increases to the solids concentration led to a reduced maximum size (Owen et al. 2008).

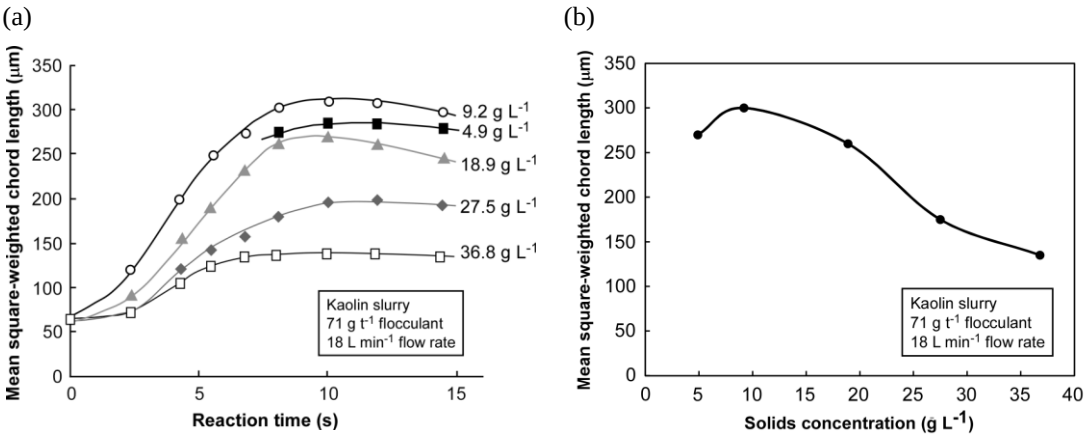


Figure 2.11. Mean square-weighted chord length of flocculated kaolin as a function of: (a) reaction time for different solids concentrations at a dosage of 71 g $t^{-1}$; and (b) solids concentration at a reaction time of 8 s. Adapted from Owen et al. (2008).

The optimum solids concentration can differ significantly between feed systems. Among the contributing factors are particle size and shape. As an example of the latter, flocculant only adsorbing on the minor edge faces of the plate-like kaolin particles will result in very "open" structures with low $D_f$ (e.g. Du et al. 2010; Fawell et al. 2009a; Hocking et al. 1999; Loan 1999; Taylor et al. 2002; Zbik et al. 2008). A lower $D_f$ heightens the increase in the effective solids volume fraction and slurry viscosity, shifting the optimum solids concentration to a lower range.

### 2.1.6 Flocculant dosing strategy

Flocculant delivery and dosing systems offer some flexibility in how flocculation is achieved, which provides options for enhanced performance. Adding flocculant in a split or step-wise basis generally enhances overall performance; e.g. an in-line mixer may be used to dose flocculant in the pipe feeding a feedwell, with additional flocculant then dosed in the feedwell (Probst 1999). Table 2.1 summarises published studies where split or step-wise flocculant addition has proven to be beneficial.

Table 2.1. Selected results showing the benefit of step-wise flocculant addition in different mineral slurries.

| Mineralogy | 1st addition | 2nd addition | Comment | Literature |
|---|---|---|---|---|
| Coal-clay | Cationic | Nonionic | -- | Baran et al. (1983) |
| Alumina | Anionic | Cationic | Alumina is positively charged, anionic added first | Yu and Somasundaran (1993) Fan et al. (2000) |
| Silica | Anionic | Anionic | Continuous dosing | Peng and Williams (1993) |
| Kaolin | Nonionic | Nonionic | Continuous dosing | Suharyono and Hogg (1996) |
| Kaolin | Anionic | Anionic | Higher proportion in 2nd addition is beneficial | Owen et al. (2008) |

It was postulated that the first addition of flocculant produces small aggregates that consist of many particles, allowing the subsequent addition(s) (which is not necessarily a flocculant of the same ionic type) to interact only with the external surface area of the aggregates (e.g. Owen et al. 2008). Fan et al. (2000) translated this into a concept of *anchoring* and *tethering*, schematically explained in Figure 2.12. The ultimate result of split or step-wise flocculant addition is an enlarged aggregate size (e.g. Moss 1978; Owen et al. 2008; Peng and Williams 1993) that is often accompanied by improved fines capture efficiency (e.g. Baran et al. 1983; Fan et al. 2000; Yu and Somasundaran 1993). It should be noted that a high solids concentration can mask the efficacy of split or step-wise flocculant addition, due to the effective solids volume fraction limiting the aggregate size, as discussed in the previous section (Owen et al. 2008).

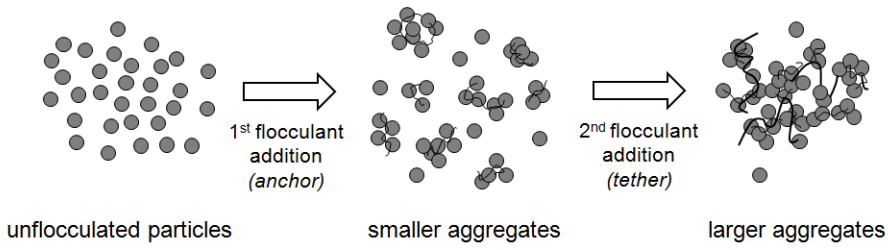


Figure 2.12. Schematic representation of the step-wise polymer flocculation process. Adapted from Fan et al. (2000).

In addition to the flocculant dosing points, the concentration of the flocculant solution being dosed also affects the flocculation process (e.g. Guibai and Gregory 1991; Moss 1978), with concentrations > 0.010% potentially decreasing the aggregate size attained and reducing the resultant settling rate. When dosed as a

concentrated solution, the flocculant can suffer from poor mixing and dispersion due to its viscosity (e.g. Fawell et al. 2009a; Owen et al. 2008; White et al. 2001). Uneven distribution of flocculant throughout the slurry leads to sub-optimal contact with the particles.

As a proof of this premise, quantification of adsorption from the turbulent pipe flocculation of kaolin at a dosage of 300 g $t^{-1}$ showed that increasing the dosed flocculant concentration from 0.003 to 0.010% reduced the amount of flocculant adsorbed from 98 to 90% (Owen et al. 2008). This effect was magnified on doubling the flocculant dosage (95 to 75%). However, it should be kept in mind that diluting the flocculant at the level that maximises mixing and distribution ($\leq$ 0.005% according to Fawell et al. 2009a) can be impractical in some applications, such as in bauxite residue primary thickening, which is discussed separately in Section 2.4.4.

## *2.2 The thickening process*

The basic features of a gravity thickener were shown in Figure 1.2, but that image is by no means representative of how all thickeners look. While thickeners in excess of 100 m in diameter are known, there are many low throughput applications where diameters may be lower than 10 m. The total height of a thickener is the sum of the vertical sidewall and the height of the cone section immediately below. While sidewall heights are often kept low to reduce capital costs, they may be increased in applications where bed consolidation is a priority. The angle of the cone section is typically low in older thickeners (14º is common), but is often higher when dealing with higher yield stress materials, such as in paste thickeners.

Figure 2.13 provides a clearer representation of the passage of solids through a thickener. After leaving the bottom of the feedwell, flocculated slurry settles towards the sedimentation zone until it reaches the thickening zone where consolidation occurs as a result of natural compression and rake action. Aggregate deformation during consolidation releases liquid entrapped in the aggregate network to flow upward and increases the solids concentration in the bed. The velocity of such streams can influence the solids concentration that reports to the thickener overflow

due to its capacity to entrain particles (dispersed or poorly flocculated) whose gravitational settling rates are lower than the upward velocity.

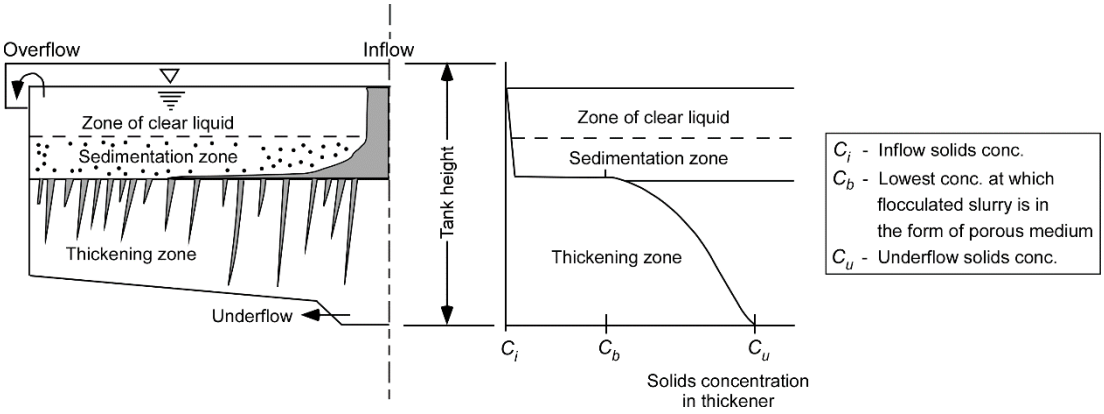


Figure 2.13. Schematic explanation of different zones in the gravity thickener relevant to the solids concentration. Reproduced from Shammas and Wang (2007).

The development of synthetic flocculant technology with the ability to give much faster settling rates drastically changed the rules for sizing and design of thickeners. In the case of the Bayer process, thickeners can be built that are 4-6 times smaller than those in 1950s refineries in which the natural flocculant starch was used to assist aggregation and improve settling rates with very limited success (Chandler 1976; Laros and Baczek 2009; Vidyasagar 1996). Without intending to diminish the role of other thickening aspects, such as rake design, overflow configuration and underflow pumping, it is apparent that the aggregate structures formed and the efficiency of particle capture achieved substantially influences all measures of thickener performance, making the feedwell the most important element in thickener design and operation.

## *2.3 Feedwell*

The original objectives for feedwells prior to the introduction of synthetic flocculants were to dissipate the feed momentum/kinetic energy and to as much as possible ensure it is distributed gently and symmetrically when leaving the feedwell. When flocculant is used, the feedwell is also required to give sufficient shear and collisions between solid substrates and flocculant to favour aggregate growth and fines capture over breakage (Heath and Triglavcanin 2010). Given that feedwells are also often

poorly controlled, it is rare that all functions are achieved to full effect. Older feedwells are generally used as flocculation vessels without any significant changes made towards this specific purpose.

The benefits from optimised flocculation are apparent from the combination of reduced flocculant consumption, rapid settling, good overflow clarity and high underflow density – all of which fall into the criteria especially desirable for bauxite residue primary thickening. Among the many feedwell aspects which have to be understood to achieve optimal flocculation are: (i) the basic feedwell flow patterns, (ii) feed throughput and feedwell dimension (in particular the feedwell aspect ratio), (iii) volumetric flow rate and (iv) feedwell internal structure.

### 2.3.1 Feedwell flow patterns

In their simplest form, feedwells are just cylinders open at both the top and bottom, with the feed effectively entering from the side in a horizontal direction; there are instances in old thickeners where feed streams are discharged above the liquor surface, but such cases are very much sub-optimal for flocculation and as they are not seen in Bayer process thickeners, they will not be discussed further. The pressurised feed should enter below the liquor surface in a tangential (or close to tangential) direction relative to the inner wall of the feedwell and in order not to cause excessive agitation, it must decay in a swirling motion while dissipating its momentum/kinetic energy (Fitch and Lutz 1960) and create a continuous vortex inside the feedwell.

The simplified flow pattern in an open tangential feedwell is drawn in Figure 2.14. A feedwell will therefore typically have two regions or compartments - a highly turbulent flow region (usually at its upper part) where the pressurised slurry is introduced and exposed to a risk of jet acceleration, and a quiescent region (usually lower down) where the slurry has dissipated most of its kinetic/momentum energy (Echeverri et al. 2012; Foster et al. 1996).

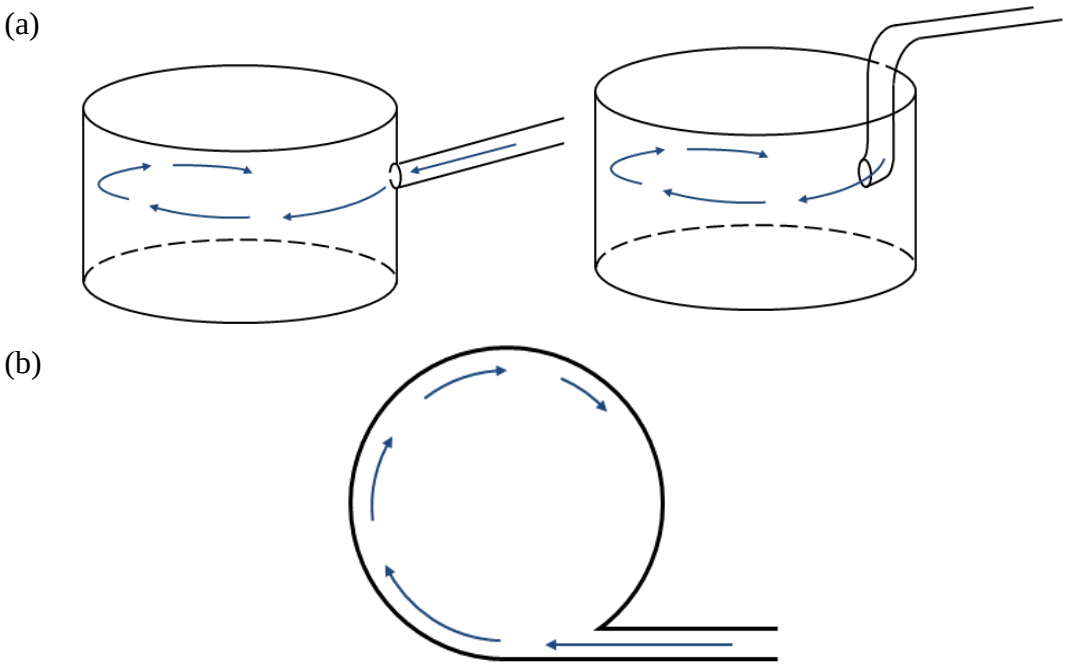


Figure 2.14. Schematic representation of fluid flow in an open tangential feedwell: (a) side view of slightly different pipe feeding systems and (b) plan view.

An open tangential feedwell not only represents the simplest feeding system but the simplest swirling flow pattern as well. In practice, a split feed arrangement is often used for high throughput applications (e.g. Fawell et al. 2009b; Fitch and Lutz 1960; Foster et al. 1996), including many designed for bauxite residue thickening. In this case, pressurised slurry is divided into two streams prior to entering the feedwell at the same level (see Figure 2.15a). In an ideal situation, the slurries going in opposite directions along the inner wall of the feedwell collide at the far side and dissipate their kinetic energy (see Figure 2.15b).

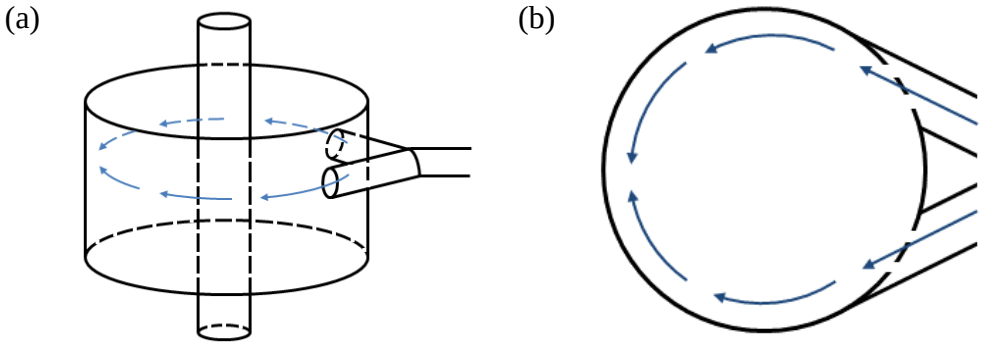


Figure 2.15. Schematic representation of: (a) open split feedwell and (b) the ideal fluid flow inside the feedwell. Adapted from Fawell et al. (2009b).

By having two different incoming streams with equal volumetric flow rate, the total flow volumetric rate can theoretically be two times higher. Increasing the volumetric flow rate in a single stream to achieve the same volumetric rate is likely to create undesirable turbulence.

It must be kept in mind that the ideal condition depicted in Figure 2.15b can only occur if the split streams have identical velocities. Actually achieving and maintaining the even split is difficult (Fawell et al. 2009b), often resulting in the domination of one stream over the other (see Figure 2.16). Depending on their velocity vectors, one (or both) of the streams may also sink out early and the collision of streams does not necessarily happen. Hence, the energy dissipation goal is not achieved and worse, short-circuiting is experienced, with the slurry preferentially discharged to one side of thickener.

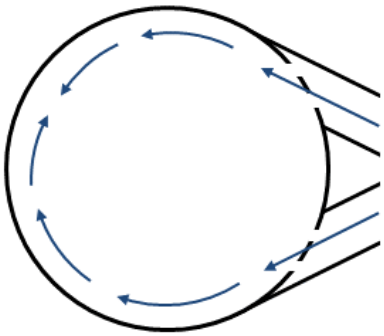

Figure 2.16. Schematic representation of the domination of one stream in an open feedwell with split feed.

In the Fitch feedwell design, the split-feeding system is mounted to the feedwell with its two branches at different levels in between the three internal shelves (Figure 2.17a) – such a configuration, where the slurry streams are in opposite directions and separated by the shelves, may (in theory) prevent them from sinking out early and eliminates the poorly controlled collision of streams seen when they both enter on the same plane. In fact, the shorter middle shelf lets the streams that go in opposite directions contact each other (see Figure 2.17b), creating a turbulent shearing zone adjacent to the central zone of the feedwell (Fitch and Lutz 1960; Foster et al. 1996). As a consequence, solid dispersion is claimed to be improved, as slurry must pass the shearing zone prior to discharge at the bottom (Fitch and Lutz 1960). Although the

Fitch feedwell may provide higher throughput, it was said to suffer from high flocculant consumption (Arbuthnot and Jagger 1999).

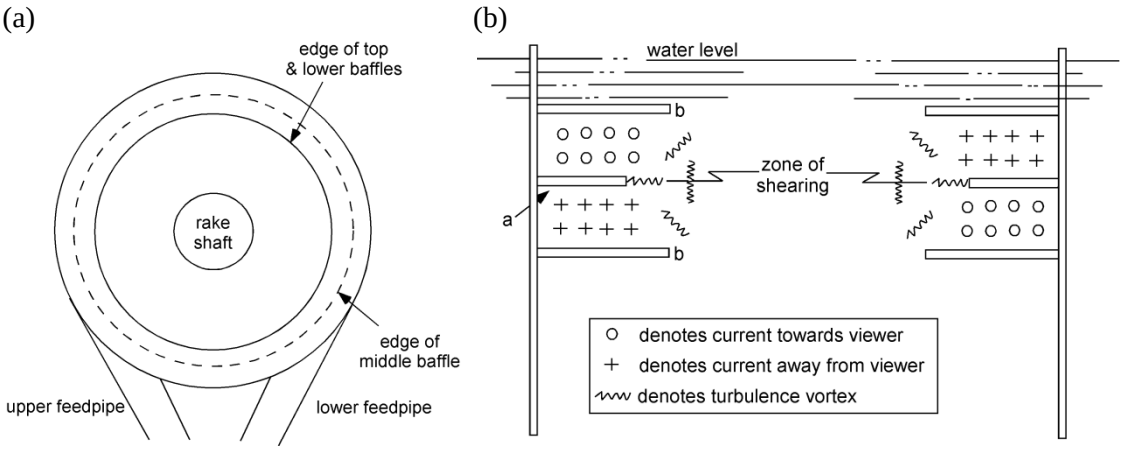


Figure 2.17. Schematic representation of Fitch feedwell: (a) plan view (adapted from Foster et al. 1996) and (b) side view (adapted from Fitch and Lutz 1960).

As stated earlier, settled bed consolidation releases liquid entrapped in the aggregate network to flow upward. While much of this is collected in the overflow launder as clarified liquor, some can re-enter the feedwell and change the fluid flow inside the feedwell. From the flocculation standpoint, this can be considered beneficial, since it gives a local dilution effect (see Section 2.1.5). However, if the upward velocity is too fast, it can entrain fines or aggregate fragments back into the feedwell, thereby increasing the solids population inside the feedwell. This is testament to the complexity of the three-dimensional flow pattern inside a feedwell. There is no one-fits-all solution, although some conditions can be manipulated to improve the flocculation process.

### 2.3.2 Throughput and dimensions

Throughput for a mineral processing plant often varies, either to meet the demand for higher production or in response to feed properties. Thickeners (and therefore feedwells) are often identified as bottlenecks in the quest for higher production, due to their limited ability to treat volumetric flow rates outside a narrow range. A thickener is actually able to treat more slurry if a higher underflow solids concentration can be produced within the same bed residence time. This can be achieved through the action of rakes or pickets that helps settled bed consolidation

(e.g. Dahlstrom et al. 1998; Loan and Arbuthnot 2010; Peloquin et al. 2002; Peloquin et al. 2005; Rudman et al. 2008; Sato et al. 1984; Schoenbrunn 2011; Suttill 1991).

However, the pressurised feed slurry must first pass through a feedwell to achieve a suitable extent of flocculation to give settling rates that sufficiently exceed the liquor rise rate in the body of the thickener. This represents the main bottleneck, as higher throughputs not only increase the liquor rise rate but also raise the mean shear rate in the feedwell, making it more difficult to grow aggregates with high settling rates. Considering that feedwell diameters in conventional gravity thickeners are about $1/10^{th}$ of the thickener diameter (Arbuthnot and Jagger 1999), it is clear that the key feature for higher throughput is to increase the effective capacity of the feedwell. There are various strategies that serve such a purpose, most often involving increasing the feedwell's depth or diameter, or both. Therefore, feedwells found in mineral processing plants vary considerably in their diameter and depth (Foster et al. 1996). In reality, there is a practical limitation of increasing the feedwell depth in many thickeners since there will often be rake structures lying underneath (Figure 2.18).

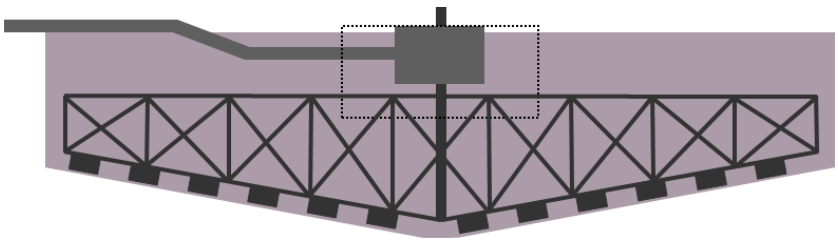

Figure 2.18. Schematic representation of a thickener with: smaller and larger feedwell (with dashed lines).

This should not be a restriction for the deep cone thickeners (DCT) with height-to-diameter ratios of at least 1:1 (Bagatto et al. 1992; Chandler 1986; Nunn 1998; Peloquin and Simard 2002), providing enough height for a "deep" feedwell. However, not all plants are equipped with this type of thickener, with thickener heights generally kept low to minimise capital costs. In most cases, increasing feedwell diameter seems to be more realistic than making it deeper (Figure 2.18). As a consequence, increasing feedwell diameter will reduce the strength of the fluid vortex inside the feedwell and result in a non-uniform solid volume fraction distribution (e.g. Echeverri et al. 2012) and sub-optimal mixing between flocculants

and particles. The inlet volumetric flow rate and feedwell internal structure (shelves and baffles) can be modified to offer solutions for the aforementioned problems.

### 2.3.3 Volumetric flow rate

A swirling flow pattern means that the solids are not evenly distributed throughout the feedwell volume, with concentrations highest near the feedwell inner walls and the feed entry. Ideally, the horizontal velocity component of the tangentially-fed slurry should be much higher than the gravitational settling of individual particles so that excessive settling of solid particles during the swirling motion does not happen.

A useful example of poor feedwell performance caused by slurry that immediately plunges can be seen in the in the historical case of an open tangential-fed primary thickener at the Worsley alumina refinery (Kahane et al. 2002; Kahane et al. 1997). By adopting simplified assumptions (initially excluding the particle and flocculant interaction), the authors used computational fluid dynamics (CFD) modelling to predict the solid volume fraction distribution in the feedwell. A typical example of the CFD output is depicted in Figure 2.19.

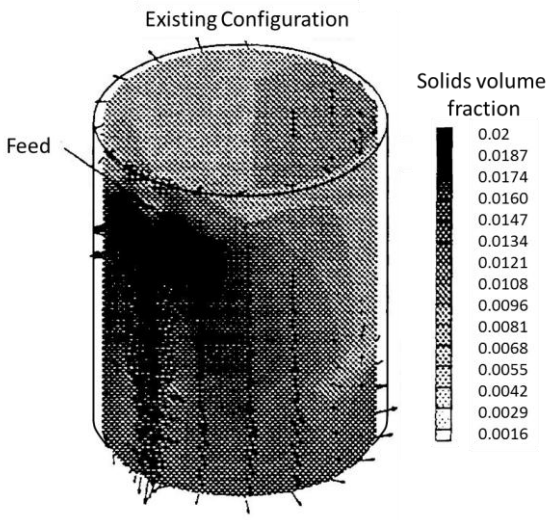


Figure 2.19. CFD modelling results showing the distribution of solids volume fraction in Worsley Alumina primary thickener. From Kahane et al. (1997).

The above figure explicitly shows that the higher solid volume fractions (marked by darker shades) are localised on the area around and vertically downward from the

slurry feed entry point, indicating that the solids only travelled a short distance from their entry point before they fell due to gravity. Regardless of the flocculant injection point, sub-optimal contact between flocculant and solid particles will result in the potential for a significant fraction of unadsorbed flocculant leaving the feedwell and poor overall flocculation.

Using CFD combined with population balance (PB) modelling of the flocculation process, Nguyen et al. (2006) demonstrated that controlling the volumetric flow rate is the simplest remedy for short-circuiting problems in a tangentially fed open feedwell. For a specific flocculation system, they predicted that increasing volumetric flow rate from 500 to 1000 to 2000 $m^3$ $h^{-1}$ would improve the solid residence time inside the feedwell, as well as the solids volume fraction distribution.

The mean shear rate across the volume of an open tangential feedwell was also considered too low (< 40 $s^{-1}$) to give optimum collision and aggregation rates when the volumetric flow rate was only 500 $m^3$ $h^{-1}$. From numerous CFD studies on a variety of feedwells, it is known that such shear rates should be in a moderate range (50-150 $s^{-1}$) to promote aggregate growth with minimum breakage (Nguyen et al. 2012), and ideally the mean shear rate should not exceed 100 $s^{-1}$ to give an optimum aggregate size (Nguyen 2013). The detrimental effect of too low a volumetric flow rate is exacerbated in feedwells with a high diameter-to-depth aspect ratio (e.g. Echeverri et al. 2012; Fawell et al. 2009b).

Table 2.2 shows how the flocculation conditions affected the predicted overall performance when the volumetric flow rate was increased in an open tangential feedwell (Nguyen et al. 2006). The results of improved solid and shear rate distributions were predicted to be a larger aggregate size (~290 μm from 2000 $m^3$ $h^{-1}$ vs. ~200 μm from 500 $m^3$ $h^{-1}$) and fewer fines < 10 μm that report to the overflow. In terms of flocculant adsorption, more than half of the flocculant was predicted to be unadsorbed in the poor mixing condition given by the 500 $m^3$ $h^{-1}$ volumetric flow rate and in contrast, almost complete adsorption can potentially be achieved after increasing the volumetric flow rate to 2000 $m^3$ $h^{-1}$.

Table 2.2. The effect of volumetric feed rate on the CFD predictions of calcite flocculation in an open tangential feedwell (Nguyen et al. 2006).

| | Volumetric feed rate ($m^3 h^{-1}$) | | |
|---|---|---|---|
| | 500 | 1000 | 2000 |
| Solid distribution | Poor | Moderate | Good |
| Natural dilution | No | Yes | Yes |
| Relative mean shear rate & shear rate distribution | Too low & non-uniform | Moderate & non-uniform | High enough & uniform |
| % flocculant unadsorbed | 60 | 14.7 | 0.2 |
| Aggregate size (μm) | ~200 | ~270 | ~290 |
| < 10 μm fraction | High | Moderate | Low |

Conditions:

- Thickener: 20 m diameter and 7 m height.
- Feedwell: 4 m diameter and 3 m height, with 0.50 m diameter feedpipe.
- Kinematic viscosity of liquor = $10^{-6}$ $m^2$ $s^{-1}$ and solid density = 2710 kg $m^{-3}$.
- PB system: calcite (50 kg $m^{-3}$). 30% anionic high molecular weight PAA (20 g $t^{-1}$).

Nguyen and co-workers later extended this study to emphasize that there is a certain volumetric feed rate limit, beyond which the benefit to flocculation is lost as aggregate breakage becomes dominant (Nguyen et al. 2012). In the same study, it was shown that feedwell design features such as a shelf can change the flow rate required for optimum flocculation. Also recognising the importance of volumetric flow rate, Triglavcanin (2008) proposed modification of the slurry feed inlet cross-sectional area to get a specific and constant flow rate entering a feedwell.

### 2.3.4 Feedwell internal structure

Internal shelves and baffles are feedwell interior features that may be added or changed to improve flocculation. The addition of an internal shelf below the slurry feed inlet has been claimed as a potential remedy for low dispersion and non-uniform solids distribution inside both open tangential and open split feedwells (Fawell et al. 2009b; Fitch and Lutz 1960; Kahane et al. 2002; Nguyen et al. 2012; Owen et al. 2009). Although not shown here, the difference in solids distribution predicted from CFD with and without an internal shelf for open tangential feedwells was significant (Owen et al. 2009). When the model was refined to allow PB simulation of the flocculant-induced aggregation of calcite (Figure 2.20), it clearly showed the improved aggregate size distribution as a result of better mixing and longer slurry

residence time that helps flocculant/solids contact (adsorption) and aggregate growth (Fawell et al. 2009b).

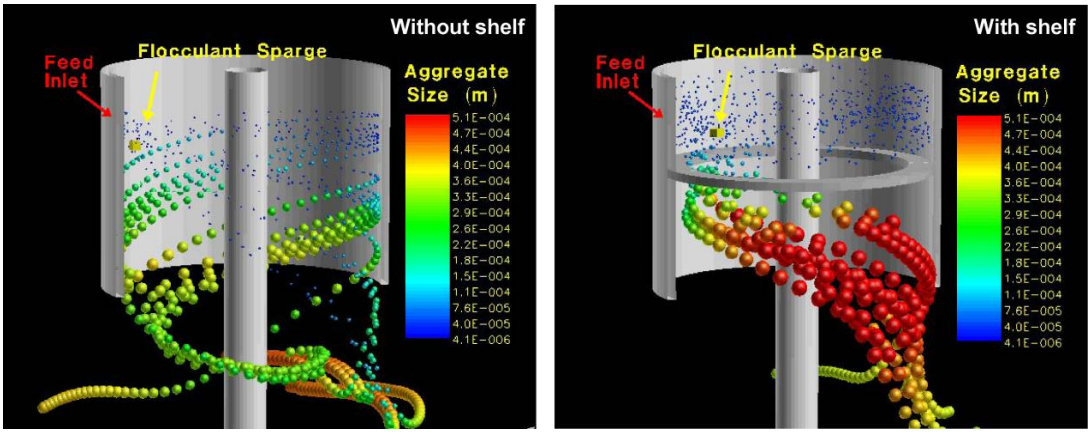


Figure 2.20. PB-CFD model of calcite flocculation in a feedwell with and without shelves. Volumetric flow rate 1000 $m^3 h^{-1}$ for 50 kg $m^{-3}$ calcite ($d_{4/3}$ 24 μm), feedwell 4×3 m, 0.5 m diam. single tangential inlet, feed, dosage 20 g $t^{-1}$. Reproduced from Fawell et al. (2009b).

Baffles positioning can also play an important role in flocculation within highly sheared feedwells. At the feed entrance, the slurry mimics a jet that breaks into vortices, creating local acceleration and high shear when it swirls down to the lower half of the feedwell (Foster et al. 1996; Triglavcanin 2008). That acceleration effect is more pronounced for feedwells with small diameter and limited depth (Echeverri et al. 2012). A high shear rate at a late stage in the flocculation process intensifies aggregate breakage and leads to smaller aggregates that settle slower in the sedimentation zone. The presence of multiple baffles on the inner feedwell wall can provide better momentum dissipation so that high shear late in flocculation can be avoided. Arbuthnot and Jagger (1999) also mentioned that baffles convert kinetic energy into high energy eddies that favours flocculant dispersion, making ideal positions for flocculant injection.

## *2.4 Bayer Process primary thickening*

As mentioned in the Introduction, flocculation during primary thickening in the Bayer process is very unique and challenging because of the highly caustic liquors at near boiling temperature. However, there are other reasons and constraints which set up specific requirements for optimum flocculation that must be understood.

Three major factors that influence Bayer process primary thickening are flocculant chemistry, residue mineralogy and solution composition. While the flocculant is an external factor which can be controlled to some extent, complex mineralogical and solution composition are internal factors that are far less controllable.

### 2.4.1 Flocculants

Flocculant use to assist solid-liquid separation in the Bayer process started with starch in the 1930s. The introduction of PAA to replace starch in the 1950s revolutionised bauxite residue thickening before HX PAM came to dominate that market from the early 1990s (Ballentine et al. 2011). Starch is a natural flocculant, while PAA and HX PAM are both synthetic flocculants whose main characteristics, such as molecular weight and anionicity, can be manipulated to some extent.

Starch was widely used because it contains amylose (molecular weight < $10^6$) and amylopectin ($10^7$-$10^8$) that belong to the general class of polysaccharides (Ballentine et al. 2011; Pearse 2003, 2005) and can assist aggregation due to their molecular weights. In caustic solution, phosphoric esters in the amylopectin are hydrolysed to amylose and phosphoric acid (Gardner and Ray 1939), increasing the concentration of amylose yet limiting the effective molecular weight to ~$10^6$.

Compared to the molecular weight of synthetic flocculants, typically up to $30\times10^6$ (Basu et al. 1986; Bublik et al. 1986; Connelly et al. 1986; Moody 1992; Pearse and Sartowski 1984), the relatively low molecular weight of starch gives limited polymer extension and minimal bridging capacity, explaining why slurry settling rates are only slightly improved. This makes the dosage requirements extremely high, once reported to reach 16 kg of starch per ton of bauxite (Chandler 1976).

At such high dosages, only a fraction of the starch will be adsorbed by the residue, with the rest remaining soluble. On the one hand, soluble amylose might further capture and aggregate particles in overflow streams about to escape from the primary thickener, but on the other hand, it contributes to an undesirably high organic

concentration in the Bayer liquor (Ballentine et al. 2011). Limited improvements in settling rate and the side effect of an increased organics liquor concentration make starch use uncommon now, although it may sometimes be looked as a co-dosing option with PAA, producing a reasonably high settling rate that is accompanied by excellent overflow clarity (Arslan et al. 2012).

PAA was the first synthetic polymer flocculant used for bauxite residue applications. Its molecular weight, which can be controlled during synthesis to be much higher than the amylose in starch, greatly improves its bridging capacity, allowing larger aggregates with faster settling rates to be formed. Yamada et al. (1980) reported that settling rates of various bauxite residue slurries were limited to 3 m $h^{-1}$ when flocculated with starch but reached up to 18 m $h^{-1}$ when PAA was used.

Although increasing PAA dosages will favour higher settling, this is not necessarily the case for overflow clarity (e.g. Ballentine et al. 2011; Spitzer et al. 1991). The correlation of supernatant solids (ppm) vs. PAA dosage for batch settling tests with an undisclosed bauxite residue sample is shown in Figure 2.21. Clearly, a faster settling rate does not automatically mean better fines capture. There is no implication that the same trend will be derived from a different bauxite residue sample, however, there is always a risk of poor overflow clarity when PAA is used. The low affinity of PAA limits extra binding that might occur between adsorbed polymer tails and iron oxide fines/micro-aggregates during settling (Kirwan 2009a).

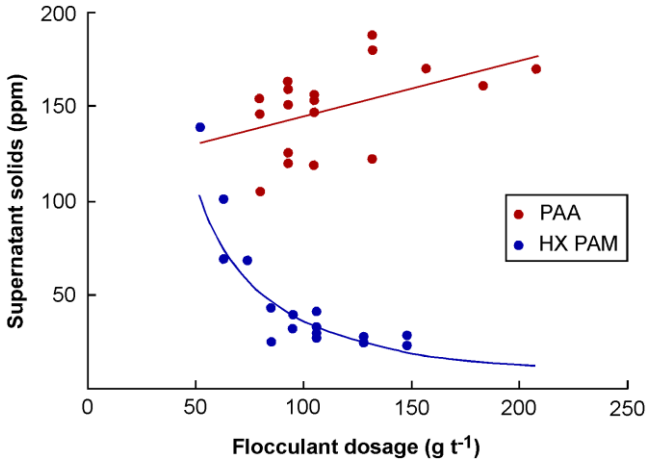


Figure 2.21. Supernatant solids derived from the utilisation of PAA and HX PAM. Adapted from Spitzer et al. (1991).

It was mentioned in Section 2.1.1 that the hydroxamate functionality adsorbs onto the surface of iron oxide through a chelating mechanism, a stronger (thermodynamic) interaction than that achieved by cation bridging with PAA products (Bremmell and Scales 2004; Chen et al. 2003; Rothenberg et al. 1989; Spitzer et al. 1991). The ultimate result from the former is a greater likelihood of flocculant binding to the iron oxide surface through multiple attachment points which then accordingly gives excellent overflow clarity of the post-flocculated slurries (Azevedo et al. 1995; Ballentine et al. 2011; Kirwan 2009a; Rothenberg et al. 1989; Ryles and Avotins 1996; Spitzer et al. 1991). Better overflow clarity from applying HX PAM is evident from Figure 2.21 (Spitzer et al. 1991), with the supernatant solids concentration dropping almost four-fold when the HX PAM dosage was increased, opposite the observation with PAA.

It is also of interest that the adsorption kinetics of PAA was reported to be slower compared to that of HX PAM (Perrier et al. 1999; Spitzer et al. 1991). In batch settling tests, this was indicated by the induction period from the moment PAA was added and mixed to the time the solid-liquid interface movement became even and clear to see. Gregory (1989) compared the $D_f$ of colloidal silica aggregates that were formed in slow and rapid aggregation and argued that the lower $D_f$ was found in the latter because particles do not have sufficient time to find a void at the inner part of aggregates. Kirwan (2009a) used this argument to explain that the slower adsorption kinetics with PAA is likely to result in more compact, denser aggregates that experience free settling. In contrast, aggregates formed by HX PAM will have lower density and be more likely to experience hindered settling, where its network acts as a bed trapping fines. Therefore, the utilisation of PAA typically corresponds to faster settling rate, while that of HX PAM gives better fines capture.

Using focused beam reflectance measurement (FBRM) to look at aggregate size decay as a function of shearing time, Kirwan (2009a) concluded that denser and more compact aggregates formed by PAA are more resistant to applied shear than those formed by HX PAM. However, Spitzer et al. (1991) varied the number of strokes during settling tests and found that after 100 strokes, the supernatant solids

concentration of the slurry flocculated by PAA was at least a magnitude higher than that flocculated by HX PAM (3700 vs. 300 mg $L^{-1}$). Apparently, the applied shear may substantially reduce the mean aggregate sizes formed with HX PAM, but the hydroxamate functionality is better able to hold the particles together within the aggregate as small settling fragments due to its high affinity for iron oxide surfaces.

Other than its major benefit of better overflow clarity, HX PAM was said to give numerous other advantages, including increased throughput, better overflow filterability (with filter by-pass possible), reduced scaling and reduced lime requirements (Avotins et al. 1999; Ballentine et al. 2011; Perrier et al. 1999; Rothenberg et al. 1989; Rousseaux et al. 2004; Ryles and Avotins 1996). From a primary thickener operational standpoint, the most important advantage could arguably be better underflow rheology (Perrier et al. 1999; Ryles and Avotins 1996; Spitzer and Avotins 1994). In general, flocculant addition to a thickener feed produces aggregate networks that substantially increase the settled bed yield stress. This limits the operating underflow density that can be achieved before the torque exceeds its tolerated limits. Slurry flocculated by HX PAM exhibits a lower yield stress at the same solids concentration (Perrier et al. 1999; Ryles and Avotins 1996; Spitzer and Avotins 1994), allowing the potential for a higher thickener underflow density. Interestingly, this tends to be in contradiction with operational experience, which may reflect the short residence times in primary thickeners, leading to the denser aggregates formed with PAA possibly giving higher solids in the underflow.

The relative impacts on underflow properties may be less important for conventional thickeners operating with low underflow density (20-30 wt/wt%), yet very crucial for modern high rate thickeners producing underflow with > 40 wt/wt%. Less scale formation on the thickener wall, base and raking system is also important as it reduces equipment downtime for scheduled maintenance (e.g. Avotins et al. 1999).

There are other groups of polymer developed specifically for application in bauxite residue solid/liquid separation. They also include functionalities other than acrylate, acrylamide or hydroxamate such as the salicylic functionality (Phillips 2003, 2004) or the silane functionality (Dai et al. 2008; 2010; Davis et al. 2010a, 2010b). However, benefitting from its ability to produce excellent overflow clarity, HX PAM

is still used as the main flocculant in primary thickeners, with PAA, salicylic and silane polymers playing a secondary role.

The most common operating strategy is to co-dose HX PAM with PAA, a compromise between the benefits of better overflow clarity brought by HX PAM and higher settling rates and denser aggregates given by PAA (Eckart et al. 2010; Filho et al. 2012; Kirwan 2009b; Perrier et al. 1999; Rousseaux et al. 2004). The lower cost of PAA also comes into this equation.

### 2.4.2 Mineralogy

Iron-bearing minerals are the major constituents of bauxite residue, with hematite and goethite being the major iron phases represented. In comparison to hematite, goethite is known for its inferior dewaterability. The main reason is the typical finer particle size of goethite solids, meaning the same unit mass of bauxite residue will contain more particles if the goethite content is higher. When the particle number was indirectly measured as specific surface area, Solymar et al. (1992) showed a perfectly linear relationship between the specific surface area of bauxite residue and its goethite content. The needle-like structure of goethite (Basu 1983; Schwertmann and Cornell 1991; Wu 2012) also suffers from the same problem as kaolin, where a plate-like structure produces aggregate structures with low $D_f$, requiring flocculation to be done at lower solids concentration (see Section 2.1.5).

The flocculation and handling of a suspension will be very much affected when it contains a higher number of particles within the same unit mass of solids. For example, a suspension of finer particles will display a higher effective volume fraction from surface chemistry effects and will lead to an increased viscosity. Roach et al. (2001) measured the viscosity of six different bauxite residue samples and found that the goethite-rich Jamaican bauxite samples have much lower solids concentration (380 g $L^{-1}$) compared with other samples (650 g $L^{-1}$) at an equivalent viscosity of 500 mPa. In combination with the greatly increased surface area, higher particle numbers will hinder flocculation and set-up requirements for high flocculant

dosages and solids dilution prior to flocculation (Basu 1983; Basu et al. 1986; Li and Rutherford 1996; Li 1998; 2001; Roach et al. 1989; Solymar et al. 1992).

Iron oxides have been often used as model substrates to investigate aspects of bauxite residue flocculation. It is of interest that within a comparable specific surface area window (2-17 $m^2$ $g^{-1}$), settling rates of flocculated hematite slurry in a synthetic Bayer liquor were not greatly diminished by a decrease in particle size from 1.5 to 0.5 μm, but those of flocculated goethite were (Basu 1983). Although that size range might not be a true representation of bauxite residue, the result hypothesized that physical properties (in this case, a finer particle size) cannot solely account for and be responsible for hindering settling on flocculation. In fact, at comparable sizes, chemical composition can be a differentiator, as in the case for aluminous goethite (aluminium substitution into the iron in goethite lattice) that was found to be much harder to flocculate than purely ferritic goethite (Li 2001).

Sodalite is the stable DSP phase found under the pre-desilication plant operating conditions (8-20 h, near boiling temperature), but it can transform to cancrinite at high digestion temperatures (~250°C) when calcium is present in the liquor or on prolonged reaction (Croker et al. 2008; Radomirovic et al. 2013; Whittington et al. 1998; Xu et al. 2009; 2010; Zheng et al. 1997). Sodalite and cancrinite are different in terms of their structure although both form cage structures that are made up of -Al-O-Si-O- rings (Hassan 1982; Lowe 2007; Smith 2009; Zheng et al. 1997). The structures of sodalite and cancrinite are presented in Figure 2.22a and b, respectively.

(a) (b)

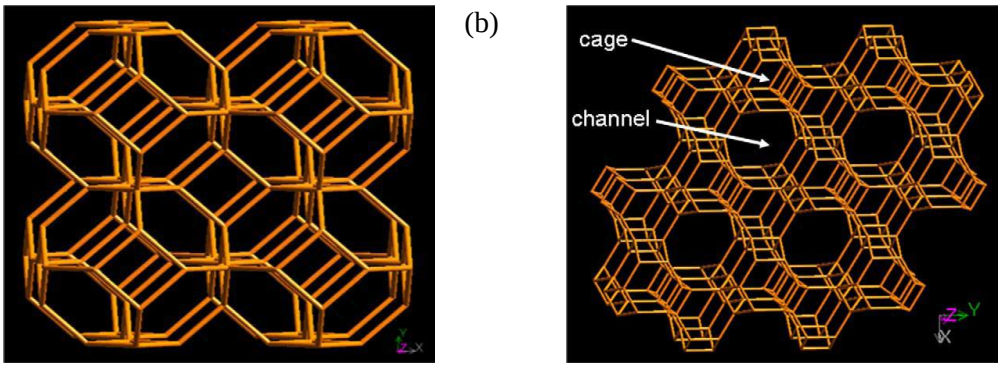


Figure 2.22. Cage structure of: (a) sodalite and (b) cancrinite. Reproduced from Smith (2009).

In bauxite residue thickening, the existence of both sodalite and cancrinite is known to result in poor dewatering characteristics, such as low settling rate, high supernatant solids and low underflow density, even at high flocculant dosages (Dai et al. 2008; Davis et al. 2010a; Liu et al. 1994; Roach et al. 1989; Rousseaux et al. 2004). Considering the lower specific gravity of sodalite relative to iron-bearing minerals (natural sodalite = 2.2 < goethite = 3.3-4.3 < hematite = 4.9-5.3), lower settling rates and underflow solids concentrations for DSP-containing bauxite residue are then expected, particularly at higher feed solids concentrations. However, high supernatant solids largely independent of flocculant dosage indicate that the problems go beyond physical properties.

In contrast to iron oxide model slurries, for which some flocculation aspects have been studied in detail, the mode and extent of flocculant adsorption onto DSP have never been investigated; nor have the effects of flocculant chemistry (i.e. PAA copolymer vs. HX PAM terpolymer), solution composition and shear on the flocculation of DSP-containing residues. To date, the only major findings are:

(i) high digestion temperatures improve the settling rate of flocculated bauxite residue that originates from high silica bauxite (Liu et al. 1994). It is still unclear whether this is due to the conversion of sodalite to cancrinite, as the latter was claimed to have a finer particle size distribution (Zheng et al. 1997) that is theoretically undesirable for flocculation,

(ii) higher kaolin content in pre-desilication produced finer (< 1 μm) DSP particles (Davis et al. 2010a),

(iii) co-dosing of HX PAM with a small amount of PAA increased primary thickener settling rates and reduced overall flocculant consumption, although HX PAM was still irreplaceable in maintaining overflow clarity (Rousseaux et al. 2004),

(iv) silane polymer added prior to PAA or HX PAM flocculants decreased the supernatant solids without a consistent trend seen in the settling rates of DSP-containing residues (Dai et al. 2010; Davis et al. 2010a).

Such poor knowledge of these processes hampers attempts to achieve the effective flocculation of DSP-containing residue and provides the main motivation of this

thesis, particularly given the on-going trend for processing high silica bauxite (Smith 2009).

### 2.4.3 Solution composition

The liquor entering the Bayer process solid/liquid separation stage is quite complex and differs from plant to plant for a variety of reasons, such as the caustic concentration and process temperature used. For example, the typical caustic (C) concentration used is in a range between 140-230 g $L^{-1}$ $Na_2CO_3$ (Jones et al. 1998a; Pearse and Sartowski 1984; The and Bush 1987). While some refineries operate at a higher caustic concentration, that rarely exceeds 300 g $L^{-1}$ $Na_2CO_3$ as it results in sub-optimal precipitation yield (Den Hond et al. 2007). Note that Bayer process uses specific liquor terminology explained separately (see Abbreviations, Nomenclature and Liquor Terminology).

Caustic concentration will then dictate the overall solution chemistry; this is the case for the alumina (A) concentration, with the equilibrium A/C ratio in Bayer liquor known to be a function of both caustic concentration and temperature. At 150°C and 250 g $L^{-1}$ caustic, the equilibrium A/C ratio equals 0.76 (Den Hond et al. 2007) or in other words, the alumina concentration entering the primary thickener will be ~190 g $L^{-1}$. This number will change if a lower or higher caustic concentration is used or if higher temperature digestion is required to dissolve boehmitic bauxite.

A similar principle applies to the soluble silica concentration, for which the post-desilication concentration obeys a function of temperature, caustic and alumina concentrations (Barnes et al. 1999a; Cresswell 1983; Jamialahmadi and Müller-Steinhagen 1998; Oku and Yamada 1971; Smith et al. 2002). Feed mineralogy also contributes to the increasing concentration of other soluble species such as organics (Kim and Lee 2003; Power et al. 2011; Power and Tichbon 1990; Yamada et al. 1973). All the above-mentioned combine to make Bayer liquor composition both complex and a critical factor to process efficiency.

Among the soluble species that have been investigated for their effect on bauxite residue flocculation are:

- caustic and alumina,
- inorganic anions (carbonate, sulphate, chloride and phosphate),
- multivalent cations (calcium and silicon), and
- organic anions (e.g. oxalate, humate).

The caustic concentration in bauxite residue solid/liquid separation peaks in the primarily thickener (generally C $\geq$ 200 g $L^{-1}$ $Na_2CO_3$), then decreases down the counter-current washing train. High caustic in synthetic liquor was found to decrease settling rates of model hematite slurries and increase the resultant supernatant solids, although this effect levelled off for C > 250 g $L^{-1}$ $Na_2CO_3$ (Jones et al. 1998b).

During flocculation tests with model hematite slurries, alumina supersaturation levels up to a maximum A/C ratio of 0.7 (C = 100 g $L^{-1}$ $Na_2CO_3$, S = 110 g $L^{-1}$ $Na_2CO_3$) gave no significant differences in the resultant settling rate or supernatant solids (Jones 1998). However, it should be kept in mind that there is no clear implication that the same observations will be seen at higher C concentrations or for different substrate mineralogies.

The effect of carbonate ions (originating from organic impurities in the raw materials and/or transferred from carbon dioxide-containing air) was far clearer, with Jones et al. (1998b) finding higher carbonate concentrations gave lower settling rates and higher supernatant solids for flocculated model hematite slurries. When flocculant adsorption was quantified by surface excess (mass of flocculant adsorbed per unit area of adsorbent), the same authors showed that the surface excess was lower in the presence of carbonate ions. It was then hypothesized that carbonate ions were adsorbed at the surfaces of hematite and thereby reduced the proportion of active sites for flocculant adsorption. They were able to experimentally confirm a lower flocculant adsorption density in the presence of carbonate ions.

It is under these exact circumstances when calcium addition will be most beneficial, precipitating soluble carbonate to form calcite (Equation 2.4 in Section 2.1.1). The

same mechanism of preferential adsorption reducing the extent of flocculant adsorption was also shown to apply for the presence of dissolved organic species, such as oxalate and humate (Hunter et al. 1991) and soluble silica (Jones 1998).

Sulphate and chloride are also major inorganic ions in Bayer liquor, but unlike carbonate, concentrations of up to 50 g $L^{-1}$ sulphate and 40 g $L^{-1}$ chloride did not change the adsorption density of flocculant and the resultant dewatering of model hematite slurries (Jones 1998). Similarly, phosphate at up to 1.2 g $L^{-1}$ (representing its typical concentration in Bayer liquor) had no effect on the settling rate, turbidity and flocculant adsorption density for flocculated hematite slurries, because it is not itself adsorbed on the iron oxide surface.

### 2.4.4 Specific requirements of Bayer Process primary thickening

In a 250 g $L^{-1}$ caustic liquor, the equilibrium A/C ratio drops from 0.76 to 0.53 when the temperature falls from 150 to 100°C (Den Hond et al. 2007) with a lower equilibrium A/C ratio expected if the temperature keeps decreasing. Digesters in a Bayer refinery dissolve aluminium-bearing minerals (gibbsite and/or boehmite) at 150-250°C and produce a slurry with an A/C ratio between 0.7-0.8. This slurry must be cooled to at least ~100°C prior to its release to atmospheric pressure to prevent excessive evaporation. Thermodynamically, alumina reversion (Equation 2.15) will naturally happen to the cooled-off slurry because its A/C ratio is higher than the equilibrium value, although the kinetics of this reaction might not be significant at ~100°C. Therefore, in the primary thickener, reasonably fast settling rates in the range 12-30 m $h^{-1}$ (Rousseaux et al. 2004) are sought to give effective liquor clarification before reversion progresses.

$$NaAl(OH)_4(aq) = Al(OH)_3(s) + NaOH(aq) \qquad 2.15$$

In the primary thickening of bauxite residue, while the majority of fines are separated as underflow, a tiny fraction of the total solids mass poisons the overflow. These fines are then captured by filtration, producing clean pregnant liquor for product precipitation. This action is known as security filtration or liquor polishing. In this

stage, pressure filters are used with a differential pressure between 1-4 bar as a driving force for filtration, decreasing the solids concentration in the liquor from up to 300 mg $L^{-1}$ to below 20 mg $L^{-1}$ while maintaining a specific liquor flow rate (per square metre of filter area) of between 0.8-2 $m^3$ $h^{-1}$ (Bott et al. 2008).

Filter aid is sometimes added during filtration operations to act as a liquor permeable coat that captures the fines and prevents cloth blinding (Svarovsky 2000). For security filtration, tricalcium aluminate (TCA, $3CaO.Al_2O_3.6H_2O$) is chosen as the filter aid because it can be produced in-house through the reactions of quicklime or slaked lime with a liquor containing sodium aluminate, such as spent liquor (e.g. Andermann and Pollet 2003; Barham et al. 2000; Malito 1996; Mugnier et al. 2001; Rousseaux and Ferland 2009).

The filtration rate $\left(\frac{dV}{dt}\right)$ is governed by Darcy's Law of filtration under constant pressure (e.g. Dickey and Bryden 1946 ; Dickey 1961; Sparks 2012; Suttle 1969; Svarovsky 2000):

$$\frac{dt}{dV} = \frac{\alpha c \mu V}{A^2 \Delta P} + \frac{\mu R_m}{A \Delta P} \qquad 2.16$$

where $t$ is the filtration time (s), $V$ is filtrate volume ($m^3$), $\alpha$ is filter cake resistance (m $kg^{-1}$), $c$ is total suspended solids concentration (kg $m^{-3}$), $A$ is filtration area ($m^2$), $\Delta P$ is differential pressure (Pa) and $R_m$ is the filter medium resistance ($m^{-1}$). According to Equation 2.16, an increase in the overflow solids concentration will slow down the filtration. Hence, producing overflow with a low solids concentration is a target of equal importance to fast settling rates, explaining the dominance of HX PAM flocculants in primary thickening.

The other problem with providing excellent overflow clarity is that the optimum shear for aggregate growth is not necessarily the same as the optimum shear for fines capture (e.g. Farrow and Swift 1996a; Gagnon et al. 2001). By using a flow-through Couette shearing device connected to a settling column which can be isolated for settling measurements (also known as Shear Vessel), Gagnon et al. (2001) found that

increasing the shear intensity can decrease the turbidity of a flocculated bauxite residue samples. However, such action also breaks aggregates into smaller fragments that settle slower (Figure 2.23).

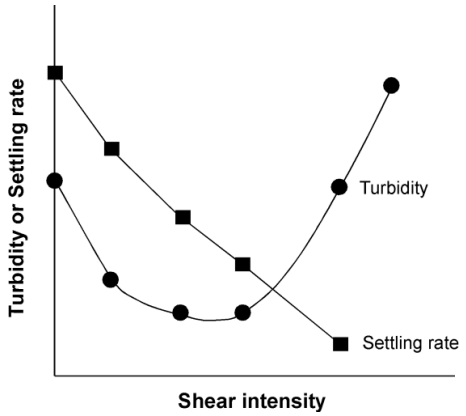


Figure 2.23. The effect of shear on settling rate and turbidity for flocculated bauxite residue. Adapted from Gagnon et al. (2001).

A flocculant that generates excellent overflow clarity (such as HX PAM) is therefore always helpful in this situation, otherwise a higher shear rate is required during flocculation and settling rate has to be to some extent sacrificed when producing overflow liquor with better clarity (faster filtration rate according to Equation 2.16).

In the security filtration stage, in addition to all the process parameters in Equation 2.16, it is known that the presence of residual flocculant also affects filtration efficiency (Malito 1996; Owen et al. 1991; Rousseaux and Ferland 2009). The most general rule-of-thumb is that the flocculant will hinder the filtration process, although a very low residual flocculant concentration (50 ppb) can give an accelerating effect (Malito 1996) and the extent of hindrance at higher concentrations is dependent upon the flocculant chemistry (Rousseaux and Ferland 2009). Although never stated within the open access literature, residual flocculant is believed to blind the pores in filter cloth.

The effect of residual flocculant concentration on filtration time as a function of filtrate weight and filtration rate as a function of time can be seen in Figure 2.24a and b, respectively, including the benefit of a very low flocculant concentration. The filtration rate drops as cake formation progresses and this reflects what actually

happens under real plant conditions. When the filtration rate no longer meets the production rate demand, the deposited cake must be washed from the filter cloth.

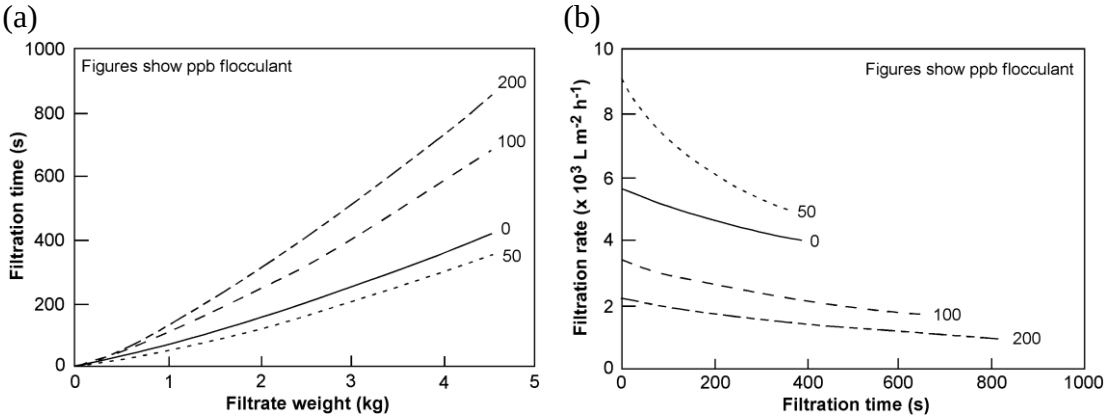


Figure 2.24. The effect of residual flocculant concentration on the: (a) filtration time as a function of filtrate weight and (b) filtration rate as a function of filtration time. PAA flocculant, 1.05 g $L^{-1}$ solids concentration. Adapted from Malito (1996).

Although a very low level of residual flocculant may be beneficial in the security filtration stage, in practical terms this circumstance may not be met, as only a small increase beyond this level sees a sharp decline in filtration performance. Poor hydrodynamic conditions are common in feedwells, which create poor flocculant dispersion regimes, reduced contact between flocculant and solid particles and accordingly the potential for a higher proportion of unadsorbed flocculant (see Section 2.1.6. and 2.3.3). The key to avoiding this undesirable condition is high dilution of the flocculant (to 0.005% or less) to enhance its dispersion, mixing and adsorption (Fawell et al. 2009a; 2009b; Heath and Arbuthnot 2013; Owen et al. 2008)

In bauxite residue thickening, flocculant is generally in the form of powder or emulsion. Unlike powder flocculants that contain ~100% active polymer, an emulsion flocculant has its active component dissolved in very fine water droplets which are dispersed in oil (Cytec 2011). Prior to use, powder flocculant has to be first made-up to 0.5-1 wt/wt% solution (Hurd et al. 1994). In contrast, emulsion flocculant has to be first "inverted" to a 1.5-4 wt/wt% solution, with this concentration calculated on the basis of product rather than active polymer (Hurd et al. 1994; Murray and Millington 2002; Rousseaux et al. 2004). The inversion is achieved by applying a high shear intensity over a short period of time, releasing the

active component that was originally "trapped" or dispersed in the emulsion (Cytec 2011). HX PAM is always provided in the form of an emulsion as incorporating hydroxamate functionality onto the PAA backbone must be done when polymer is in the liquid form (Ballentine et al. 2011), while PAA can be in powder or emulsion form (Hurd et al. 1994; Murray and Millington 2002).

In reality, a 4 wt/wt% emulsion flocculant solution may contain the same amount of active component as a 1 wt/wt% powder flocculant solution, since there is less active component in every unit mass of an emulsion product. These "stock" solutions have to be further diluted prior to introduction to the flocculation system in order to decrease its viscosity and improve its mixing through the solids.

To avoid confusion, the liquor used in the initial preparation of flocculant stock solutions is defined as "make-up" liquor, whereas that used for further dilution is defined as "dilution" liquor. It was once considered that the make-up and dilution liquors in Bayer applications could be anything, including water for make-up (Rousseaux et al. 2004) and primary thickener overflow for dilution liquor (Hurd et al. 1994), although other studies latter revealed that they were not the best options.

Cytec Industries, the manufacturer of HX PAM flocculants, specify that 0.5-1 M NaOH (27-53 g $L^{-1}$ $Na_2CO_3$) is used for make-up (Cytec 2011), in agreement with the observation reported by Ferland et al. (2003) where alumina content in the make-up liquor can reduce the specific viscosity (activity) of the flocculant solution.

Perrier et al. (1999) tested a range of alternatives for dilution liquor, including:

(i) condensate with pH ~10 (liquid recovered from the condensation of vapour exiting liquor cooling process),
(ii) 1st washer overflow (94 g $L^{-1}$ $Na_2CO_3$),
(iii) filtered pregnant liquor and
(iv) condensate + caustic (40 g $L^{-1}$ $Na_2CO_3$)

and found that the 1st washer overflow gave diluted flocculant of highest activity.

Linking the above findings to the precipitation process, diluting flocculant to a super-dilute condition (≤ 0.005%) with liquor having a low alumina content (such as 1st washer overflow) will slightly decrease the alumina supersaturation level and potentially the product growth rate during the precipitation (Den Hond et al. 2007). This paradoxically creates a constraint of not diluting the flocculant to the level that favours optimal dispersion and mixing.

Underflow density is also one of the main concerns in the primary thickening of bauxite residue. A low underflow density indicates a high proportion of liquor in the consolidated bed and means a greater burden of caustic and soda (S) in the counter-current washing stages. Table 2.3 compares the mass of soda that will be deported to the 1st washer from different primary thickener underflow densities. It implies that there will be 20% less soda transferred to the 1st washer if the underflow density in the primary thickener can be increased from 30 to 45 wt/wt% solids.

Table 2.3. The effect of underflow density on the soda content of bauxite residue.

| | Unit | underflow density (wt/wt% solids) | | | |
|---|---|---|---|---|---|
| | | 30 | 35 | 40 | 45 |
| mass of residue | (g) | 300 | 350 | 400 | 450 |
| mass of liquor | (g) | 700 | 650 | 600 | 550 |
| vol. of liquor | (mL) | 583 | 542 | 500 | 458 |
| C | (g) | 117 | 108 | 100 | 92 |
| S | (g) | 137 | 127 | 118 | 108 |
| $S / S_{30}$ ratio | - | 1 | 0.93 | 0.86 | 0.79 |

Assumptions: 1 kg of bauxite residue (as received basis), liquor density = 1.2 kg $m^{-3}$, C = 200 g $L^{-1}$ $Na_2CO_3$, C/S ratio = 0.85.

Achieving 45 wt/wt% solids is not unrealistic, as it is the typical underflow density target in the modern high-rate thickener (Arbuthnot and Jagger 1992; Jagger and Arbuthnot 1991; Laros and Baczek 2009; Vidyasagar 1996) except for the case of Jamaican bauxite residue, where the existence of very fine goethite particles limits underflow densities to ≤ 35 wt/wt % solids (Roach et al. 2001). From mathematical modelling, it is known that decreasing the size of mono-sized spheres from 10 to 1 μm increases the packing porosity from 0.58 to 0.82 and this is exacerbated if the

particle shape is not perfectly spherical – both statements clearly show the problem associated with handling goethite-rich bauxite residue (Roach et al. 2001).

While the role of flocculant is probably less significant for the underflow than in the feedwell, combining PAA that gives higher density aggregates and HX PAM that gives better rheological property can potentially give further increments in underflow density (Eckart et al. 2010; Rousseaux et al. 2004).

Scale that builds up over a long period of time also indirectly makes optimum flocculation even more difficult to achieve. The propensity of scaling stipulates that reduced surface areas of stainless steel structures are used and immersed in the liquor (Chandler 1986; Emmett 1986; Emmett and Klepper 1991; Laros and Baczek 2009), and a similar expectation also applies for feedwell design, particularly in the primary thickening process that treats pregnant liquor. Feedwells in a primary thickener should therefore have minimum internal and external structural features. As a consequence, novel feedwell designs, such as the Outotec Vane feedwell that is claimed to provide better performance through its more complex internal design (Heath and Triglavcanin 2010; Henriksson et al. 2011; Loan et al. 2009; Triglavcanin 2008) are not favoured.

In summary, optimum flocculation in primary thickening of bauxite residue seeks to achieve a balance of: (i) reasonably fast settling rates, (ii) overflow clarity of a level that is acceptable for subsequent liquor filtration and (iii) high underflow density that minimises the deportment of liquor to the washing stages. Such performance must be derived under constraints that prohibit the dilution of flocculant solutions to an ideal level and prefers feedwell designs with minimum interior and exterior design features, even though they may not give the best hydrodynamics and mixing conditions. These multiple aspects makes primary thickening as practiced in the Bayer process very distinctive and much more difficult to control than most other thickening processes.

## *2.5 Monitoring flocculation by Focused Beam Reflectance Measurement (FBRM)*

As previously mentioned in Section 2.1.2, aggregate properties such as size and structure (density/porosity, shape) dictate the settling rate and extend through to the settled bed. The challenge in any particle aggregation study is to obtain reliable characterization under relevant conditions.

### 2.5.1 Advantage of FBRM

Aggregates, whether formed by charge-based coagulation or polymer-bridging flocculation, exhibit fragile structures of low effective density, and are highly sensitive to any handling or treatment applied post-formation. For "real" systems in which the particles are mostly micron-sized and the aggregates have the potential to approach millimeters, reaction times will be measured in seconds, shear effects will be heightened and settling also becomes a consideration.

Direct characterisation of aggregate structure (typically through $D_f$) is complex and time-consuming. Image analysis techniques, sometimes combined with settling rate measurements of individual aggregates (e.g. Farrow and Warren 1993; Gagnon et al. 2003), require sampling and very high dilution that alters structures. In practice, it is often sufficient to indirectly infer relative aggregate structural behaviour from the variation in flocculation response (aggregate size, settling rate) at different solids concentrations.

A summary of common methods available for monitoring particle/aggregate size is represented in Figure 2.25, together with their expected size ranges and solids loading that can be tolerated for direct measurement. It must be acknowledged that this last point is somewhat subjective, as the practical solids loadings will often vary with particle size. These methods are also distinguished by whether they can be applied *in-situ* or *ex-situ*, the latter implying slurry has to be sampled and possibly diluted for measurement. The essential criteria in this discussion have to include applicability to monitor flocculation at practical solids concentrations for mineral processing (as opposed to low solids water treatment).

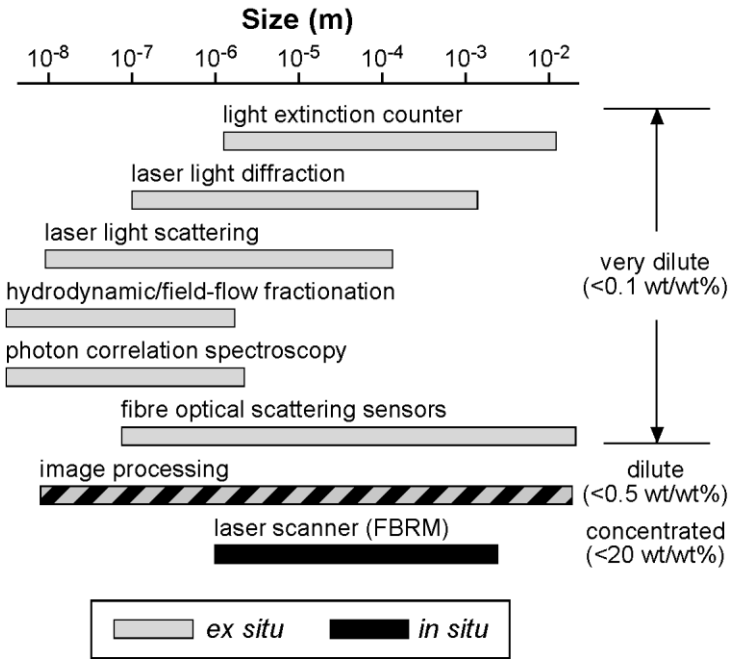


Figure 2.25. Optical methods for measuring geometry of particles in suspensions. Adapted from Heffels et al. (1998).

The majority of techniques available for the sizing of particle systems fail when applied to polymer-flocculated aggregates in real-time studies. While commercial particle sizing instruments that utilize laser diffraction or low angle light scattering have proven useful to characterize $D_f$ for coagulated sub-micron latexes and other similar materials (Spicer et al. 1998), dilution is still necessary for the solids concentrations considered in most mineral systems and the measurements cells (even in a flow-through configuration) are likely to impose some shear to the fragile aggregates. The distributions that are obtained may also be of questionable value, given that they are unlikely to capture the often transitory real-time peaks in aggregate size, or may even represent artifacts of the sample handing (e.g. further growth on dilution).

Optical/microscopic techniques cannot be applied during the aggregation process, and either require very high dilution or immobilization of the aggregates being studied. Aggregation monitoring by turbidity fluctuations was not included in Figure 2.25 as it only offers a "flocculation index" as a relative indication of aggregation rather than a size, but has had some success for qualitative comparisons in water

treatment applications (Gregory and Nelson 1986). However, this is again an instrument better suited to lower solids concentrations.

In the early 1990's a new technique termed scanning laser microscopy became available for monitoring particle and aggregate properties with the potential to be directly applied to suspensions across a wider concentration range. It is now better known as FBRM and it has been successfully used to study a variety of aspects of the flocculation process.

### 2.5.2 Principles of FBRM

In FBRM, a rotating lens provides a highly focused laser beam at the external surface of a sapphire window that scans in a circular path at a fixed velocity (Figure 2.26a). When the beam meets the suspended solids at the focal plane (Figure 2.26b), backscattered light is generated and the measured time lag between laser emission and reflection is multiplied by the velocity of the scanning laser to calculate a "chord" length. A chord for any geometric shape may be defined as the line segment whose endpoints both lie on the external surface of that shape. Thousands of chords can be measured during a single measurement duration (as short as 2 s), generating a chord length distribution. Measurements occur in dilute or concentrated flowing slurry with no sampling or sample preparation necessary.

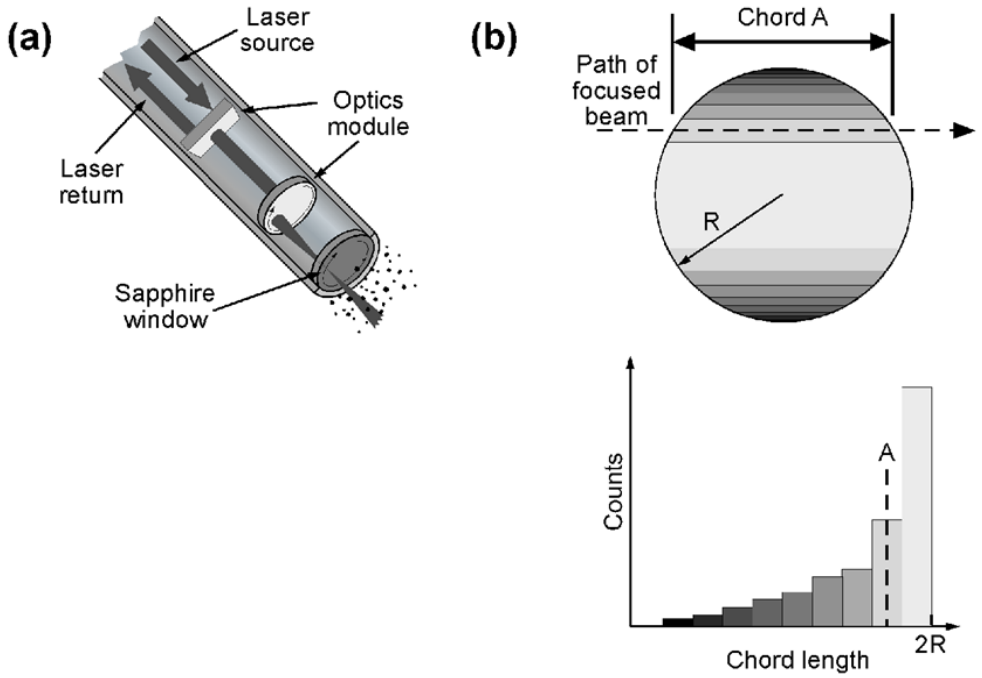


Figure 2.26. Schematic representations of (a) FBRM probe and particle sensing, and (b) generation of a chord length distribution for mono-dispersed spherical particles.

Figure 2.26b also demonstrates schematically how the chord distribution would appear for mono-dispersed spherical particles. The largest chord length is near the diameter (2R in the figure), where there is a high probability of chords being measured, but shorter chord lengths will also be represented in the distribution.

### 2.5.3 Refinement of the FBRM approach

Despite the clear advantages of FBRM in many applications, there have also been limitations that cannot be ignored and, in some situations, may raise concerns as to the true relevance of the results. Greaves et al. (2008) observed that for bimodal systems, large particles will often diminish the ability of FBRM to quantitatively measure small particles; certainly this is the case for volume-weighted chord length distributions, although the unweighted distributions should still provide sensitivity to the fines. Vay et al. (2012) determined that the FBRM response is influenced by the surface characteristics of the tested materials (e.g. reflectivity, translucence), an issue when studying emulsions, but not really a concern for flocculation.

Heath et al. (2002) noted the non-linear response to increases in solids concentration, but potentially more significant was the tendency to oversize solids in the 1 to 10 µm

range, a point also identified by others which can typically be attributed to the addition of the beam's width to the chord length (Vay et al. 2012). Again, in flocculation studies, this does not impact upon the measurement of the volume weighted distributions used as an indication of the extent of flocculation. Such distributions are largely unaffected when flocculation is inefficient, whereas the unweighted distributions should show the impact of residual particles that are not captured within aggregates. This is certainly the case in many applications, but it is likely that the poor discrimination of sizes at the lower end of the distribution diminishes the sensitivity to such inefficiencies.

The G-series FBRM systems (released 2012) were developed to address some of these perceived problems. Of the improvements over the previous generation probes, the most significant were (a) higher resolution/greater accuracy in characterising fine particles and bimodal distributions, and (b) higher sensitivity in concentrated particle systems. Figure 2.27 seeks to represent in simple terms how such improvements have been achieved, using information from the manufacturer (Smith 2013).

When backscattered intensity is measured as a reflection from the suspended solids, the intensity will vary, with surface roughness one factor that causes localised noise. Previous generation FBRM instruments applied a fixed intensity threshold above which the chord length will only be measured, however, when the localised noise from surface roughness is near the threshold limit (Figure 2.27a, particle 3), some of the intensity will fall below this limit and register as the occurrence of several distinct chord lengths, when in reality there was only one particle. The new G-series instruments instead use enhanced edge detection to determine the measured chords, reducing the influence of surface roughness. Another improvement in the new generation instruments is related to the consistency of the counts generated at higher solids loadings.

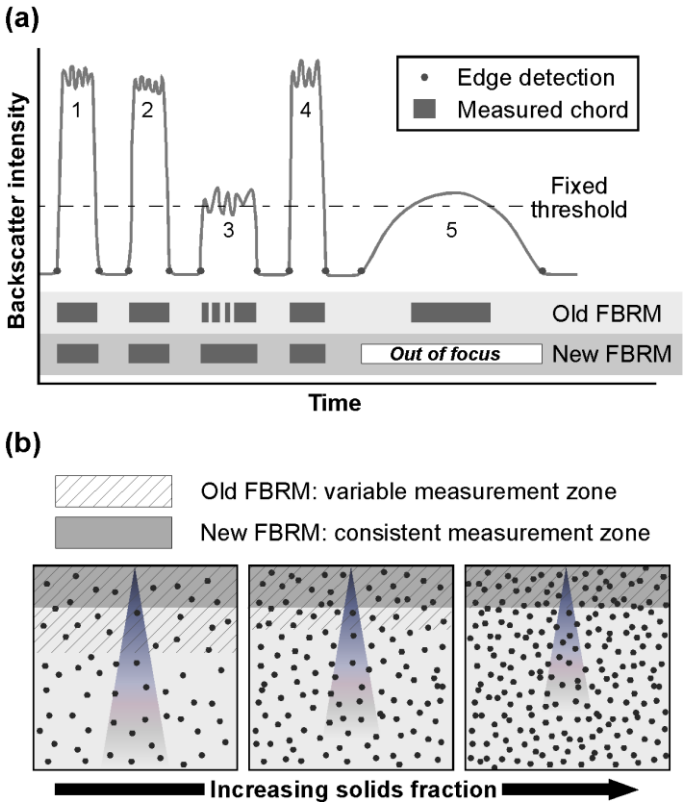


Figure 2.27. Schematic representations of (a) FBRM chord detection methods and (b) the impact of solids concentration on measurement zones. Adapted from Smith (2013).

As illustrated in Figure 2.27b, an increasingly dense population of particles obscures the laser intensity and in the older generation FBRM instruments this resulted in a reduction in the measurement zone (represented by the hatching), which contributed to the non-linear response of counts to solids concentration. For FBRM as achieved with the G-series instruments, the measurement zone is fixed (shading) and the non-linearity of the solids response is greatly reduced.

The first image in Figure 2.27b shows that at low solids concentrations, the laser beam becomes quite diffuse at the extremes of the measurement zone, and for highly reflective particles this could lead to chord length over-estimation by older generation FBRM instruments if the fixed threshold was exceeded; e.g. the measured chord length for particle 5 in Figure 2.27a would be higher than the true value. In this case, edge detection with the G-series would lead to even greater over-estimation, but combined with slope rejection, this chord is now rejected as out of focus. All these factors contribute to the potential for greater resolution and accuracy, which will be attested in this thesis.

# 3 Thesis objective

There have been numerous fundamental studies of flocculation in Bayer primary thickening that were performed on either bauxite residue samples or iron oxide model substrates. These have provided insights on (i) the flocculant adsorption mechanism (Bronswijk et al. 2006; Fawell et al. 2002; Jones et al. 1998c; Kirwan et al. 2004), (ii) the effect of shear on flocculation kinetics and breakage (Gagnon et al. 2001; 2002; Kirwan 2009a; Spitzer et al. 1991), (iii) the flocculated aggregate characteristics, including size and density distribution (Gagnon et al. 2003; Kirwan 2009b; Phillips 1999), and (iv) the effect of flocculant functionality (Arslan et al. 2012; Eckart et al. 2010; Phillips 2003; Phillips and O'Brien 2006; Rothenberg et al. 1989).

However, few considered the effect of DSP and those that did concentrated on whether commercial flocculants new to the market improved the settling rate and supernatant solids in cylinder settling tests (Dai et al. 2008; 2010; Davis et al. 2010a, 2010b). Although improvements were evident, such information does not necessarily reveal the mechanism by which this was achieved. Critically, such effects may not be seen in the more complex conditions that mimic the real plant situations.

This study therefore aims to fundamentally understand the effect of DSP on bauxite residue flocculation and sedimentation. Realising the importance of aggregate characteristics, especially size as an indication of extent of flocculation, the first priority in this study was to understand and assess the ability of FBRM in measuring aggregate size *in-situ* while providing extra information about fines capture through the number of counts measured within a specific size window (e.g. 0-20 μm). Chapter 4 discusses these aspects in more details as the performance of the new generation G series FBRM was contrasted to that of the older generation M series with the same flocculation system

The ‘genesis’ of DSP itself needs to be first well-understood, especially how this can potentially impact on subsequent flocculation processes. For instance, so far there is no definitive information as to whether DSP grows at the surface of residue solids or

if it instead tends to precipitate as a distinct phase. The mode of flocculant adsorption onto DSP is also not known. DSP that (at least partially) grows and covers the residue (or model substrate) surface may result in fewer active sites for the attachment of flocculant functionalities that favour such surfaces. Alternatively, if DSP precipitates as a distinct phase, it will increase the number of particles and thereby the solid volume fraction. This also hinders flocculation, but in a different manner from DSP that covers the surface. Chapter 5 presents the results from: (i) settling tests, (ii) zeta potential measurements, (iii) pre-desilication experiments and (iv) scanning electron microscopy (SEM) applied on model iron oxide and DSP mixtures that were prepared differently (with and without iron oxide seed particles), elucidating the 'genesis' of DSP.

Most studies that use DSP-containing residues only focus on very specific conditions. For example, residue samples produced in a refinery are often used (e.g. Dai et al. 2008; Rousseaux et al. 2004), however, the concentration of DSP per unit mass of residue in such cases is not under proper control and a detailed study on the effect of increasing/decreasing DSP concentration becomes problematic. Davis et al. (2010a, 2010b) mixed residue derived from bauxite digestion with pre-made DSP to control the concentration (wt/wt%) of DSP in the mixture. This again does not represent the actual conditions for full-scale pre-desilication, which is performed in the presence of other mineral phases within bauxite. Moreover, their tests were only done at one particular solids concentration (45 g $L^{-1}$ solid) which is insufficient for supplying mechanistic information.

In Chapter 6, model hematite was mixed with high purity kaolin in different mass ratios and digested under conditions close to those in the plant situation, producing a range of synthetic residue slurries with different DSP concentrations. Those slurries were then subjected to physiochemical characterisations and standard settling tests to gain insights into the flocculation of DSP-containing synthetic residue, applying the most widely-used flocculant chemistries (PAA and HX PAM) to different solids concentrations. FBRM was employed to monitor the extent of aggregation and link the findings to explain the variances seen in settling rates and supernatant solids concentrations measured during standard settling tests. The adsorption density of

flocculant was also quantified for iron oxide (hematite), iron oxide and DSP mixtures and for pure DSP to see if the presence of DSP inhibits flocculant adsorption.

After the DSP 'genesis' was understood and its impact on flocculation and sedimentation behaviour of flocculated slurries defined, the next step was to look at the possible remedy for the problems introduced by DSP in the primary thickening of bauxite residue. Polymer with silane functionalities have been claimed to offer a partial solution (Dai et al. 2008; 2010; Davis et al. 2010a, 2010b), but no mechanistic study has been published so far. Chapter 7 therefore looked at the effects of silane polymer that was co-dosed with PAA and HX PAM. Besides the flocculant type, other variables considered were the method of addition, the solution composition and solids concentration. SEM and X-Ray diffraction (XRD) analysis of supernatant solids revealed which mineralogical constituents (hematite or DSP) was preferably aggregated by silane polymer, PAA and HX PAM. Experiments were also extended to investigate the effect of shear under relative conditions that represent three different feedwell flocculation scenarios (low, medium and high shear). All findings were rationalised so that guidance can be given as to which conditions silane polymer addition provides the best outcomes.

In summary, this study is the first systematic examination of DSP effects on the flocculation and sedimentation behaviour of bauxite residue under closely controlled conditions. It benefits from access to the new generation FBRM system for aggregate characterisation and the first-of-its-kind silane polymer flocculant. While mainly seeking fundamental insights into the process, all the findings are also interpreted in terms of providing better knowledge of how to achieve optimum flocculation under real plant conditions. The discussions about how to extend the experimental results towards the ideas that may improve flocculation process in Bayer process primary thickener's feedwell becomes the core of the last result and discussion chapter, Chapter 8.

# 4 Monitoring hematite flocculation by FBRM

## *4.1 Introduction*

### 4.1.1 Application of FBRM in flocculation

Despite widespread use in a range of industries; studies of mineral systems, including bauxite residue, have been comparatively rare and often lacking in detail. A number of groups have recognised that FBRM offers significant advantages for the study of flocculated systems, primarily through the ability to provide real-time *in-situ* or in-stream information, avoiding the need for sampling and dilution. Examples of the use of FBRM for studying aggregation phenomenon in the mineral processing context can be found in Table 4.1, including the evolution of the equipment model indicated by the change in its commercial name. FBRM has been utilised as a primary tool to investigate the effect of process variables such as mixing intensity/shear rate, flocculant chemistries or flocculant dosage on aggregate dimensions.

Table 4.1. Examples of FBRM studies in mineral systems.

| | Feed | Flocculant/coagulant | Variables | FBRM type |
|---|---|---|---|---|
| Williams et al. (1992)<br>Peng and Williams (1993,1994) | silica | cationic | (1) mixing intensity<br>(2) solids conc.<br>(3) flocculant dosage | Partec 100 |
| Spears and Stanley (1994) | silica | 97% cocoalkylamine acetate & 3% dicocoalkyl acetate | (1) mixing intensity<br>(2) coagulant dosage<br>(3) solids conc. | Partec 100 |
| Honaker et al. (1994) | fine coal | - | pH | Partec 100 |
| Caron-Charles and Gozlan (1996) | $MnO_2$ | high ionic and nonionic | flocculant type | Partec 100 |
| Sengupta et al. (1997) | kaolinite | cationic PAA | (1) mixing intensity<br>(2) pH<br>(3) solids conc. | Partec 200/300 |
| Fawell et al. (1997) | hematite | undisclosed | flocculant dosage | Lasentec M500 |
| Jones (1998) | hematite | PAA | caustic conc. | Lasentec M500 |
| Hecker et al. (1999)<br>Heath et al. (2002, 2006a,b,c)<br>Swift et al. (2004)<br>Owen et al. (2007, 2008)<br>Fawell et al. (2009a)<br>Grabsch et al. (2013) | various | various | (1) mixing intensity<br>(2) mixing time<br>(3) flocculant type<br>(4) flocculant dosage | Lasentec M500 |
| Blanco et al. (2002) | $CaCO_3$ | cationic | flocculant type | Lasentec M500 |
| Phillips (2004) | bauxite residue | various | (1) mixing intensity<br>(2) flocculant type | Lasentec M500 |
| Negro et al. (2005)<br>Jarabo et al. (2010) | cement and fibre | PAA | (1) flocculant type<br>(2) fibre composition | Lasentec M500 |
| Kirwan et al. (2009a,b) | bauxite residue | PAA and HX PAM | flocculant type | Lasentec M500 with D600 probe |

The U.S. Bureau of Mines used an early FBRM system (Partec 100) for an *in-situ* study of the shear aggregation of silica (Murphy et al. 1994; Spears and Stanley 1994). They observed that large aggregates became unstable at higher mixing speeds, resulting in a narrower distribution. In a study of the centrifugal dewatering of polymer flocculated suspensions of manganese dioxide, Caron-Charles and Gozlan (1996) used a Partec 100 to measure "size" distributions of the products formed. The dewatered cakes were suspended in clarified supernatant and mixed to allow the probe to be used. They considered the use of the Partec 100 to be suitable because it eliminated the need for high dilution, which may have modified the aggregate size.

Sengupta et al. (1997) used FBRM to examine kaolin flocculation by a cationic polyacrylamide in a stirred glass beaker. They studied the effects of mixing speed and time, staged flocculant addition, pH and solids concentration. Their main performance measure was a "relative size" term, being the ratio of the mean aggregate size over the primary particle size. More detailed studies were carried out by Williams and co-workers (Peng and Williams 1993, Williams et al., 1992). They examined the flocculation of silica by cationic polyacrylamides in a stirred baffled vessel. By recording distributions every 16 seconds, they were able to extract information on the kinetics of both the flocculation and aggregate rupture processes. They were also able to show that, for this particular substrate, multi-stage addition of flocculant produced larger aggregates than a single dose.

Peng and Williams (1994) completed a detailed investigation of aggregate rupture in pipe flow. Silica was flocculated in a 360 L stirred baffled tank by the addition of a cationic polyacrylamide. The tank was sealed and pressurised to control the flow rate through the pipe outlet. A Partec 100 probe was inserted at the base of the tank to allow aggregates to be characterised before entering the pipe. Aggregates were ruptured in a 0.8 m long pipe with a uniform internal diameter of 22 mm. A second probe was fitted at the end of this pipe, allowing the extent of aggregate rupture to be monitored as a function of the velocity gradient. From this a quantitative assessment of aggregate strength could be obtained.

Flocculation of hematite in stirred beakers has been examined by FBRM and compared to classical settling and turbidity measurements (Fawell et al. 1997). The hindered settling rate and average chord length displayed similar trends with increasing dosage, while the total counts below 9.3 µm correlated with residual turbidity results. However, FBRM offered a real time continuous analysis of the reaction, compared to the batch settling rate and turbidity measurements.

A major concern with many FBRM flocculation studies has been the poor control of mixing. Batchwise mixing in stirred vessels is known to be inefficient, generating a wide range of shear rates with only particles close to the impellor experiencing high shear (Dippenaar 1985). Residence times within the mixing zone are invariably higher than optimal, leading to aggregate rupture.

Blanco and co-workers used FBRM (now the M series, a significant upgrade on the early Partec instruments) in the study of flocculation in papermaking (Blanco et al. 2002) and cements (Jarabo et al. 2010; Negro et al. 2005), in both cases considering mixtures of mineral particles and fibres. They compared the extent of flocculation achieved with different flocculant products over time in stirred beakers and the capacity for reflocculation when the applied shear conditions are reduced. Such reflocculation is rarely if ever observed in hydrometallurgical applications, for which the polymer-bridged aggregates are irreversibly ruptured on extended shear (see Section 2.1).

Hecker et al. (1999) inserted a similar FBRM probe below the settling tube of the Shear Vessel for a study of kaolin flocculation. They established some rough correlations between the mean square-weighted chord length and the hindered settling rates measured from flocculation at a fixed solids concentration with different flocculants. A scaled down version of this Shear Vessel was latter used with FBRM to examine flocculant make-up effects (Owen et al. 2007).

The greatest control over flocculation conditions has come from using turbulent pipe flow, with FBRM detection and variation of pipe length after flocculant dosing allowing reaction times to be controlled to a fraction of a second (e.g. Heath et al.

2006a; Swift et al. 2004). Kinetic measurements of such real systems were only possible through FBRM use, leading to the development of a population balance model for polymer-bridging flocculation (Heath et al. 2006b), more advanced relationships between chord length statistics and settling rates (Heath et al., 2006a) and new insights into flocculation process (e.g. Fawell et al. 2009a; Owen et al. 2008).

In their use of FBRM to monitor flocculation in paper-making, Blanco and co-workers proposed a simple test that allowed semi-quantification of aggregate strength, although this appears best used for direct product comparisons under selected conditions (Blanco et al. 2002).

The potential for FBRM to provide number-sensitive information from unweighted chord length distributions and volume-sensitive information from application of length-square weightings is a significant advantage in flocculation studies, offering discrimination of flocculation efficiency and extent, respectively. That the results differ from classical particle sizing does cause some confusion. Thapa et al. (2009) incorrectly described the counts from the unweighted chord length distributions as representing the number of particles; while the total counts can be number-sensitive, the relationship with number is certainly not linear and may be complex, especially when sizes (or shapes) are broad or changing. De Clercq et al. (2004) were aware of this when submerging an FBRM at various locations within a full-scale municipal wastewater clarifier, but then only compared the unweighted chord length distribution, thus neglecting the impact of passage through the clarifier on the relative aggregate sizes.

### 4.1.2 Bauxite residue flocculation

In the case of bauxite residue flocculation, Jones (1998) used FBRM M500 to study the non-aggregating behaviour of a specific hematite sample, observing that the mean chord length did not improve when flocculant was added. Such behaviour also confirmed the results derived from settling tests. The author proposed that this was due to the inherent surface contaminant (silicate) found in that hematite sample.

Phillips (2004) took advantage of the ability of FBRM to record counts for specific chord length channels (see Figure 2.26), using the unweighted counts at the lower end of the chord length distribution to establish how different flocculant products impacted upon fines capture.

Kirwan (2009a) extended the quantification of aggregate strength proposed by Blanco et al. (2002) to contrast the behaviour of the two most widely used flocculants in bauxite residue primary thickening, HX PAM and PAA (Section 2.4.1). In a separate study, the same author co-dosed HX PAM with PAA and the mean square-weighted chord length measured was then used to approximate the settling rate at various solids concentrations (Kirwan 2009b). The relevance of the results to primary thickening of bauxite residue is still questionable because lower alkalinity 1.2 M NaOH solutions were used instead of actual or synthetic Bayer liquor.

Aside from the studies mentioned above, there are no other known open access studies that discuss the use of FBRM in bauxite residue flocculation. Even with those studies, their focus was not on the critical aspects of bridging flocculation, such as flocculant dosage, shear rate or solids concentration (see Section 2.1.3-5). This underlines the need to provide fundamental information of the flocculation response under such variables.

## *4.2 Objectives and approaches*

In many thickening applications the feed properties are quite amenable to flocculation, i.e. there are no colloidal solids and the surface chemistry favours flocculant adsorption. In such cases the primary concern in characterizing the flocculation process is the *extent* of aggregation, through measuring the size achieved and relating this to settling rate or settling flux, for which the older generation FBRM instruments have proven valuable.

However, bridging flocculation with high molecular weight polymer flocculants becomes more problematic as the feed particle size becomes finer, with the

aggregation process very much affected by the efficiency of flocculant distribution. In addition, for some systems the surface chemistry (either through mineralogy or pH) leads to a reduced fraction of the particle surface being available to flocculant adsorption, thereby impacting on subsequent aggregate growth.

The *extent* of aggregation still remains important, but characterization of the *efficiency* of the process (i.e. the ability to capture fine particles) is also required, particularly when the nominally clarified liquors after thickening undergo downstream processing (e.g. precipitation, electrowinning, solvent extraction). It is in terms of monitoring flocculation efficiency in real time that it is believed that the G-series FBRM may provide additional insights not achieved with the older generation instruments.

This Chapter therefore considers the relative merits of old (M-series) and new (G-series) generations of FBRM instruments in studying bauxite residue flocculation, with residue being represented by synthetic iron oxide and liquor to provide far greater reproducibility than can be achieved from plant or laboratory digested bauxite. This was done to understand how the instruments may perform differently under identical flocculation conditions, revealing their limitations and advantages. The results were further used to refine the experimental methods in Chapter 6 and 7. Both M and G-series FBRM instruments were still used throughout this thesis, except in the particular condition where one of them fails to observe the difference given by changing flocculation conditions, simply due to equipment limitation.

How aggregate characteristic is affected by fundamental parameters such as flocculant dosage, solids concentration and mixing intensity is of interest. It is worth noting that the experimental conditions in the FBRM studies are inevitably different from those in a cylinder settling test, a turbulent pipe flow reactor or a full-scale gravity thickener. Variables that give optimum flocculation in FBRM studies will not necessarily give similar results in cylinder settling tests. Nevertheless, they do provide comparable trends of how the aggregate size changes when the process parameters are varied. The sensitivity of FBRM to discern such changes can also be the key towards better process control in thickener operation. This Chapter therefore

focuses on the flocculation mechanism of hematite as a model substrate for bauxite residue, prior to the extension to the DSP/hematite mixtures in the subsequent Chapters.

## *4.3 Materials and methods*

The FBRM instruments examined were the M500 and G400, both obtained from Mettler-Toledo. The diameter of the probe tip immersed in the slurry was 25 mm for the old M500 version and 9.5 mm for the new G400 version. The M500 can be used with either "Fine" or "Coarse" electronics, the slower response of the latter enabling aggregates to be more reliably measured, but adding to the over-sizing of finer particles. Changing to the Fine-electronics requires the physical swapping of an internal module, and therefore the Coarse-electronics was maintained throughout (in later D-series instruments, this change could be done through the flicking of a software switch). For the G-series, Fine and Coarse are now referred to as "primary" and "macro" chord selection models, and both are measured concurrently, with the ability to choose between the two depending on the application or aspect of greatest interest.

For both instruments, distributions were measured every 2 s and averaged over five measurements; the M500 provides distributions from 1 to 1000 μm, whereas the range for the G400 is extended to 4000 μm (these larger chord lengths could also be accessed by some of the D-series instruments). Particle and aggregate size distributions are usually presented as line graphs for ease of comparison, but in reality should be column graphs, with chord lengths divided into channels distributed in a logarithmic spacing. Such spacings are done in post-processing and therefore do not affect data collection. The chords are integrated to give a "total counts" value (or counts up to a nominated chord length). A volume-weighting is achieved by applying a square-weighting to the chord length distribution:

$$n_{i,2} = n_i M_i^2 \qquad 4.1$$

where $n_i$ and $n_{i,2}$ are the counts and square-weighted counts in a chord channel, respectively, and $M_i$ is the midpoint of the channel. The mean of this distribution is also derived:

$$\text{Mean square-weighted chord length} = \frac{\sum_{i=1}^{k} n_i M_i^3}{\sum_{i=1}^{k} n_i M_i^2} \quad 4.2$$

This work uses specific Bayer industry liquor properties terminology for describing liquor concentrations (see Abbreviations, Nomenclature and Liquor Terminology). The "testwork" liquor was made by adjusting a commercial sodium aluminate solution (Coogee Chemicals, WA) to target alumina and caustic concentrations (C = 230 g $L^{-1}$, A/C = 0.35, C/S = 0.99, liquor density ($\rho$) = 1200 kg $m^{-3}$) by using sodium hydroxide and deionised water (Xu et al. 2010).

The testwork liquor represents spent liquor composition found in Bayer refineries, having a typical low A/C ratio. Although a primary thickener treats slurry containing bauxite residue and pregnant liquor with a high A/C ratio (~0.7-0.8), using such liquor in laboratory testing is complicated by the risk of gibbsite precipitation. If some degree of such precipitation occurs, the implication for flocculation studies will be significant, as gibbsite is known to precipitate at the surface of hematite (Webster et al. 2011) and is also not responsive to polyacrylate flocculant (Yamada et al. 1980). Jones (1998) demonstrated that reproducible settling results were derived from using synthetic Bayer liquor with A/C ratio ≈ 0.3 during cylinder testing and furthermore found that increasing the A/C ratio (in the absence of precipitation) had very little effect on the flocculation process. Thus, unless stated otherwise, synthetic liquor with the aforementioned composition was used throughout this Chapter.

Hematite has often been used as a synthetic substrate to represent bauxite residue in studies of flocculant adsorption and flocculation performance (Hulston 2005; Jones 1998; Kirwan 2002) with the source varying in terms of the particle sizing required for the study. As this study sought to emphasize the impact of flocculation efficiency, a fine hematite powder from Sigma Aldrich (Iron (III) oxide, ≥ 99%) was used.

The chemistry of flocculant products that can be applied in bauxite residue flocculation have been discussed in Section 2.4.1. Representatives of various flocculant chemistries used in this study are described in Table 4.2. It is important to stress that some physicochemical properties of those polymers, such as % hydroxamate, remain proprietary information. All, except S-10292, are claimed as nominally high molecular weight and it should be noted that molecular weight itself is not a variable considered within this study, as it is expected to have only an incremental effect of the behaviours being considered. As S-10292 is claimed as the first generation of its kind, its molecular weight and other physicochemical properties remained undisclosed by its provider.

The simplest among them is the polyacrylate (PAA) product, having little or no amide character. This was preferred over other flocculant chemistries as it is known to give relatively poor fines capture for residues having high fines contents – a characteristic that the new generation of FBRM may able to distinguish over its older version. Alclar 665 (BASF) was selected as a representative PAA. Many comparable products are available and there is no implication this was an optimized selection.

Table 4.2. List of flocculant used in this thesis.

| Flocculant | Form | Supplier | Remarks |
|---|---|---|---|
| Alclar 665 | Powder | BASF | Polyacrylate (100% anionic) |
| Cyfloc HX-300 | Emulsion | Cytec Industries | HX PAM |
| Cyfloc HX-600 | Emulsion | Cytec Industries | HX PAM |
| Magnafloc 919 | Powder | BASF | Polyacrylate/acrylamide (50% anionic) |
| S-10292 | Water continuous | Cytec Industries | silane-containing PAA |

To prepare a 0.5 wt/wt% stock flocculant solution, Alclar 665 powder (1.0 g) in a glass jar was wetted with ethanol (1.5-2 g) before the required mass of deionised water was added and the jar sealed. This was placed on a shaking table and maintained in gentle motion for at least 24 hours at room temperature to ensure full dissolution and close to equilibrium deagglomeration of polymer chains (Owen et al.,

2007). The stock was diluted to 0.0125 or 0.025 wt/wt% with a 20 g $L^{-1}$ NaOH solution immediately prior to flocculation tests. The dosage of flocculant added into the system is expressed as grams of flocculant per tonne of hematite solids (g $t^{-1}$).

Slurries of different solids concentrations were prepared by adding a known amount of hematite to the testwork liquor, then pre-conditioned at a high mixing intensity (700 rpm, 70°C) for 15 minutes in a 2.5 L baffled stainless steel beaker (diameter 12.5 cm, height 25 cm) fitted with a 8.9 cm diameter A310 impeller. Testing indicated that the flocculation response for such slurries remained consistent for pre-conditioning times of up to 90 minutes, with some ageing effects apparent at longer times (i.e. a slow decline in the aggregate sizes attained). All testing was therefore completed within the 90 minute period.

For the main flocculation tests, 150 mL of slurry was transferred to a water jacketed standard 500 mL tall-form glass beaker (internal diameter 7.0 cm, height 13 cm) and placed in the FBRM beaker stand (Mettler-Toledo), equipped a four-blade turbine impeller (each blade 2.1×0.8 cm, angled at 45°C, shaft 0.8 cm). The stand supports the FBRM probe in a vertical position near the inner wall of the beaker and above the impeller, such that slurry is directed towards the probe tip, ensuring good sample presentation (Hukkanen and Braatz 2003).

Note that the M500 and G400 each have a dedicated beaker stand, and the different dimensions of the two probes leads to their positioning within the beaker being different (Figure 4.1). Unless otherwise stated, the stirring rate was fixed at 300 rpm throughout. The slurry was equilibrated at 70°C for 5 minutes before the required volume of dilute flocculant solution was injected.

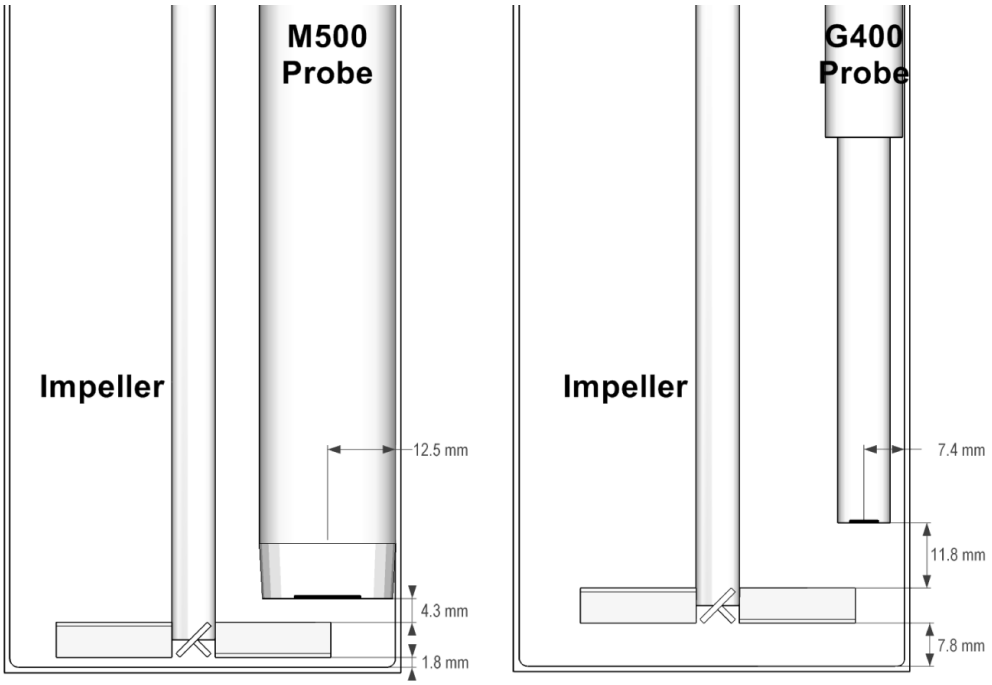


Figure 4.1. Beaker measurement geometry with M500 and G400 FBRM probes. Sapphire window position on each probe shown by thick black line. Beaker, probe and impeller dimensions are given in the text.

To measure supernatant solids concentrations in selected slurries post-flocculation in the G400 beaker stand, the same preparation and flocculation methods as described above were applied before agitation was stopped at a selected duration after flocculant addition. Settling was allowed to proceed for 60 s after this time, then supernatant (25 mL) was carefully removed with a syringe positioned ~1 cm below the liquor surface. This was vacuum filtered through a 0.45 µm membrane filter, washed by hot water (2×100 mL) to remove all salts and dried in an oven at 90°C, with the solids then determined gravimetrically.

While examination of Figure 4.1 may suggest otherwise, neither beaker stand allowed both probes to be used simultaneously, as the probe bodies above the measurement heads are significantly wider. A larger scale geometry was therefore used for a limited number of flocculation tests monitored with both FBRM probes, as well as *in-situ* imaging with a Particle Vision & Measurement probe (PVM, Mettler-Toledo). The PVM probe tip has identical dimensions to the M500 probe, with a number of strobing laser lights focused near the external surface of the sapphire

window allowing images to be captured in stirred suspensions. The images as measured are 880×660 µm, with a resolution of 5 µm.

To accommodate the three probes, a water jacketted 5 L stainless steel baffled tank (diameter 16 cm, height 26.5 cm) was used in combination with an A310 impeller (diameter 8.6 cm). The probes were vertically positioned near the inner wall and in advance of the baffles, ~1-2 cm above the impeller.

Hematite slurry (2 wt/wt%, 2 L, C = 230 g $L^{-1}$, A/C = 0.35 and C/S = 0.99) held at 70°C was initially dispersed at high intensity mixing (700 rpm) for 15 minutes, with the stirring speed decreased to 300 ppm prior to addition of the flocculant (0.0125 wt/wt % Alclar 665). FBRM distributions were recorded every 2 s; PVM images were acquired at a rate of one per second with the manual control of the focal plane and contrast to get the best image quality.

Particle size distributions were also measured on selected samples by low angle laser light scattering with a Malvern Mastersizer 2000. Mie theory is used to calculate the particle size from the scattering data through an iterative least square minimisation matrix inversion process (ISO 2009). No assumptions about the number of modes or breadth/narrowness of the distribution were made.

In contrast to FBRM tests, the Malvern measurements required high sample dilution and cannot be applied to slurries in the full-strength (i.e. high C) synthetic liquor. Sufficient sample was added to the analysis cell to obscure between 10 and 30% of the laser beam. To obtain a primary particle size distribution, hematite in water was treated with a dispersant (100 ppm sodium hexametaphosphate) and sonication applied prior to dilution and measurement.

To obtain an indication of the likely extent of hematite coagulation in the synthetic liquor, sapphire windows were used with the Malvern instrument and hematite solids were physically dispersed (by stirring) in a 3 M NaCl solution at pH ~10; no dispersant was added. Surface area analyses were performed on washed and dried solid samples using a Micrometrics Tristar 3000 instrument.

## *4.4 Results and discussion*

### 4.4.1 Feed properties

The fully dispersed particle size distribution measured by laser light scattering (Malvern Mastersizer) is presented in Figure 4.2, giving $d_{10}$ 0.34 µm, $d_{50}$ 0.76 µm, $d_{90}$ 4.8 µm and $d_{4/3}$ 1.80 µm. The measured specific surface area was 5.1 $m^2$ $g^{-1}$.

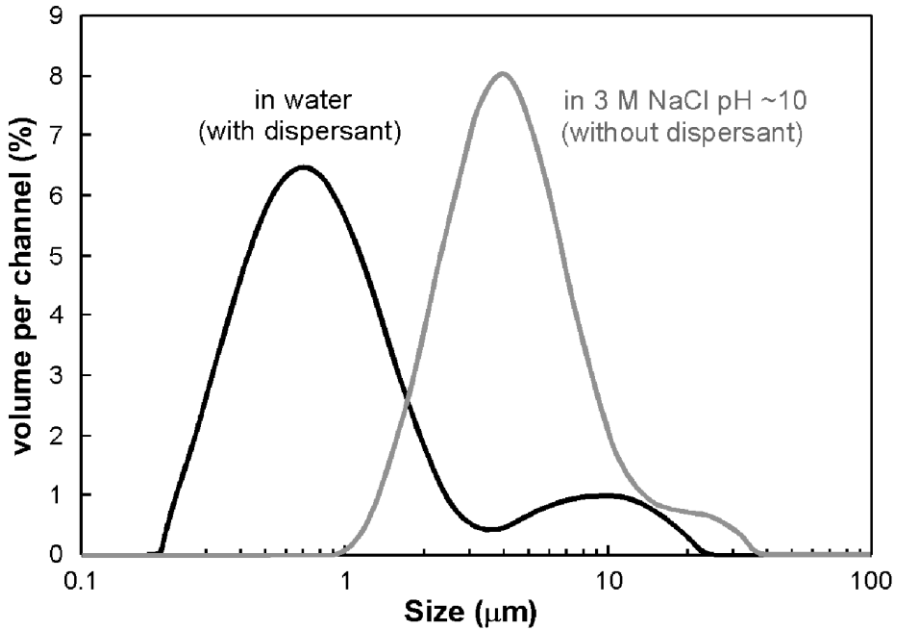


Figure 4.2. Particle size distribution for hematite (~0.05 wt/wt%) as measured by Malvern Mastersizer.

It is immediately apparent from the fully dispersed hematite particle size distribution that the majority of the free particles (certainly on a number basis) are below the detection limit for FBRM. For a particle suspension with a significant submicron fraction, flocculation studies by FBRM are potentially complicated by the aggregation of effectively invisible submicron particles to larger sizes that can be detected and this would be seen as an apparent shift in the chord length distribution to lower sizes.

However, submicron solids are expected to be significantly coagulated within the highly ionic synthetic Bayer liquor. The subsequent aggregation response will reflect the bridging flocculation of coagulated particles rather than the primary particle size,

thereby substantially reducing the required flocculant dosages. The Malvern Mastersizer cannot be used with full strength Bayer liquors, even with sapphire windows, the pH should ideally be kept at 10 or below. When suspended in 3 M NaCl at high pH prior to determining the particle size distribution, Figure 4.2 shows the hematite distribution to be significantly shifted to larger sizes relative to dispersion in water with the peak near 4 µm; significantly, almost nothing is seen below 1 µm.

Figure 4.3 shows the unweighted chord length distributions measured for hematite suspended in the testwork liquor using both the M500 and G400 FBRM probes under continuous mixing. The coarse-electronics and macro modes for each probe, respectively, represent the approach to chord length measurement that favours aggregate sizing (as opposed to distinct particles), but this reduces sensitivity to fines. They are observed here to give a similar peak near 20 µm, although the G400 distribution is broader, with some hint of a small shoulder at ~100 µm and more counts from 2-10 µm. The latter was expected, but at this stage it cannot be said with any certainty if the former is a consequence of the refined measurement process. That no such shoulder exists in the primary distribution may suggest its presence in the macro distribution results from aggregation.

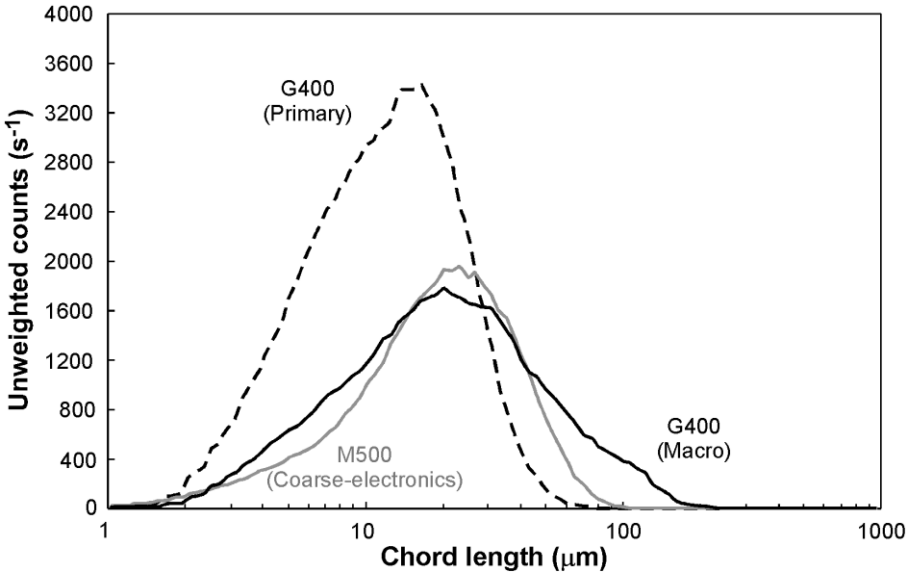


Figure 4.3. Unweighted FBRM chord length distribution for hematite (2 wt/wt%) within the testwork liquor, comparing the use of G400 and M500 instruments.

A significant shift in the distribution to smaller chord lengths was seen by changing the G400 processing from macro to primary, with the counts also elevated, although the peak was above 10 µm, still greater than that expected from the Malvern result in 3 M NaCl (Figure 4.2) acquired at a much lower solids concentration. Higher size seen in the FBRM (both M500 and G400) than that measured in 3 M NaCl with laser light scattering could be due to different extents of aggregation. Bayer liquor with A = 81 g $L^{-1}$ and C = 230 g $L^{-1}$ contains 4.3 M NaOH and 1.6 M $Al(OH)_3$ and has higher total ionic strength (coagulation tendency) than 3 M NaCl. Note that the counts below 2 µm remain lower than might be expected, which is not necessarily an indication of insensitivity to species at the lower end of the measurement range, but may instead reflect a greater impact of adding the beam width to these shorter chord lengths (Vay et al., 2012).

Using primary mode to examine aggregation may be in conflict with normal expectations, and certainly the macro mode would be used exclusively for examining the square-weighted (volume-weighted) chord length distributions and associated statistics when the extent of aggregation after flocculant addition (i.e. the aggregate size achieved) is the major goal. Access to the primary mode provides the ability to give some enhanced sensitivity to the low end of the distribution, and should at the very least be considered when investigating fines formation or capture processes.

### 4.4.2 Flocculation: M500 and G400

#### *4.4.2.1 Volume weighted FBRM results*

A major attraction of using FBRM to monitor flocculation processes is the option of following a range of chord length statistics for a reacting system with measurement intervals as short as 2 s. Typical statistics used are shown below for flocculation with the G400 and M500 probes at two different dosages. Figure 4.4a presents the mean square-weighted chord length as a function of reaction time, used most commonly as the indication of aggregate dimensions. The corresponding results for the total unweighted counts over the full chord length range are given in Figure 4.4b as a guide to the efficiency of aggregation; integrating the counts across a narrower chord length range (e.g. 1 to 10 µm) can also emphasize particular trends.

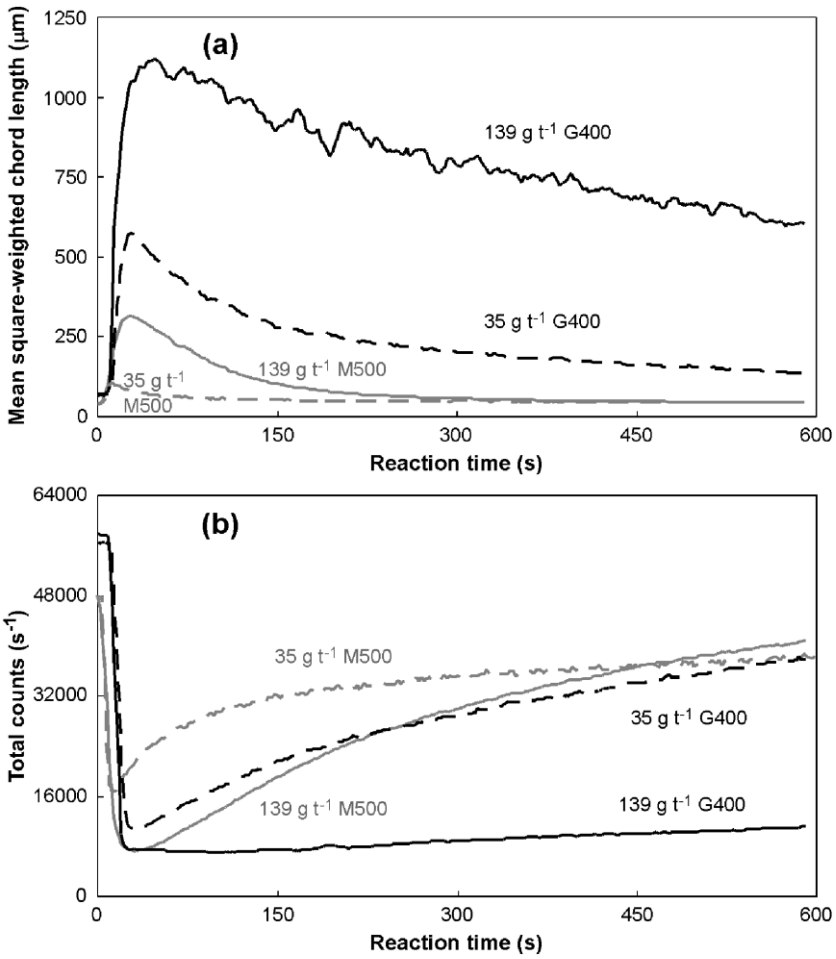


Figure 4.4. (a) Mean square-weighted chord length and (b) total counts for hematite flocculation (2 wt/wt%) at 300 rpm as a function of reaction time with G400 (macro) and M500 (coarse-electronics) instruments.

The reaction profiles for the mean square-weighted chord length data all show the expected response of a sharp rise upon flocculant addition, reaching a peak in aggregate size that is followed by a slower decline at longer reaction times. The corresponding profiles for the total counts display a minimum near the same reaction times as the peaks in size, beyond which the counts increase, consistent with the breakage or erosion of aggregates.

It is apparent from Figure 4.4 that the G400 results indicate a greater degree of aggregation. That the G400 total counts for the unflocculated solids were higher than the M500 value was an expected consequence of higher sensitivity, but fewer counts were observed by the former after flocculation (Figure 4.4b), while the mean square-weighted chord lengths were more than three times higher.

The interpretation of these results is complicated by the changed physical dimension of the G400 probe relative to the M500 (diameter 9.5 mm cf. 25 mm), combined with an altered positioning within the beaker stand arrangement (Figure 4.1). These factors inevitably lead to a change in the hydrodynamic conditions for flocculation, with the results obtained indicating a lower effective shear intensity experienced at the same rotation rate in the presence of the smaller probe, allowing larger aggregates to form and reducing the degree of aggregate rupture on extended mixing.

It is frequently assumed that mixing conditions within stirred vessels are determined by the impeller and its rotation rate; this may be the case for coagulation reactions for which aggregation is more likely in higher shear regions, but for polymer bridging flocculation processes it is expected that aggregates will grow in all vessel regions. As a consequence, the observed extent of aggregation after any reaction time, whether inferred from settling rate or aggregate size measurements, is an averaged response across products from all these zones.

To better understand the impact of the different hydrodynamics, a stainless steel sleeve was constructed for the G400 probe that increases its effective diameter to 25 mm, thereby allowing it to be inserted into the same beaker measurement configuration as the M500 probe (Figure 4.1). Figure 4.5 shows the square-weighted chord length distributions for both probes at selected reaction times at a fixed flocculant dosage of 139 g $t^{-1}$, confirming that the G400 probe is indeed observing much larger aggregate sizes. For comparison purposes, G400 results obtained in the absence of the sleeve are also shown, with the larger aggregate sizes able to be obtained at a much lower dosage.

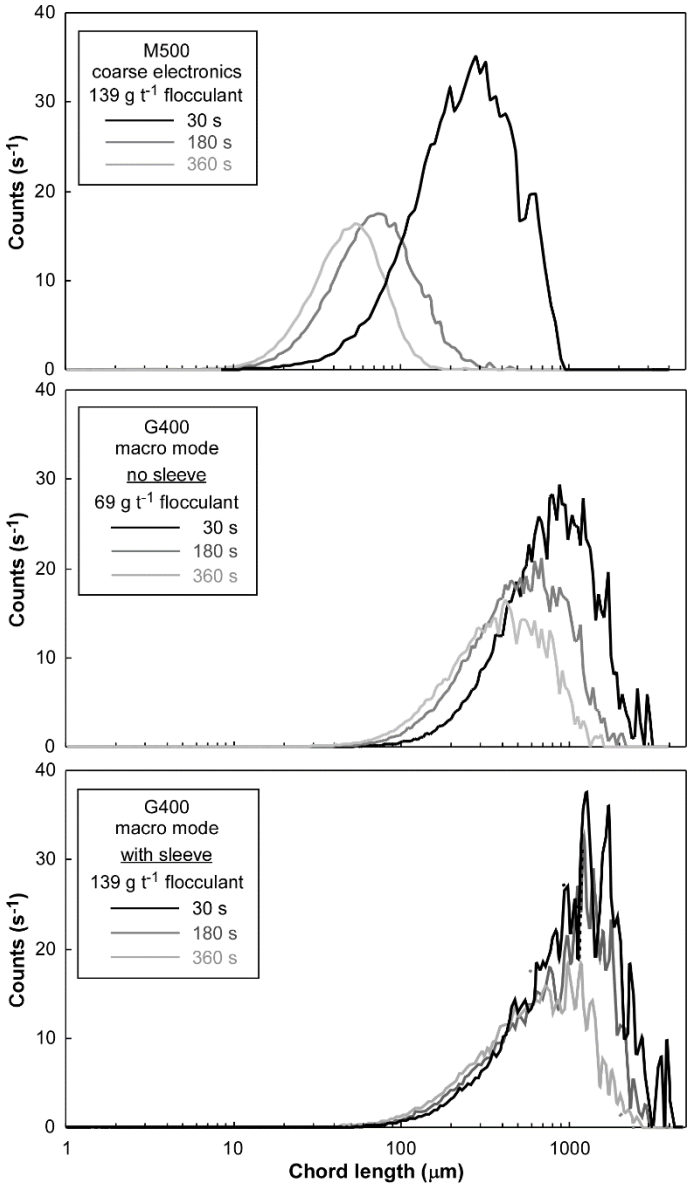


Figure 4.5. Square-weighted chord length distributions for different reaction times after flocculant addition to a hematite slurry (2 wt/wt%), comparing the use of M500 (coarse-electronics) against G400 (macro mode) at a dosage 139 g $t^{-1}$, with the latter in a stainless steel sleeve to match the hydrodynamic conditions of the former (see Figure 4.1). G400 results without the sleeve are also shown (dosage 69 g $t^{-1}$).

Comparisons between two different geometries must therefore be viewed with caution, and will potentially create some issues for those who attempt to quantify aggregate breakage processes by FBRM within the beaker stand geometry (Alfano et al. 1998; Blanco et al. 2002; Kirwan 2009a). It also highlights an important practical qualification that needs to be placed on all cylinder or stirred vessel tests, in that the flocculation performance measured is of relevance to the mixing conditions applied

in that test, but not necessarily to those experienced within full-scale flocculation vessels (feedwells or feedpipes/launders).

This concern was the primary motivation behind using turbulent pipe flow with FBRM detection for flocculation kinetics measurements, as the mean shear rate and reaction time can be controlled accurately, although requiring much larger sample volumes (Grabsch et al. 2013; Heath et al. 2006a; Owen et al. 2008). The small scale (bench top) turbulent pipe flow experiment requires as minimum 50 L of slurry for generating chord length profile in a closely controlled shear rate or mixing time. A massive amount of sodium aluminate slurry must be then prepared for the duration of the experiment, thus, although it may have been the ideal mode to study turbulent pipe flow, it was neither practical nor achievable.

Having considered the contribution from the measurement geometries, differences in the square-weighted chord length distributions in Figures 4.5 must be a consequence of the refined capabilities of the new generation probe. Most obvious is the impact of the expanded detection limit, which allows detection of chords up to 4000 µm and reliable measurements up to 2000 µm. Even with exercising caution and limiting the mean sizes measured to below 1500 µm, this still represents a significant extension beyond the capability of the M500 probe, for which mean sizes above 400 µm were rarely practical.

While this extended range for the G400 probe may contribute to the differences seen in the 30 s distributions in Figure 4.5, it cannot be a factor in those for the longer reaction times. To better discern the true impact of the different processing approaches for the two probes, a limited number of experiments were conducted at a larger scale in which both FBRM probes and the PVM imaging probe were all used simultaneously in a baffled vessel (5 L total volume). The intention was that the images would provide some indication as to which FBRM probe was better capturing the actual aggregate properties.

The PVM probe is more limited in the conditions that can be studied, with higher dilution preferred to minimise the overlap of aggregate boundaries; in this case

2 wt/wt% was the highest solids concentration that could be considered. Positioning of the probes to give comparable presentation was difficult and the vessel used represents yet another distinct hydrodynamic environment, but that was of lesser importance than achieving a degree of general validation. It should also be stressed that this larger vessel is far from ideal for detailed study of flocculation responses, given the broad shear rate distribution, and was only used to allow image acquisition with the FBRM results. Suitable presentation to the FBRM probes is obtained under milder mixing conditions with the smaller beaker geometry, making it better suited for comparison of flocculation efficiency.

The insert plot within Figure 4.6 shows the reaction profiles obtained from both FBRM probes and the four selected reaction times for which the full distributions are given in the main plot. Again the aggregate sizes measured with the G400 probe are substantially larger than those from the older M500 across all reaction times, although the relative differential appears less than in the smaller scale tests. It can therefore be concluded that vessel hydrodynamics and the expanded measurement window for the G400 probe are not the only factors in the larger sizes observed in these flocculation studies.

The PVM images from the different reaction times were taken in a different physical location within the vessel from the FBRM data, and therefore cannot be assumed to directly represent the chord length distributions from those times. However, the aggregates captured within each image do indicate that the M500 probe may be undersizing, particularly when examining the longer reaction times, at which the majority of visible aggregates extend well beyond 100 μm in one direction.

Many of these aggregates are quite elongated, and chord length measurements will inevitably have a higher probability of producing shorter chords. This will undoubtedly influence the unweighted chord length distribution, but the very nature of the square-weighting process emphasizes the relative contribution of any larger chord lengths. That the square-weighted chord length distribution for the M500 probe sees a very low contribution from aggregates over 200 μm in size at a reaction time of 90 s is at odds with the image taken at that time.

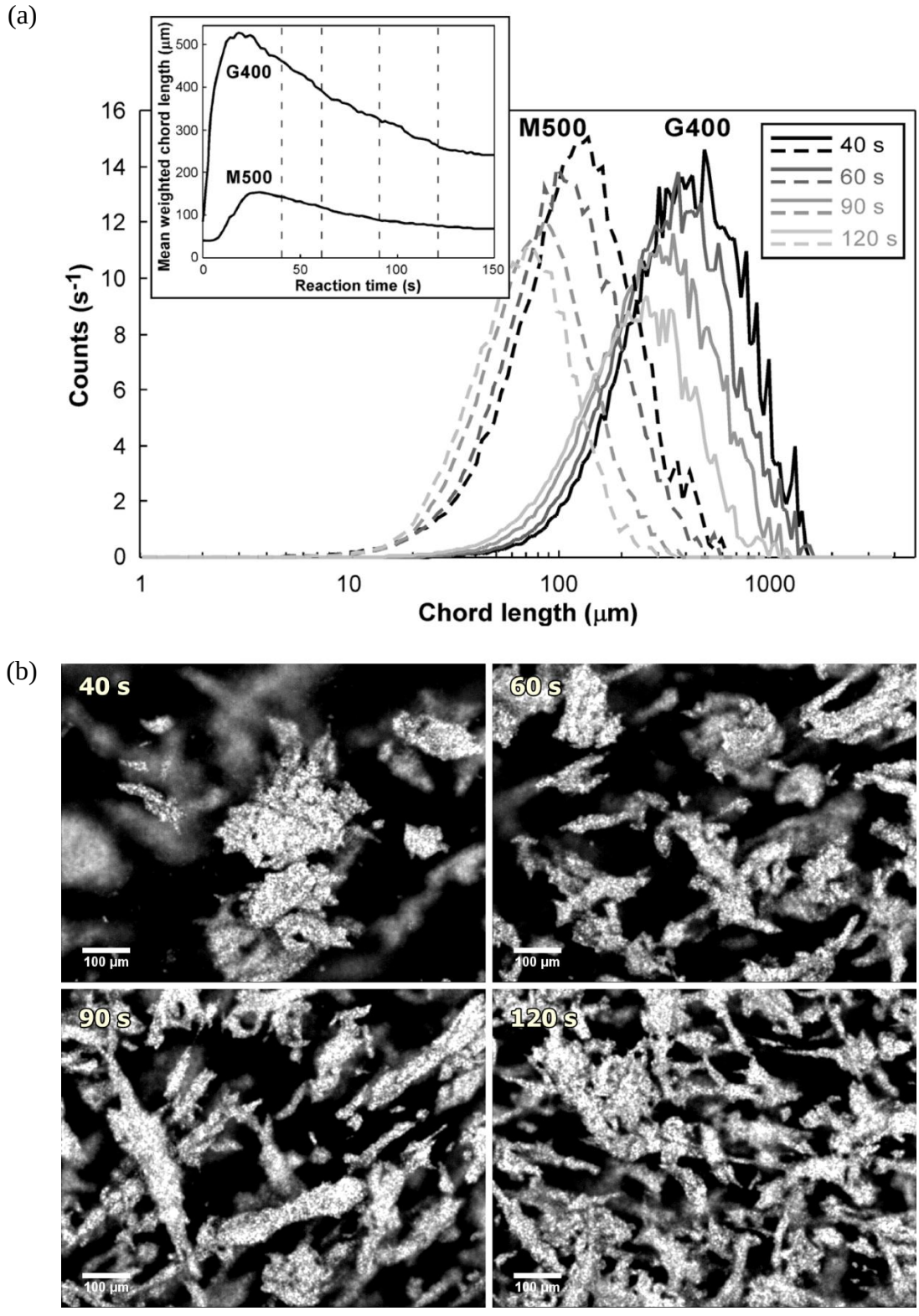


Figure 4.6. Effect of reaction time on: (a) square-weighted chord length distributions of flocculated hematite slurry and (b) the corresponding PVM images at 40, 60, 90 and 120 s after flocculation. Conditions: 2 wt/wt% solids concentration in a 5 L baffled tank, flocculant dosage 139 g $t^{-1}$, comparing the use of G400 (macro, solid lines) and M500 (coarse-electronics, dashed lines), FBRM and PVM recording were done simultaneously.

It is highly likely that the enhanced edge detection and removal of the fixed threshold for the G400 probe (as discussed in Section 2.5.3) contribute to the reporting of larger chord lengths, and the square-weighting process serves to give them further emphasis. Considering the schematic in Figure 2.27a, aggregates may be considered as equivalent to "particle 3", in that the old measurement principle may undersize due to a single aggregate being reported as multiple smaller chord lengths.

Figure 4.7 illustrates how chord length measurements with both the M500 and G400 probes may be affected by the high porosity of aggregates. The use of the coarse-electronics with the M500 probe reduces this effect, but fractal aggregates become increasingly porous at larger sizes, reducing their potential to produce reflected chords across their full dimensions. If chord length measurement as performed with the G400 probe is increasing this probability of seeing larger aggregates as a single body, then it may represent a major advantage, as these larger aggregates have a much greater practical significance to industrial flocculation processes.

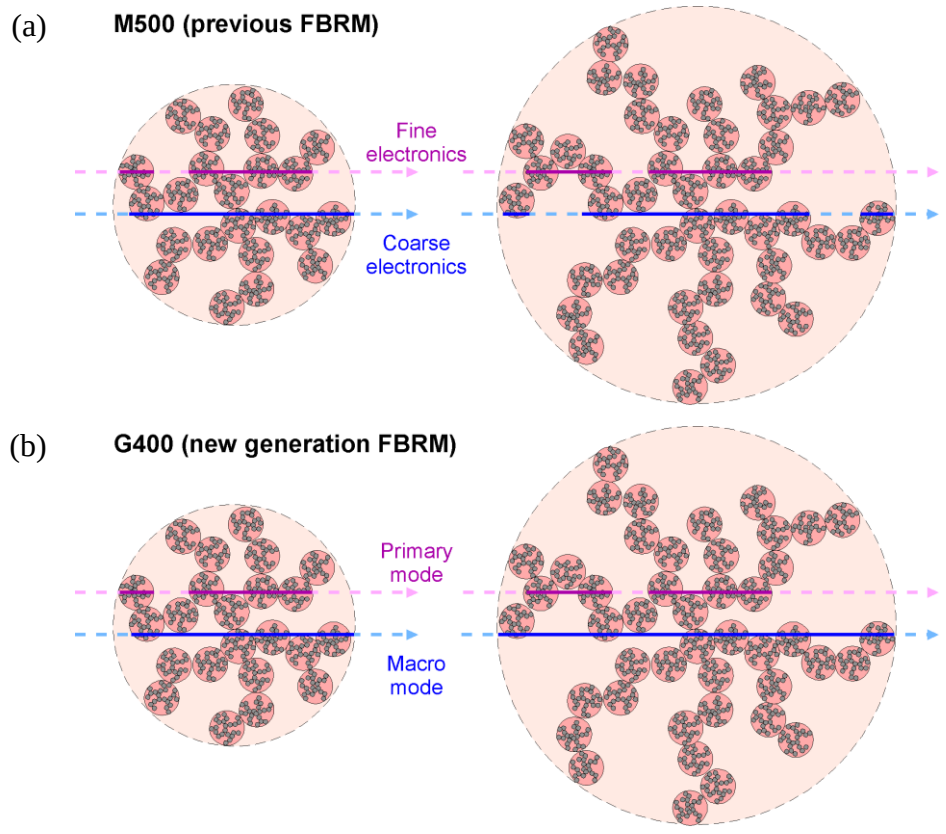


Figure 4.7. Schematic illustrations of the differences between FBRM: (a) M500 and (b) G400 in interpreting a large aggregate. (Red lines: fine electronics in M500 or primary mode in G400 and blue lines: coarse electronics in M500 or macro mode in G400).

### *4.4.2.2 Unweighted FBRM results*

Figure 4.8 shows the unweighted chord length distributions obtained with both FBRM probes at different reaction times following hematite flocculation in the 5 L baffled tank. As flocculation substantially reduces the total counts, these distributions can be almost an order of magnitude lower in their count scale in comparison to the corresponding unflocculated distributions (Figure 4.3), which can lead to an increased degree of noise. However, the flocculated distributions highlight the distinctions between the two probes. Unweighted chord length distributions from the M500 system have often been used as an indication of flocculation efficiency, and can be seen here to display a clear increase in counts as the reaction time increased. However, results with the G400 probe provide greater sensitivity to the change in chord lengths as the aggregates are sheared. That larger aggregates are seen raises the prospect of better resolving the peaks from aggregates and fines, an aspect examined in more detail in the next section.

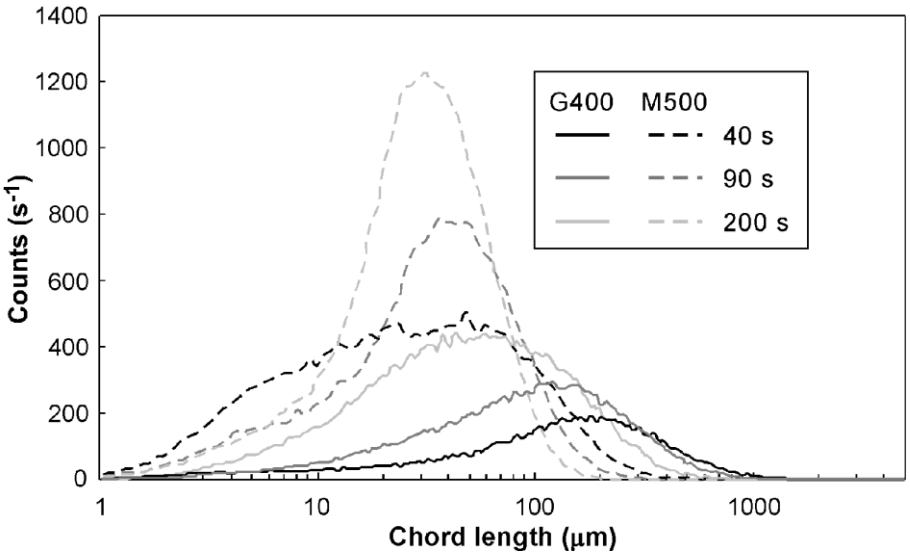


Figure 4.8. Unweighted chord length distributions at different reaction times after flocculation of a hematite slurry (2 wt/wt%, dosage 139 g $t^{-1}$) in a 5 L baffled tank, comparing the use of G400 (macro, solid lines) and M500 (coarse-electronics, dashed lines) FBRM instruments.

Any improved sensitivity to fines offers considerable scope for the optimisation of flocculant selection and flocculation conditions for bauxite residue flocculation after digestion, for which effective fines capture is a primary concern, particularly if it reduces the need for filtration prior to product precipitation. The subsequent sections

therefore only consider results for the G-series FBRM instrument. The small-scale beaker measurement geometry (with no sleeve on the G400 probe) was used, as this provided access to the mildest mixing conditions.

#### *4.4.2.3 Practical considerations*

The mean square-weighted chord lengths reported from older generation FBRM for flocculated minerals are typically under 400 µm, and yet the naked eye can frequently see much larger aggregates being formed in laboratory tests and thickener feedwells. The G400 probe consistently measures larger chord lengths, and this is seen as a significant advantage. Of course, aggregates are rarely spherical, in some instances becoming quite elongated. It is therefore a consequence of the square-weighting applied to such chords that the mean values may in fact be much larger than for more spherical aggregates. Given that the main use of FBRM is in detecting changes, this is not necessarily a concern, but something that users need to be alert to.

Another consequence of measuring larger chord lengths, which inevitably contribute only a low number of counts, is a greater degree of noise in the square-weighted distributions, as evident in Figures 4.5 and 4.6. Such noise can be reduced by acquiring the chord length data over longer time intervals or averaging over multiple measurements. This is viable in continuous processes such as flocculation in a pipe reactor, but attempting this in a batch reactor or a full-scale feedwell risks the masking of true peaks in aggregate size or process fluctuations. In reality, the magnitudes of the changes that can be detected from swings in flocculation performance are sufficiently large that they should exceed any contributions from such noise. The results obtained in this study were acquired every 2 s and averaged over five consecutive measurements, but only after checking that this did not influence the trends. Longer measurement durations would only be considered for much slower processes and fail to the capture the gradual change in flocculation response when its kinetics is fast.

While the chord length measurement principle applied with the G400 probe leads to an enhanced sensitivity to species at the lower end of the measurement range relative

to previous generation FBRMs, the lower limit still remains around 1 μm. For the vast majority of hydrometallurgical applications this is of little concern, particularly given the ionic nature of most process liquors and the likelihood of colloidal particles being aggregated. However, this limit remains well above what would be considered appropriate for the direct study of nanoparticles, and the detection of aggregation of such particles may only be practical in limited circumstances.

### 4.4.3 The mechanism of hematite flocculation

#### *4.4.3.1 Effect of flocculant dosage*

Understanding the flocculant dosage response is always a key aspect in any flocculation study, allowing the comparison of different flocculant products and ideally an indication of the effectiveness of the aggregation process. The dosage that produces the desired settling rate is not necessarily the same as that required for optimal fines capture.

Settling rate measurements from cylinder tests relate to the aggregate size and solids concentration, and are generally useful if the tests are done well. Supernatant clarity measurements are more problematic for tests done at the solids concentrations appropriate for thickening (they are of greater value in jar tests at very low starting solids concentrations). Settling mudlines within cylinders in the absence of any other flows can ‘drag-down” suspended solids, artificially enhancing the clarity result. Small-scale testing is considered to produce unreliable predictions of full-scale clarification performance, and yet this can often be a key priority in optimizing and controlling a process.

The effect of five different flocculant dosages (from 35 to 174 g $t^{-1}$) on the G400 FBRM flocculation response for a hematite slurry under constant mixing was examined, with the mean square-weighted chord length (Figure 4.9a) and total unweighted counts (Figure 4.9b) monitored as a function of time. As expected, higher dosages led to higher mean square-weighted chord lengths; while dosage increases beyond 104 g $t^{-1}$ had a comparatively smaller impact on the peak size, on extended mixing it was apparent that the additional flocculant imparts a degree of

strength to the aggregates, with significantly larger sizes maintained at a reaction time of 600 s, especially when looking at the decay rate of the mean square-weighted chord length for the first 150 s of reaction time.

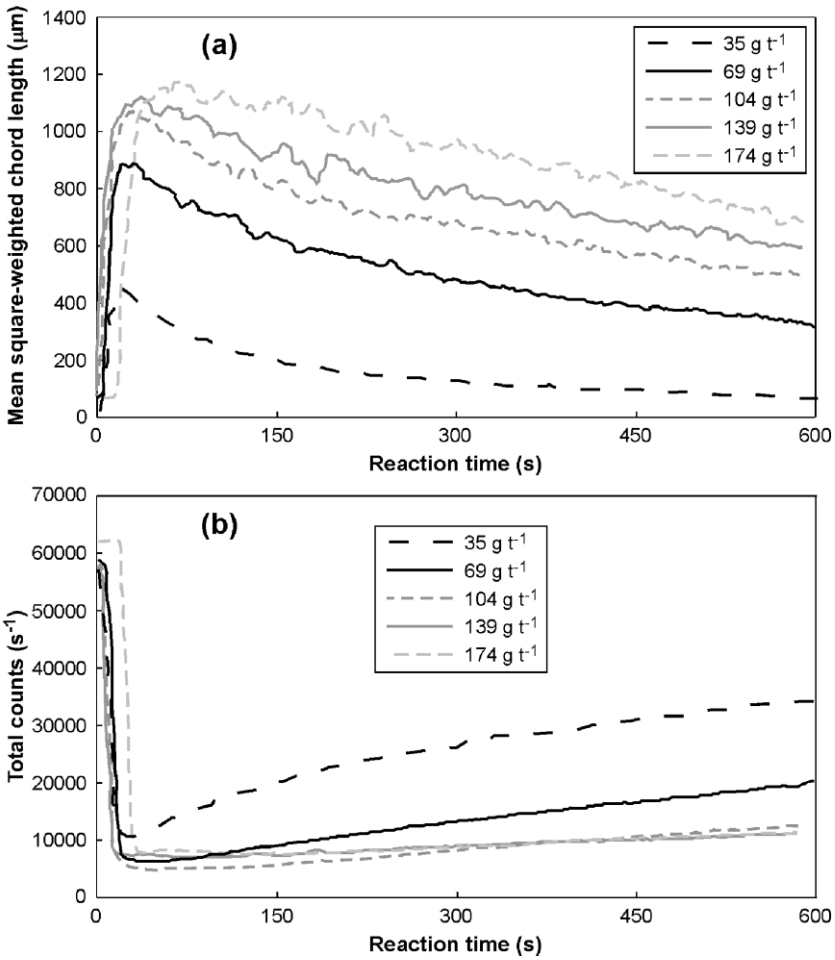


Figure 4.9. (a) Mean square-weighted chord length and (b) total counts as a function of reaction time for different flocculant dosages (G400 probe in macro mode, 2 wt/wt% hematite, 300 rpm).

Higher dosages also greatly reduced the total counts, with comparatively little change in the initial extent of this reduction beyond a dosage of 69 g $t^{-1}$ (Figure 4.9b). Extended mixing had a greater detrimental effect at the lower dosages, again consistent with weaker aggregates leading to breakage and/or erosion processes.

The sensitivity of maximum mean square-weighted chord length as a consequence of increasing flocculant dosage is best portrayed in Figure 4.10, which also shows the decline of total counts measured at the point when the maximum mean square-weighted chord length was achieved. If the total counts in Figure 4.9b and 4.10 are

taken as pre-cursors in fines capture efficiency, it seems that increasing flocculant dosage will generate larger aggregates while providing extra probability of the flocculant adsorption onto the submicron hematite particles, hence enhancing its collision efficiency (Section 2.1).

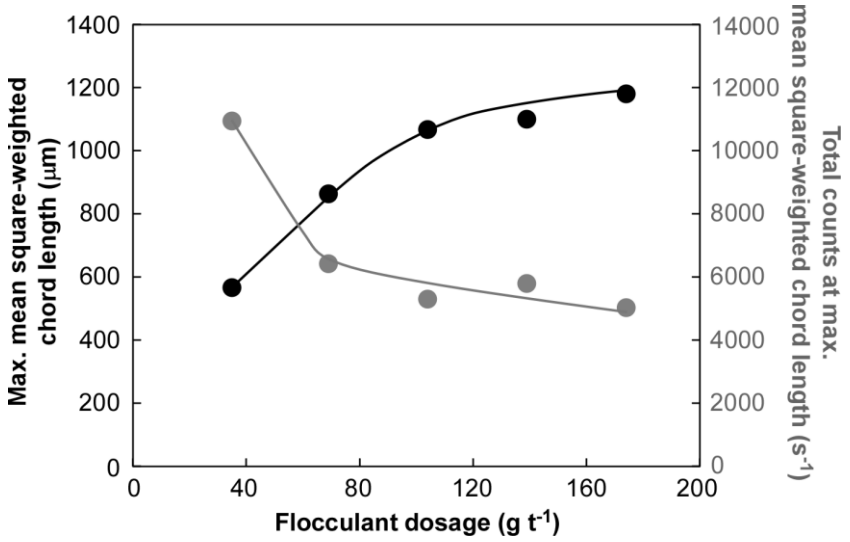


Figure 4.10. Maximum mean square-weighted chord length and its total counts as a function of flocculant dosages (G400 probe in macro mode, 2 wt/wt% hematite, 300 rpm).

From the plant operator point of view, improved fines capture can be perceived as the opportunity for better clarity, potentially increasing the filtration rate in security filtration (Equation 2.16 – Section 2.4.4). While the above interpretations of the total counts are useful, they only provide part of the picture, with the large reduction seen on flocculation actually masking detail that is best seen by considering the full unweighted chord length distributions after flocculation. Figure 4.11 shows these distributions at three dosages for three different reaction times. The macro mode for these distributions is shown; the primary mode gave additional counts and gave greater emphasis to the lower end of the distribution, but did not change the observed trends.

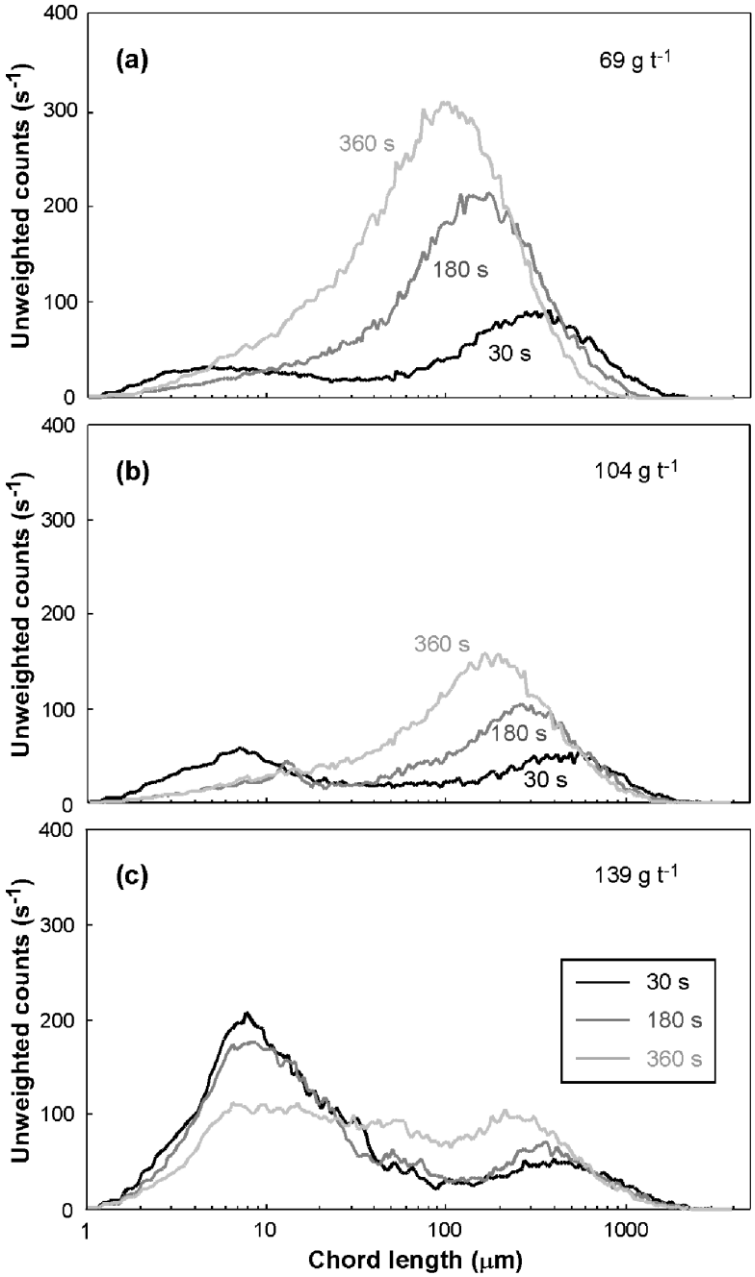


Figure 4.11. Unweighted chord length distributions at three different reaction times for flocculation at dosages of (a) 69, (b) 104 and (c) 139 g $t^{-1}$ (G400 probe in macro mode, 2 wt/wt% hematite, 300 rpm).

For the lowest of these dosages (69 g $t^{-1}$, Figure 4.11a), the distribution after 30 s was clearly bimodal, with the lower peak at ~5 μm representing the contribution of fines and coagulated fines that were not yet flocculated, while flocculated aggregates made up the peak at ~300 μm. This was consistent with the short reaction time under fairly mild shear conditions giving sub-optimal mixing, initially forming some very large aggregates but not efficiently capturing fines/micro-aggregates. Such peaks have never been clearly resolved in unweighted distributions with the M500 probe.

Note that the large aggregates (> 500 µm) that contribute most to the effective aggregate volume fraction will actually provide few counts to this distribution. Longer reaction times favour more efficient fines capture, almost eliminating the lower peak, but the fragile larger aggregates are readily ruptured, leading to the upper peak shifting to shorter chord lengths and higher intensity (i.e. a greater number of smaller aggregates).

The response was similar on increasing the applied dosage to 104 g $t^{-1}$ (Figure 4.11b), although the upper peak was shifted to larger chord lengths and was of a lower intensity at all three reaction times shown. The latter is indicative of the lower population of fragments that form as a result of aggregate break-up. Thus, higher dosage is not only increasing aggregate size but also imparting a degree of strength to the aggregates. However, analysis of data in this region is much better done through the weighted distributions that highlight the volumetric contribution and show distinct shifts in response to higher dosages; in contrast, the low counts at larger chord lengths in the unweighted distributions for higher dosages offer very little sensitivity to minor changes in conditions.

Figure 4.11b provides a hint of an increase in counts in the lower peak at a reaction time of 30 s, and this is clearly evident in Figure 4.11c for a dosage of 139 g $t^{-1}$ for all three reaction times. While this may seem counter to expectations for a high flocculant dosage that has produced larger aggregates, it is most likely a consequence of the mild mixing and the addition of a larger volume of flocculant contributing to localized overdosing, i.e. a small fraction of the solids immediately contacted with the flocculant which is quickly adsorbed, leading to a high effective surface coverage. These particles or small aggregates are either thereby stabilized or at least have a reduced probability of being incorporated into larger aggregates, as is evident from the distributions after longer reaction times.

Table 4.3 compares the FBRM counts below 10 and 20 µm during flocculation (300 rpm, 30 s) at different dosages with the solids concentrations measured in supernatant samples taken 60 s after mixing was stopped. Interestingly, the supernatant solids results show a distinct step-change improvement in performance

on increasing the dosage from 69 to 104 g $t^{-1}$, whereas the corresponding FBRM counts actually show significant increases.

Table 4.3. G400 FBRM counts in selected chord length ranges during hematite flocculation (2 wt/wt%, 30 s reaction time) with supernatant solids measured after 60 s of settling.

| Dosage (g $t^{-1}$) | Mixing (rpm) | Counts ($s^{-1}$): Primary mode | | Counts ($s^{-1}$): Macro mode | | Supernatant solids (mg $L^{-1}$) |
|---|---|---|---|---|---|---|
| | | 1-10 µm | 1-20 µm | 1-10 µm | 1-20 µm | |
| 35 | 300 | 992 | 1780 | 449 | 809 | 120 |
| 69 | 300 | 1080 | 1450 | 684 | 958 | 136 |
| 104 | 300 | 1570 | 2050 | 1020 | 1470 | 24 |
| 139 | 300 | 3330 | 4040 | 2180 | 2900 | 28 |
| 139 | 400 | 731 | 1020 | 445 | 651 | 84 |
| 139 | 500 | 2060 | 4410 | 751 | 1710 | 304 |
| 139 | 600 | 7410 | 16600 | 2060 | 4410 | 380 |

This highlights the non-equivalence of the two measures, with the supernatant solids measurement representing not only the 30 s reaction time under the applied mixing, but additional aggregation that can occur during the 60 s that follow. FBRM provides chord length information representative of the aggregation state under the conditions applied at the time of the measurement, and it must always be remembered that the conventional measures of flocculation performance are conducted under conditions that cannot be an exact match. Settling rates and supernatant clarities are acquired from batch tests in which there will inevitably be a delay after the applied mixing regime is completed. This delay represents a period of gentle (or tapered) mixing prior to the onset of mudline settling, with the potential for additional aggregate growth to occur and settling rates to be enhanced (Owen et al. 2008).

The same can be assumed for flocculated solids that are discharged from a feedwell. Supernatant clarities from cylinder tests are measured after an even longer delay, and unflocculated or poorly flocculated fines detected by FBRM can be dragged down with large aggregates that then occupy a greater effective volume fraction, leading to higher than expected clarities. Conversely, clarities in full-scale thickeners can be adversely affected by currents outside the feedwell entraining solids that would

otherwise settle. This is where high flocculant dosage and the resulting stabilization can be dangerous and to some extents, can be predicted from the use of FBRM.

### *4.4.3.2 Effect of applied mixing*

As discussed, estimating mean shear rates near impellers as a measure of mixing intensity within stirred vessels in batch flocculation is of little (if any) value, given that aggregation also takes place in the larger regions of lower shear (Dippenaar 1985; Fawell et al. 2009a; Swift et al. 2004). That said, higher stirring rates will lead to more intense mixing and can provide useful qualitative comparisons.

The effect of applied mixing on the maximum mean square-weighted chord length and the total counts measured at which maximum mean square-weighted chord length was achieved is described in Figure 4.12. Increasing stirring rate from 300 to 600 rpm clearly led to a gradual decrease of the maximum mean square-weighted chord length. However, it seems that the total counts increased considerably only when the stirring rate was higher than 500 rpm, indicating a critical mixing intensity where, beyond that, flocculant has no ability to hold and preserve the aggregates structure.

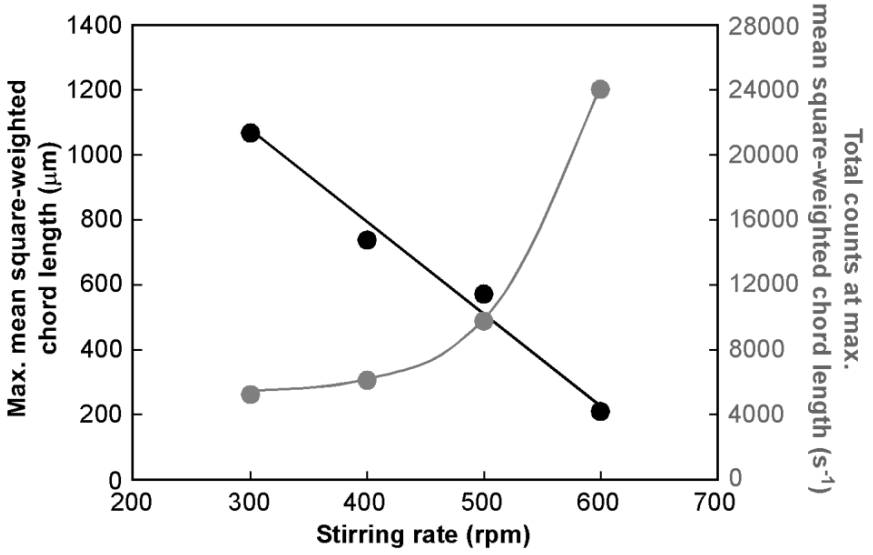


Figure 4.12. Maximum mean square-weighted chord length and the corresponding total counts as a function of stirring rate (G400 probe in macro mode, 2 wt/wt% hematite, 300 rpm, 139 g $t^{-1}$ flocculant).

The flocculant dosage of 139 g $t^{-1}$ was chosen because the mild mixing at 300 rpm failed to incorporate the smaller and stabilized aggregates into the bigger ones (Figure 4.11). Therefore, the effect of higher stirring rate on the unweighted chord length distributions at such dosage is of importance. Figure 4.13 shows the effect of increasing the applied mixing in the G400 beaker stand configuration on the unweighted chord length distributions for hematite slurry flocculated with 139 g $t^{-1}$ of flocculant. The volume-weighted distributions are not presented; while they demonstrate the expected reduction in aggregate size and greater degree of breakage at longer reaction times, in this case it is the relative efficiency of flocculation that is of more interest.

The ability to clearly distinguish between conditions that do or do not favour fines capture represents possibly the most valuable enhancement from the G400 probe, providing far greater sensitivity than was ever seen with the earlier FBRM chord detection principles. In particular, this may offer major advantages in the screening of different flocculant products.

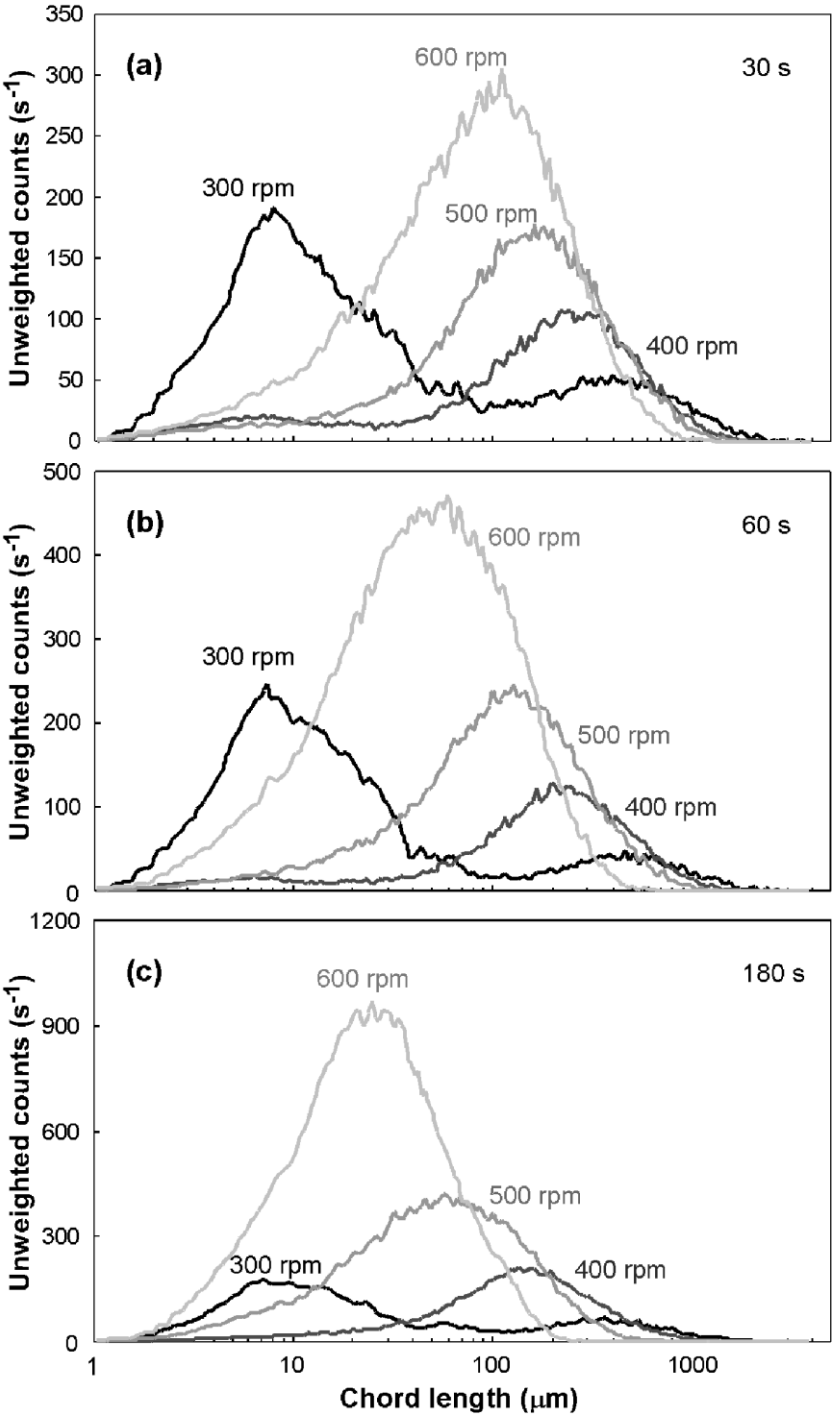


Figure 4.13. Effect of mixing on unweighted chord length distributions at different reaction times for flocculation at 139 g $t^{-1}$ PAA (G400 probe in macro mode, 2 wt/wt% hematite).

Supernatant solids concentrations were again determined following flocculation at each mixing intensity for 30 s and compared with the FBRM counts below 10 and 20 μm (Table 4.3). As was the case for the effect of dosage, the trends are different, although the effect of mixing did produce larger effects on both forms of measurement. While FBRM suggested fines capture was best at 400 rpm, each

increase in mixing intensity led to higher solids in the supernatant; the latter results are probably influenced by the reduced aggregate size and the possibility that bigger aggregates can drag down the fines.

The enhanced counts for FBRM in primary as opposed to macro mode was evident in the results from different dosages, but the primary mode also proved much more sensitive to the effect of mixing. The substantial elevation in counts for primary vs. macro mode at 600 rpm also coincided with a significant shift to lower sizes. In this case the relative closeness in size between coagulated fines and small flocculated aggregates may prevent any resolution of their contributions in either distribution, but the variations between modes do at least indicate the presence of both.

#### *4.4.3.3 Effect of solids concentration*

The flocculation process is very much affected by the solids concentration, and in mineral systems an optimum value is always observed; below this optimum, aggregation is often inefficient, while above it the aggregate size achieved will be limited by viscosity effects and the settling rates greatly reduced. One of the attractions of FBRM in the study of flocculation is its ability to be applied in real-time across a wide range of solids concentrations, and the reader is directed to the work of Heath et al. (2006a) and Owen et al. (2008) for further details. The potential for application of the G400 probe to produce better information on aggregate sizes formed in high solids systems is of great interest.

Figure 4.14 compares the evolution of mean square-weighted chord length as a result of flocculant addition and mixing at different solids concentrations (2, 4, 6 and 8 wt/wt%), capturing the existence of an optimum value. A larger peak aggregate size was formed when the solids concentration was increased from 2 to 4 and then to 6 wt/wt%. A further increase to 8 wt/wt% led to the smallest aggregates size of all, indicating that the optimum solids concentration had been passed.

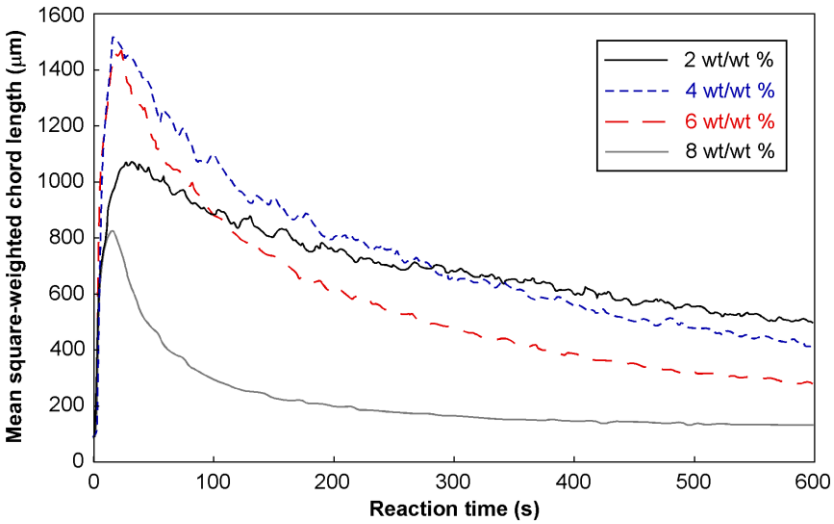


Figure 4.14. Mean square-weighted chord length as a function of reaction time for different solids concentration (G400 probe in macro mode, hematite, 104 g $t^{-1}$ flocculant, 300 rpm).

From the size reductions observed in the reaction profiles, it is clear that an increasing solids concentration accelerated aggregate break-up. This was explained in Section 2.1.3 and 2.1.5, where higher viscosity as a result of increasing solids concentration increases not only the aggregation rate but also the breakage rate. This was most obvious when contrasting the 4 and 6 wt/wt% profiles, where comparable peak values of the mean square-weighted chord length were reached. The 6 wt/wt% profile displayed a greater extent of size reduction after longer reaction times. The degree of aggregate break-up was even more pronounced at a solids concentration of 8 wt/wt%, although the maximum mean square-weighted chord length was achieved 10-20 s earlier than in the other profiles because the relatively higher viscosity improved the initial aggregation kinetics (Equations 2.7-2.9 in Section 2.1.3).

The effect of increasing the solids concentration on unweighted chord length distributions obtained with the G400 probe is shown in Figure 4.15a and b for two different reaction times: 30 and 120 s. At 30 s, doubling the solids to 4 wt/wt% led to a slight reduction in the fine counts below 20 µm, behaviour maintained at the longer reaction time (120 s). This clearly indicates that 4 wt/wt% is closer to the optimum concentration, although the lower concentration had served to provide greater sensitivity to variations in conditions.

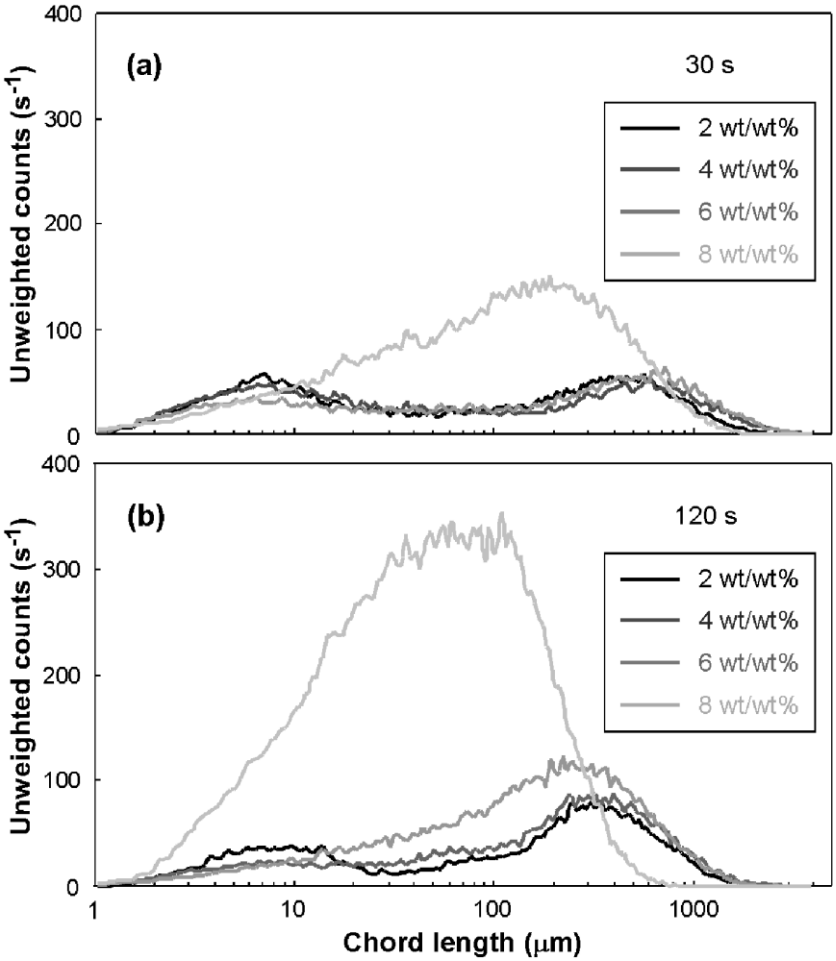


Figure 4.15. The effect of hematite solids concentration on unweighted chord length distributions at reaction times of (a) 30 s and (b) 120 s for flocculation at a dosage of 104 g $t^{-1}$ (300 rpm, G400 in macro mode).

The 30 s distribution on increasing the solids concentration to 6 wt/wt% suggests that the aggregate size was comparable and fines capture was slightly better (especially for < 10 μm particles). However, at 120 s the aggregate peak was shifted to shorter chord lengths and higher counts, with more frequent aggregate collisions leading to an increased degree of breakage to mid-sized fragments (10-300 μm) which may still settle in a gravity thickener.

At 8 wt/wt%, the aggregate size became much more limited – very few chords near 1000 μm are measured at 30 s but the majority are centered around 200 μm. The inevitable long tail in the unweighted chord length distribution to the left of a peak means that the contribution of fines can no longer be readily inferred, although this may change at higher dosages. Increasing the reaction time to 120 s saw a very high degree of breakage, and the shift in the aggregate peak well to the left effectively

merged it with the fines peak. This does not imply that the chord length information would necessarily lose its value for detecting flocculation inefficiency; comparison of the integrated counts below a selected chord length threshold under carefully controlled conditions would still provide an option for rapid screening.

## *4.5 Summary*

The main attraction of FBRM has always been real-time direct monitoring of particle systems without the need for dilution, highly desirable in most applications but absolutely essential in flocculation studies. The aggregates formed are fragile, and for the majority of mineral systems, irreversibly ruptured by excess shear. Assessing a flocculation process should involve estimating both the size of the aggregates formed and the efficiency of fines capture, information readily derived from FBRM through the square-weighted and unweighted chord length distributions, respectively.

By setting a much lower reflected intensity threshold for the measurement of chord lengths, the new generation G-series instruments substantially enhance the information obtained from flocculated systems by FBRM. The probability of measuring chord lengths more representative of larger aggregates is increased, while clearer discrimination of the contribution of fine particles or small aggregates to the unweighted chord length distributions greatly increases the value of FBRM in screening products or conditions that lead to inefficient aggregation.

While the new G-series FBRM has undeniable advantages, this does not automatically discount information obtained with the previous M-series generation, particularly given that the main value of FBRM in many situations is to monitor real-time trends, rather than to provide absolute size measurement. Under a high flocculant dosage regime, low populations of very large aggregates ($\geq$ 1000 μm) tend to add too much noise on the volume-weighting of the chord lengths measured by the G400 probe (see Figure 4.5). The mean-square weighted chord length is usually only required as a representation of size under specific conditions, often to capture the onset of significant aggregation as a consequence of small shifts in such conditions. There may therefore be no disadvantage to using the M500 probe when comparative

numbers are sought, such as when contrasting the mean square-weighted chord lengths for hematite and DSP/hematite slurries flocculated by the same polymer.

Flocculation of hematite in synthetic Bayer liquor with different variables (flocculant dosage, mixing intensity and solids concentration) proved that there were different optimum flocculation conditions in terms of aggregates size and fines capture. Too high a dosage would produce larger aggregates but may also create local overdosing where fines or smaller aggregates were stabilised and not flocculated. Excessive surface coverage from high flocculant dosage lowers the collision efficiency and hence more collisions are required to provide higher probability of successful bridging collisions between barren surfaces and polymer attached to surfaces.

Increasing stirring rate facilitates more collisions, however, it also accelerates aggregate break-up. A higher shear intensity aids fines capture but decreases aggregate size (and accordingly the settling rate), following the generally accepted behaviour for bridging flocculation (see Section 2.4.4). In the case of hematite in synthetic Bayer liquor, a critical stirring rate was observed, beyond which aggregate break-up dominated and relatively small aggregate fragments (< 20 μm) were produced on extended stirring. The insights gained from experiments that varied the stirring rate were also useful towards predicting what may happen in a feedwell.

While increasing solids concentration favoured the kinetics of initial aggregate formation, it also enhanced aggregate break-up due to the higher viscosity. In fact increasing solids concentration beyond its optimum value greatly limited the aggregate size that could be formed. This emphasizes the necessity of high solids dispersion and internal dilution in plant feedwell flocculation procedures if the solids concentration is too high. In laboratory scale experiments, 2 wt/wt% was below the optimum solids concentration, however, it did offer the greatest sensitivity to changes in process variables, particularly in the lower chord length region of 1-20 μm. The improved sensitivity to fines provided by the G-series instrument, reflected in bimodal distributions measured after flocculation, is of particular interest in terms of assessing the performance of new silane-containing polymers that are claimed to give better fines capture when flocculating DSP-rich residue.

# 5 Sodalite solids formation at the surface of iron oxide

## *5.1 Introduction*

The poor flocculation of DSP-containing residue under primary thickener conditions has been repeatedly reported from both plant observations (Faneitte et al. 1994; Perrier et al. 1999; Rousseaux et al. 2004) and laboratory simulations (Dai et al. 2008; 2010; Davis et al. 2010a, 2010b; Liu et al. 1994; Roach et al. 1989). The latter were derived from substrates prepared by different methods, with the DSP origin referred to as either "made *in-situ*" or "physical mixture". The former refers to DSP from either the mineral's reactive silica or kaolin that was added and co-digested with residue (see Figure 5.1a), and the latter to addition of DSP that was separately pre-prepared (see Figure 5.1b).

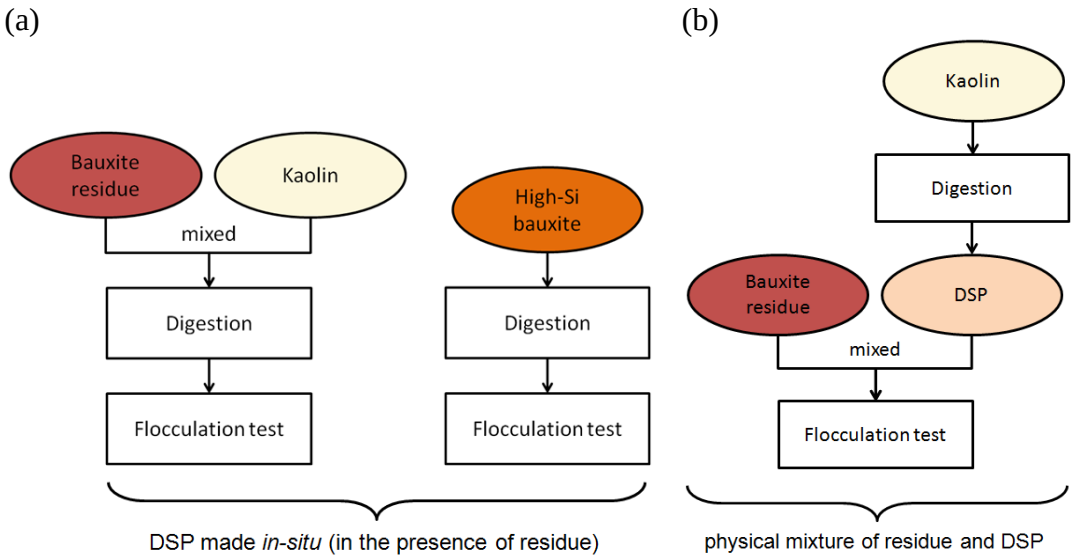


Figure 5.1. Method of DSP synthesis for flocculation tests: (a) DSP made *in-situ* (in the presence of residue) and (b) physical mixture of residue and DSP.

Although the residue slurry with the DSP made *in-situ* is different from the physical mixture of both, both types of slurry showed similar trends for bridging flocculation. Reduced settling rates, high supernatant solids and poor settled bed densities were reported for both conditions, regardless of their preparation methods. Most previous studies were carried out for the evaluation of flocculant products (Dai et al. 2008; 2010; Davis et al. 2010a, 2010b) without seeking insights into how the preparation

method may subsequently influence the solid substrate surface properties. To date, no detailed investigation has been undertaken to explain whether (i) DSP precipitates onto the major substrate surface, thereby changing the surface properties, or (ii) it precipitates as a distinct minor phase. From a flocculation perspective, it is important to answer this fundamental question, as it potentially affects how the industrial process may be optimised.

Surface coverage by nuclei may lead to less surface being available for flocculant adsorption, influencing aggregation kinetics and aggregate density (see Figure 5.2a). Precipitation as a separate phase increases the number of particles in the slurry, with aggregation then dependent on the activity of the new surfaces (see Figure 5.2b). Both processes can lead to a reduction in the optimum solids concentration for flocculation, but for very different reasons. The responses will also be very much dependent on the active flocculant functionalities and their potential to interact with the surfaces.

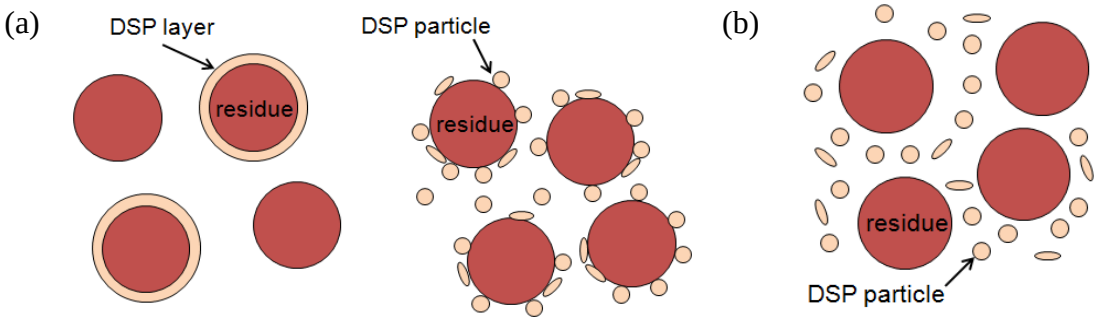


Figure 5.2. Precipitation of DSP in the presence of residue solids: (a) as complete or partial coverage on the seed particles and (b) as a distinct phase.

Various forms of iron oxide are reported to host the precipitation of different solid species in sodium aluminate solution. Goethite, hematite and magnetite can act as seed surfaces in Bayer liquor to promote $Al(OH)_3$ precipitation (Webster et al. 2011). DSP (sodalite) can also deposit onto 316-stainless steel surfaces (Addai-Mensah et al. 2001). These facts suggest that iron oxide (either as a major residue phase or a model substrate) might potentially exhibit the same seeding characteristic for DSP.

## *5.2 Objectives and Approaches*

The objective of the work discussed in this Chapter was to gain fundamental understanding of DSP formation (precipitation) in the presence of iron oxide model phase (hematite). The experiments were also designed to find evidences if DSP can coat and change the physicochemical characteristic of the iron oxide seed particles.

Cylinder settling tests following flocculation are by far the most common method used to identify changes in particle properties and are also applied here. However, they need to be viewed with some caution. The reproducibility of settling rate measurements is hampered by a high standard error, which even in the best circumstances can be 8-12% (Farrow and Swift 1996b).

Additional supporting evidence is therefore required, preferably by direct measurements on the solids and slurries. Hence, in the present work, the following measurements were performed on DSP/hematite mixtures prepared by different methods:

- Zeta potential as a function of pH in order to derive isoelectric points (iep). Such measures are well known for their relevance to coagulation and flocculation phenomena, as explained in Section 2.1. Zeta potentials for bauxite residue have been found to be sensitive to aggregation state, ionic strength and mineralogy (Hirosue et al. 1980; Karakyriakos and Patrick 2005; Liu et al. 2013).
- Desilication rates. If the presence of hematite results in a higher sodalite precipitation rate, it can be implied that it promotes crystallization and DSP might partially or completely cover the hematite surface, similar to the case of gibbsite precipitation on iron oxide seed particles (Webster et al. 2011).
- SEM of the post-digested hematite surface. An SEM image will display the proliferation of DSP precipitate on the hematite surface if heterogeneous nucleation is the rate determining step (Addai-Mensah et al. 2001).

### 5.2.1 Zeta potential: theory and measurement

The nature of a particle surface when immersed in an aqueous phase and how it influences the distribution of surrounding ions is best explained by the *electrical double layer concept* that leads to the Gouy-Chapman-Stern model (Hunter 1981; Karakyriakos and Patrick 2005; Klimpel 1998; Riley 2005; Shaw 1992).

It was mentioned in Section 2.1.1 that the particle surface will have a distribution of neutral, negatively-charged and positively-charged sites that together determine the net surface charge. Charged surfaces attract ions of opposite charge (counter-ions) to the solid/liquid interface while repelling ions of similar charge (co-ions) across the diffuse layer (Figure 5.3a). The relative concentration of counter-ions is therefore at its highest at the interface and that of co-ions is highest in the bulk solution (Figure 5.3b). In the earlier Gouy-Chapman model, ions in the diffuse layer are assumed to be as point charges, their distribution obeying the Boltzmann function and making the potential drop as a function of distance from the surface, as seen in Figure 5.3c, obeys the following equation:

$$\sigma_0 = \epsilon \kappa \psi_0 \qquad 5.1$$

where $\sigma_0$ is charge density, $\epsilon$ is permittivity, $\kappa$ is the ionic composition of the medium and $\psi_0$ is the potential (e.g. Hunter 1993; Riley 2005; Shaw 1992). At low potentials, the double layer behaves similar to a capacitor between two parallel plate electrodes in elementary physics and its thickness will be equal to 1/κ (Figure 5.3c).

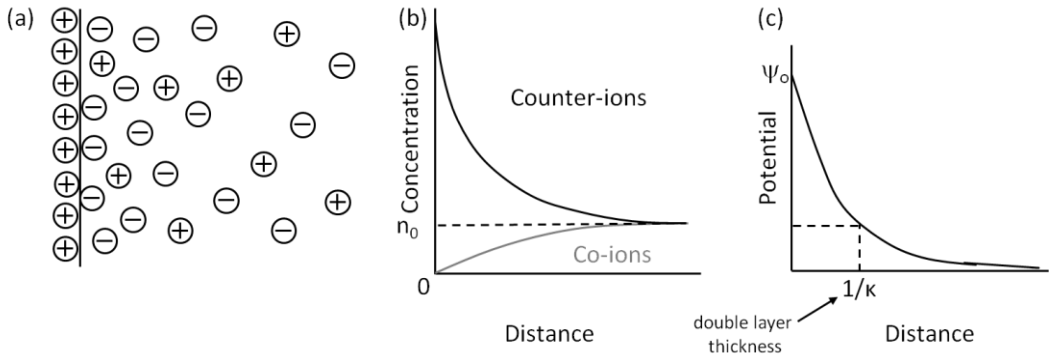


Figure 5.3. Schematic representations of: (a) diffuse layer and (b) distributions of counter and co-ions and (c) surface potential as function of distance from the positively charged surface. Adapted from Shaw (1992).

In the Gouy-Chapman-Stern model, the double layer is further refined to have an inner layer, a plane of shear and a diffuse layer (Figure 5.4a). The inner layer (Inner Helmholtz plane of IHP) which accounts for the distance between the centre of a hydrated ion and the particle surface is located between the particle surface and the Stern layer (also known as the outer Helmholtz plane or OHP), according to the Helmholtz model (e.g. Hunter 1993; Riley 2005; Shaw 1992). The potential will be linear up to the Stern layer (Figure 5.4b). In the diffuse layer, there is also the plane of shear, defined as the effective boundary of the solid/liquid interface (Riley 2005) as ions adsorbed to the surface are assumed to be 'stuck' (Figure 5.4a). Electrokinetic experiments measure the potential at the plane of shear, reported as the zeta potential. Although it is not exactly the same as the surface potential, the zeta potential is the closest representation of the surface potential that can be realistically measured.

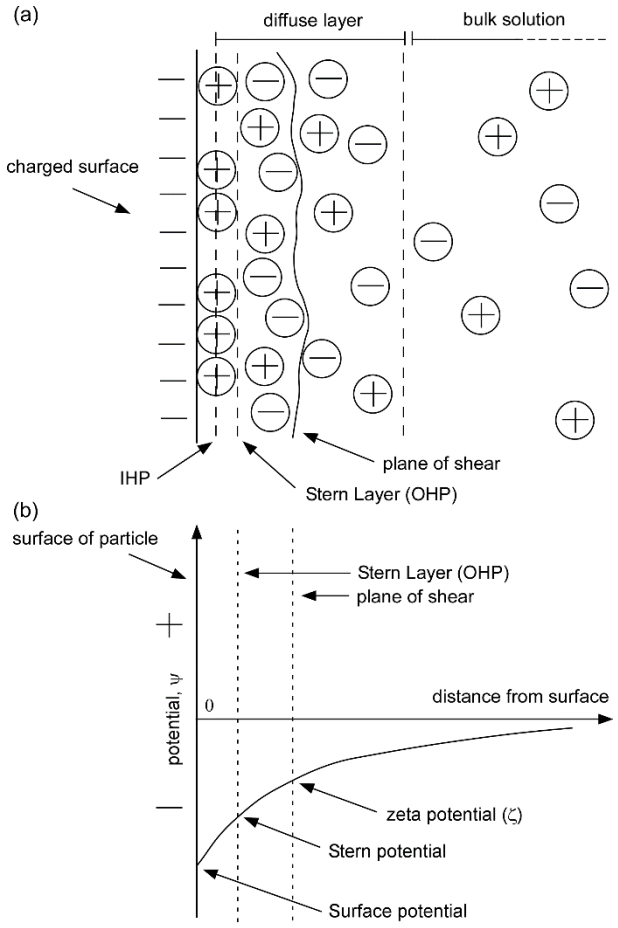


Figure 5.4. Schematic representations of: (a) ion distribution and (b) potential gradient in Gouy-Chapman-Stern model for the negatively charged surface. Adapted from Klimpel (1998) and Riley (2005).

Under the influence of an applied electric field, charged particles in the electrolyte are attracted towards the electrode of opposite charge, with viscous forces opposing this motion (Malvern 2004). When an equilibrium between attractive and opposing forces is achieved, the particles move with a constant velocity, known as the electrophoretic mobility ($U_E$), which is a function of the dielectric constant ($\varepsilon$), the fluid viscosity ($\eta$) and the zeta potential ($\zeta$), as per Henry's equation:

$$\zeta = \frac{3\,U_E\,\eta}{2\,\varepsilon\,f(ka)} \qquad 5.2$$

where *f(ka)* is the Henry function. For a particle-electrolyte system, *f(ka)* equates to 3/2 and Equation 5.2 becomes the Smoluchowski relationship (Riley 2005).

Zeta potentials in the range of -80 to +100 mV are commonly reported for aqueous colloidal systems (e.g. Kirwan 2002; Tscharnuter 2001). Under conditions that give large negative (< -30 mV) or large positive (> +30 mV) zeta potentials, particles will tend to repel each other (Malvern 2004). On the other hand, negative or positive zeta potentials of small magnitude (0 ± 5 mV) may promote coagulation and marginally improve the settling rate and overflow clarity of settled slurries from the limited degree of aggregation achieved (Dihang et al. 2008; Harif et al. 2012; Holt et al. 2002; Ma 2011; Vergouw et al. 1998). A reduction in the magnitude of zeta potential can be achieved by adding salt, thereby increasing the concentration of counter-ions in diffuse layer, compressing the thickness of double layer and eventually decreasing the repulsive forces among particles (e.g. Riley 2005; Shaw 1992).

In flocculation studies, a change in zeta potential can indicate the relative extent of flocculant adsorption (Bárány et al. 2011; Karakyriakos and Patrick 2005; Kirwan et al. 2004; McGuire et al. 2006; Mpofu et al. 2004; Nasser and James 2006; Sivamohan and Cases 1990), although this may only be relevant for charged flocculants at significant dosages.

In this Chapter, zeta potential measurements were employed to detect any change in surface properties that may originate from the deposition of DSP on the surface of a

model iron oxide substrate. When zeta potential is plotted as a function of pH, the pH where zeta potential equals to 0 is defined as the isoelectric point (iep). A shift in iep to a lower pH reflects an increased proportion of negatively charged surface sites at most slurry pH values (Chvedov et al. 2001).

Liu et al. (2013) measured the zeta potentials of bauxite residue samples from Australia and China, which would be expected to vary greatly as a consequence of mineralogical and pre-treatment differences. Higher Al/Fe molar ratios (resulting from increasing DSP contents) were found to shift the iep to the higher pH region. This is in contrast with the results from (Chvedov et al. 2001) where a high DSP bauxite residue exhibited a lower iep value. Bauxite residue with high DSP content exhibiting a lower iep does also make sense, as silica and silicates are known to have iep values lower than hematite (Kosmulski 2002, 2004, 2006, 2009, 2011).

Such contradictions should not be overlooked, as there could be unknown factors influencing the zeta potentials, such as high CaO contents bringing the iep to close to that of pure CaO (Liu et al. 2013) or adsorbed flocculant introducing negatively charged $COO^-$ sites, which shift the iep to lower values (Chvedov et al. 2001; Zhang et al. 2008). To isolate the results from such factors, zeta potential experiments in this Chapter only considered high purity kaolin as the feed for synthesizing DSP. If hematite is required, as in the *in-situ* prepared DSP/kaolin slurry, pure hematite was also added.

### 5.2.2 Pre-desilication: theory and measurement

During digestion of gibbsitic bauxite at 150°C, gibbsite dissolves at a much faster rate than reactive silica (1996a; Harato et al. 1996b; Oku et al. 1973). For an unidentified bauxite sample, Harato et al. (1996b) found that 90% of gibbsite dissolution was achieved within 5 minutes, while only ~40% of the reactive silica had dissolved. This implied that during processes downstream from digestion, reactive silica could continue to slowly dissolve (Equation 1.1) and then undesirably precipitate as DSP (Equation 1.2), either becoming a final product impurity or

forming scale in process equipment. This emphasizes the need for effective pre-desilication.

During the pre-desilication step, kaolin is reacted with barren liquor containing caustic at near boiling temperature (90-102°C) for 10-20 h, depending on the reactive silica content (Cousineau and Fulford 1987; Ostap 1985; Roach and White 1988; Thomas and Pei 2007). The aim is to achieve complete DSP formation at an early stage, thereby mitigating the risk of post-digestion clay (or other reactive silica) dissolution and DSP precipitation. In the pre-desilication process, kaolin will first dissolve, increasing the concentration of soluble silica (Kotte 1981). Once the degree of silica supersaturation (or the difference between the actual and equilibrium silica solution concentrations) is high enough, precipitation will take place and decrease the soluble silica concentration to its equilibrium level (Figure 5.5).

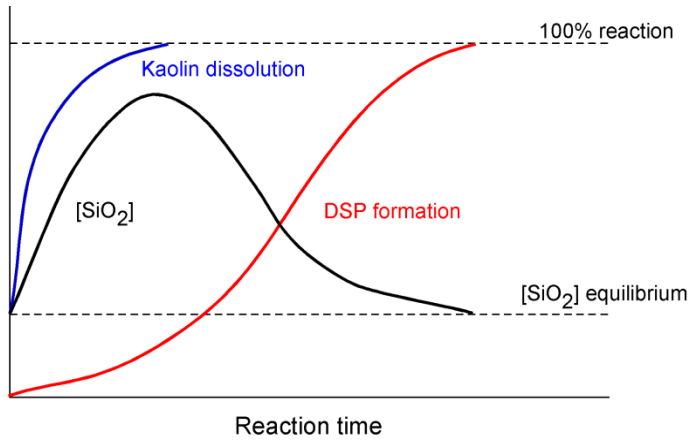


Figure 5.5. Schematic representations of kaolin dissolution, DSP formation and soluble silica concentration in Bayer liquor during pre-desilication. Adapted from Kotte (1981).

The rate of pre-desilication therefore depends on the rates of reactive silica (kaolin) dissolution and DSP precipitation, both determined by numerous factors. In addition to the temperature, the particle size and crystallinity play important roles in kaolin dissolution, with fine and poorly-crystalline kaolin dissolving more quickly than coarse and well-crystalline kaolin (Ostap 1985). For DSP formation, the supersaturation level achieved from kaolin dissolution, process temperature, solution composition and the presence of DSP seed particles determine the precipitation rate (Cousineau and Fulford 1987; Jamialahmadi and Müller-Steinhagen 1998; Kotte 1981; Oku and Yamada 1971; Smith et al. 2002). In operating plants, DSP seed

particles are often prepared separately and added to the pre-desilication reactors to promote precipitation.

Thomas and Pei (2007) modified the second-order pre-desilication kinetic equation from Duncan et al. (1995) to quantify the role of seed particles and proposed that the rate of reactive silica conversion to DSP can be written as:

$$\frac{dX}{dt} = k(1 - X)^2(\alpha + X) \qquad 5.3$$

where $X$ is the fraction of reactive silica that has been converted to DSP, $k$ is the pre-desilication rate constant and $\alpha$ is the amount of seed particles present in the starting material. More importantly, they also mentioned that the seed particles do not necessarily have to be DSP, as other minerals present could act as seed particles for initiating DSP formation. Oku and Yamada (1971) reported that a slightly higher pre-desilication rate was seen on increasing the bauxite residue concentration from 45 to 90 g $L^{-1}$, however, they did not compare these results to conditions without bauxite residue.

In relation to this study, it is important to clarify if iron oxide (hematite) promotes DSP nucleation during the initial period of precipitation and thereby changes the iron oxide surface properties. This can be accomplished by comparing the DSP precipitation rates in the absence and presence of iron oxide seed particles.

## *5.3 Experimental*

The experimental part of this study focused on two aspects: (i) synthesizing a variety of DSP-hematite slurries (through digestion) and (ii) comparing physicochemical properties of the slurries through settling tests, zeta potential analysis, desilication tests and SEM.

### 5.3.1 Materials

Figure 5.6 outlines the steps by which either *in-situ* prepared or physical mixtures of DSP and iron oxide were made. The difference between the two approaches is that kaolin was mixed with the iron oxide prior to hydrothermal (digestion) reaction if making an *in-situ* prepared DSP/iron oxide slurry. For producing the physical mixtures of DSP and iron oxide, iron oxide was only added after the hydrothermal conversion of kaolin to DSP reaches completion. The same fine hematite powder from Sigma Aldrich (Iron (III) oxide, ≥ 99%) described in the previous Chapter was used as the iron oxide model phase.

For *in-situ* DSP formation in the presence of a model phase, hematite and kaolin (Eckalite, Imerys Minerals) were mixed at a ratio of 3:1 and heated in the "digestion" liquor (C = 230 g $L^{-1}$, A/C = 0.35, C/S = 0.84 $SO_4^{2-}$ = 20 g $L^{-1}$, $Cl^-$ = 10 g $L^{-1}$) at a solids concentration of 60 g $L^{-1}$ and temperature of 90°C for 24 h in a bench top oven. Subsequent gravimetric measurement indicated the presence of ~31 wt/wt% DSP within the final product. The procedure for the liquor make-up follows the same details given in Section 4.3.

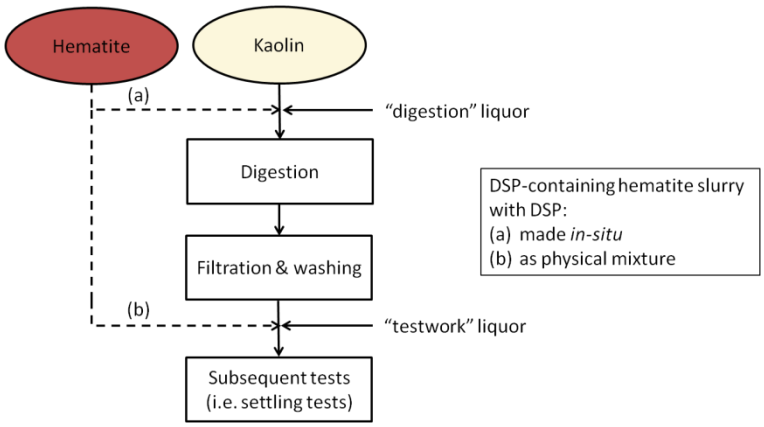


Figure 5.6. Schematic representation of the preparation of DSP-containing hematite slurry with DSP either made *in-situ* or added as a physical mixture.

To confirm that kaolin is fully transformed to DSP after reacting with "digestion" liquor at 90°C for 24 h, kaolin slurry reacted in the absence of hematite was sub-sampled and prepared for XRD phase identification. This preparation started with filtration of the sub-sample through a 0.45 μm pore size Supor®-450 membrane before washing the solids with 5×200 mL aliquots of hot deionised water to flush

anions/cations that may be physically adsorbed. The washed cake was then dried overnight at 105°C before being hand-ground. $CaF_2$ was added as an internal standard (~10 wt/wt%) and mixed during grinding. A Phillips X'pert diffractometer was used to generate diffractograms using Co Kα emission (λ = 1.7889 Angstrom); 2 theta (θ) diffraction angle measurements were acquired in a standard window of 5-90° (step size of 0.02° and step length of 1 s).

### 5.3.2 Settling tests

To remove any remaining soluble silica and ensure stability for settling tests, digested slurries were filtered (Supor®-450, 0.45 µm pore size membrane), and the solids were washed (5×200 mL aliquots of deionised water) before the "testwork" liquor was added (C = 230 g $L^{-1}$, A/C = 0.35, C/S = 0.99) to make a 5 wt/wt% solid solution. This replenished slurry was then allowed to equilibrate overnight (~18 h) at room temperature without stirring. Settling experiments were also conducted on slurries immediately after digestion, without involving filtration and washing, to confirm that differences seen when comparing *in-situ* prepared and physical mixture samples were not due to the preparation method.

To avoid slurry ageing and achieve stable dispersions, the stock slurry that had been equilibrated overnight was subjected to further treatments involving continuous stirring and sonication as explained below:

(1) stir at 700 rpm for one hour in the 2.5 L stainless beaker used in Section 4.3, fitted to the circulating water bath set at 70°C (Grant GR 150),

(2) stir at 300 rpm for another hour,

(3) transfer the slurry to 3 L plastic container using a hose clamped to a peristaltic pump (Cole-Parmer Masterflex L/S Easy Load model 7518-10),

(4) place the container filled with slurry inside the ultrasonic bath (Cole-Parmer 8853) containing hot water (70°C) and sonicate for 10 minutes,

(5) pour the slurry back to stainless steel beaker,

(6) stir at 450 rpm and 70°C for 5 minutes,

(7) transfer into 250 mL graduated cylinders (Azlon M101198, diameter: 3.5 cm and height: 23.5 cm),

(8) place the cylinders in an aquarium filled with polyethylene glycol whose temperature is maintained at 95°C by a Grant immersion thermo-control unit (a slurry temperature of 95°C was achieved in 15 minutes),

(9) apply 5 plunger strokes to equilibrate prior to flocculant addition.

The equipment set-up for slurry preparation (stirring and sonication) is captured in Figure 5.7. The aquarium acting as an oil bath in which settling tests were carried out is shown in Figure 5.8a. The plunger used throughout this Chapter consisted of a 3.5 cm diameter stainless steel disc with six inner radial holes of 0.7 cm diameter at the end of a shaft 47 cm long, 0.7 cm in diameter (Figure 5.8b).

(a)

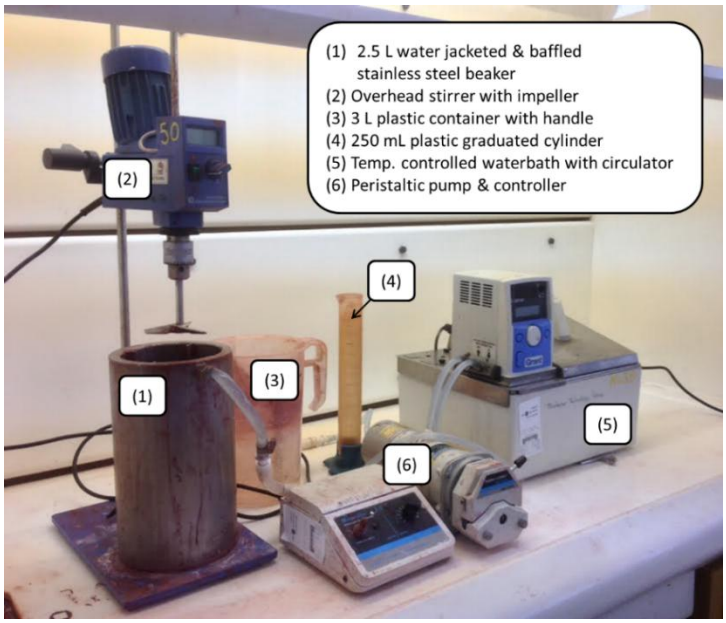


(b)

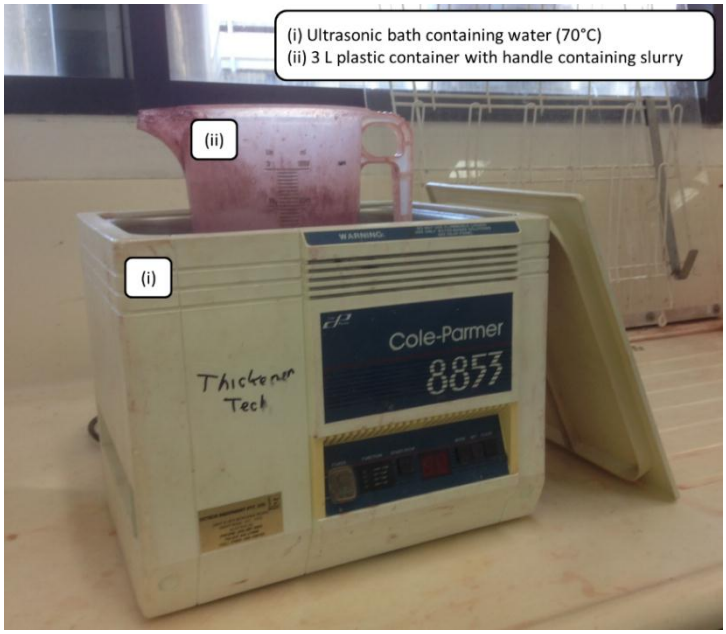


Figure 5.7. Equipment set-up for slurry preparation: (a) stirring and (b) sonication.

(a)

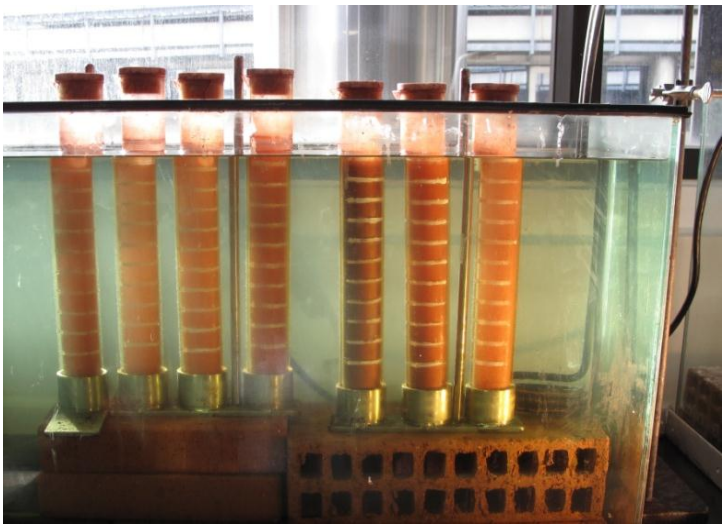

(b)

Figure 5.8. Settling test equipments used throughout this Chapter: (a) temperature controlled oil bath and (b) plunger.

Only one flocculant (Alclar 665, BASF) was considered in settling tests related to studying the effect of DSP origin. The flocculant stock solution (0.5 wt/wt%) was made-up following the procedure in Section 4.3. Stock solutions were diluted in 20 g $L^{-1}$ NaOH to 0.025% prior to use. The 0.025% flocculant solution (at 45°C) was added as a single dose to the slurry within a measuring cylinder and mixed with five plunger strokes (a single "stroke" considered as both down and up movements of the plunger).

Settling rates were calculated from the initial linear portion of the plot of mud-line height vs. time. To measure the supernatant solids concentration, a 20 mL sample of supernatant solution was taken from a given height (~4.5 cm from the top of solution level) 60 s after the last plunger stroke (or immediately after the mud-line passes that point in slow settling cases). This sample was vacuum filtered through a 0.45 µm

membrane filter, washed by hot deionised water (2×100 mL) to remove all salts and the solids then determined gravimetrically (dried in an oven at 105°C). Consolidation behaviour was quantified from the bed height after 0.5 h.

*Note that gravimetric analysis applied to small sample size (~20 mL) causes large variability in the results. 1 mg difference in such sample size is translated as 50 ppm difference in supernatant solids concentration. Therefore, a difference of supernatant solids concentration that lies within the range of 50-100 ppm may not be sufficient to prove that the fine capture efficiency is better in one test when compared to the other.*

### 5.3.3 Zeta potential measurements

Electrophoretic mobility measurements were carried out with a Malvern Zetasizer ZS that combines both Laser Doppler Velocimetry (LDV) and Phase Analysis Light Scattering (PALS) methods for enhanced sensitivity in measuring very low mobility samples. Under controlled conditions within the U-shaped zeta cell (represented in Figure 5.9), applying a potential will make charged particles travel along the provided pathway to approach the oppositely charged electrode. A laser beam is fired at a particular point where any intersection with a travelling particle will create a scattered beam (see Figure 5.9b). The properties of the scattered beam can be further analysed, as its frequency or phase shift will be proportional to the velocity of the particles (Malvern 2004).

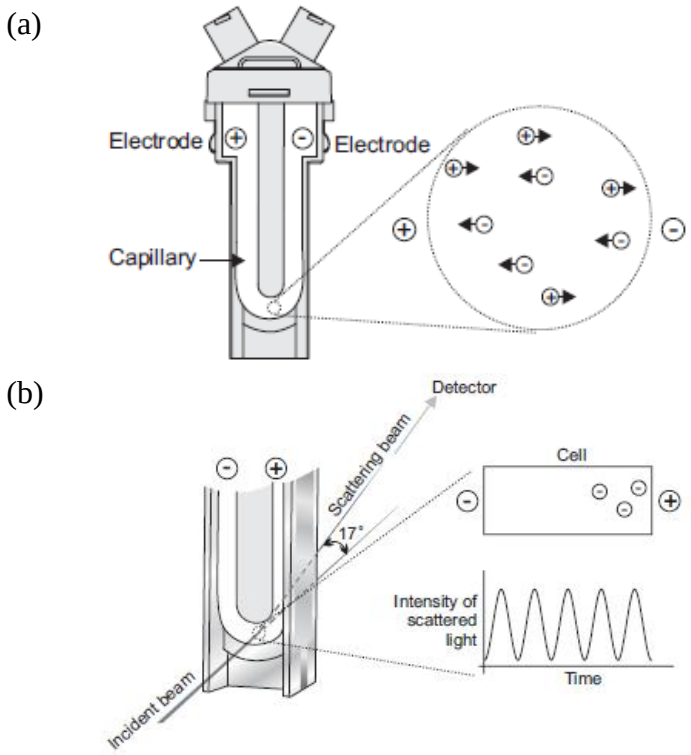


Figure 5.9. Schematic representations of: (a) particle movement in the U-shaped zeta cell and (b) intensity of light scattered as incident beam collides with moving particle. Reproduced from Malvern (2004).

In LDV, the Doppler frequency shift is used to back-calculate the particle velocity, while in PALS technology, the phase shift caused by the interaction of laser beam and moving particle is compared to the phase of a reference beam (Malvern 2004). In addition to measuring electrophoretic mobility, phase analysis is also claimed to be able to separate other effects, such as thermal drifts.

Electrophoretic mobility measurements are difficult to obtain in high ionic strength liquors (such as Bayer liquor), a consequence of the large current required and its resultant distortion of particle movement (Kosmulski and Rosenholm 2004). Therefore, the filtration and washing steps performed for settling tests were also required before the cake was re-suspended in 0.01 M NaCl (ambient temperature) and sub-sampled for the mobility measurement. In such dilute NaCl solutions, the physical properties of pure water, such as dielectric constant and viscosity, can be used in the calculations without introducing significant errors. For all zeta potential determination experiments, the hematite:kaolin ratio in the digestion process was

fixed at 10:1, giving a final product containing ~11 wt/wt% DSP (from gravimetric measurement).

The iep values for various hematite samples have been reported to range from 5.5 to 9.3 (Kosmulski 2011). Zeta potential determinations were therefore conducted on pure hematite, pure DSP and their mixtures over a pH range of 5 to 11. Sodalite will start to dissolve at a pH less than 5.5 (Hongting et al. 2004), and accordingly, the measurements were done immediately (well within 10 minutes) after pH adjustment. The procedure of pH control involved drop-wise addition of 0.005 M HCl or NaOH solution, with pH measurements by an Orion SA 720 pH meter equipped with an Ionide IJ44 pH probe that was calibrated prior to use.

Zeta potential measurements at every pH unit from 5-11 were repeated four times for each of the following samples: pure hematite, pure DSP, the *in-situ* prepared DSP/hematite and the physical mixture of DSP and hematite. Standard deviations resulting from repeat measurements were calculated and plotted as the error bars.

### 5.3.4 Desilication kinetics

It was stated in Section 5.2.2 that comparing the DSP precipitation rate in the presence and absence of hematite can reveal whether hematite has a tendency to promote DSP nucleation. In practice, such experiments are not straight-forward to achieve – as any unreacted kaolin might also behave as a seed material and mask the efficacy of iron oxide seeding precipitation. Hence, kaolin cannot be employed as a source of soluble silica and precipitation rates were measured in barren liquor in which a known soluble silica concentration could be achieved. Both silicic acid and sodium metasilicate dissolve in Bayer liquor and there was no implication that the former was an optimised selection. Note that for all experiments other than precipitation kinetics (settling tests, zeta potential measurements and SEM studies), the use of kaolin as a source of soluble silica does not complicate any of the results obtained.

Batch precipitation tests in "testwork" liquor doped with $SiO_2$ = 2 g $L^{-1}$ from dissolving silicic acid (precipitation time: 2.5-30 minutes) were conducted. Preliminary tests performed at 90°C in a stirred beaker showed that the unseeded desilication rate from soluble silica sources was very slow (~0% conversion after 8 h). Hence, the temperature was raised to 150°C by using a 250 mL stainless bomb (diameter 4.3 cm and height 13 cm) connected to a thermocontroller and heated by a gas-fired flame while rotating. Photographs of the stainless bomb and the thermocontrolled gas-fired chamber are given in Figure 5.10a and b, respectively.

(a) (b)

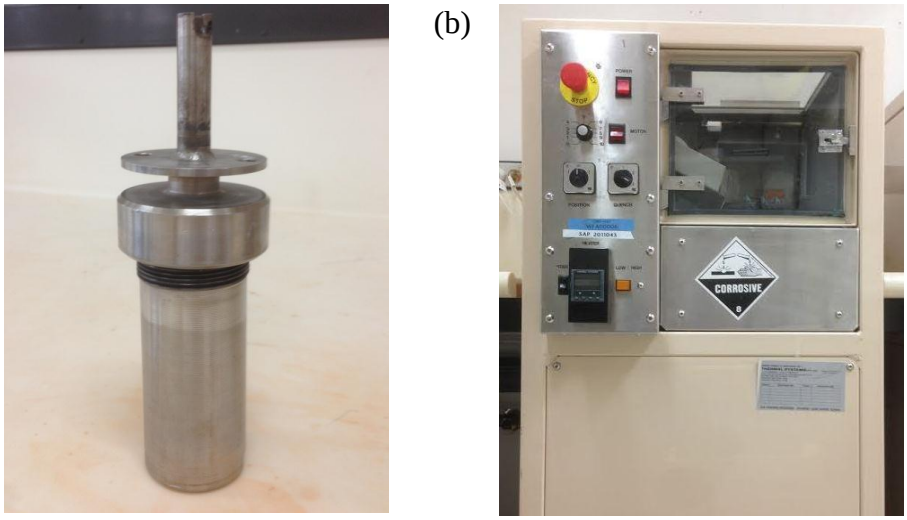


Figure 5.10. (a) Stainless steel bomb and (b) gas fired reactor.

After a specific reaction time, the bomb was quenched with a continuous cold water spray to 40°C for subsequent safe handling. The pulp was then removed and filtered through a Supor®-450 0.45 μm pore size membrane, with the filtrate centrifuged for 10 minutes to achieve a clear solution free from colloidal particles. The soluble silica concentration in this solution was determined by inductively coupled plasma – atomic emission spectrometer (ICP-AES), using an Agilent model 735-ES instrument.

### 5.3.5 SEM examination

Visual evidence for deposition and/or growth of DSP on a hematite surface was sought from SEM examination. The flat surface ideally required for SEM was provided by polishing a natural hematite rock sample (obtained from Mt Newman)

mounted in high-temperature resistant resin on 400 and then 1200 grit sandpapers. Reaction of this hematite slab in the presence of 40 g $L^{-1}$ kaolin was carried out for 24 h at 90°C in the "digestion" liquor to generate the post-desilication surface profile.

After this simulated digestion, the slab was sonicated for 10 minutes in an ultrasonic cleaner to release physically attached DSP. Its surface was rinsed and carbon coated (5 nm) prior to viewing on an Evo Zeiss SEM instrument. In addition, Energy Dispersive X-ray spectroscopy (EDX) was used to determine elemental composition, with the data collected at a working distance of 9.5 mm at a voltage of 15 or 20 kV.

## *5.4 Results and discussion*

### 5.4.1 XRD analysis

The XRD profile of sodalite formed at 90°C is presented in Figure 5.11. From the peak matching results relative to the kaolin pattern, it is clear, without the need for detailed quantitative analysis, that the reaction conditions (90°C for 24 h) have converted all kaolin to sodalite (89-843 and 24-1045 are variants of DSP found in Inorganic Crystal Structure Database which match the collected patterns). A trace amount of muscovite was evident, but any cancrinite was below the detection limit of XRD (< 1 wt/wt%). Muscovite formed during desilication in the presence of kaolin in synthetic Bayer liquor is also reported by Jones (1998). No cancrinite was found in the XRD pattern and this agrees with observations from other researchers that propose cancrinite forms through the slow transformation of sodalite, a process which can be accelerated by increasing the process temperature (≥ 200°C) or by adding calcium (Croker et al. 2008; Radomirovic et al. 2013; Whittington et al. 1998; Xu et al. 2009; 2010; Zheng et al. 1997). That sodalite is the dominant DSP phase makes data rationalisation throughout this study less complicated.

During precipitation kinetics experiments, the reaction temperature must be raised to 150°C due to the very slow precipitation rate that hampered both the seeded and unseeded conditions reactions at 90°C. Figure 5.12 displays the XRD profile of the sodalite produced at 150°C. Note that although the precipitation temperature was

raised from 90 to 150°C, it did not change the DSP phase formed, with XRD results showing that sodalite was still the only DSP phase detected (see Figure 5.12) and although it is not shown here, the presence of residual kaolin was very minimal, as in the case of reactions at 90°C for 24 h.

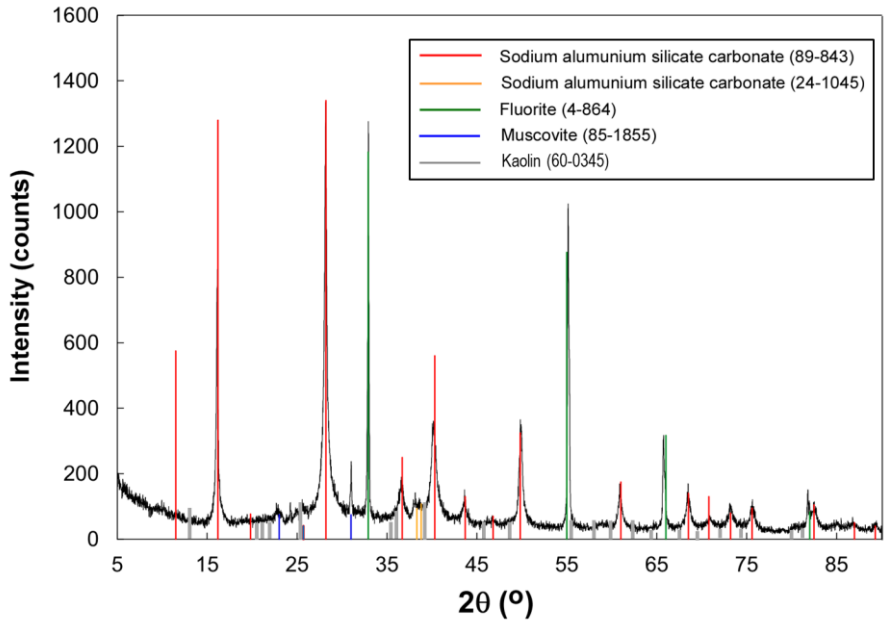


Figure 5.11. XRD pattern and phase identification of DSP sample made from reaction of kaolin with "digestion" liquor at 90°C for 24 h: (a) without and (b) with kaolin pattern (in red). Fluorite was the internal standard.

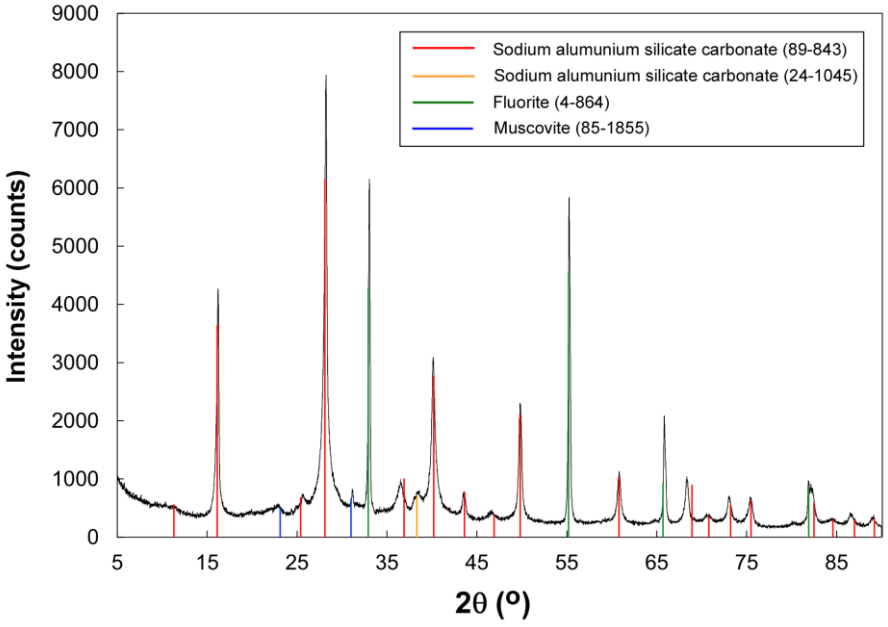


Figure 5.12. XRD pattern and phase identification of DSP sample made from reaction of kaolin with "digestion" liquor at 150°C for 30 minutes. Fluorite was the internal standard.

### 5.4.2 Settling test results

Figure 5.13 shows the settling rates results for DSP/hematite slurries prepared by the different methods. For comparison, the settling rates of pure hematite slurry are also shown at the same figure. The settling rates of pure DSP slurry could not be presented as it was too cloudy to measure the mudline. The settling rates of hematite and DSP as a physical mixture were higher than when DSP was made *in-situ* although they were still lower than those measured from the pure hematite slurry. Pre-treatment that included filtering, washing and replenishing with fresh testwork liquor did not change the trend of higher settling rate given by the physical mixture.

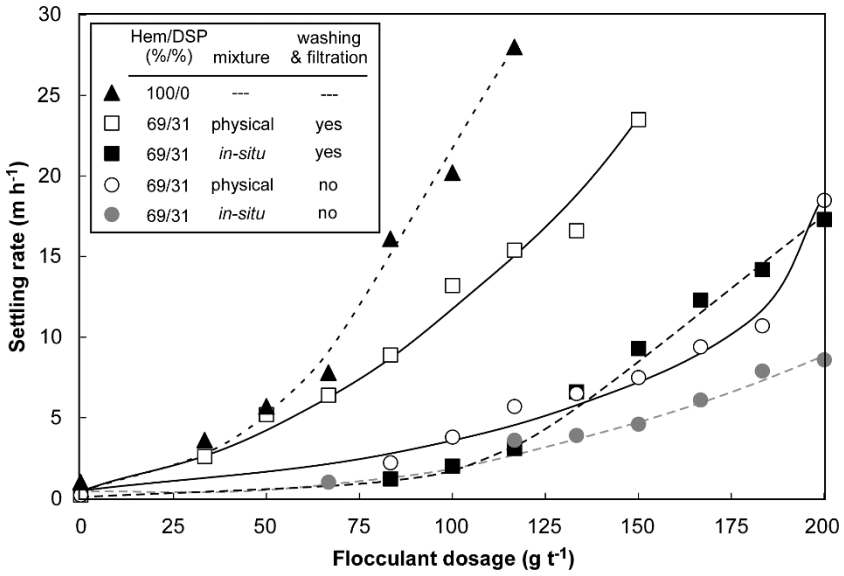


Figure 5.13. Settling rate vs. dosage for hematite and DSP slurries. Series refer to Table 5.1, solids concentration = 5 wt/wt%.

While the post flocculation supernatant solids are within experimental error for the DSP/hematite slurries prepared by different methods, the settled bed heights were also generally higher when DSP was made in the presence of hematite (Table 5.1). All the above results demonstrate that there is a surface interaction between the DSP and hematite phases during DSP formation that changes the surface properties of hematite, resulting in a different response during flocculation.

Table 5.1. Settling properties of hematite and DSP slurries at 5 wt/wt% solids concentration.

| Mixture | Washing & filtration | Settling rate ($m\ h^{-1}$) | Supernatant solids (ppm) | Bed height (mL) | Dosage ($g\ t^{-1}$) |
|---|---|---|---|---|---|
| *In-situ* | Yes | 9.3 | 410 | 72 | 150 |
| Physical | Yes | 23.5 | 430 | 61 | 150 |
| *In-situ* | No | 8.6 | 340 | 84 | 200 |
| Physical | No | 18.5 | 380 | 81 | 200 |

The difference in settling rate was less pronounced in the absence of washing and filtration (Figure 5.13 and Table 5.1) but was still discernible across the full dosage range. This may be due to the deleterious effect of remnant silica, as reported by Jones (1998), where dissolved silica is adsorbed onto hematite and decreases the settling rate proportionally. Liquor analysis proved there was ~120-130 ppm of $SiO_2$ in the unwashed slurry samples; Jones (1998) attributed a substantial reduction in settling rate (~10 $m\ h^{-1}$) to similar levels of solution $SiO_2$.

Focusing on the results where washing and filtration were applied, decent settling rates of ~15 $m\ h^{-1}$ were achievable although the *in-situ* prepared DSP/hematite slurry required at least 50% extra flocculant when compared to the physical mixture of DSP and hematite (see square data points with and without shading in Figure 5.13). In fact, the physical mixture of DSP and hematite that was filtered and washed behaved quite similar to the pure hematite slurry except that the settling rate response to the flocculant dosage curve was not as steep as that in the pure hematite slurry. At this point it can only be surmised that the surface interaction mentioned previously is a consequence of DSP formation (precipitation) at the active sites of hematite, blinding some of them during contact with flocculant and therefore creating the need for higher flocculant dosage to improve its collision efficiency. Chapter 6 considers in more detail the aspect of flocculant adsorption.

### 5.4.3 Zeta potential determination

The real challenge of interpreting zeta potentials for the *in-situ* prepared DSP/hematite slurry lies in distinguishing the hematite particles, which could be partly or completely covered by DSP nuclei and mimic the behaviour of DSP, from

distinct DSP particles. A characteristic observed from PSD measurements (procedures given in Section 4.3) is that hematite is typically 0.1-10 µm and synthetic DSP 0.3-40 µm. The PSDs of hematite and synthetic DSP are contrasted in Figure 5.14a and b, respectively. This difference in PSD provides some scope for isolating hematite particles with a diameter of less than 0.3 µm, which might possibly be covered by DSP.

By filtering hematite slurry through a 0.3 µm membrane, a small fraction of very fine hematite particles (< 0.3 µm) will go to the filtrate. If this principle is used for the *in-situ* prepared DSP/hematite slurry, very fine hematite (potentially) with DSP at its surface can also pass through the membrane while any distinct DSP will remain on the membrane filter as its size is larger > 0.3 µm. If the filtered suspension (< 0.3 µm) has only pristine hematite (i.e. no hematite with DSP at its surface), the measured zeta potential will likely be identical to that of pure hematite. However, if it does contain a fraction of hematite with DSP at its surface, the filtered suspension zeta potential will be a blend of that from pure hematite and pure DSP.

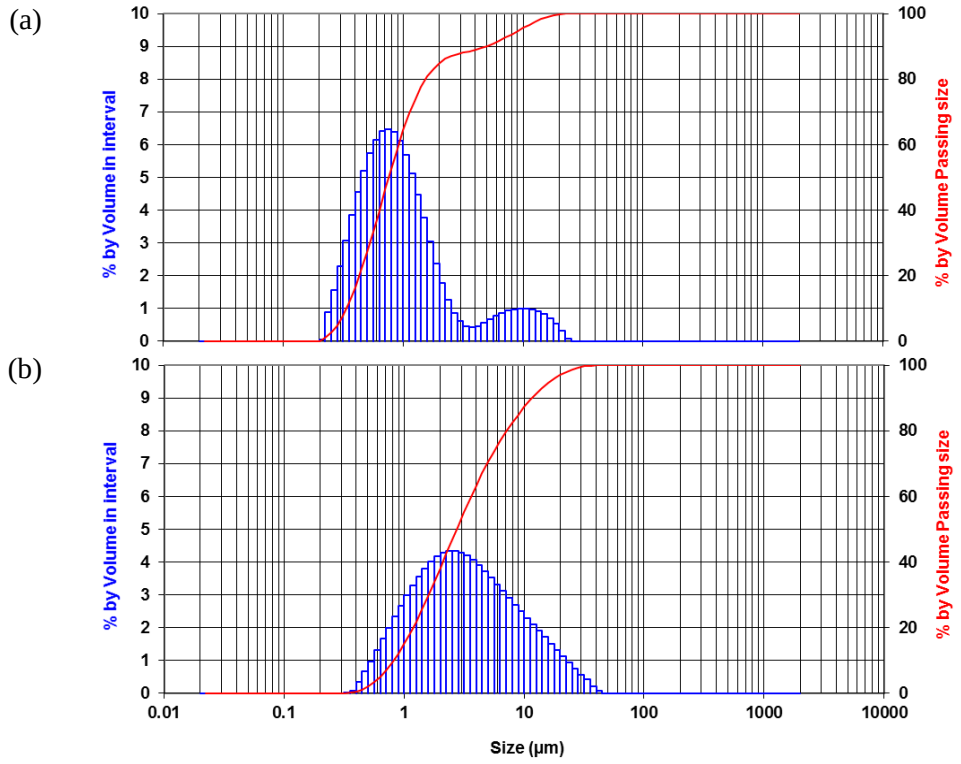


Figure 5.14. Particle size distributions for: (a) hematite model phase and (b) pure DSP as measured by laser sizing in deionised water.

For other substrate samples (physical mixtures of DSP and hematite, pure DSP and pure hematite), a 5 μm membrane was used to generate suspensions with a narrow size distribution, as coarse particles tend to settle within the cell used for electrophoretic mobility measurements during transport under an applied voltage.

Figure 5.15 shows the zeta potential of the (i) digested hematite, (ii) physical mixture of DSP and hematite, (iii) *in-situ* prepared DSP/hematite and (iv) pure DSP suspended solids as a function of pH. For pure hematite the zeta potential was ~15 mV at pH 5, gradually decreasing to approximately -25 mV at pH 11. The iep was observed to be in between pH 6-7, as the zeta potentials at both pH values were very close to zero.

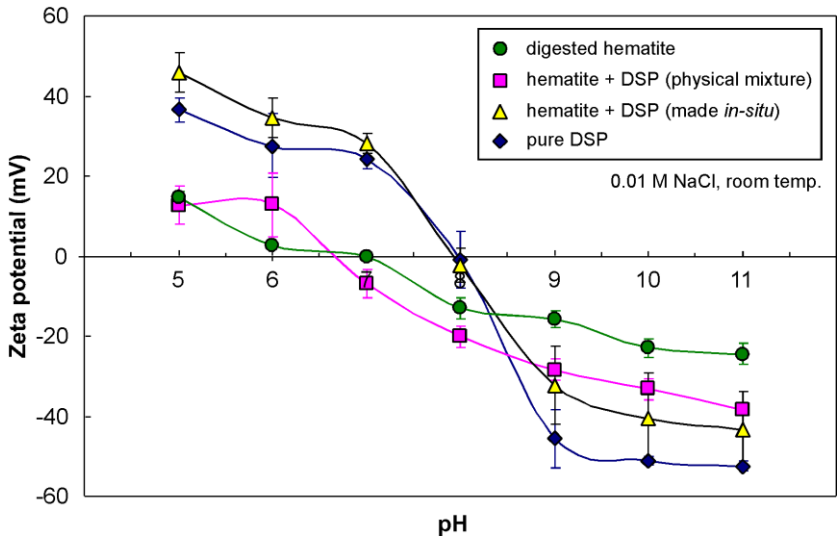


Figure 5.15. Measured zeta potentials of hematite and other suspensions as a function of pH.

The zeta potential of hematite as a function of pH has been reported in numerous studies which are available for comparison. The study conducted under conditions close to those in this Chapter are those from Pan et al. (2004). In their case, pure hematite (< 5 μm) was suspended in 0.03 M NaCl for zeta potential determinations from pH 3 to 11. At pH 5 and 11, the zeta potentials measured were 20 mV and -25 mV, respectively, with the iep reached at pH 7. This is very similar to the behaviour derived from the present measurements. Other studies reported higher iep (i.e. Kirwan et al. 2004 observed the iep of colloidal hematite at pH 10). However,

those studies were conducted in conditions that were totally different from the present work, making the comparison questionable.

The zeta potentials of *in-situ* prepared DSP/hematite slurries (≤ 0.3 μm) were very similar in magnitude to those of pure DSP, whereas those of the physical mixture of DSP and hematite appeared to represent a combination between the values of the pure phases. The fact that there was a substantial difference between the zeta potential of digested hematite and that of the *in-situ* prepared DSP/hematite is evidence of a proportion of hematite particles with surface properties different from pristine hematite. This observation also extends to the iep values, which increased in the order: hematite (6-7) < physical mixture DSP/hematite (6.5-7) < *in-situ* prepared DSP/hematite (8) ≈ pure DSP (8). It can then be inferred that DSP, to at least some extent, coats the surface of the hematite solids.

The magnitude of zeta potential for the different phases is also of interest. The zeta potentials of hematite over the pH range examined lies within a band from 20 to -20 mV while that for DSP from 40 to -50 mV. If values within ±30 mV are said to represent systems amenable to coagulation (Section 5.2.1), DSP may then display a high tendency to remain dispersed. However, it must be remembered that these zeta potential measurements were conducted in a low ionic strength matrix (0.01 M NaCl). According to Siebentritt et al. (2014), the zeta potential of hematite in 0.01 M NaOH (pH = 12) can be in the range -50 to -80 mV, however, increasing the NaOH concentration to 1 M brought the zeta potential to the region of 1-5 mV, well within the range for coagulation.

Coagulation of hematite by increasing salt concentrations was demonstrated in Section 4.4.1. Similar to hematite, DSP is also expected to coagulate in high ionic strength solutions, such as Bayer liquor. Therefore, zeta potentials reported in this Chapter do not represent those measured in typical Bayer liquor since the cation screening effect given by the high ionic strength Bayer liquor will make the zeta potential of any solid sample closer to zero (Sections 2.1.1 and 5.2.1), with less differentiation among various mineralogies. The zeta potential values reported in this

Chapter are merely used to distinguish hematite particles, which are likely to be covered by DSP on its surface.

The iep for the pure DSP suspension is higher than most published values for silica or kaolin (e.g. Kosmulski 2011). However, the iep of the DSP/hematite suspensions for both the physical mixture or when DSP was made *in-situ* fall within the expected range of 6.5-8.5 for bauxite residues samples. The DSP presence also shifts the iep of hematite to higher pH, as reported in the DSP-rich bauxite residue (Liu et al. 2013).

### 5.4.4 DSP precipitation kinetics

Figure 5.16 contrasts the results from DSP precipitation kinetics experiments conducted in the presence and absence of hematite as a seeding phase. The percentage conversion of soluble silica and the depletion of the soluble silica concentration are plotted as a function of reaction time in Figure 5.16a and b, respectively.

In general, the precipitation behaviour at 150°C for both seeded and unseeded conditions from a dissolved silica source followed the classical precipitation behaviour, initially being relatively fast before slowing as approaching an equilibrium level. Under unseeded conditions, a typical S-curve was observed as a result of an initial slow reaction rate, when only few DSP particles were present and not sufficient to act as seed particles (Kotte 1981). The precipitation rate increases proportionally once there are enough DSP particles in the system to act as seeds (Equation 5.3; Thomas and Pei 2007).

It is then hardly surprising that an S-curve response was not observed under seeded conditions where sufficient hematite particles are present from the beginning. After only 2.5 minutes, remarkably contrasting behaviour was observed, with the seeded experiment achieving 58% conversion (precipitation) compared to only 1% in the unseeded case (Figure 5.16a). When those numbers are presented as the remaining $SiO_2$ concentration, they represent 844 vs. 1990 ppm in the seeded and unseeded experiments, respectively (Figure 5.16b). The differential in this silica concentration

became smaller as both cases approached ~75% desilication. Like the zeta potential results, the desilication experiment also indicates that hematite seed particles may partly be covered by DSP since they gave a seeding effect during precipitation.

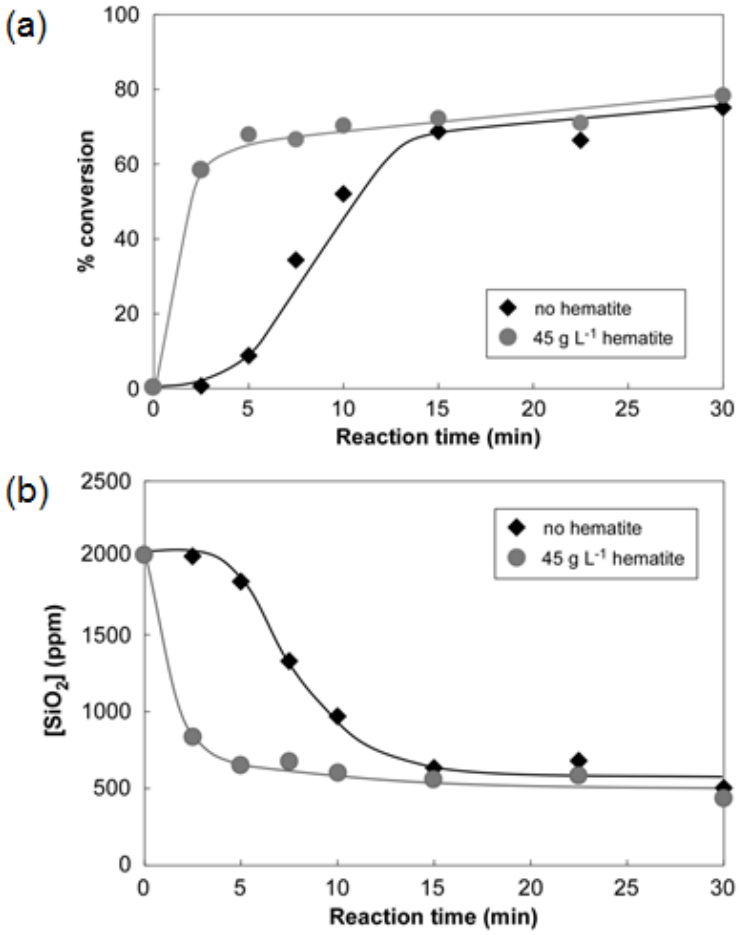


Figure 5.16. Desilication results in the presence and absence of hematite, expressed as (a) % conversion and (b) $SiO_2$ concentration in solution as a function of time.

The post-desilication concentrations of soluble silica at prolonged reaction times were very similar in each case, regardless of any rate acceleration from the action of the seed particles. The soluble silica concentration in both seeded and unseeded experiments was still declining at a very slow rate after 25 minutes at 150°C, suggesting that the solubility limit was not reached yet. Although it was not achieved in this experiment, the solubility limit of DSP is determined by the solution composition and the temperature and not affected by the precipitation kinetics (Barnes et al. 1999a; Cresswell 1983; Jamialahmadi and Müller-Steinhagen 1998; Oku and Yamada 1971; Smith et al. 2002).

### 5.4.5 SEM Examination

Typical SEM images of the hematite surfaces before and after desilication are shown in Figure 5.17a and b, respectively. The post-desilication surface clearly shows the appearance of nodules on the hematite surface. There is a much greater likelihood that those nodules are DSP rather than hematite, considering the very minimal extent of hematite dissolution and precipitation expected within a highly alkaline medium (Basu 1983; Basu et al. 1986). The authors reported that iron solubility in caustic solution with C = 250-350 g $L^{-1}$ is very low (< 10 ppm) even at 150°C, therefore iron oxide dissolution and re-precipitation could at best be very minor. Hence, the present work strongly suggests that the formation of DSP can occur via heterogeneous nucleation on hematite.

(a)

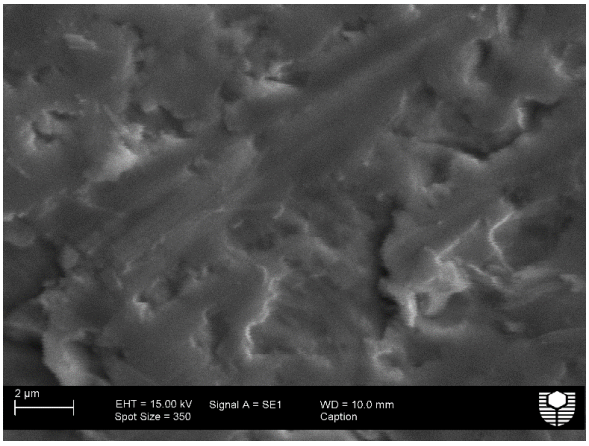


(b)

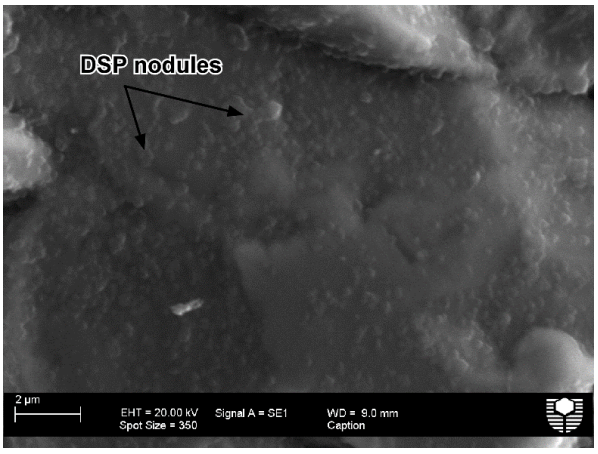


Figure 5.17. SEM of hematite surface: (A) before and (B) after desilication (magnification ×4000).

In addition, the sample preparation steps that involved sonication and rinsing of the surface effectively rule out the possibility that those nodules exist because of the physical adsorption of DSP onto the surface of iron oxide. Analysis by EDS failed to observe any localisation of silicon and aluminium content at those nodules; in fact, both elements were found to be evenly distributed across the area examined. This could be due to a thin layer of DSP covering the surface of hematite, explaining why the texture of post-desilicated surface looked less sharp than its original appearance. It is also worth noting that the surface area of natural hematite rock exposed in the desilication was very limited (~4 $cm^2$). Therefore, it is still an open question if all hematite particles in the *in-situ* prepared DSP/hematite slurry will be completely covered by DSP.

From the PSD of the *in-situ* prepared DSP/hematite slurries presented in Figure 5.18, it is immediately clear that the presence of DSP increased the population of 2-20 μm particles when compared to the original PSD of the pure hematite in Figure 5.13a. This could be due to the continuous growth of DSP on the hematite seed particles or precipitation of DSP as distinct particles (see Figure 5.16).

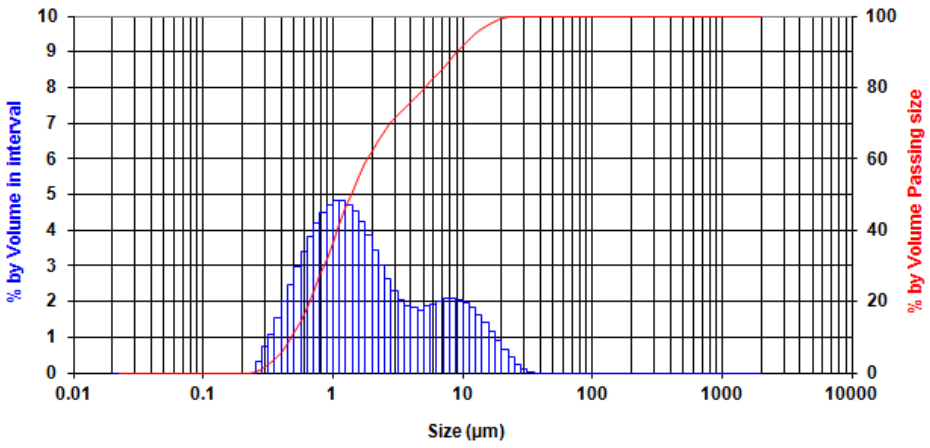


Figure 5.18. Particle size distributions for the *in-situ* prepared DSP/hematite slurry (31 wt/wt% DSP) as measured by laser sizing in deionised water.

Interestingly, the results from SEM imaging differ from those published by Ho et al. (1992), in which SEM applied to bauxite residue particles gave an indication of iron oxide particles "coating" the DSP particles. The existence of submicron hematite particles adjacent to the larger DSP particle could be interpreted as coating. This was

a noted obstacle in the preliminary experiments conducted in this study and a motivation for using a flat hematite surface for electron microscopy analysis. Such a surface gives results that are more easily interpreted and do not suffer from the complication of the size differential issue mentioned above.

## *5.5 Summary*

The work described in this Chapter addressed the need to better understand DSP formation in the presence of iron oxide from the flocculation point of view. From the desilication kinetics experiment it was demonstrated that hematite, as an iron oxide model phase for bauxite residue, can act as an effective seed for DSP precipitation. In fact, the % conversion of soluble silica to DSP was almost a magnitude higher when hematite was present at the initial precipitation stage. Visual evidence of DSP formation at the surface of hematite was derived from the SEM examination applied to a flat hematite surface that had undergone desilication reaction. DSP proliferation on this surface changes the hematite surface chemistry, as detected during the zeta potential measurements. Changes in the surface properties of hematite result in lower settling rates in flocculation tests.

SEM examination applied to the post-desilicated surface of hematite rock (~4 $cm^2$) indicated complete coverage of hematite surface by DSP. There is no implication that a similar observation will be met in the *in-situ* prepared DSP/hematite slurries where fine hematite particles contributed to the large surface area. Meanwhile, PSD measurements hinted that DSP might also precipitate and grow as distinct particles. Having DSP at the surface of hematite and as distinct particles influences aggregate properties, as will be discussed in Chapter 6. A lower settling rate itself is an indication of a changed flocculant-solid interaction when DSP partially covers the surface of hematite, a domino effect from DSP formation in the presence of hematite. More detail about the adsorption of flocculant onto the surface of hematite and DSP is also given in Chapter 6.

# 6 The impact of desilication products on flocculation

## *6.1 Introduction*

Throughout the discussion in Chapter 2, it is explained that the presence of DSP in bauxite residue creates problems in primary thickening. The problems are clear-cut, involving decreased settling rate, poor overflow clarity and low underflow solids density – all impacting on the success of the thickening process. However, little is known about the mechanism by which DSP has this impact. The reason behind this is that to date, there has been no systematic study that attempted to:

(i) gain insights into the flocculation mechanism over a wide range of solids concentrations.

To compare settling behaviour at only a single fixed solids concentration is a major flaw in many flocculation studies. Changes in particle size and aggregate structure both alter the flocculation response, and this can only be properly captured by quantifying flocculation at a range of solids concentrations.

(ii) identify the change in aggregate characteristic caused by the presence of DSP in bauxite residue.

Batch settling is the most practical way to study flocculation under different conditions. However, the flocculation measures obtained (settling rate, supernatant solids and settled bed height) do not provide direct information about an aggregates' intrinsic properties.

(iii) study the adsorption of flocculant onto the DSP-containing bauxite residue.

This aspect is extremely important, as it was demonstrated in Chapter 5 that DSP partially covers the surface of iron oxide, and this would decrease the extent of flocculant adsorption if DSP has a lower affinity for carboxylate or hydroxamate functionalities.

### 6.1.1 Effect of DSP content with *in-situ* prepared DSP

The study of the fundamental aspects of how increasing DSP content affects primary bauxite residue thickening is of growing interest, due to the anticipated further decline in bauxite feed quality (higher reactive silica content – Section 1.3). From all published literature on the impacts of DSP on bauxite residue thickening (e.g. Dai et al. 2010; Davis et al. 2010a, 2010b; Liu et al. 1994; Roach et al. 1989; Rousseaux et al. 2004; Yamada et al. 1980), only Dai et al. (2008) and Davis et al. (2010b) considered varying the relative ratio of bauxite residue and pre-made DSP. In addition to their *ex-situ* DSP formation method not representing the process as it occurs in a refinery, their batch settling tests were also done at fixed flocculant dosages. Although a decline in settling rate due to increased DSP content mixture was evident, the absence of dosage and settling rate response curves for different DSP contents means full rationalisation of the results cannot be satisfactorily undertaken.

As an example, the settling rate resulting from the addition of 250 g $t^{-1}$ HX PAM decreased from ~25 to ~5 m $h^{-1}$ when the proportion of DSP in the mixture increased from 0 to 40 wt/wt% (Dai et al. 2008). However, it was not confirmed whether increasing the flocculant dosage would significantly improve the settling rate. In a separate study; Davis et al. (2010a) reported that the detrimental effect on settling rate cannot be overcome by the addition of more flocculant.

### 6.1.2 Effect of solids concentration with *in-situ* prepared DSP

The importance of solids concentration in promoting or hindering flocculation is discussed in Section 2.1.5. Table 6.1 compiles previous studies relevant to bauxite residue primary thickening, and shows that the majority were conducted at a fixed solids concentration. For specific purposes, such as investigating flocculant ageing, fixing the solids concentration is perhaps the easiest approach and may be acceptable, provided the concentration is not too high. However, examining a single fixed solids concentration is certainly not sufficient for providing mechanistic information related to flocculation. Phillips and O'Brien (2006) varied the solids concentration to compare the performance of two different flocculants and noticed

that the difference, which was not seen in low solids concentration, became substantial when solids concentration was increased. This suggested that the flocculants had different optimum solids concentrations.

Table 6.1. Selected bauxite residue flocculation studies.

| | Solids concentration | | Solution composition | | | T |
|---|---|---|---|---|---|---|
| | g $L^{-1}$ | wt/wt % | C (g $L^{-1}$) | A/C | C/S | (°C) |
| Yamada et al. (1980) | 30 | - | 205 | 0.60 | - | 95 |
| Basu (1983) | 30 | - | 243 | 0.24 | | 90 |
| Sato et al. (1984) | 83 | - | 70 | - | - | 90 |
| Connelly et al. (1986) | - | 4.5-28.5 | | N/R | | N/R |
| Hunter et al. (1991) | 25 | - | 265 | - | 0.84 | N/R |
| Perrier et al. (1999) | N/R | - | | primary thickener feed | | N/R |
| Jones (1998) | 60-120 | - | 100 | 0.3 | 0.9 | 95 |
| Li (1998) | 33-43 | - | 200-300 | 0.60 | - | 103 |
| Phillips (1999) | 40 | - | | plant slurry | | N/R |
| Gagnon et al. (2001) | 50 | - | 13 | - | 0.30 | 21 |
| Rousseaux et al. (2004) | 40-74 | - | | primary thickener feed | | N/R |
| Normandin et al. (2006) | 50 | - | 13 | - | 0.30 | 21 |
| Phillips and O'Brien (2006) | 55-100 | - | | washer slurry | | N/R |
| Dai et al. (2008) | 40 | - | 235 | 0.60 | 0.85 | 100 |
| Kirwan (2009a) | 40 | - | | primary thickener feed | | 95 |
| Kirwan (2009b) | 20-80 | - | 64 | - | - | room temp. |
| Dai et al. (2010) | 98 | - | | primary thickener feed | | N/R |
| Davis et al. (2010a) | 40 | - | | primary thickener feed | | 95 |
| | | | | lab digested slurry | | |
| Davis et al. (2010b) | 40 | - | 277 | 0.69 | 0.87 | 100 |
| Arslan et al. (2012) | N/R | - | | N/R | | 95 |
| Soliz et al. (2012) | N/R | - | | primary thickener feed | | N/R |

Note: Except for Jones (1998) who used hematite, all studies used bauxite residue; synthetic liquors were used unless stated otherwise; N/R: not reported.

There are only a few open access studies which have looked at the flocculation of bauxite residue over a range of solids concentrations. Often those studies were not done under conditions (solution compositions or temperature) that represent primary thickening (e.g. Kirwan 2009b; Phillips and O'Brien 2006). Studies that tested at high sodium aluminate concentrations ($\geq$ 100 g $L^{-1}$ C) and at elevated temperatures ($\geq$ 90°C) were not focusing on the effect of DSP (e.g. Jones 1998; Li 1998). Therefore, a primary objective in the present study is to assess the effect of solids concentration on the flocculation of the hematite model substrate, both in the absence

and presence of DSP. This may help in identifying the optimum solids concentration for flocculation, which is expected to change because of the presence of DSP in the solid phases.

### 6.1.3 Aggregate characteristics

The intrinsic properties of aggregates (size, density, etc.) are known to greatly influence the settling characteristic of flocculated slurries (see Section 2.1.2). For DSP-containing bauxite residue, it is still an open question as to whether the low specific gravity of sodalite (Section 2.4.2) leads to the lower effective density of the aggregates formed and consequently their lower settling rate. Yamada et al. (1980) provided a qualitative comparison of flocculation response for different minerals that may be found in bauxite residue (see Table 6.2). While hematite can produce large aggregates, it was claimed that sodalite cannot. Thus, it is of great interest to find out if a limitation in aggregate sizes formed from DSP-containing residues is also a reason for slower settling compared to residues with negligible or low DSP content.

Table 6.2. Flocculation of minerals in the Bayer liquors. Adapted from Yamada et al. (1980).

| | Flocculation response | Settling rate (m $h^{-1}$) | |
|---|---|---|---|
| | | Synthetic liquor | Plant liquor |
| Hematite | O | 15 | 10 |
| Goethite | X | - | - |
| Anatase | O | 92 | 78 |
| Rutile | X | - | - |
| Sodalite | X | - | - |
| Boehmite | O | 33 | 26 |
| Gibbsite | X | - | - |
| Quartz | X | - | - |
| Kaolinite | X | - | - |

Note: particle diameters of minerals were less than a few micron, O: large aggregates formed by the addition of PAA, X: large aggregates were not formed by the addition of PAA.

Visual observation can only provide qualitative information, reporting “small” or “large“ aggregate formation (as in Table 6.2). *In-situ* measurement with FBRM offers real-time quantification of aggregate dimension/size through mean square-

weighted chord lengths (see Sections 2.5 and 4.4.2). Measuring mean square-weighted chord lengths as a function of time under applied shear may also shed more light on relative aggregate strength.

In several flocculation studies (Alfano et al. 1998; Blanco et al. 2002; Kirwan 2009a), the decrease in mean square-weighted chord length over time that is caused by shear has been fitted by the following equation:

$$y = C_0 + A\, e^{\left(\frac{-x}{Tb}\right)} \qquad 6.1$$

where $y$ is the mean square-weighted chord length at time $x$, $C_o$ is the steady-state mean square-weighted chord length after extended stirring, $A + C_o$ is the maximum mean square-weighted chord length achieved and $1/Tb$ is the rate of decay. A representation of how Equation 6.1 is applied to FBRM data is provided in Figure 6.1a.

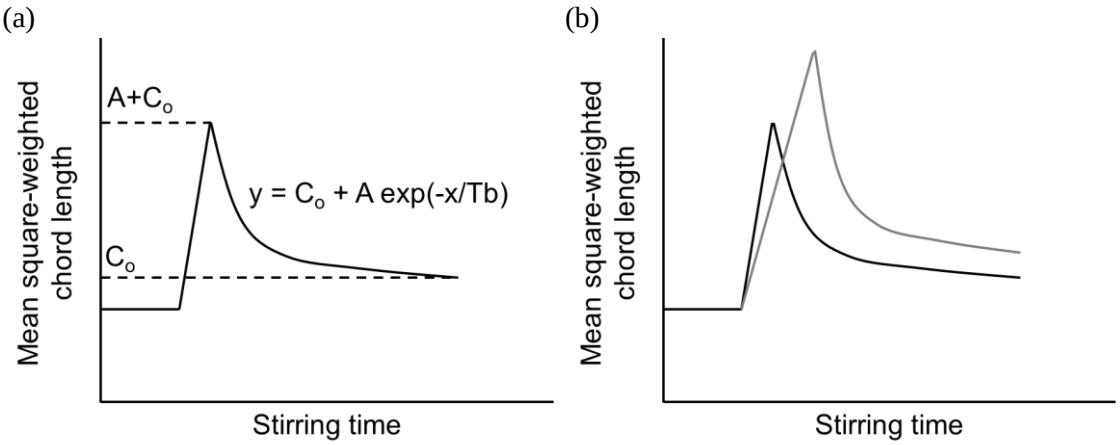


Figure 6.1. Schematic illustrations of: (a) aggregate rupture as a function of stirring time (adapted from Kirwan 2009a) and (b) different ruptures scenarios of aggregates with different mean square-weighted chord lengths.

Although Equation 6.1 seems to provide useful quantification of the aggregate breakage kinetics, it needs to be viewed with caution, especially when systems with different mean aggregate sizes are compared (see Figure 6.1b). Larger aggregates may have a lower fractal dimension or may simply form because of a higher effective flocculant dosage. In either case, a larger aggregate will be more

susceptible to breakage (having lower *Tb*). Therefore, the approach in Equation 6.1 would only give more reliable information about relative aggregate strength when contrasting the size reduction as a function of shearing time for aggregates with comparable starting sizes ($A+C_o$).

The FDA method was employed to calculate the effective density of the aggregates formed from flocculation. By using a video camera, the settling of individual aggregates within a transparent analysis cell can be recorded. The vertical and horizontal dimensions of aggregates and their settling rate can be determined from the images for the effective density calculation by a modified version of Stokes' Law (Bushell et al. 2002; Farrow and Warren 1993; Gagnon et al. 2003; Owen et al. 2002; 2007). Details of the FDA method are described in Section 6.3.5. The characteristic responses of densities and settling rates as a function of size are illustrated in Figure 6.2a. If the existence of DSP results in lower densities and settling rates (as represented in Figure 6.2b), then the assumption that sodalite contributes to a lower aggregate density may be correct, although this will need to be normalised to account for the different solids densities of the two phases (details in Section 6.5.3).

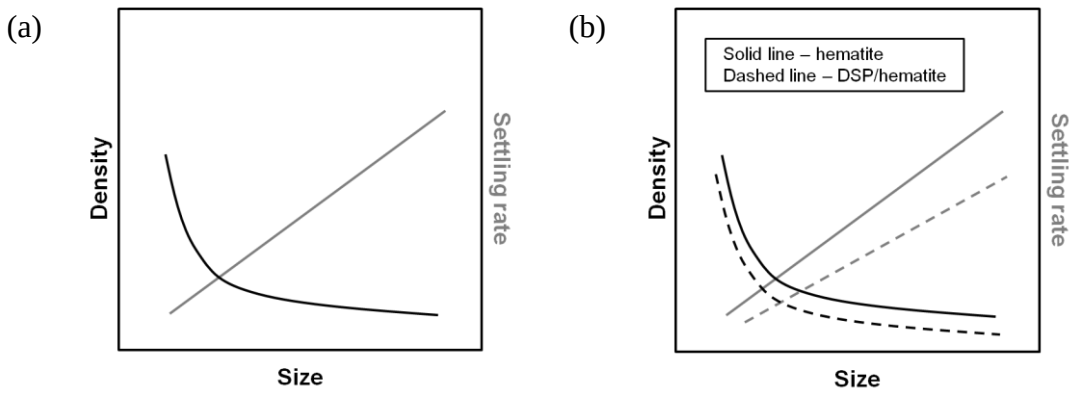


Figure 6.2. Possible scenario for the relationship of density or settling rate vs. size from FDA measurements for: (a) hematite and (b) DSP/hematite slurries.

### 6.1.4 Adsorption of flocculant

Matter adsorbed at a solid surface can be classified into three different states: gases, liquids and dissolved solids or solutes (Giles et al. 1974). The last is the most relevant to the case of flocculant adsorption. Seminal work by Irving Langmuir (Langmuir 1918) defined for the first time a linear relationship between the

concentration of solute absorbed on a solid substrate and that remaining in the solvent. At very high solute concentrations, adsorption is hindered as fewer active sites are available for adsorption, and it eventually reaches a limiting value due to surface saturation caused by monolayer coverage (see L-type curve in Figure 6.3). Since increasing solute concentration was done at constant temperature, the curve of equilibrium concentration of solute adsorbed on solids vs. that remaining in solvent is known as an adsorption isotherm.

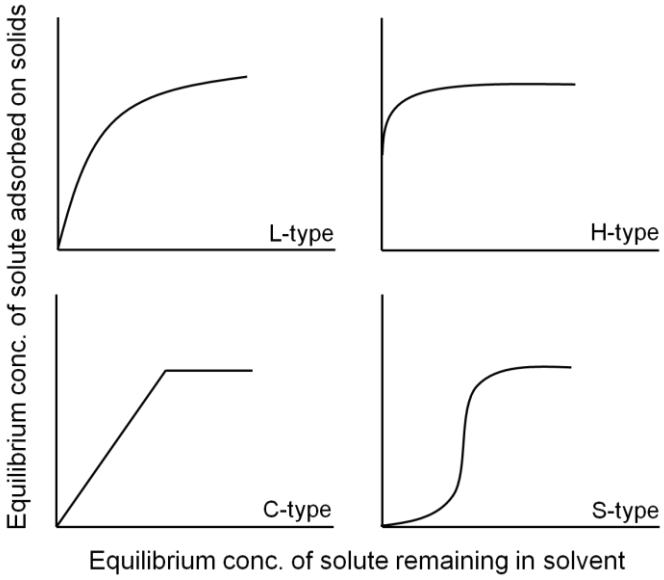


Figure 6.3. Classification of adsorption isotherms: Langmuir (L), high affinity (H), constant partition (H) and S-shaped. Adapted from Giles et al. (1974) and McGuire (2008).

The slope of the concentration of solute adsorbed on the solids substrate against that remaining in the solvent is a measure of how easily solute molecules find and adsorb onto active sites (Giles et al. 1974). It was later established that there are behaviour variants that depart from the Langmuir-type adsorption isotherm (e.g. Fleer and Scheutjens 1993; Giles et al. 1960; Giles et al. 1974; McGuire 2008; Nakagaki et al. 1973). For example, Giles et al. (1974) found that some solutes have a high affinity for the solid substrate, resulting in a very steep isotherm slope (see H-type curve in Figure 6.3).

Besides the L or H-type curves discussed above, C-type and S-shaped isotherms are also known (Giles et al. 1974). The C-type isotherm gains its name from "constant partition" adsorption. In this case, solutes can penetrate into the micropores of the

solid substrate, slowly saturating the surface and the internal voids (see C-type curve in Figure 6.3). An isotherm slope that makes an S-shaped curve as in Figure 6.3, is an indication of multilayer adsorption where solute-solute interaction provides additional sites for adsorption. The C-type and S-shaped isotherms are not common for polymer adsorption (McGuire 2008), whilst L and H-type isotherms have been reported for the adsorption of PAA onto mineral surfaces (Dash et al. 2011; Jones et al. 1998a; Loan 1999; Morris et al. 2002; Mpofu et al. 2003).

In Chapter 5, DSP nodules were found to be extensively deposited on the surface of hematite. When this finding is viewed from the flocculant adsorption standpoint, it emphasizes the need to understand whether the presence of DSP will retard this process and thereby affect the extent of aggregation achieved. If DSP that exists at the surface of iron oxide has much lower affinity for the added flocculant (PAA or HX PAM), the *in-situ* prepared DSP/hematite slurry will adsorb far less flocculant than the pure hematite slurry (Figure 6.4a).

If a solid substrate that has a much higher maximum adsorption capacity is considered as having a fraction of active sites ($\phi$) equal to 1 (or all sites at the surface are active), then according to Moudgil et al. (1987), the fraction of active sites for the solids substrate having a lower maximum adsorption ($\phi'$) can be approximated from the ratio of maximum adsorptions (or $\Gamma_{\text{higher adsorption}} / \Gamma_{\text{lower adsorption}}$ in Figure 6.4a). By taking into account that not all sites are uniformly active in the latter case, the collision efficiency factor can be rewritten as:

$$E = 2\,\theta\ (\emptyset')^2(1-\theta) \qquad 6.2$$

Solid substrates that have a very low affinity for the flocculant will suffer a low collision efficiency that cannot be substantially improved even with excessive addition of flocculant, as illustrated in Figure 6.4b (Moudgil et al. 1987). To date, there is no detailed information as to whether DSP at the surface of a hematite model phase will potentially give a similar effect, and the answer to this question is sought in this study.

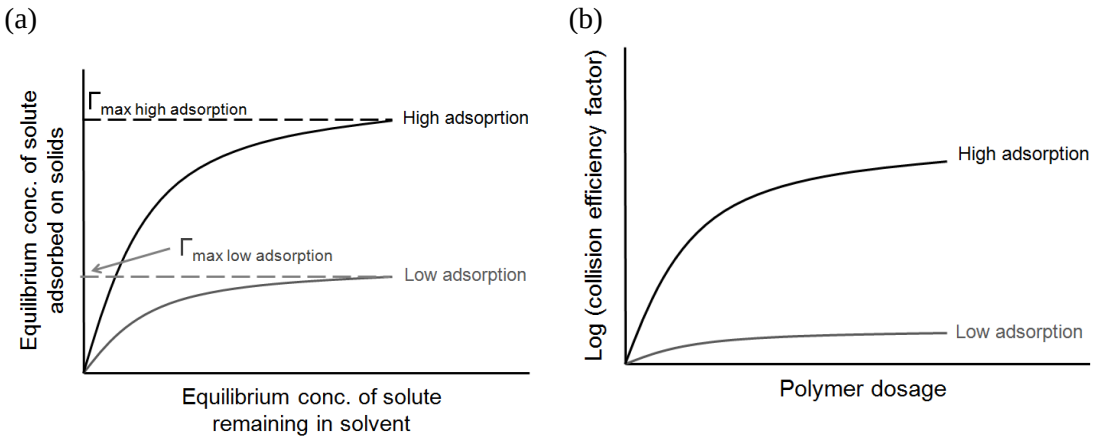


Figure 6.4. Schematic illustrations of (a) high and low adsorption isotherms and (b) collision efficiency vs. polymer dosage in high and low adsorption conditions.

### 6.1.5 Flocculant handling

A complication within many flocculation studies is that flocculant solutions often suffer from reduced or irreproducible activity. This is generally because of poor procedures in the preparation stage, either preventing a flocculant from achieving optimum activity, or leading to degradation from prolonged agitation. In a binary solids system such as the *in-situ* prepared DSP/hematite slurry, the use of flocculants with reduced activity may lead to major misinterpretation, where sub-optimal results are perceived as resulting from DSP in the system. Therefore the effects of flocculant make-up and handling need to be well understood.

In Section 2.4.4, it was discussed how the selection of "process water" used for flocculant stock solution make-up and subsequent dilution prior to dosing affects flocculation performance. Using kaolin as the model substrate, Owen et al. (2002) focused not on the chemistry of make-up or dilution liquor but on the ageing of stock solutions during gentle motion on a table-top shaker (~145 rpm). They showed that significant ageing times ($\geq$ 24 h), were required to transform powder flocculants to being close to completely dissolved with chains almost fully dispersed. In between, the flocculant becomes a swollen gel before adopting a highly agglomerate structure.

Similar ageing behaviour was also shown by an emulsion PAA flocculant with moderate (30%) anionic character (Owen et al. 2007). Whilst ageing stock solutions could be beneficial, Sato et al. (1984) observed that in the case of bauxite residue

flocculants, an emulsion polymer solution that had been diluted from its stock solutions was less active when held for 12 h. All these findings highlight the importance of optimising flocculant preparation and handling in the present study.

The approach taken for flocculant addition is also of particular interest. Sankey and Schwarz (1984) demonstrated that the split (dual) addition of a PAA flocculant solution was beneficial for bauxite residue flocculation. To achieve a settling rate of 12 m $h^{-1}$, 20 and 35% less flocculant were required by splitting into two and four distinct doses, respectively. This agrees with observations for other mineral systems (Section 2.1.6). In contrast, Spitzer et al. (1991) claimed that split addition only gave improvement if used for HX PAM. Figure 6.5a shows the settling rates of an undisclosed bauxite residue flocculated with PAA and HX PAM flocculants. Almost no difference between single and split additions was observed for the polyacrylate flocculant, whilst the improvement from dual addition of HX PAM was substantial. A similar trend was observed for the supernatant solids measurements. An improvement in clarity was expected from HX PAM in any case, but was even better with split addition (Figure 6.5b).

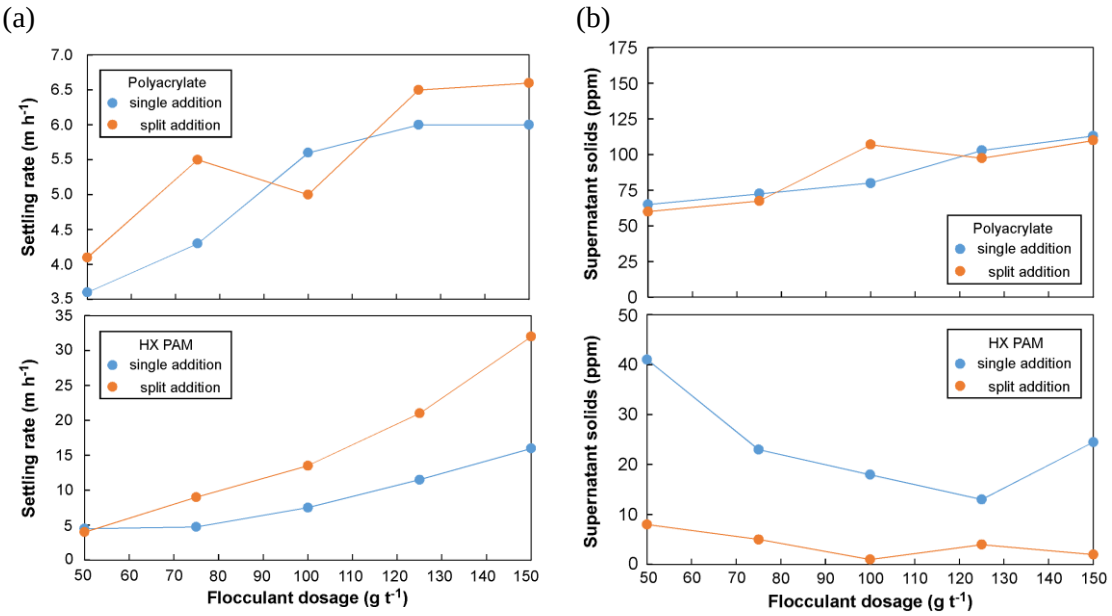


Figure 6.5. The effect of single and split additions of PAA and HX PAM flocculants to the: (a) settling rates and (b) supernatant solids of flocculated bauxite residue. Adapted from Spitzer et al. (1991).

Phillips (2003) later found that the impact of flocculant split addition largely depends on factors such as shear intensity, flocculant chemistry and the applied total dosage. For instance, varying the number of plunger strokes immediately after flocculant addition, he showed that the benefit of split addition was negated by excessive shear experienced by aggregates. Furthermore, the advantage of split addition for certain flocculant chemistries may only manifest at very low or very high dosage regimes. For the method optimisation conducted in this study (Section 6.4), clarification as to whether split addition will benefit flocculation of the *in-situ* prepared DSP/hematite slurries was also considered important.

## *6.2 Objective and Approaches*

The work described in this Chapter investigates the impacts of DSP formation at the surface iron oxide on the flocculant adsorption and the characteristics of aggregate formed under the influence of the following variables: DSP content in the *in-situ* prepared DSP/hematite slurries, solids concentration and flocculant chemistry. Such goals were achieved by conducting:

- optimisation on flocculant make-up and preparation.
- settling tests on DSP/hematite slurries with varying solids concentration, DSP content and flocculant type (PAA vs. HX PAM).
- real-time monitoring of flocculation reactions by FBRM to collect information about aggregate dimensions (size).
- estimation of the aggregate density on selected samples using the floc density analyser (FDA).
- flocculant adsorption isotherm measurements on the following samples: pure hematite, pure DSP, *in-situ* prepared DSP/hematite and physical mixture of DSP and hematite.

The experimental for this chapter is therefore divided into the following main categories: (i) DSP synthesis and characterisation, (ii) flocculant make-up and preparation, (iii) settling tests, (iv) FBRM, (v) FDA and (vi) flocculant adsorption; with the details for each category explained in the following section.

## *6.3 Experimental*

### 6.3.1 DSP synthesis and characterisations

Synthesis of the *in-situ* prepared DSP/hematite slurries followed exactly the same method described in Section 5.3.1, except that hematite-to-kaolin ratios were varied in order to produce different DSP contents (wt/wt%). No physical mixtures of DSP and hematite were examined in this Chapter. Table 6.3 lists the ratios of hematite and kaolin used and the resultant DSP contents. Note that when pure hematite slurries were used, hematite was not reacted (digested) at 90°C because: (i) there was no need when not synthesising DSP, (ii) hematite is known to be inert in highly alkaline media and (iii) the zeta potential of digested hematite was found to be very similar to that of the undigested phase, indicating no change in surface properties.

Table 6.3. DSP concentrations (wt/wt %) in the *in-situ* prepared DSP/hematite slurries.

| Ratio | | DSP in *in-situ* prepared mixtures |
|---|---|---|
| Hematite | Kaolin | (wt/wt %)* |
| 1 | 0 | 0 |
| 10 | 1 | 11 |
| 8 | 1 | 14 |
| 7 | 1 | 16 |
| 6 | 1 | 18 |
| 5 | 1 | 21 |
| 4 | 1 | 25 |
| 3 | 1 | 31 |

(*) measured gravimetrically.

For subsequent PSD analysis, sub-samples of slurries produced from reacting hematite, kaolin and sodium aluminate liquor at elevated temperature were then filtered (0.45 μm) and washed with 5×200 mL aliquots of hot deionised water before being re-suspended in deionised water. Details regarding PSD measurement and data treatment can be found in Section 4.3. By preserving the sub-sample as a suspension to avoid drying and regrinding routines, the PSD can be maintained as close as possible to its original condition.

In contrast, dry samples are required for specific surface area, pore structure and particle density measurements. Drying at an elevated temperature (105°C) leads to a

compact cake that needs intensive grinding, which may change the physical properties of the solids. Therefore, initial drying of the filtered and washed sub-samples was done at room temperature in a vacuum desiccator for a week before lightly grinding and re-drying to constant weight at 105°C. Analysis of surface area and pore structure was conducted using the Brunauer, Emmet and Teller (BET; Brunauer et al. 1938) and Barrett, Joyner and Halenda (BJH; Barrett et al. 1951) gas adsorption methods, respectively. A Micrometrics Tristar 3000 instrument was used for both the BET and BJH measurements. Mercury picnometry (e.g. Lynch 2003) was also employed to measure the particle density in a Quantachrome Multi Picnometer.

To assess the variability of the DSP chemical composition for different batches, XRF analysis was conducted on selected dry samples through a commercial analytical company (Ultra Trace Pty. Ltd). Their procedure followed the standard XRF analysis, where borate flux is mixed with a small amount of ground sample prior to fusing at 1100°C. The cooled fused bead is then loaded into a fluorescence spectrometer for metal content determination. The content of the selected elements (Si, Al, Fe, Na, S, Ti and Cl) was back-calculated and reported as their oxides.

Table 6.4 summarises the elemental analysis results from XRF conducted on pure DSP synthesised in different batches under standard conditions (24 h, 90°C, digestion liquor – see Section 5.3.1 for its composition). Hematite was not added in this instance to avoid effective dilution of minor elements. The XRF results in Table 6.4 show very little deviation for each element of interest, with the biggest standard deviation (0.39 wt/wt%) observed for $SiO_2$. From the XRF results alone, it can be implied that the DSP produced in different batches would have consistent characteristics.

Table 6.4. Chemical composition of sodalite produced from different batches.

| (%) | Batch A | Batch B | Batch C | Batch D | Batch E | Mean | SD |
|---|---|---|---|---|---|---|---|
| $SiO_2$ | 34.8 | 33.8 | 34.7 | 34.4 | 34.3 | 34.4 | 0.39 |
| $Al_2O_3$ | 31 | 30.8 | 30.9 | 30.9 | 30.9 | 30.9 | 0.07 |
| $Fe_2O_3$ | 0.41 | 0.4 | 0.41 | 0.4 | 0.41 | 0.406 | 0.01 |
| $Na_2O$ | 22.6 | 23 | 22.7 | 22.8 | 22.8 | 22.78 | 0.15 |
| $SO_3$ | 4.62 | 4.58 | 4.62 | 4.61 | 4.56 | 4.60 | 0.03 |
| $TiO_2$ | 0.49 | 0.48 | 0.49 | 0.49 | 0.48 | 0.49 | 0.01 |
| Cl | 0.631 | 0.66 | 0.622 | 0.628 | 0.649 | 0.638 | 0.016 |
| LOI | 6.14 | 6.72 | 6.19 | 6.25 | 6.24 | 6.31 | 0.23 |

### 6.3.2 Flocculant make-up and preparation

The products chosen to represent polyacrylate and HX PAM chemistries were the powder flocculant Alclar 665 (BASF) and emulsion flocculant Cyfloc$^{TM}$ HX-300 (Cytec Industries). For simplicity, the latter is referred to as HX-300 throughout the text. There was no implication that these were optimised product selections. Unless stated otherwise, Alclar 665 was made to a 0.5 wt/wt% stock solution, with the complete procedure given in Section 4.3. HX-300 was made to 1 wt/wt% stock solution by injecting 3 g of the product into the vortex formed while stirring a caustic solution (297 mL of 20 g $L^{-1}$ NaOH in a 500 mL tall form beaker with a diameter of 7 cm and height of 13 cm) with a cage impeller (Jiffy mixer, Aldrich). The stirring rate was maintained at 1100 rpm for the first 2 minutes and then reduced to 400 rpm for another 20 minutes. The cage impeller and the experimental set-up for emulsion flocculant inversion are shown in Figure 6.6a and b, respectively.

Another HX PAM flocculant (Cyfloc$^{TM}$ HX-600, Cytec Industries) was used in a limited number of tests in Section 6.4, and was made-up by the same method applied to HX-300. Magnafloc 919 (powder flocculant with ~50% anionic character, BASF) was also used for a comparative study of flocculant adsorption at lower pH (Section 6.3.6). It was made-up by the standard procedure for powder products, although the make-up and dilution liquors were 0.2 M NaCl.

(a) (b)

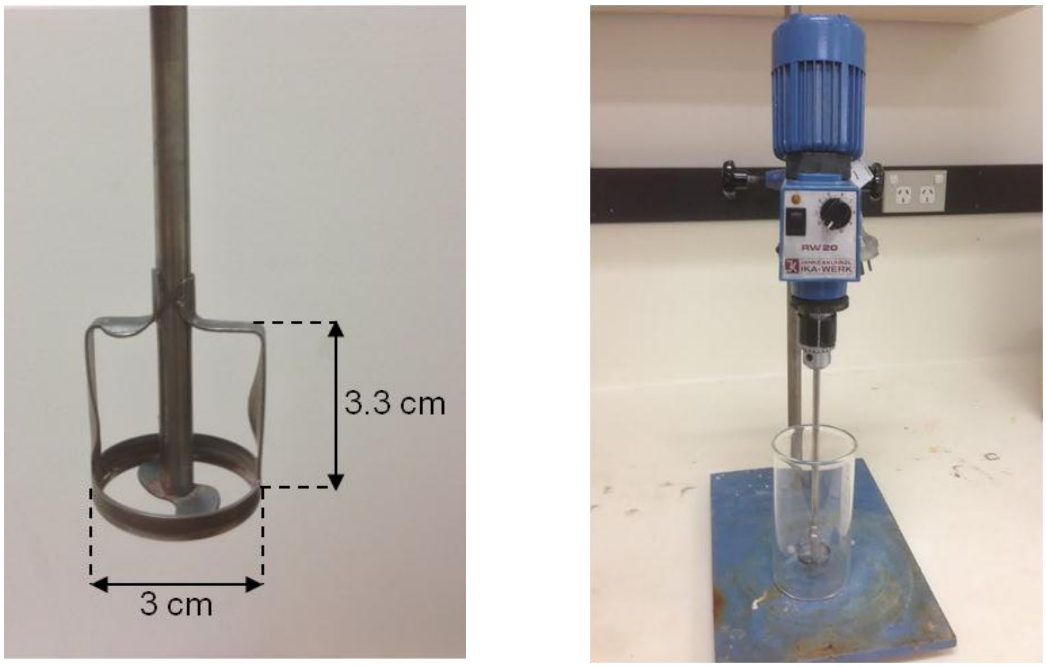


Figure 6.6. Emulsion flocculant inversion equipment: (a) cage impeller and (b) set-up.

### *6.3.2.1 Flocculant aging*

Stock flocculant solutions ageing can lead to problems in batch laboratory tests, although it is far less of an issue for a refinery, where the flocculant is continuously added to the pipe entering the feedwell or directly to the feedwell. In this case, flocculant stock solutions management is complicated by the fact (established early in this project) that after inversion of HX PAM flocculants to 1 wt/wt%, the use of those stock solutions on the following days often led to reduced flocculation performance.

Such ageing was not observed for 0.5 wt/wt% stock solutions made from the PAA powder flocculant, even after storage for 2 weeks. The stability of PAA stock solutions is in agreement with results from Jones (1998), who observed no degradation in flocculant activity for the unsheared PAA stock solutions aged for up to 72 days.

It was proposed that contact with air may have accelerated the time-based loss of activity for 1 wt/wt% solutions of HX PAM flocculants. To test this premise, 300 mL

of 1 wt/wt% HX-300 was prepared in 20 g $L^{-1}$ NaOH, of which 200 mL was kept in a 200 mL jar, thereby ensuring a minimal presence of air. The remaining 100 mL portion was also stored in an equivalent jar, such that 50% of the volume is occupied by air (Figure 6.7).

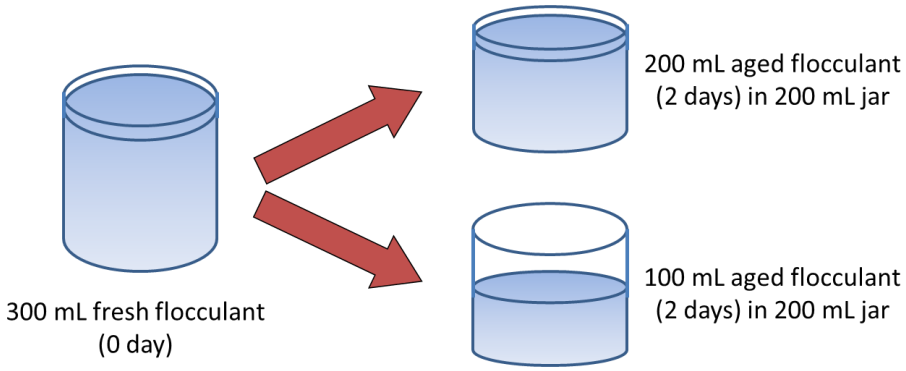


Figure 6.7. Schematic illustrations of flocculant storage with control to the air exposure.

Settling tests (details of protocols given in Section 5.3.2) conducted at a fixed dosage after 2 days of ageing (Figure 6.8) showed the settling rate from the flocculant solution with minimum air contact to be at least six-fold higher than the solution for which air exposure was significant (46 vs. 6.7 m $h^{-1}$), confirming that air does induce degradation of the HX PAM flocculant. The ageing problem was therefore overcome by storing HX PAM solutions in several small bottles (50 mL) with a very limited head space, and no stock solution was retained for longer than 2 days.

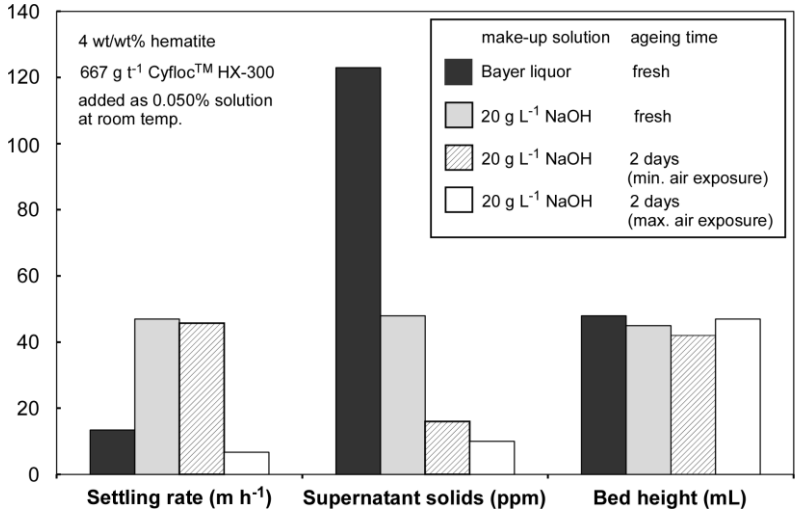


Figure 6.8. The effects of made-up liquor and air exposure to the stock solutions on the performance of flocculants (stock solutions were made-up by different liquors and further diluted by 20 g $L^{-1}$ NaOH).

When synthetic Bayer liquor (composition similar to the testwork liquor) was used to dilute 1 wt/wt% HX PAM solutions, the reduced activity in settling tests was evident immediately (dark vs. grey bars in Figure 6.8). Unlike diluting stock solutions with 20 g $L^{-1}$ NaOH, using synthetic Bayer liquor as dilution liquor maintains the solution composition in the slurry that is prepared for settling test. Nevertheless, the fact that Bayer liquor reacts in some way with the hydroxamate functionality of the flocculant makes its use as a make-up liquor inadvisable – especially in this study where the comparison of HX PAM and PAA performance was sought. Hence, both stock solutions were further diluted to different concentrations by using 20 g $L^{-1}$ NaOH.

#### *6.3.2.2 Temperature of dosed flocculants*

At some Bayer plants, the dilution of flocculant stock solutions prior to dosing is undertaken with hot liquors. This not only increases the volume added, but the lower viscosity of the flocculant at temperature is also thought to help mixing through the slurry. In such cases the dilution is typically only achieved just seconds prior to dosing into the slurry. Contrast this with a batch settling test performed at a high temperature (≥ 90°C), for which the flocculant solution is inevitably held for longer prior to addition, either at room temperature, 45 or 75°C.

Ageing was also minimal over a 45 minute period when flocculant solutions were held at 45°C (Figure 6.9). No ageing was observed within 6 h for any of the dosed flocculants when added as a room temperature solution to the hot slurry. The HX PAM flocculant (HX-300) did display some loss in activity over time at 75°C, even at a higher concentration. It is important to stress that this result is again not directly relevant to plant applications, but has important implications for laboratory comparisons of flocculants, stressing the need to hold diluted flocculant solutions at a low-to-moderate temperature. If this is not done, this can lead to irreproducible results and invalid product comparisons.

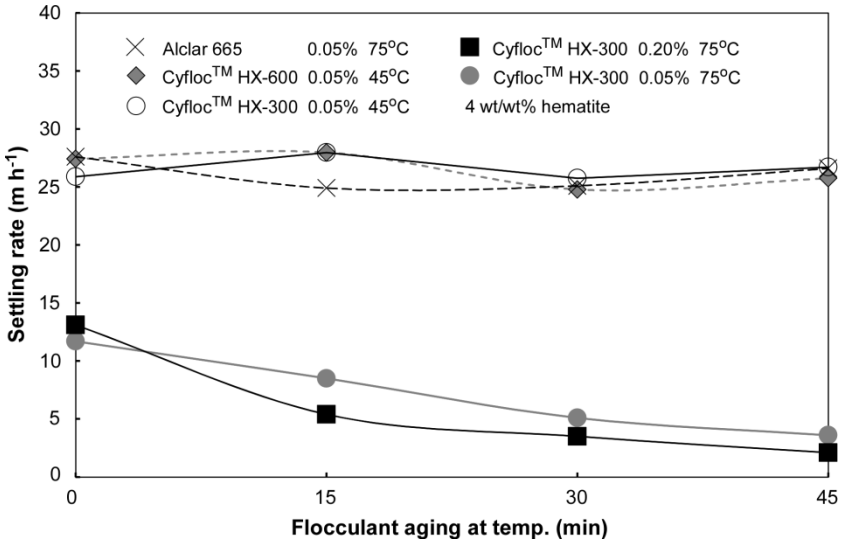


Figure 6.9. The effect of holding temperature to the performance of diluted PAA powder and HX emulsion flocculant solutions (dosages: Alclar 665 = 150 g $t^{-1}$, HX-300 = 800 g $t^{-1}$, HX-600 = 800 g $t^{-1}$).

### *6.3.2.3 Concentration of dosed flocculants*

The concentration of the flocculant solution as applied during flocculation (while still maintaining the required dosage) is one of the more significant factors that affects the subsequent settling properties, because the degree of mixing (and as a consequence, the effectiveness of flocculant distribution and adsorption) can also be greatly affected (Section 2.4.4). To assess this, a 0.5 wt/wt% stock solution of the Alclar 665 flocculant was further diluted to the following concentrations: 0.0125, 0.025 and 0.05 wt/wt%. The flocculation response of these diluted solutions with hematite slurries as a function of the applied dosage was compared.

Settling rates were used to measure the flocculant performance over a wide range of dosages (0-150 g $t^{-1}$) that gave settling rates between 5 and 45 m $h^{-1}$ (Figure 6.10a). The corresponding supernatant solids can be found for comparison in Figure 6.10b. The dosed flocculant concentration did not substantially change the flocculation response across the dosages examined. There was some variation in the very high settling rate region ($\geq$ 35 m $h^{-1}$), but measurements for such high settling rates can be hampered by a lack of accuracy in capturing the very fast mud-line movement within a cylinder of limited height, and therefore should always be viewed with caution.

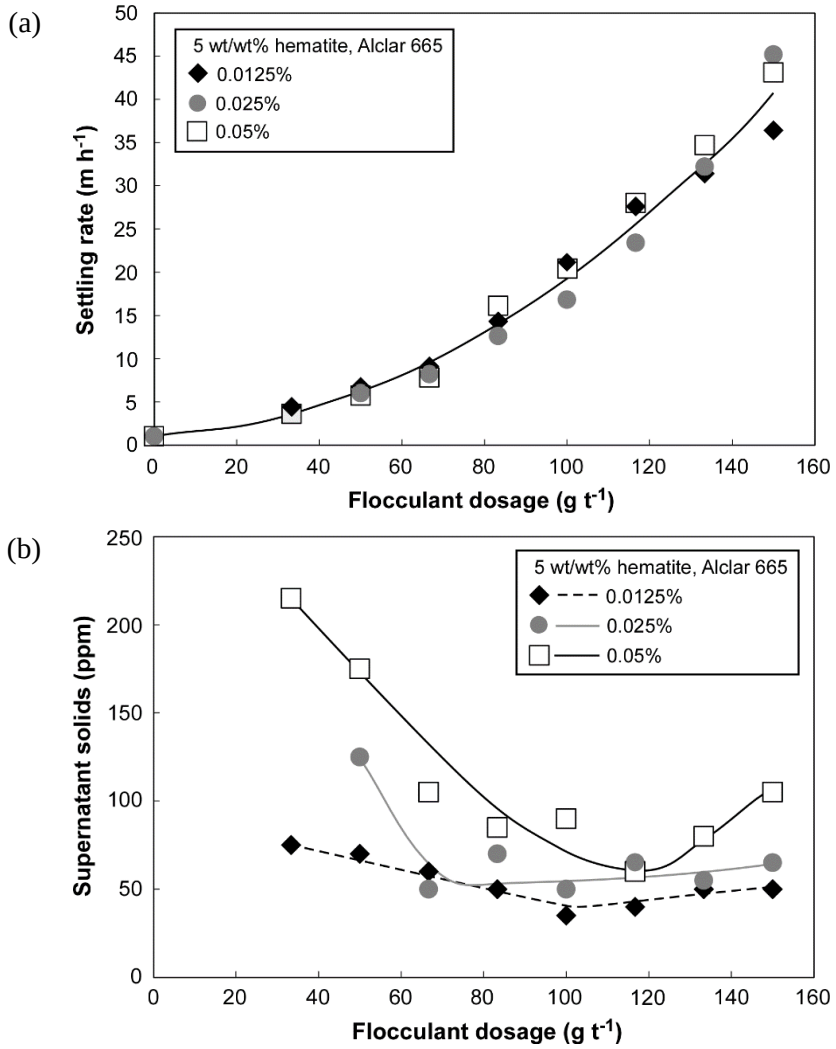


Figure 6.10. The effect of dosed Alclar 665 flocculant concentration on the: (a) settling rate and (b) supernatant solids of hematite slurries. Flocculants were added at 45°C.

The difference in performances was more significant when contrasting the supernatant solids measured. Increasing the flocculant concentration (while fixing the total applied dosage) had a negative impact on fines capture, resulting from relatively poor mixing of a polymer solution with increased viscosity. This was evident from the decreasing trend of supernatant clarity. This effect was heightened at lower dosages and it is in this region that higher dosed concentration would have the greatest effect. It is also of interest that the supernatant solids decreased until a certain flocculant dosage where beyond that, the trend was less definitive because the small difference (50 ppm) in the supernatant solids could be due to experimental error related to the small sample size for gravimetric measurement.

Despite the better fines capture efficiency when PAA flocculant is dosed at lower dosing concentration (0.0125% vs. 0.05%), the comparison between the flocculation of hematite and the *in-situ* prepared DSP/hematite slurry was done with the same dosed concentration (0.05%). A lower dosed concentration was less suitable simply because DSP-containing slurry required a much higher total flocculant dosage, and therefore much more total added volumes for dilute flocculants. This can change the system (i.e. the total solids concentration) as explained below for the case of HX PAM utilisation.

For HX-300 flocculant solutions, the options for dilution were limited to 0.05 or 0.1 wt/wt%; due to its high dosage requirement that can be 4-5 times higher than PAA on the basis of product mass. As an emulsion flocculant, only a fraction of the HX PAM total mass (~10-12%) represents the active polymer component, and therefore the stock solution itself is moderately dilute. To aim for adding 800 g $t^{-1}$ of HX PAM in a 250 mL slurry with solids concentration of 40 g $L^{-1}$, 20 mL of HX PAM solutions with a product concentration of 0.05% needs to be dosed. This action would change the liquor composition (as flocculants were diluted by 20 g $L^{-1}$ NaOH) as well as the total solids concentration. Results in Figure 6.10 indicate that the performances of 0.05 and 0.2 wt/wt% HX PAM were almost equal. Hence, for a very limited number of tests conducted with dosages > 1000 g $t^{-1}$ HX PAM (as in Section 6.4.4), a concentration of 0.2 wt/wt% was accordingly used.

#### *6.3.2.4 Method of addition: single or split addition?*

Section 6.1.5 discussed whether flocculation of bauxite residue is improved by split addition of flocculant (i.e. less total flocculant required when targeting comparable settling rates). For HX PAM, the benefit is clear, with split addition strongly advised by its suppliers. Whether this benefit extends to the dosing of PAA flocculants is the subject of debate.

To elucidate that issue, settling tests were conducted to compare single and 50:50 split addition of the Alclar 665 PAA flocculant to the pure hematite slurries and the *in-situ* prepared DSP/hematite slurries (with 31 wt/wt% DSP). Figure 6.11 plots the

settling rates of flocculated pure hematite slurries as a function of Alclar 665 dosage. For single dosing, the number of strokes following flocculant addition was either five or ten. For split dosing, the number of strokes accompanying every addition was five.

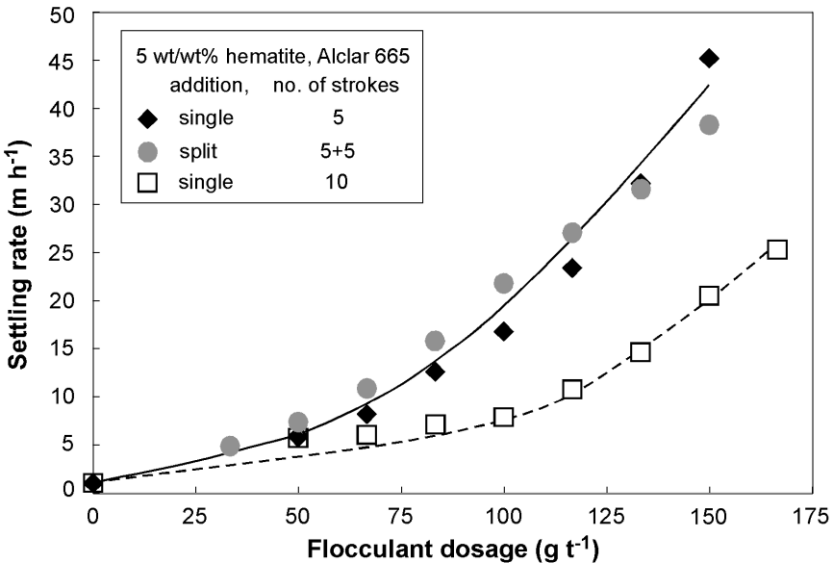


Figure 6.11. The effect of single and split PAA flocculant additions on the settling rate of hematite slurries.

Figure 6.11 confirmed that the results for single or split addition of Alclar 665 were comparable, agreeing well with the observation from Spitzer et al. (1991). However, more shearing (number of strokes) applied to the single addition significantly decreased the settling rate. Only one PAA flocculant was studied here but the results in Figure 6.11 highlights that the applied mixing is likely to have a much greater impact on flocculant performance than the practise of single or split dosing.

The settling rate data as a function of Alclar 665 dosage for the flocculation of *in-situ* prepared DSP/hematite slurries with single or split addition is presented in Figure 6.12. The results are also similar to those from the flocculation of pure hematite slurries, where single or split addition did not substantially change the flocculation response. It is worth noting that twice the flocculant dosage was required by the *in-situ* prepared DSP/hematite slurries to maintain a reasonable settling rate between 10-15 m $h^{-1}$. This aspect is further discussed in Section 6.4.1.

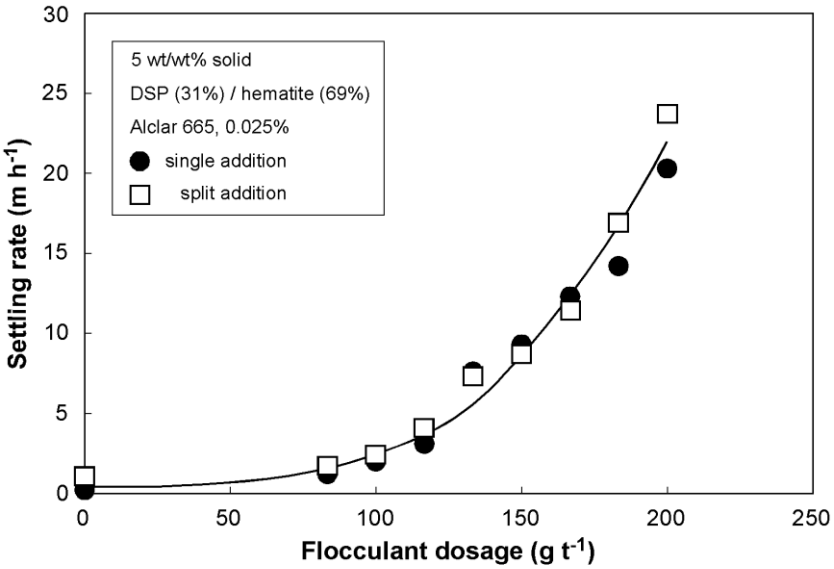


Figure 6.12. The effect of single and split PAA flocculant additions on the settling rate of the *in-situ* prepared DSP/hematite (31 wt/wt% DSP) slurries. The number of strokes accompanying every addition was five.

### 6.3.3 Settling tests

The *in-situ* prepared DSP/hematite slurries with differing DSP contents were subjected to cylinder settling tests to quantify their flocculation response. Slurry preparation includes filtration, washing, overnight equilibration in fresh testwork liquor (see Section 4.3 for its composition) and then re-dispersion. The amount of testwork liquor added was adjusted to give stock slurries with solids concentrations in the range 3-7 wt/wt%.

The complete procedures followed that detailed in Section 5.3.2. The main concern was to find out if there is a slurry ageing effect that occurs when following those protocols. The knowledge of slurry ageing is particularly important in this Chapter since the difference of dewatering properties derived from varying flocculant/DSP content could be masked by the ageing effect.

The first experimental set was therefore carried out to assess the effect of slurry ageing time on the flocculation done in settling tests. The slurry ageing time refers to the time after the slurry has been stirred (700 rpm for 1 h and 300 rpm for 1 h) and sonicated (10 minutes) – see Section 5.3.2 for details. Pure hematite slurry was chosen in order to avoid the possible complication arising from the presence of DSP.

Settling rates of slurries were found to be independent of the slurry ageing time, with a standard deviation of 1.4 m $h^{-1}$ for the five measurements done within 75 minutes of ageing (details given in Appendix A). This suggests that complete dispersion had been achieved through the "standard" slurry preparation that involved stirring (at 700 and 300 rpm) and sonication (10 min).

It is worth noting that fresh HX PAM flocculant solution was used here to minimise the effect of flocculant instability. "Fresh" flocculant solution refers to 1 wt/wt% stock solutions that were made ~4 h before and diluted by 20 g $L^{-1}$ NaOH ~1.5 h prior to the use. The supernatant solids still showed a slight but significant increasing trend with respect to flocculant ageing time, most evident at times approaching 130 minutes. To minimise any risk of ageing effects; in all subsequent experiments, a set of settling tests with up to 10 individual cylinders should always be completed within 60 to 90 minutes of commencement.

After knowing that the slurry preparation method had given repeatable results, ensuring the reproducibility of settling tests for *in-situ* prepared DSP/hematite slurries emerged as the next concern. The settling rates of five nominally identical DSP/hematite slurries (31 wt/wt% DSP), prepared in separate batches were within the range 14.5-18 m $h^{-1}$ (details in Appendix A). Considering that differences of 2-3 m $h^{-1}$ are very common for repeat tests on the same slurry when flocculation is achieved within the cylinders, the reproducibility here was considered acceptable. The small variation observed in the *in-situ* prepared DSP/hematite slurries settling tests can be explained to some extent by the chemical composition of DSP produced (Section 6.3.1).

### 6.3.4 FBRM

Slurries of *in-situ* prepared DSP/hematite with different DSP contents were filtered, washed and equilibrated in fresh testwork liquor and then redispersed, following the procedure in Section 5.3.2. Testwork liquor was added to make slurries for FBRM tests of 2 wt/wt% solids concentration. Methods and equipment used for FBRM tests

are given in Section 4.4. Both the M500 and G400 probes were employed to gain better insights on aggregate characteristics. The temperature was maintained at 70°C during both preparation and testing. Unless stated otherwise, the stirring rate inside the 500 mL tall form water jacketed FBRM beaker (150 mL of slurry) was fixed at 300 rpm.

Similar to the settling tests, PAA and HX PAM flocculant were added in single and split doses, respectively. The concentration of dosed flocculant was 0.0125% and 0.025% for PAA and HX PAM, respectively. In the FBRM study, the second addition of HX PAM flocculant was done 3 minutes after the first addition, while maintaining continuous mixing of the slurry. All flocculant solutions were added at room temperature, as continuous mixing given by the rotating impeller minimises the risk of low dispersion of flocculant even when its viscosity is higher at room temperature.

### 6.3.5 FDA

While FBRM offers *in-situ* measurement of aggregate sizes, FDA requires sub-samples to be carefully diluted prior to image capture and further analysis. Thus, the experiment was divided into three sequences: aggregate sampling, the collection of images of the settling aggregates, and the use of image analysis software to provide individual aggregate dimensions and settling characteristics.

#### *6.3.5.1 Aggregation and sampling*

The initial sample preparation for producing aggregates was similar to that for FBRM (see the first paragraph of Section 6.3.4), except that no FBRM probe was immersed when pure hematite or *in-situ* prepared DSP/hematite slurries were flocculated with 139 g $t^{-1}$ Alclar 665. A sub-sample for FDA measurement was carefully withdrawn by syringing 40 s after flocculant addition. Preliminary experiments by FBRM have shown that the maximum aggregate size was achieved within 30 s and no further aggregate growth would be expected after sampling. It is important to emphasize that the tip of the syringe (Terumo® 20 mL DVR-5174) was only 1 mm in diameter and there is a possibility that some aggregates were bigger

than that (see Section 4.4.3). Therefore, in order not to deform the aggregates, a plastic tube (7 mm in a diameter) was connected to the tip of the syringe via a plastic junction (see Figure 6.13a). Sampling involved withdrawing the slurry into the 7 mm diameter tube section only.

(a)

(b)

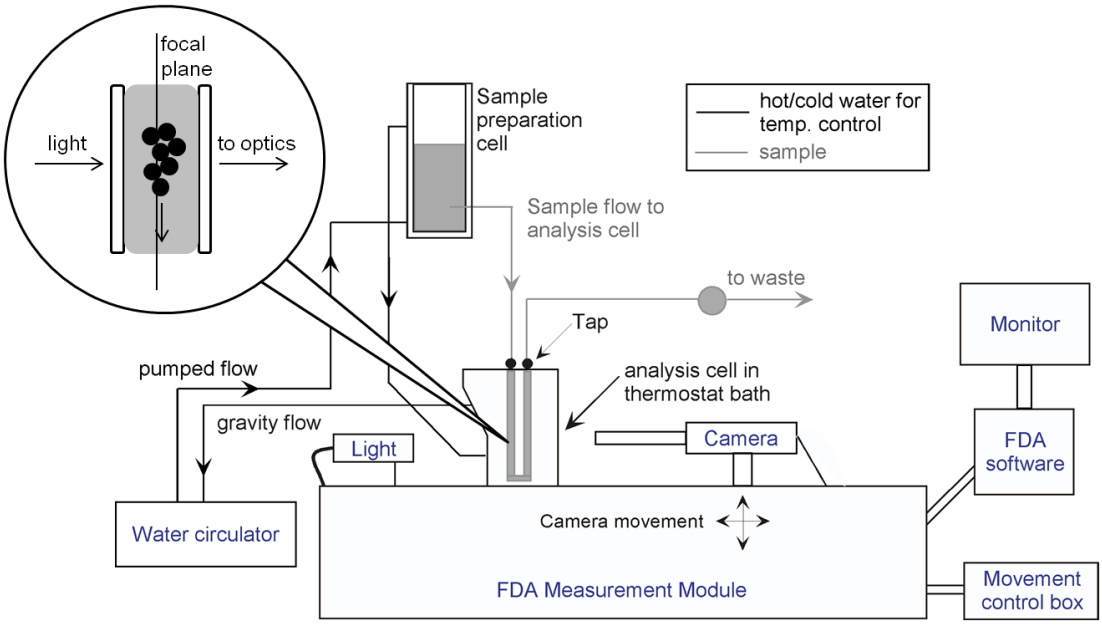


Figure 6.13. Schematic illustration of: (a) syringe for sampling and (b) FDA set-up.

The sub-sample is not ready for direct measurement since it has to be further diluted (by a factor of ~50) and re-suspended in the sample preparation cell before the suspension is pumped to the analysis cell (see Figure 6.13b). Careful solids dilution and resuspension are crucial, as free settling of individual aggregates is sought to provide suitable data for the calculation of aggregate density. A plastic plunger was employed to promote dispersion by applying ten gentle strokes. The plunger was

similar to that used in settling tests (Figure 5.8b) but with different dimensions (3.8 cm diameter plastic disc with six inner radial 0.6 cm holes at the end of a shaft 25.5 cm long, 1.4 cm in diameter). Diluted and re-suspended sample was then pumped to the analysis cell for video recording.

Post-formation shear from sampling and other handling steps (e.g. dilution) may potentially either destroy aggregate structures or promote densification (Owen et al. 2008). The possibility that the action of dilution and resuspension induces some degree of breakage or densification cannot be ruled out in this study, however, every effort was made to minimise such effects, and the results are the most realistic that can be achieved.

#### *6.3.5.2 Collecting images of settling aggregates*

Once diluted slurry was pumped into the U-shape transparent borosilicate glass cell (see Figure 6.14 for detail), the taps on each arm were tightened to isolate the system. For monitoring and recording purposes, a digital camera (JAI Navitar Progressive Scan; 0.58-7× optical magnification – 24 frames per second) was used. The camera position was controlled by a movement control box (see Figure 6.7b). The digital camera was connected to a computer via a VESA digital flat panel connector. Software package supplied by the camera vendor (Aes PcCamLink HighSpeed HardDisk Acquire) was able to present the real-time images from the digital camera on the computer screen and save them as a .raw video file (Benn 2013).

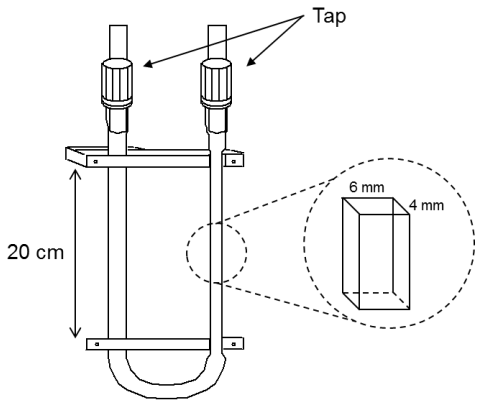


Figure 6.14. U-shape borosilicate glass in FDA analysis cell.

The recording was paused when most of the aggregates in the U-shape glass had sunk to the bottom of the cell and outside the measurement window. The taps were opened to flush the old sample and then introduce the new sample before the video recording was restarted. The entire video file was stored for further processing with different image analysis software package (explained in Section 6.3.5.3).

The quality of the images taken is a key to success in this experiment. The best image quality is derived from the adjustments of shutter speed, backlighting intensity, focal point (camera position) and optical magnification (see Figure 6.13b). A 1/800 shutter speed was found to be optimal and was set within the Camera Control software. The light source, positioned 50 mm behind the thermostat bath, provides an intensity control function and fine-tuning was done by putting a diffuser (round Teflon disc) in front of it. Meanwhile, camera position was adjusted by using the keyboard in the movement control box. Through trial-and-error, magnification by 3 to 6× was chosen to capture the motion of a statistically representative number of aggregates (250-300) of medium size (up to 250 μm but mostly in the range 25 to 150 μm).

The medium size aggregates were preferred over larges aggregates, given that the latter formed from particles of high density tend to settle too fast to be well captured or do not settle along a perfectly vertical axis. Aggregates that suffer from such issues are also found in the images captured at 3-6× magnification, but can be manually eliminated from processing by the software operator.

#### *6.3.5.3 Image analysis*

A DOS-based software package (AssistedTracking) was developed by the Solid/liquid Handling Team in CSIRO Process Science and Engineering for image analysis. In this case, analysis of settling aggregates was done frame by frame. Therefore, the recorded video must first be converted to individual images (1 s of movie = 24). The Aes PcCamLink HighSpeed HardDisk Acquire package was used to extract frames from the movie and save them as individual images (.bmp).

The AssistedTracking software can access the selected folder containing tens of thousands of individual images, presenting them continuously like a movie to the software operator. The software has a “screening” function that indicates aggregates that are suitable for the “size” determination and settling rate calculation. The screening function works by implementing selection criteria such that it only accepts aggregates that:

(1) are completely in screen view,
(2) are relatively in focus,
(3) are settling vertically (not diagonally),
(4) whose settling rate is not influenced by other faster settling aggregates,
(5) are not streaming (settling at the same rate despite the size differential).

Aggregates that fall into all the criteria mentioned above are marked with red dots by the software (e.g. Figure 6.15a). The software operator can choose (click) any of them for the first step of size determination where the top-left and bottom-right boundaries to the image of aggregate were set by the software operator. The size determination was done based on the assumption that individual aggregates have an overall ellipsoidal shape (Farrow and Warren 1993). It assumes that the third dimension of the aggregate is assumed to be similar to its horizontal dimension (Farrow and Warren 1993). These two dimensional size determination procedures in the AssistedTracking software are best explained in the Figure 6.15a and b (Benn 2013).

(a)

(b)

(c)

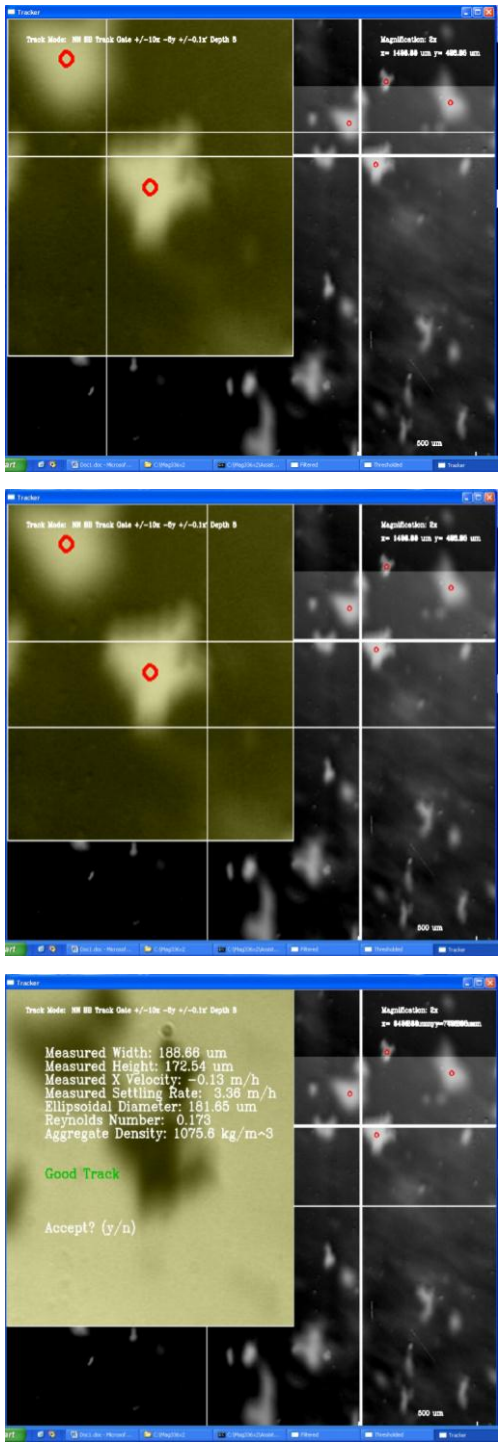


Figure 6.15. Aggregate analysis through the AssistedTrackingTest FDA software: (a) choosing top-left boundary, (b) choosing bottom-right boundary and (c) result of settling rate calculation. Adapted from Benn (2013).

Settling rate was calculated from the position of the aggregate after advancing 8 frames. There are cases where settling is accelerated over this time or displayed a significant diagonal component. This can be detected from the results of settling rate calculations, with the software categorising the settling behaviour as "good" or

"poor" track – only the former will be accepted and taken into account in subsequent calculations (see Figure 6.15c).

The results of aggregate dimension determination and settling rate calculation were saved in a spreadsheet file (.csv). This file was then used as an input for a Visual Basic Macro program (FlocCalc 4.xlsm). In this program, the 'single size parameter' and the effective density of the aggregates were calculated. The single size parameter refers to the size of a sphere with equivalent settling rate. The background theories and complete calculations for the single size parameter and the effective density are given in Appendix B.

For internal quality control purposes, two different trendlines (Standard Fit and Internal Average Fit) were applied to the settling rate vs. (single) size plots. Both are based on the following relationship:

$$SR = A\, d^B \qquad 6.3$$

where SR is settling rate of aggregate, A and B are constants and d is aggregate size. In the Standard Fit, all data generated from the FlocCalc 4.xlsm program are used. In the Internal Average Fit, the size range of aggregates measured is divided into twenty internal channels and the average size of aggregates in every channel is used in Equation 6.3, together with the average settling rate in every channel. In this case; the error introduced by specific channel(s), which has a large number of aggregates that are not that dissimilar in size but vary greatly in settling rate, can be minimised.

Aggregates that suffer from anomalies (i.e. whose settling rate was too low for its size when compared to a number of aggregates with comparable sizes), can be deleted from the calculation. Such action will make the Standard Fit trendline come closer to the Internal Average Fit trendline although the two trendlines may not necessarily form a single line. The aggregates that have passed the software selection criteria and the manual acceptance criteria are plotted in the form of settling rate or effective density vs. size (Figure 6.2).

### 6.3.6 Flocculant adsorption tests

The adsorption behaviour of PAA and HX PAM flocculant solutions to the DSP containing solids is of particular interest. This is best quantified by deriving adsorption isotherms from solution depletion measurements. The experimental set-up and initial procedures for the flocculant adsorption tests were similar to that described in Section 6.3.4 (FBRM experiments), except that the solids concentration was increased to 5 wt/wt%. The higher solids concentration was chosen so that the results are more relevant to the settling tests.

As in the FBRM experiments, the PAA flocculant solution was added to the slurry in a single dose while the HX PAM flocculant solution was split dosed, with the second addition 3 minutes after the first. The solids and flocculant contact (mixing) was maintained at 300 rpm for 15 minutes in total before stirring was stopped. For HX PAM, this meant another 12 minutes after the second dose. The slurry was then transferred to a 200 mL glass jar and allowed to settle for 1 h. Supernatant was sampled for the residual flocculant concentration analysis.

#### *6.3.6.1 Flocculant concentration determination: Hyamine method*

The determination of residual flocculant concentration in the liquor followed the procedure developed by Jones (1998), using a cationic surfactant (Hyamine 1622 – BDH Laboratory Supplies, Prod. No. 560162Y) that reacts with the carboxylate functionalities (and other anions), completely precipitating the polymer as fine colloidal particles. The turbidity resulting from the flocculant precipitation process is proportional to the flocculant concentration (Crummett and Hummel 1963; Kang et al. 2013; Michaels and Morelos 1955). Jones (1998) successfully applied this method to PAA flocculants.

The turbidity measurement itself is very sensitive to the presence of any solid contaminants. Therefore, supernatant solutions that still contained very fine and non-settling particles required further treatment, prior to reaction with Hyamine. The pre-treatment involved centrifugation for 30 minutes at 4500 rpm before 30 mL of solids-free solution was taken and mixed with 10 mL of sodium gluconate solution

(concentration 400 g $L^{-1}$) to prevent the precipitation of gibbsite (Jones 1998). The centrifugation was done in a 50 ml plastic vial fitted into Heraeus Multifuge 3 S-R. The mixture was hand-shaken for a few seconds before being allowed to equilibrate on standing for 15 h.

After equilibration, a 20 mL sub-sample was added to a vial containing 5 mL of Hyamine 1622 solution (concentration = 4 g $L^{-1}$) and mixed by hand for 3 s. The turbidity (NTU) measured by Hach Ratio/XR turbidimeter and was converted to ppm following calibration with known flocculant-containing solutions. The calibration curve is presented in the method optimisation section.

The Hyamine method is claimed to be more sensitive to the presence of pure polyacrylate polymers than to the polyacrylate/acrylamide copolymer (Allison et al. 1987), due to the higher proportion of carboxylate functionalities. Addition of hydroxamate functionalities into the polymers can decrease the sensitivity even further if Hyamine reacts exclusively with carboxylate. A comparison of turbidity vs. flocculant concentration for the flocculants used in the synthetic Bayer liquor and 0.2 M NaCl is given in Figure 6.16a and b, respectively.

It is clear that all flocculants gave linear plots of turbidity vs. flocculant concentration in the testwork liquor, providing scope for residual flocculant determination. However, Alclar 665 and Magnafloc 919 display better sensitivity at very low dosages, giving a linear calibration in the concentration windows up to 1-30 and 2.5-10 ppm, respectively. The corresponding relationship of turbidity and HX-300 concentration is linear for concentrations exceeding 25 ppm.

The slope of turbidity vs. flocculant concentration obeys the following decreasing order: Alclar 665 > Magnafloc 919 > HX-300. Even allowing for the fact that HX-300 may contain 10-12% active polymer, the difference in slopes suggests HX-300 may contain much less than 50% carboxylate functionalities. Better sensitivity at lower flocculant concentration makes Alclar 665 the preferable selection for adsorption isotherm tests in the synthetic Bayer liquor.

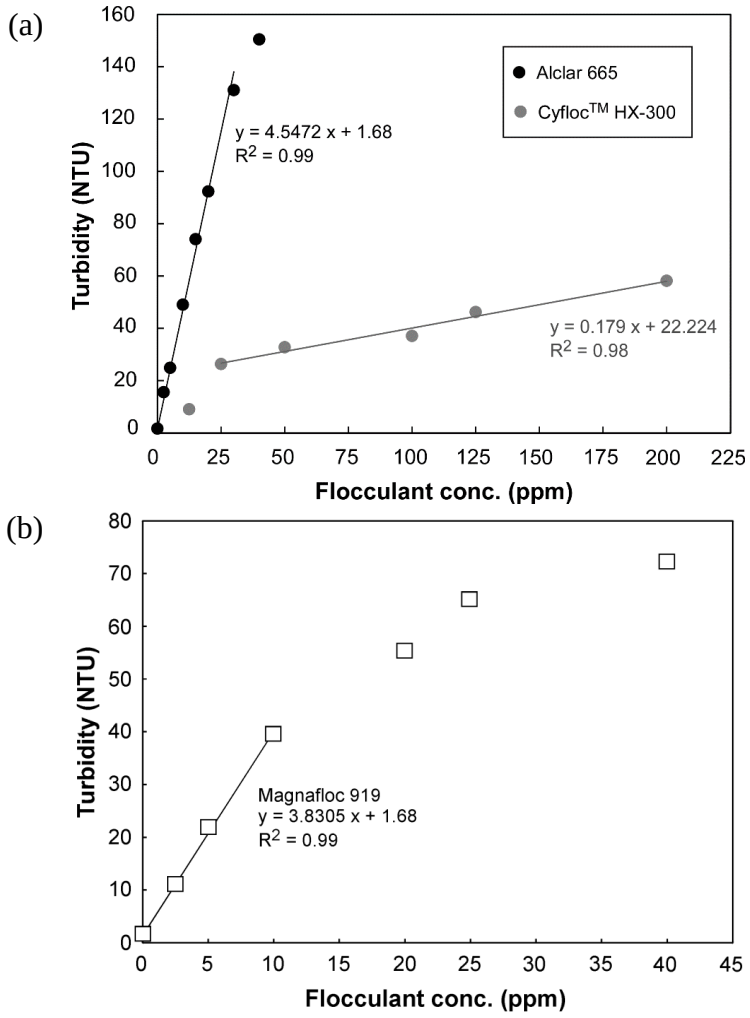


Figure 6.16. Turbidity as a function of : (a) Alclar 665 and HX-300 flocculant concentrations in the testwork liquor (b) Magnafloc 919 in the 0.02 M NaCl at pH 5.

The adsorption test was also carried out at pH 5 and room temperature for pure hematite slurry. This was done to elucidate if highly caustic solutions and elevated temperature influence the adsorption, as they are generally expected to do (see Sections 1.2 and 2.1.1). Since adsorption at pH 5 occurs through the attachment of nonionic amide and (potentially) anionic carboxylate functionalities, Magnafloc 919 (~50% anionic) was therefore purposely chosen to ensure a high degree of flocculant adsorption. A background solution of 0.2 M NaCl was used to minimise any complications from flocculant solution viscosity. Owen et al. (2008) had found that the adsorption of a mildly anionic flocculant (~20% anionic character) to kaolin was impeded by the high viscosity of the anionic flocculant in the absence of salts, mainly an effect of poor mixing. The pH of the hematite slurry was adjusted by the drop-wise addition of 0.005 M HCl or NaOH as explained in Section 5.3.3.

### *6.3.6.2 Flocculant concentration determination: filtration method*

It is worth noting that the Hyamine method works for the analysis of flocculant solutions that had been in contact with slurries of pure hematite, *in-situ* prepared DSP/hematite (31 wt/wt% DSP) or physical mixtures of DSP and hematite (also 31 wt/wt % DSP), but not with slurries of pure DSP. Even without the presence of flocculant, addition of Hyamine solution to the solids-free liquor derived from stirring pure DSP slurry for 60-75 minutes at 70°C and 300 rpm resulted in unidentified precipitation.

It is likely that higher DSP content in the slurry increases the concentration of dissolved silica to a level that exceeds its critical concentration for precipitation with Hyamine. However, the detail of this phenomenon was outside the scope of the present study. As an alternative to the Hyamine method, a filtration protocol was used which utilises the relationship of filtration time vs. flocculant concentration in the liquor (Jungreis 1981; Taylor and Nasr-El-Din 1994; Wickramanayake et al. 1987).

An increasing concentration of flocculant in the liquor is expected to correlate to the liquor viscosity and accordingly to the inverse of the filtration rate. This was calibrated by measuring the filtration time of synthetic Bayer liquor with different flocculant concentrations and plotting against the concentration of flocculation in the solution. In order to measure the filtration rate of liquor samples, 60 mL of solids-free solution from centrifugation was cooled to room temperature and vacuum filtered through a 4.7 cm diameter laboratory filtration unit (Millipore®, XX1104700) fitted with a 0.45 μm pore size membrane filter (Supor®-450). The filtration unit was connected to a vacuum pump that gave a constant vacuum pressure of 20 mm Hg. An illustration of the filtration equipment and process is given in Figure 6.17.

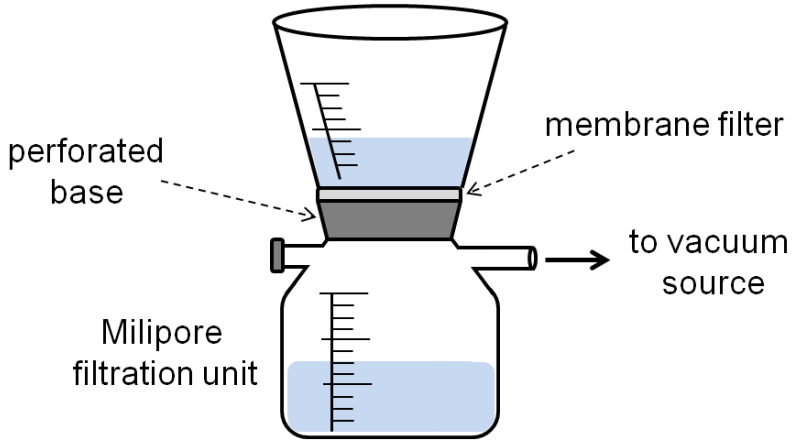


Figure 6.17. Schematic illustration of vacuum filtration for residual flocculant determination in supernatant after contact with pure DSP slurries.

The calibration curve of filtration time vs. Alclar 665 concentrations is shown in Figure 6.18. Four different measurements applied to the standard solutions prepared in different batches showed good repeatability at low flocculant dosage (≤ 4 ppm). A linear fit in the region of 1-4 ppm was also derived from repeat measurements. Such a small window for effective quantification means that high sample dilution is sometimes required, which can be a source of error. The filtration method for determining the residual flocculant concentration in the liquor was therefore reserved for certain conditions where the Hyamine method cannot be applied.

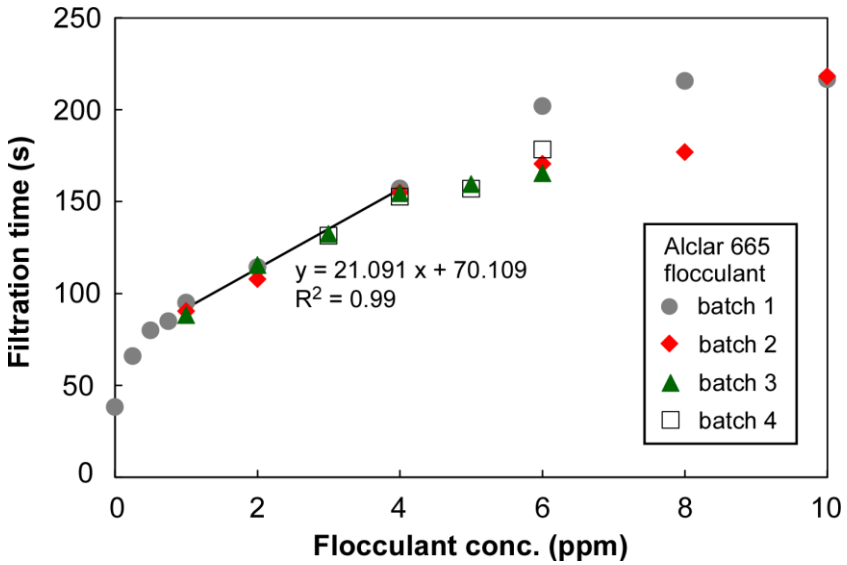


Figure 6.18. Filtration time for a 60 mL sample as a function of Alclar 665 flocculant concentration in the testwork liquor.

## *6.4 Results and discussion*

### 6.4.1 Settling tests

#### *6.4.1.1 The effect of DSP content*

The settling rate responses to flocculant dosage for 5 wt/wt% slurries with varied DSP contents (0-31 wt/wt%) are presented in Figure 6.19. The hematite and *in-situ* prepared DSP/hematite slurries have a standard deviation of approximately 1.5 m $h^{-1}$ (Sections 6.4.1 and 6.4.2), the changes in settling rate as a consequence of the increasing DSP content were definitely of a higher magnitude and therefore were not due to reproducibility issues.

For both PAA and HX PAM flocculants, increasing the DSP content led to higher dosages being required to achieve settling rates similar to pure hematite slurries. A reasonable settling rate of 15 m $h^{-1}$ can still be achieved with HX PAM even at a very high DSP content (31 wt/wt%), as seen in Figure 6.19a. However, an increase in DSP content reduces the settling rate response to flocculant dosage curve. The same observation was made when PAA was used to flocculate the *in-situ* prepared DSP/hematite slurries (Figure 6.19b). Settling rate data for HX PAM dosages $\geq$ 1000 g $t^{-1}$ are not shown in Figure 6.19a, but gave no significant increment in terms of the settling rates produced.

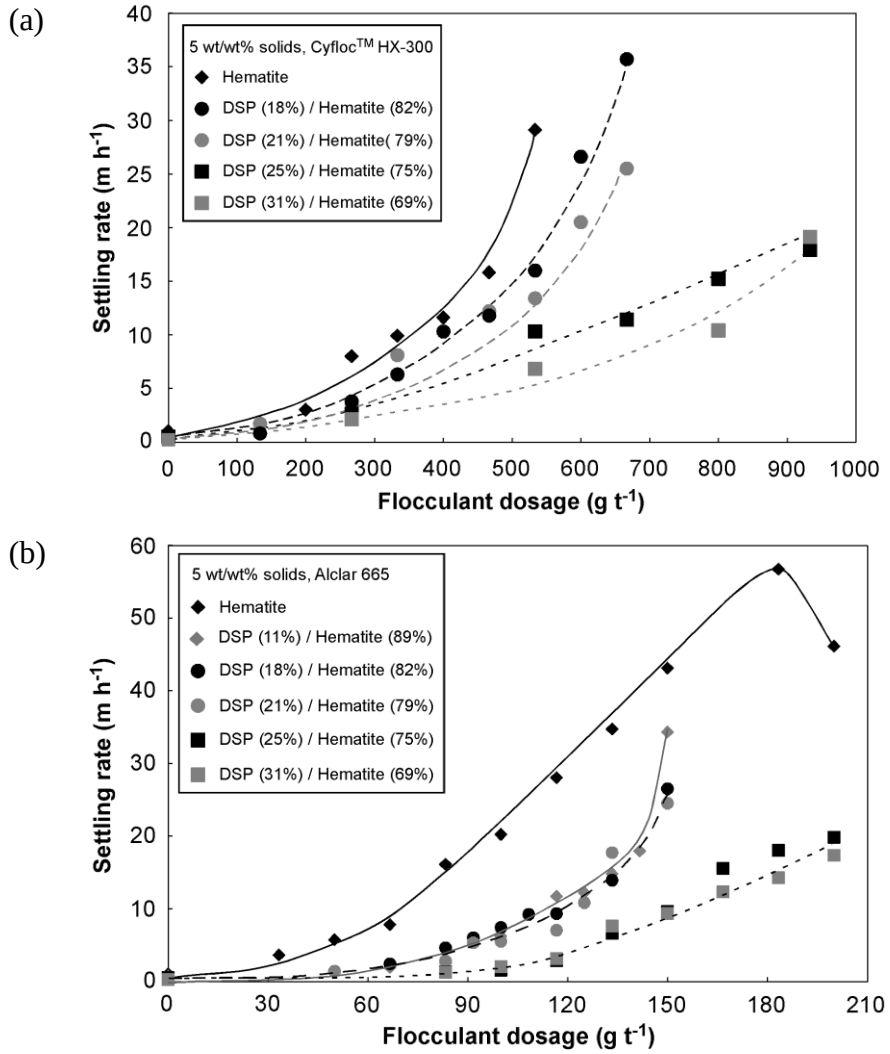


Figure 6.19. Settling rates as a function of: (a) HX PAM and (b) PAA flocculant dosages for slurries with different DSP contents.

Note that settling rates were generally higher with PAA, especially for pure hematite slurries, for which PAA generated settling rates of up to ~55 m $h^{-1}$ before dropping at higher dosages. Decreased settling rate at a high flocculant dosage is likely due to the over-flocculation phenomenon discussed in Section 2.1.4. Higher settling rates being given by PAA than HX PAM for bauxite residue flocculation has been reported elsewhere (Eckart et al. 2010; Filho et al. 2012; Kirwan 2009b; Perrier et al. 1999), including for DSP-rich residues (Rousseaux et al. 2004).

It is unfair to directly compare the relative flocculant consumptions of PAA and HX PAM given that the latter, as an emulsion product, only contains a minor active fraction per unit of product mass. In this case, the relative trends with regards to increasing DSP content were sought. At fixed flocculant dosages, HX-300 and Alclar

665 of 533 and 117 g $t^{-1}$, respectively, the settling rate dropped from 30 to ~5 m $h^{-1}$ when the DSP content increased from 0 to 31 wt/wt% (Figure 6.20). While the performance of both flocculants deteriorated, the HX product gave an overall better resistance to the increase in DSP content.

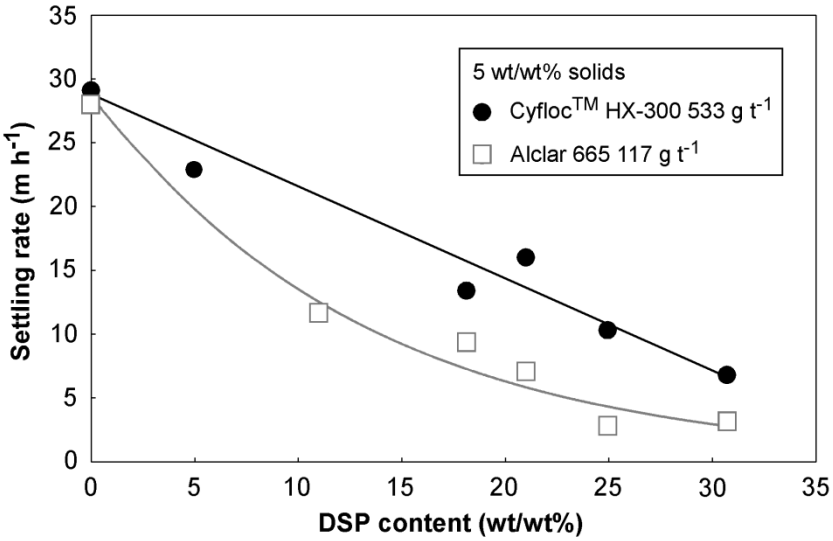


Figure 6.20. The effect of DSP content on the settling rate of the *in-situ* prepared DSP/hematite slurries from present work.

Figure 6.21 shows the results from the measurement of supernatant solids and settled bed heights after flocculation of *in-situ* prepared DSP/hematite slurries, corresponding to the settling rates given in Figure 6.20. The supernatant solids increased almost an order of magnitude higher as a consequence of the DSP content increase.

As was the case for sedimentation, the utilisation of HX PAM tends to give better results for supernatant solids, except at very high DSP contents where both HX PAM and PAA give poor clarity. At a DSP content of 18 wt/wt%, for example, the supernatant solids after flocculation with PAA was 150 ppm (or >50%) higher than when HX PAM was used. That number is beyond the experimental error which was estimated in the range of ~50 ppm. The gap diminished at very high DSP contents ($\geq$ 25 wt/wt%) where the difference is within experimental error. Also note that the supernatant solids shown in Figure 6.21 were from fixed flocculant dosage (either 533 g $t^{-1}$ HX-300 or 117 g $t^{-1}$ Alclar 665); more detailed discussion about the fines capture efficiency given by HX PAM and PAA-type flocculants for DSP/hematite

slurry, including the full dosage response curve, can be found in Chapter 7. It is also of interest that no significant adverse effect was seen in the case of consolidation behaviour when HX PAM was used, yet an increasing bed height (lower settled density) resulted at higher DSP content for PAA. There is no implication that this particular observation will be seen in a full gravity thickener with raking action.

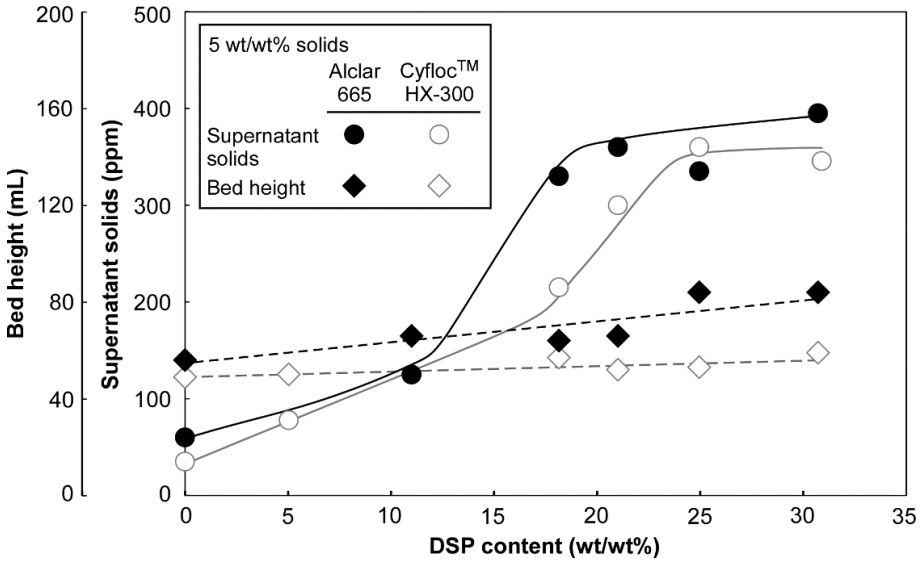


Figure 6.21. The effect of DSP content on the supernatant solids and bed height of flocculated slurries (flocculant dosage: 533 g $t^{-1}$ for HX-300 and 117 g $t^{-1}$ for Alclar 665, bed height measured 30 min after flocculant injection).

In their study of DSP effects, Davis et al. (2010a) added DSP to a bauxite residue from an operating refinery, observing settling rates and supernatant solids higher than obtained here for DSP/hematite mixtures. The very fine hematite (mostly 0.1-5 µm) used in this study largely explains the slower settling rates, and may contribute towards lower supernatant solids, given that a more definite mudline may help to "drag down" some unflocculated fines during batch cylinder settling. However, the latter result could also be evidence of other solid phases within the complex mineralogy of bauxite residue solids that are not captured by the flocculant.

Laser sizing was applied on selected samples to establish if any reduced flocculation performance from increasing DSP content was because of a change in particle size distribution. The PSDs of the *in-situ* prepared DSP/hematite slurries presented in Figure 6.22 suggest an increase in size. A higher proportion of 5-20 µm solids with increasing DSP content was apparent, especially in the case of 14-31 wt/wt% DSP.

This might explain the significant increase in the supernatant solids measured when the DSP content was between 11-20 wt/wt% (Figure 6.21), hinting that there are some fractions of relatively larger DSP particles which were poorly flocculated. These PSDs are presented in terms of their main size statistics in Figure 6.22b, $d_{10}$, $d_{50}$, $d_{80}$ and $d_{90}$ referring to the volume fraction or % volume of particles below a certain diameter.

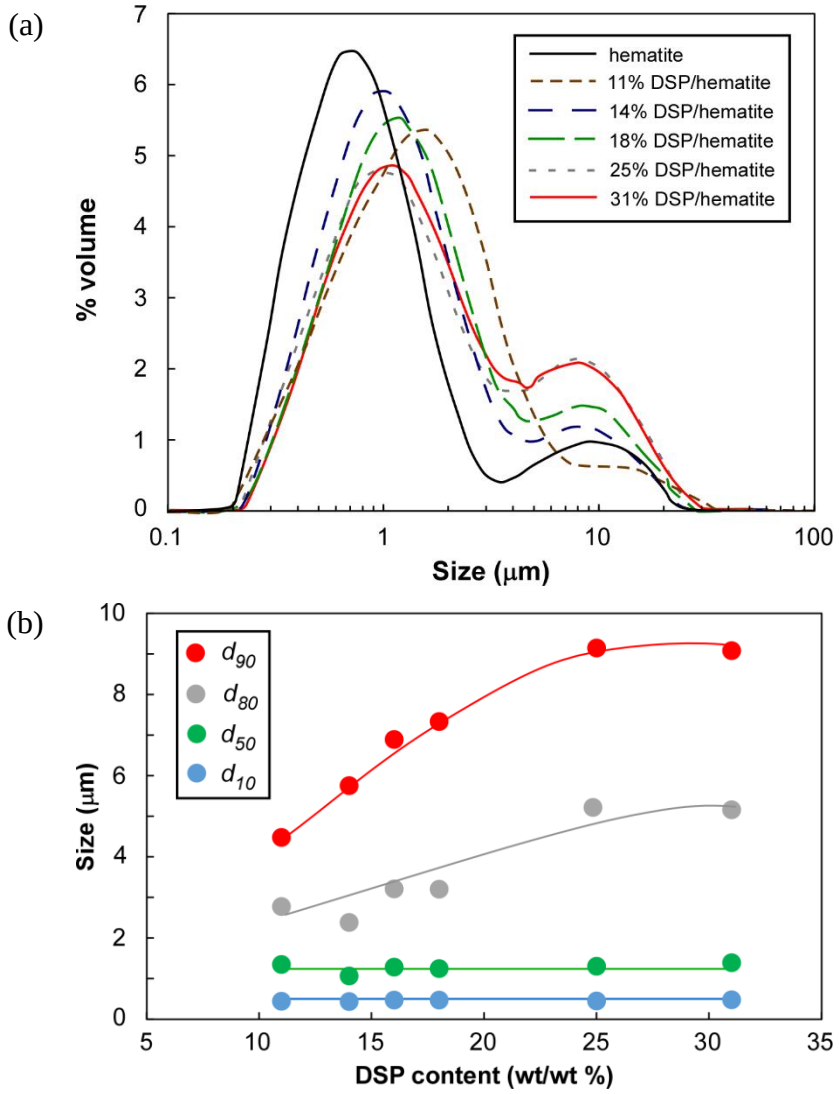


Figure 6.22. The effect of DSP content on the: (a) PSD and (b) size characteristics of the *in-situ* prepared DSP/hematite slurries.

The statistics in Figure 6.22b provide no evidence that DSP increases the population of the fines in the system, with the addition of a coarse fraction actually indicated. This is in contrast to the results from Davis et al. (2010a) who claimed that the proportion of submicron particles increases with a higher kaolin loading in digestion. This aspect receives more attention in the next Chapter. While much of the hematite used is finer than the DSP formed (Figure 5.14), it is the presence of DSP that results in the decline in flocculant performance seen in Figure 6.20 and 6.21.

#### *6.4.1.2 The effect of solids concentration*

Curves of settling rate as a function of HX-300 dosage for the flocculation of both hematite and hematite with 31% DSP made *in-situ* at a range of solids concentrations are presented in Figure 6.23a and b, respectively. They show that higher flocculant dosages are required as the solids concentration increases. The shift to higher dosages is significant for hematite alone, but the dosage curves remains quite steep, bearing in mind that the figures have different magnitudes on the dosage axis.

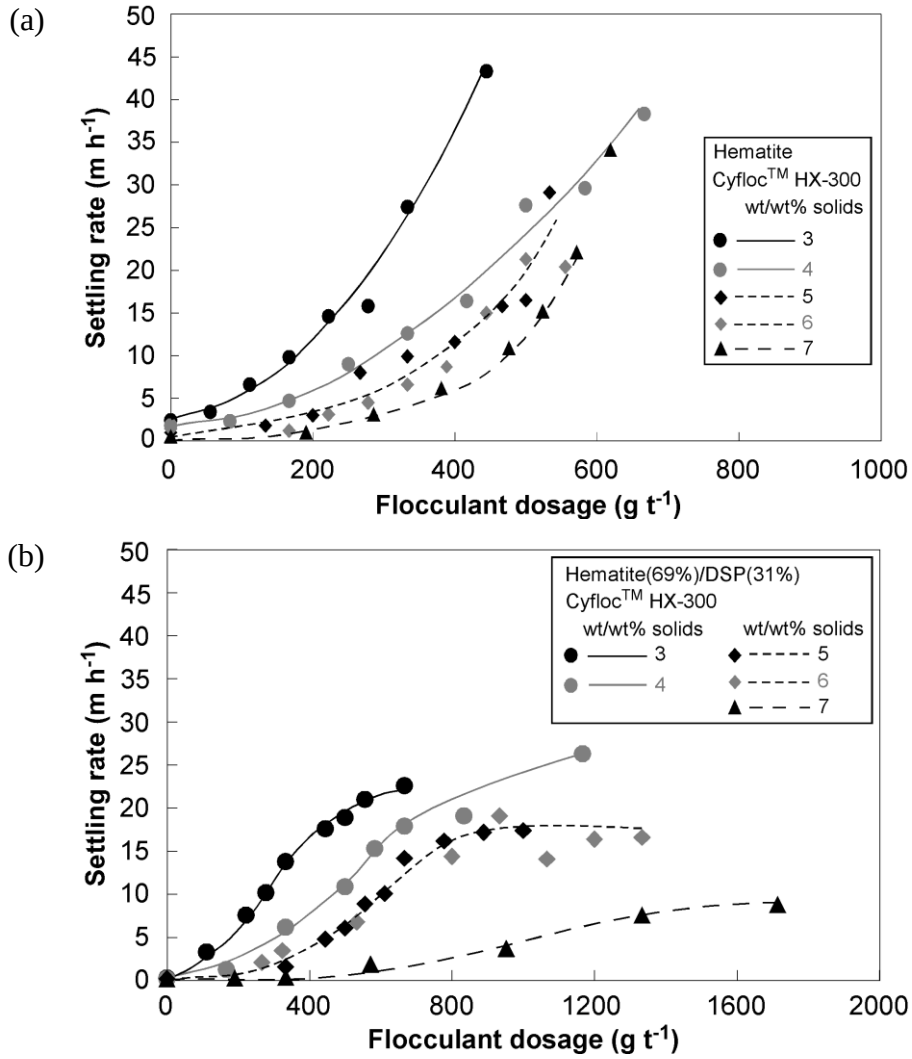


Figure 6.23. The effect of solids concentration on the settling rates of: (a) hematite and (b) the *in-situ* prepared DSP/hematite slurries (31 wt/wt% DSP).

In contrast, the increase in total solids in the presence of DSP resulted in the dosage curves flattening out such that high settling rates could not be achieved. For hematite, a settling rate as high as ~45 m $h^{-1}$ was reached at a low solids concentration (3 wt/wt%), however, this is not the case for the DSP/hematite slurries, for which the maximum settling rates were less than 25 m $h^{-1}$. A similar observation was made in the study by Rousseaux et al. (2004) where changing the refinery feed from their standard bauxite to its mixture with high silica bauxite (undisclosed reactive silica content) limited the settling rate in the primary thickener to < 12 m $h^{-1}$, down from 20-30 m $h^{-1}$ for the standard silica bauxite.

For further analysis, the settling rates in Figure 6.23 are multiplied by the solids concentration to calculate the settling fluxes (units of kg $m^{-2}$ $h^{-1}$), which is considered a better indication of achievable throughput in a thickening application. When the settling fluxes are plotted as a function of wt/wt% solids at a fixed flocculant dosage (333 g $t^{-1}$ HX-300), it can be seen in Figure 6.24 that in the presence of DSP, the settling flux was consistently lower and was very sensitive to solids concentration. The dosage in this example was not arbitrarily chosen; for a 3 wt/wt% hematite slurry, it corresponds to a settling rate of ~25 m $h^{-1}$ or what is practically aimed in a primary thickener (e.g. Rousseaux et al. 2004).

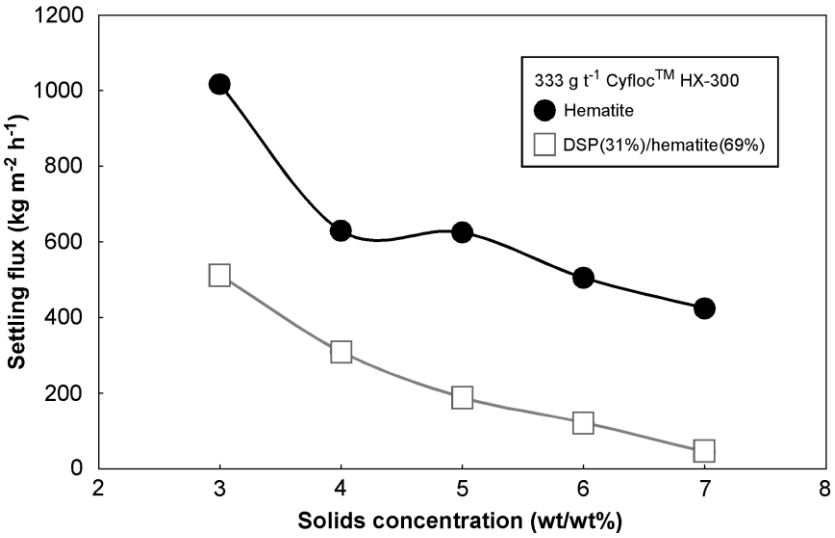


Figure 6.24. The settling flux as a function of solids concentration for hematite and the *in-situ* prepared DSP/hematite slurries at a fixed flocculant dosage (333 g $t^{-1}$ HX-300).

The sensitivity of DSP-containing slurries to the change of solids concentration has very important implications for the primary thickening process. If the slurry fed to the thickener feedwell contains a significant portion of DSP; effective internal dilution mechanism is required, otherwise optimum flocculation will not happen and the resultant settling flux will be relatively low. Even with suitable solids dilution, the settling flux will be unlikely to approach what is possible with DSP-free residue, possibly favouring a larger thickener diameter.

## 6.4.2 Size characteristics by FBRM

### *6.4.2.1 The effect of DSP content*

Mean square-weighted chord lengths were measured by the FBRM M500 probe (coarse electronics) and are shown as a function of stirring time for the addition of HX-300 (split) and Alclar 665 (single dose) to *in-situ* prepared DSP/hematite mixtures in Figure 6.25. The flocculant dosages were fixed at 556 g $t^{-1}$ and 139 g $t^{-1}$ for the HX PAM and PAA flocculants, respectively. Those dosages produced aggregates with comparable maximum mean square-weighted chord lengths (300-350 μm) for pure hematite slurries.

In both cases the decline in aggregate size with increasing DSP content is captured, as is the aggregate sensitivity to prolonged agitation. The higher maximum mean square-weighted chord length of aggregates formed by HX PAM cannot be taken as an advantage for this flocculant because dosage increase for polyacrylate flocculants also gives larger sizes (discussion on flocculant dosage effects is given in Section 6.5.2.2). An aggregate size range of 300-400 μm measured by the M500 probe is an under-estimation when compared to ~1 mm aggregates reported by the G400 probe under the same conditions (Section 4.4.3). However, this is not an issue here, as trends in response to increasing DSP content were primarily sought for comparative purposes.

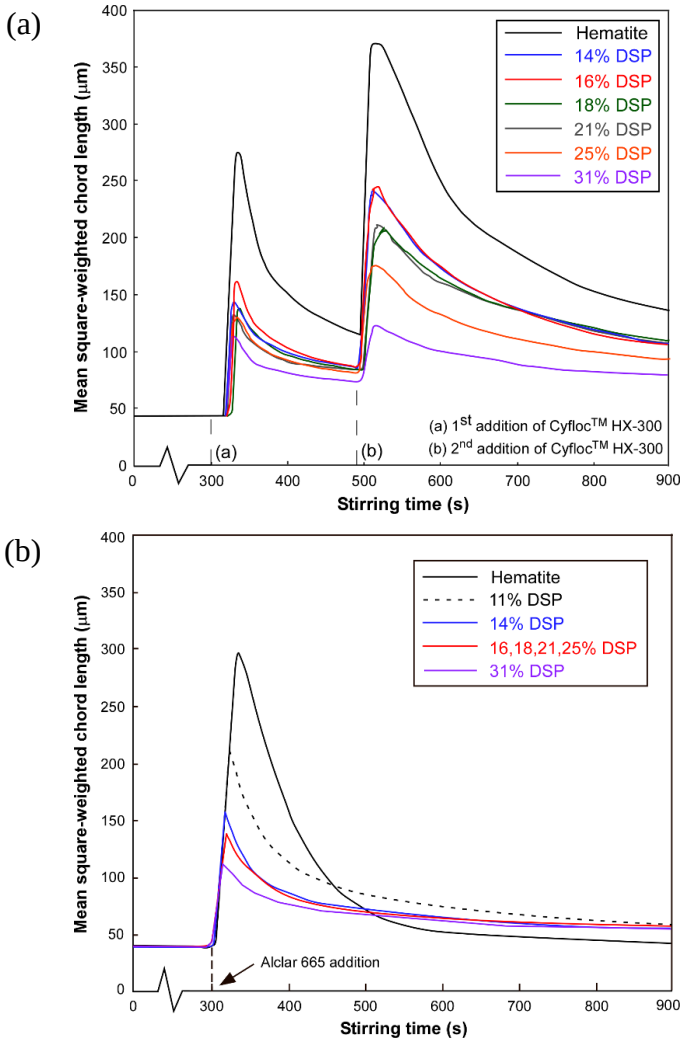


Figure 6.25. Plot of mean square-weighted chord length as a function of stirring time of hematite and DSP/hematite slurries flocculated by: (a) 556 g $t^{-1}$ HX-300 and (b) 139 g $t^{-1}$ Alclar 665 (M500 probe, coarse-electronics).

When the results in Figure 6.25 are replotted to show the maximum mean square-weighted chord length as a function of slurry DSP content (Figure 6.26), an increase in DSP was found to decrease the maximum aggregate size in a manner that was clearly flocculant dependent. For the slurry flocculated by HX-300, the maximum aggregate size decreased linearly with DSP content, whereas with Alclar 665 the size dropped sharply on the introduction of a low (11 wt/wt%) DSP content. For the latter flocculant, the drop in aggregate size then slowed, reaching a plateau at between 15 and 31 wt/wt% DSP. These trends are consistent with the settling rates responses for HX PAM and PAA use shown in Figure 6.20.

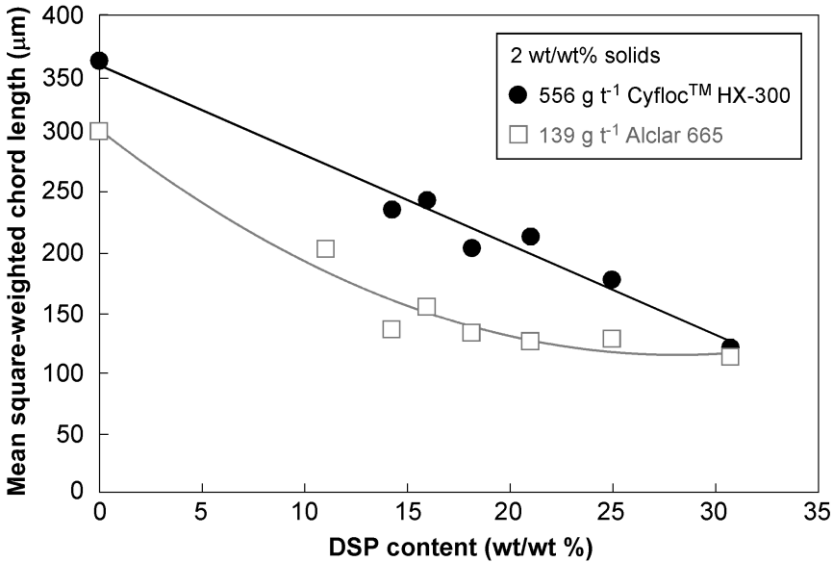


Figure 6.26. The effect of DSP content on the maximum mean-square weighted chord length of the DSP/hematite mixtures. HX-300 dosage = 556 g $t^{-1}$ and Alclar 665 dosage = 139 g $t^{-1}$ (M500 probe, coarse-electronics).

Figure 6.27a shows the unflocculated unweighted chord length distributions, while Figure 6.27b shows the corresponding distributions for HX-300 flocculated slurry after it has reached its maximum mean square-weighted chord length soon after the second addition of flocculant (i.e. the second peak in Figure 6.25a). In terms of the unflocculated feeds (Figure 6.27a), the unweighted chord length distributions shift slightly to the left (lower size) with the presence of DSP (i.e. 14 wt/wt%). This was in contrast to the PSD results measured by Malvernsizer (Figure 6.22). It was possible that hematite particles, which were mostly finer than DSP, experienced a greater degree of coagulation in high ionic strength synthetic Bayer liquor.

It is of interest that there was almost no difference detected when the DSP content was further increased to 31 wt/wt%. In addition to the natural coagulation of hematite in the high ionic strength solutions, the lower sensitivity of the M500 probe in the lower chord length range may also be a factor.

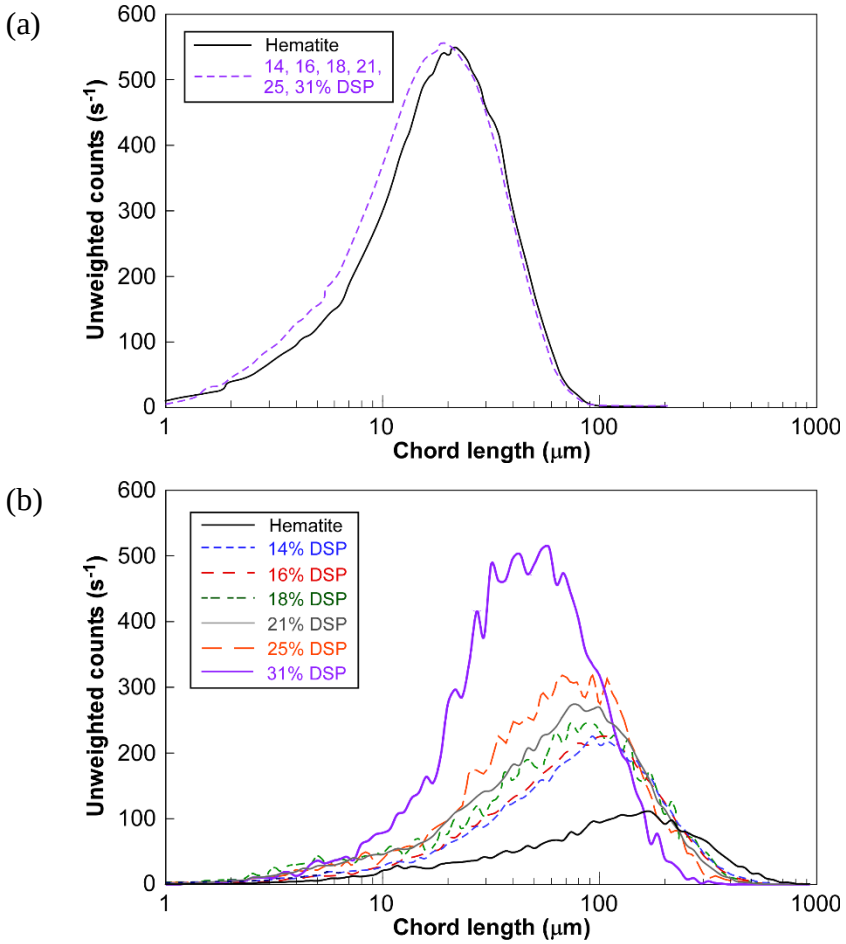


Figure 6.27. The effect of DSP content on the unweighted counts of hematite and the *in-situ* prepared DSP/hematite slurries: (a) unflocculated and (b) flocculated by 556 g $t^{-1}$ HX-300 at the 2$^{nd}$ peak in Figure 6.25a (M500 probe, coarse-electronics).

The work summarised in Chapter 4 has shown that unweighted chord length distributions are sensitive to both the extent of flocculation and the efficiency of the process (i.e. the presence of fines). In the flocculation of *in-situ* prepared DSP/hematite (Figure 6.27b), increasing DSP content led to an elevation in the proportion of counts < 40 µm. The absence of bimodal character in these distributions suggests that while the extent of flocculation is limited, the majority of particles are still being captured, i.e. most of DSP is being flocculated. This is more obvious when comparing the unweighted counts at the chord length ≤ 10 µm, which dropped by a factor of five-fold after flocculation despite the DSP content. However, it must be taken into account that the newer generation FBRM probe (G400) may give different results, especially due to its enhanced sensitivity in the lower size region. This aspect is discussed separately in Chapter 7, where the G400 probe was used specifically to study fines capture efficiency with different polymer reagents.

### *6.4.2.2 The effect of flocculant dosage*

The use of the M500 probe was extended to study how the aggregate size evolved after the first and second addition of HX-300 at various dosages. The response of the mean square-weighted chord length over time to HX-300 dosage is presented in Figure 6.28a and b for pure hematite slurry and *in-situ* prepared DSP/hematite slurry (31 wt/wt% DSP), respectively.

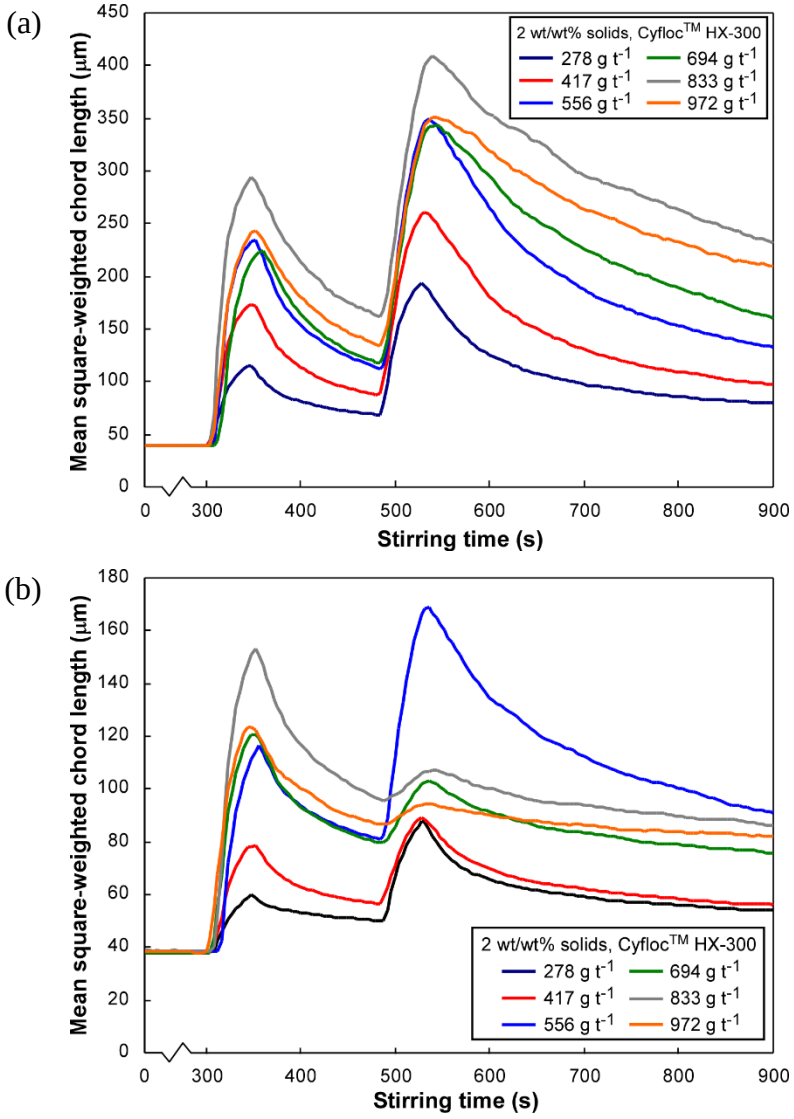


Figure 6.28. Plot of mean square-weighted chord length as a function of stirring time for the: (a) hematite and (b) DSP/hematite slurry (31 wt/wt% DSP) at various HX PAM flocculant dosages (M500 probe, coarse-electronics).

Note that Figure 6.28a and b have different scales on the chord length axis as a consequence of DSP/hematite slurry forming aggregates of a more limited size compared to the pure hematite slurry. In the absence of DSP, the second addition of HX-300 produced much larger aggregates than those from the first addition. This obeys the anchoring and tethering concept, where smaller aggregates are initially formed, enabling the polymer chain added in the second dose to attach only to a few points on the external surface of smaller aggregates (not necessarily to all particles) and improve the bridging capacity (see Section 2.1.6).

In contrast to the pure hematite slurries, the second stage addition of HX-300 to 31 wt/wt% DSP slurries did not in all cases generate aggregates larger than those produced following the first addition (Figure 6.28b). The expected size enhancement from the second addition was evident in the presence of DSP up to a combined dosage of 556 g $t^{-1}$, but beyond this dosage the maximum aggregate size from the second addition never approached that initially achieved, despite representing a large additional dose. The impact on the maximum aggregate size is shown in Figure 6.28b, and it is consistent with the settling rate results presented in Figure 6.23b, in which high DSP content led to a plateau in the flocculant dosage response.

The data in Figure 6.28 were then reprocessed to present the maximum mean square-weighted chord lengths achieved following the first and second flocculant additions as a function of the total dosage (Figure 6.29). It is clear that for the *in-situ* prepared DSP/hematite slurry (31 wt/wt% DSP), the second HX-300 addition gave very little improvement in terms of the aggregate size, in stark contrast to the behaviour shown by the pure hematite system. This phenomenon has not been previously reported, although it may explain why increasing flocculant dosages do not lead to better flocculation results in some cases, as claimed by Davis et al. (2010a) and discussed in Section 6.1.1.

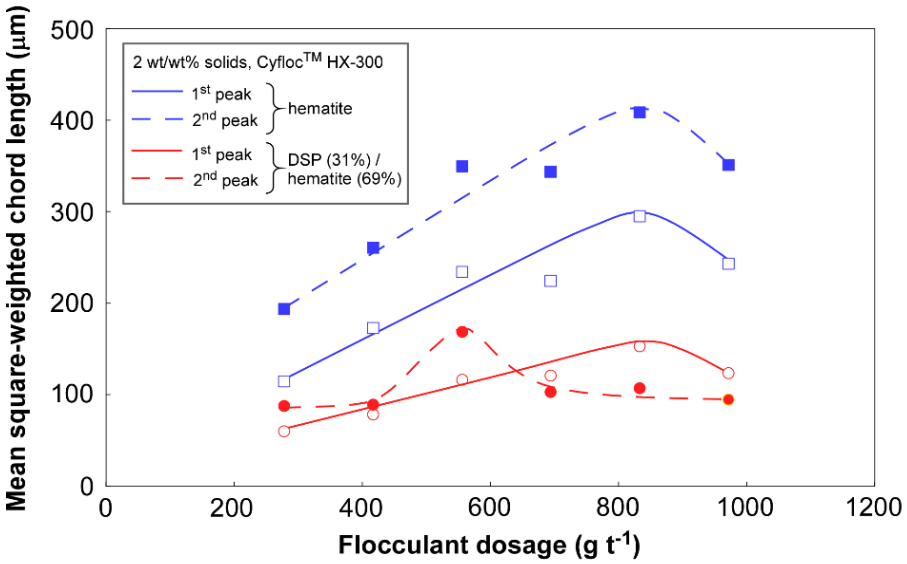


Figure 6.29. Mean square-weighted chord length as a function of flocculant dosage for the hematite and the *in-situ* prepared DSP/hematite slurries (31 wt/wt% DSP). M500 probe, coarse-electronics.

The relationship between collision efficiency and surface coverage has been explained in Section 2.1.4. With all other variables remaining constant, the collision efficiency will only be related to dosage through the fraction of surface coverage, and at high surface coverage, the collision efficiency can begin to decline. In most mineral processing applications, surface coverage will be quite low, and aggregation increases with increasing dosage. The results in Figure 6.29 suggest that the presence of DSP interacting with the hematite surface may in effect deactivate the available sites for flocculant adsorption, thereby leading to a reduction in collision efficiency. This is an area of considerable interest in understanding the influence of DSP, and is examined in more detail in Section 6.5.4.

### 6.4.3 Aggregate density characteristics by FDA

FDA experiments were conducted to investigate if there is any difference in the effective density between the hematite and *in-situ* prepared DSP/hematite aggregates (31 wt/wt% DSP). Figure 6.30a displays the settling rate as a function of size for aggregates that were in the range of 20-250 µm. After eliminating aggregates that did not satisfy the strict criteria outlined in Section 6.3.5, the number of measured hematite and the DSP/hematite aggregates were 262 and 267, respectively. The

settling rates were then used in the modified Stokes's Law (see Appendix B) to calculate their corresponding densities (Figure 6.30b).

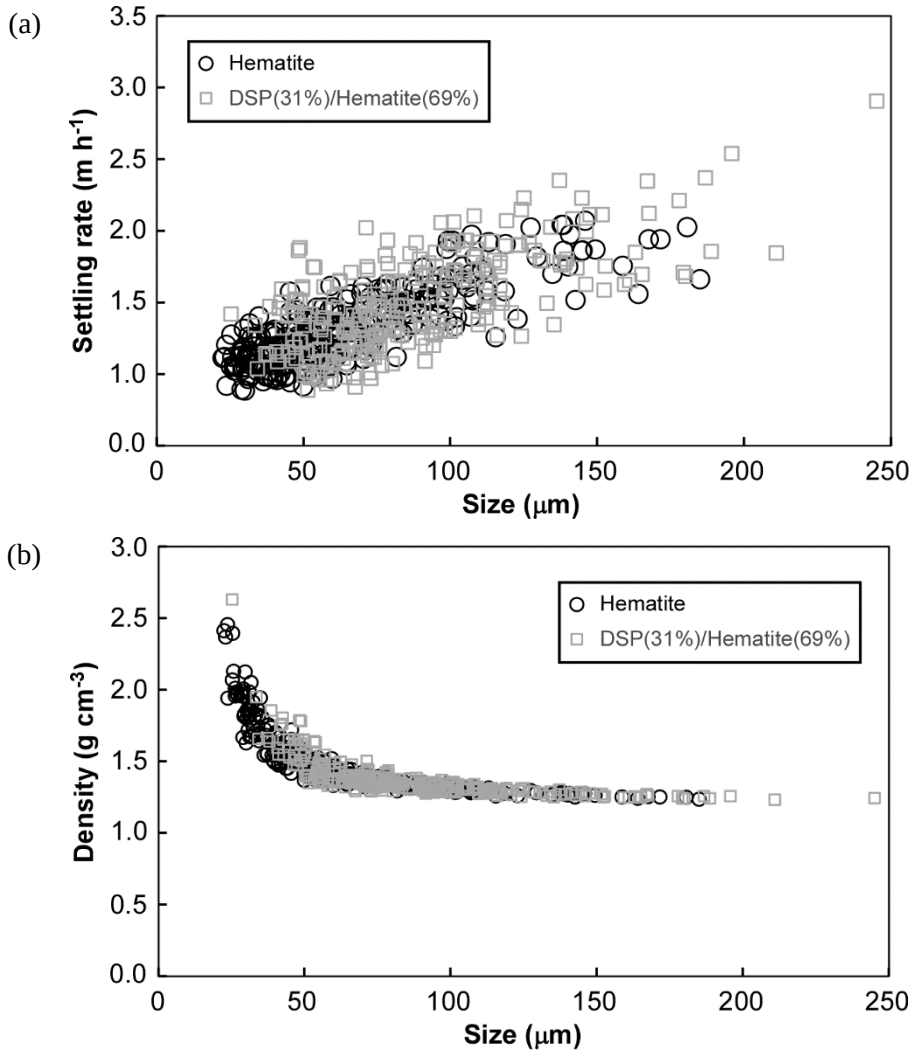


Figure 6.30. The plot of aggregate: (a) settling rate and (b) density vs. size for hematite and DSP/hematite (31 wt/wt%) slurries (flocculated for 40 s with 139 g $t^{-1}$ Alclar 665).

Surprisingly, the effective density of the hematite aggregates was not dissimilar to that of the DSP/hematite aggregates of a similar size. The presence of sodalite apparently did not contribute to a decrease in aggregate effective density, as was anticipated from sodalite's relatively low specific gravity (see Section 6.1.3). In other studies, the FDA has given insights into the effect of process parameters (such as solids-flocculant contact time or shear rate) on the aggregate density for the same solid substrate (e.g. Owen et al. 2008). In this case, the solid substrates compared are different in terms of their physicochemical properties. The measured specific gravity of hematite and DSP were different (hematite = 4.98 g $cm^{-3}$ cf. DSP = 3.98 g $cm^{-3}$).

Achieving the same effective aggregate densities from two solid substrates with different specific gravities can be achieved when there are differences in the aggregate solid volume fractions.

The plot of aggregate solid volume fraction vs. size derived from the FDA data for both pure hematite and DSP/hematite mixture is presented in Figure 6.31. The conversion from effective density to solid volume fraction follows the relationship given by Gregory (2009):

$$svf = \frac{\rho_A - \rho_L}{\rho_S - \rho_L} \qquad 6.4$$

where $svf$ is the solid volume fraction, $\rho_A$ is the effective aggregate density, $\rho_s$ is the specific gravity of the primary particle(s) and $\rho_L$ is the specific gravity of the liquor. In Figure 6.31, the difference in solid volume fraction for hematite and DSP/hematite aggregates is evident. DSP/hematite aggregates produced higher solid volume fractions than the hematite aggregates of the same size. The difference diminished for larger aggregates (≥ 150 μm) due to the fractal nature of large aggregates.

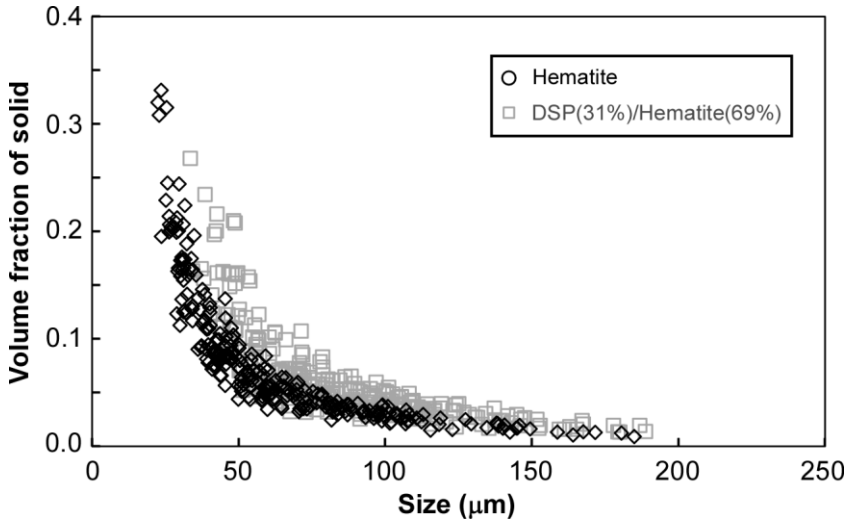


Figure 6.31. The plot of aggregate solid volume fraction vs. size for hematite and DSP/hematite (31 wt/wt%) slurries (flocculated for 40 s with 139 g $t^{-1}$ Alclar 665).

A remaining question is, how the presence of DSP in the system increased the solid volume fraction of individual aggregates? Figure 6.32 schematically explains the coverage of the hematite surface by DSP (see Section 5.4.5) and the presence of

some larger DSP-containing particles (see Figure 5.14 and 6.22) could potentially increase the solid volume fraction while the overall aggregate structure remains essentially unchanged when the same flocculant was used. The formation of DSP on the surface of iron oxide particles could incrementally increase the total solid volume fraction of the aggregate with the same size and structure. Meanwhile, larger size DSP-containing particles, either as a distinct phase or with a hematite core, could have the same mass as some hematite particles and substitute for them in the structure, which may increase the solid volume fraction of the aggregate while maintaining its effective density.

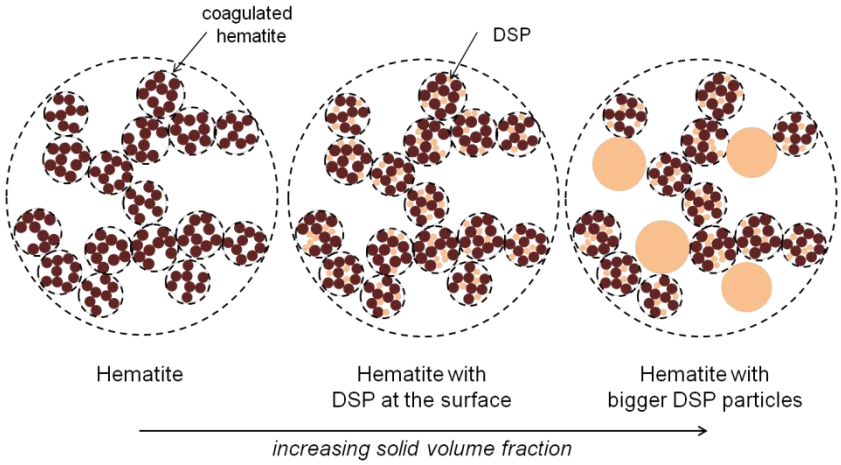


Figure 6.32. A two-dimensional illustration of the effect of partial coverage and larger DSP particles on the solid volume fraction of hematite aggregate.

What can be concluded is at this point there is no evidence that the presence of DSP contributes to a lower effective density of the aggregate. Lower settling rate for the DSP/hematite slurries could be as a consequence of the size limitation detected by FBRM (see Figure 6.25). Whether such a size limitation is driven by DSP formation at the surface of hematite that consequently deactivates sites for flocculant adsorption can be determined from adsorption isotherm for the systems, which are discussed in the following section.

### 6.4.4 Flocculant adsorption

A complete understanding of polymer adsorption during flocculation is difficult to achieve due to the broad overlapping influences of factors such as the electrokinetics at the interface, mixing hydrodynamics and availability of active sites for flocculant

adsorption. Quantification of flocculation kinetics involves larger scale experiments under controlled shear conditions, such as in turbulent pipe flow, but this requires slurry volumes that are impractical to achieve. The initial focus of adsorption studies within this Chapter was to quantify the maximum extent of flocculant adsorption for each of the different solid phases and mixed phases. Such values are obtained at dosages many times higher than would ever be applied in practice, but serve as a useful guide to the surface sites available to flocculant for adsorption and thereby may provide insights into collision efficiency effects on aggregation.

Adsorption isotherms are often presented as plots of surface excess (g $m^{-2}$) vs. residual flocculant concentration in the liquor (ppm). It is done in such a way as to take into account the significant surface area provided by fine particles, although their contribution to the total mass fraction might be limited. The plots of surface excess vs. residual flocculant concentration in the liquor for the pure hematite, pure DSP, physical mixture of hematite and DSP and the *in-situ* prepared DSP/hematite slurries are depicted in Figure 6.33. At a first glance, it was observed that adsorption onto hematite gave a higher surface excess (µg $m^{-2}$) than the other substrates, while DSP, either as a pure DSP or as 31 wt/wt% DSP in the mixture with hematite, was responsible for a lower surface excess.

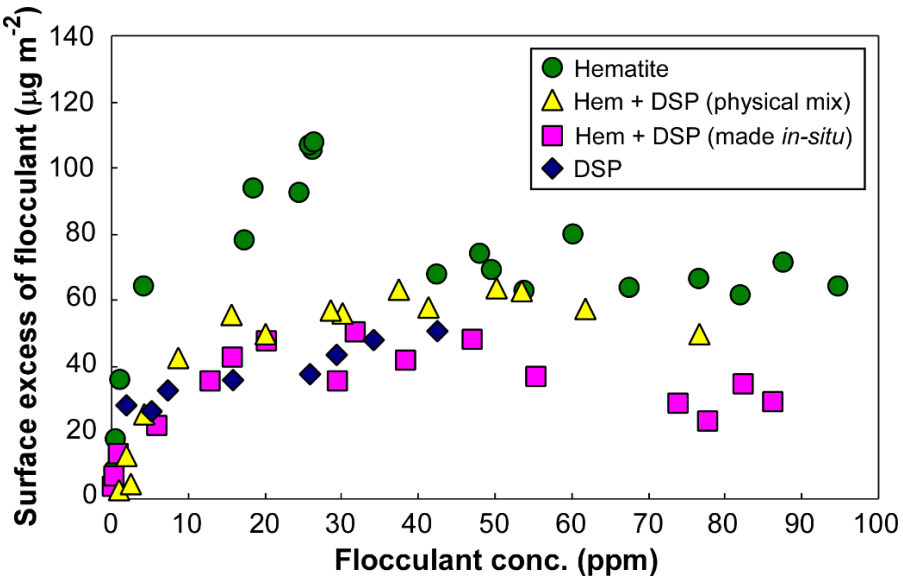


Figure 6.33. Flocculant adsorption in hematite and DSP slurries (µg $m^{-2}$) vs. flocculant concentration (ppm) (conditions: testwork liquor, 70°C, 15 minutes of stirring at 300 rpm, Alclar 665 flocculant).

The decline of flocculant adsorption (surface excess) was observed in the hematite samples at the flocculant concentration > 30 ppm. This corresponds to flocculant dosages that exceed 1000 g $t^{-1}$, and is behaviour that appears to be present to varying extents in most adsorption isotherms for flocculants on mineral systems, suggesting it may be a characteristic for bridging aggregation (e.g. Costine et al. 2014). Such aggregates are expected to be ruptured during the mixing process, which exposes fresh surfaces to the flocculant. At the same time, higher dosages impact a degree of additional strength to the aggregates, which may reduce the total surface area available and thereby lower the surface excess. There is recent evidence that extremely high dosages lead to the formation of denser aggregates (Costine et al. 2014), possibly indicating a change in aggregation mechanism.

It should also be kept in mind that the calculation of surface excess is based on the measured surface area, which is higher for DSP because of its porosity as a zeolite type mineral (Table 6.7). To date, there is not enough evidence to support porosity playing a role in flocculant adsorption, i.e. the flocculant's large dimensions in solution are likely to prevent access to surfaces within such pores. Jones (1998) measured the radius of gyration of PAA flocculant in synthetic Bayer liquor and found that it was limited to 140-160 nm due to a more coiled conformation in high ionic strength solutions. However, such dimensions are still much larger than the average pore size in DSP, preventing adsorption within the micropores. Moudgil et al. (1987) made similar observations in their study of flocculant adsorption, and proposed an alternative approach to avoid complication given by the porosity, in which the surface area from BET measurement was replaced by an estimated surface area from the average particle size.

Table 6.7. Physical properties of hematite and DSP.

| Parameter | Unit | Method | Sample | |
|---|---|---|---|---|
| | | | Hematite | DSP |
| Specific surface area | $m^2\ g^{-1}$ | BET | 5.08 | 34.2 |
| Average pore size | $10^{-9}$ m | BJH | 14.6 | 18.6 |
| Average pore volume | $cm^3\ g^{-1}$ | BJH | 0.02 | 0.16 |
| Density | $g\ cm^{-3}$ | Picnometry | 4.98 | 2.48 |
| Average size ($d_{(50)}$) | μm | Laser sizing | 0.76 | 2.74 |
| Surface area | $m^2\ g^{-1}$ | Calculation | 0.79 | 0.44 |

Note:
(i) area per g = (no. of particle per g) × (area per particle).
(ii) no. of particle per g = 1 / (mass per particle at average size).

In the work by Moudgil et al. (1987), average particle sizes were controlled by grinding and sizing, giving quite comparable calculated surface areas. For this work, without grinding and sizing, calculated surface areas of pure hematite and DSP were substantially different (0.79 vs. 0.44 $m^2\ g^{-1}$). Grinding and sizing could be applied to narrow differences in calculated surface area, but as a consequence, the adsorption measured may not then represent the conditions under which the original feed is used for the flocculation studies. The flocculant adsorption data is therefore re-presented as the mass of adsorbed flocculant per gram of solid substrate in Figure 6.34.

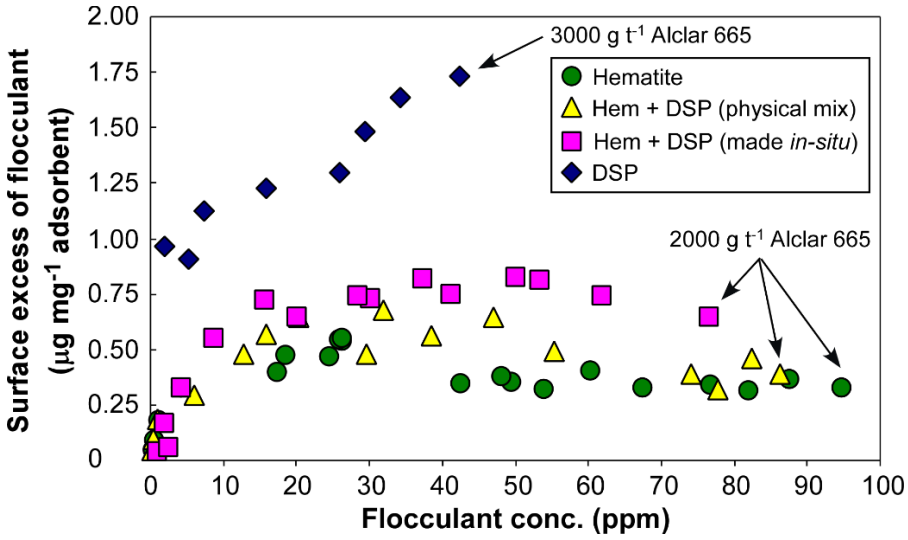


Figure 6.34. Flocculant adsorption in hematite and DSP slurries (μg $mg^{-1}$) vs. flocculant concentration (ppm) (conditions: testwork liquor, 70°C,15 minutes of stirring at 300 rpm, Alclar 665 flocculant).

From Figure 6.34, it can be inferred that the extent of polyacrylate adsorption is higher when DSP is present in the system and adsorption still gradually increases at a flocculant dosage of 3000 g $t^{-1}$ Alclar 665. For hematite and DSP/hematite slurries (both as physical mixture or when DSP was made *in-situ*), a maximum adsorption was reached with a dosage of 2000 g $t^{-1}$.

How the extent of flocculant adsorption is best compared is still debatable, but what cannot be questioned is that flocculant does adsorb on DSP. In fact, it was still adsorbed at a very high flocculant dosage. Assuming that the pore size is smaller than the flocculant dimension, the reduced bridging efficiency in the case of the *in-situ* prepared DSP/hematite slurry must therefore be due to aspects other than flocculant adsorption. Another aspect could be the aggregate strength, and a discussion of aggregate strength when DSP is present in the system is given in Section 6.5.5.

It is important to also note that the fraction of the surface area on a substrate available to the flocculant may be affected by the solution conditions and the flocculant adsorption mechanism. This can be illustrated by comparing the adsorption of flocculants of comparable solution dimensions onto hematite under different solution conditions. This requires additional measurement of maximum adsorption for an acrylamide/acrylate copolymer flocculant (Magnafloc 919) in 0.02 M NaCl at pH 5 and room temperature. The results for Magnafloc 919 adsorption under these conditions and Alclar 665 adsorption in the synthetic Bayer liquor at elevated temperature (70°C) are contrasted in Figure 6.35.

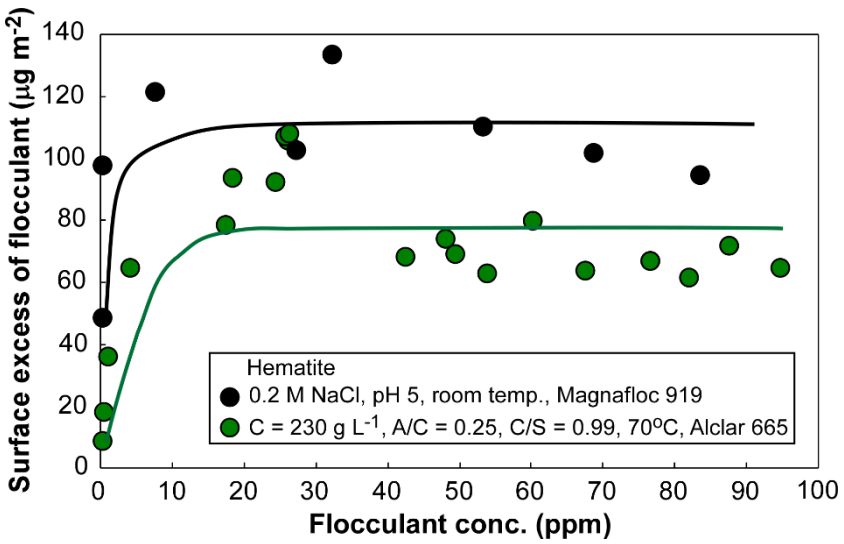


Figure 6.35. Flocculant adsorption in hematite (µg $m^{-2}$) vs. flocculant concentration (ppm) in Bayer testwork liquor and 0.2 M NaCl at pH 5.

At pH 5, flocculant adsorption reached a plateau of ~110 µg $m^{-2}$, while in synthetic Bayer liquor the corresponding plateau was only ~75 µg $m^{-2}$ (Figure 6.35). By applying the Fleer and Scheutjens model (Appendix C; Fleer and Scheutjens 1993) that relates adsorption to flocculant molecular weight and radius of gyration, the maximum hematite surface coverage by the adsorbed flocculant can be estimated. The molecular weight of both flocculants was assumed to be ~18 × $10^6$ while the radii of gyration of PAA in Bayer liquor and in 0.2 M NaCl were 140 and 170 nm (Jones 1998). In the case of solid substrates with low porosity, such as pure hematite, the surface area from BET measurement is appropriate to be used. The complete calculations can be found presented in Appendix C.

The calculated maximum surface coverage of hematite by PAA in synthetic Bayer liquor at 70°C was ~18%. This value is close to the 16% of surface coverage reported by Jones (1998) for the adsorption of PAA onto a different hematite substrate, but also in synthetic Bayer liquor. A significantly higher coverage (~34%) could be achieved for the same hematite substrate in 0.2 M NaCl solutions at ambient temperature. This is clear evidence that effective flocculation is more difficult to achieve under Bayer primary thickening conditions. At the much lower dosages applied during flocculation, a reduced fraction of the surface being available to the flocculant could lead to lower collision efficiencies during aggregation (Figure 6.4b).

### 6.4.5 Aggregate strength

While the presence of DSP does still provide active sites for flocculant adsorption (Figure 6.34), FBRM monitoring of flocculation has confirmed that higher adsorption (from increasing flocculant dosage) does not result in larger aggregate sizes (Figure 6.29). Such a limitation in the aggregate size raises the possibility of aggregate strength issues that could reflect reduced bridging capacity for adsorbed flocculant, thus preventing the formation of larger aggregates. Discussion in Section 4.4.2 underlines that the M500 monitoring is undersizing large aggregates and may in some situations be less sensitive to changes in size when shear is applied. Therefore, supporting measurements with the G400 probe were required on selected samples. The smaller dimensions of the G400 probe also give milder shear conditions than the M500 probe during beaker flocculation, and this potentially helps to preserve the fragile aggregates for a longer period during the tests.

Flocculation monitoring with the G400 FBRM probe as a function of time was carried out for hematite and *in-situ* prepared DSP/hematite (31 wt/wt% DSP) slurries at a fixed flocculant dosage. The mean square-weighted chord lengths of the hematite and DSP/hematite slurries flocculated with 35 and 69 g $t^{-1}$ Alclar 665 are shown in Figure 6.36a and b, respectively. The mean square-weighted chord length for unflocculated samples was higher for pure hematite slurry than the *in-situ* prepared DSP/hematite slurry. This is consistent to the mean square-weighted chord lengths measured by the M500 instrument (Figure 6.27) and can also be explained by the coagulation effect (Section 6.5.2).

At the lower flocculant dosage, hematite was aggregated to a peak of ~600 μm compared to the DSP/hematite aggregates, whose average peak size was limited to ~350 μm. Interestingly, at 35 g $t^{-1}$ Alclar 665, larger hematite aggregates and smaller DSP/hematite aggregates produced aggregates of relatively similar size on extended mixing.

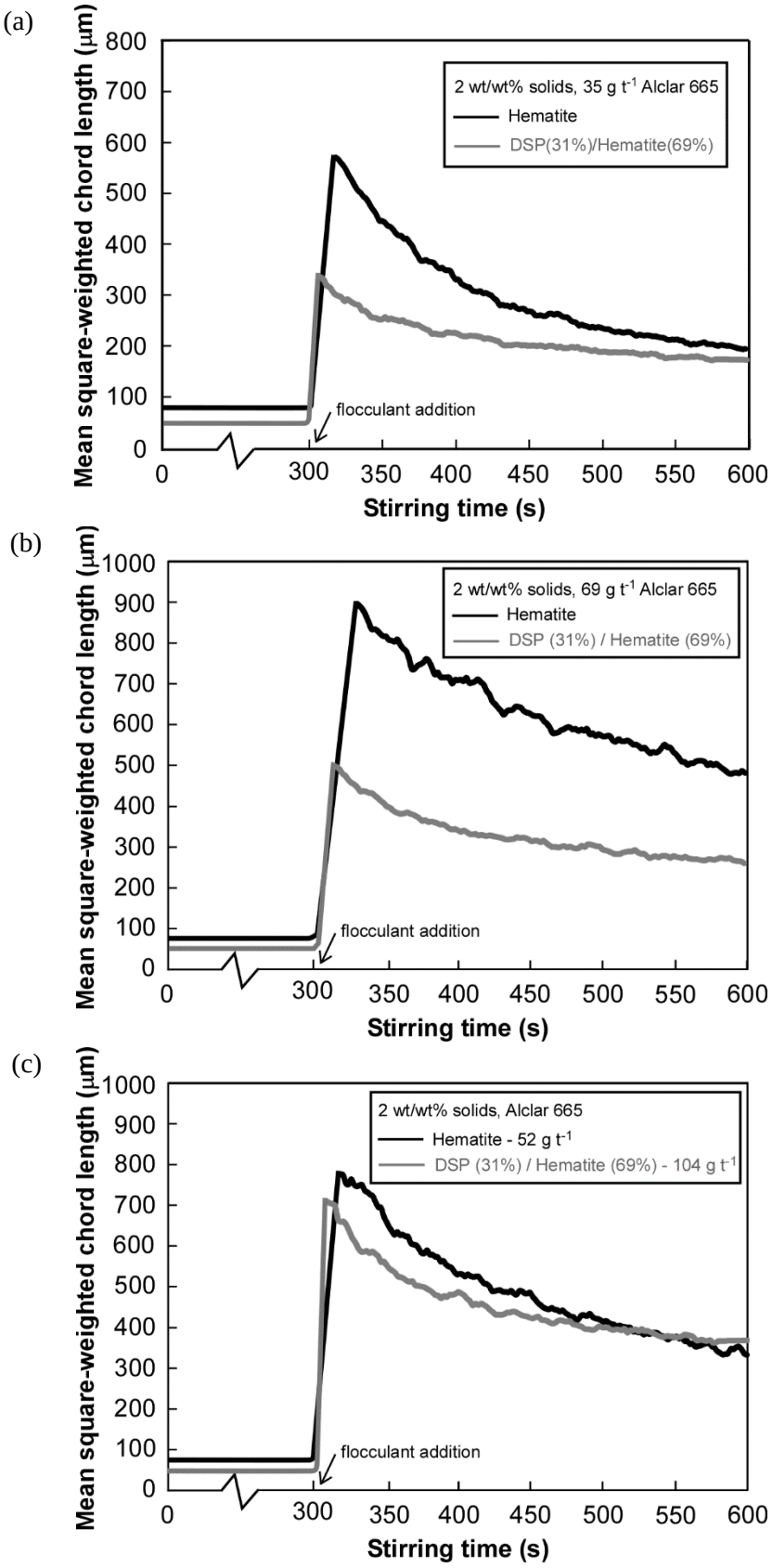


Figure 6.36. Plot of mean square-weighted chord length as a function of stirring time for hematite and DSP/hematite (31 wt/wt% DSP) slurries: (a) 35 g $t^{-1}$ Alclar 665, (b) 69 g $t^{-1}$ Alclar 665 and (c) at comparable peak sizes (G400 probe, macro mode).

Increasing the flocculant dosage to 69 g $t^{-1}$ provided further size enhancement for both systems. In this case, the maximum mean square-weighted chord length of the flocculated hematite slurries reached ~900 μm, almost twice as large as that derived from the flocculation of DSP/hematite slurries (~500 μm). Again, a greater degree of size reduction was apparent at longer reaction times for the flocculated hematite, although in contrast to the lower dosage results, the steady-state values never dropped near the same level as that obtained with Alclar 665. Hematite aggregates cannot be assumed to be weaker as a consequence of the more substantial drop in size, given that the peak sizes (the maximum mean square-weighted chord lengths achieved) before breakage predominates were so much higher. The larger fractal aggregates formed from hematite flocculation are inarguably more open and branched than the smaller ones from the DSP/hematite flocculation, and will consequently break faster.

Figure 6.36c displays the size reduction behaviour after flocculation of the hematite and the DSP/hematite mixture slurries, with the dosages adjusted so that both systems gave comparable maximum (peak) mean square-weighted chord length. Both had similar breakage profiles, hinting that the breakage rate largely depends on the initial aggregates size. However, substantially different flocculant dosages were required to produce aggregates with comparable maximum mean square-weighted chord lengths. To produce 700-750 μm average aggregates size, the DSP/hematite mixture required twice as much flocculant as the pure hematite. This extra flocculant gives supplementary strength to the aggregates, as was seen in Section 4.4.3. Based on this fact, it can be concluded that the aggregates with DSP present are intrinsically weaker.

This experiment was extended to see if a similar trend in aggregate strength was observed in the settling tests. Figure 6.37 shows the settling rates of hematite and DSP/hematite mixture (31 wt/wt% DSP) plotted against the total number of strokes applied during flocculation. The flocculant dosages were again adjusted so that both slurries gave comparable settling rates under standard mixing conditions. The HX-300 dosages were 417 g $t^{-1}$ for the hematite slurry and twice of that (833 g $t^{-1}$) for the

DSP/hematite mixture slurry. As HX-300 was added in split (50:50) mode, the number of strokes was for the total strokes equally shared between the first and the second additions. The total number of strokes itself represents the degree of shear (agitation) applied to the aggregates.

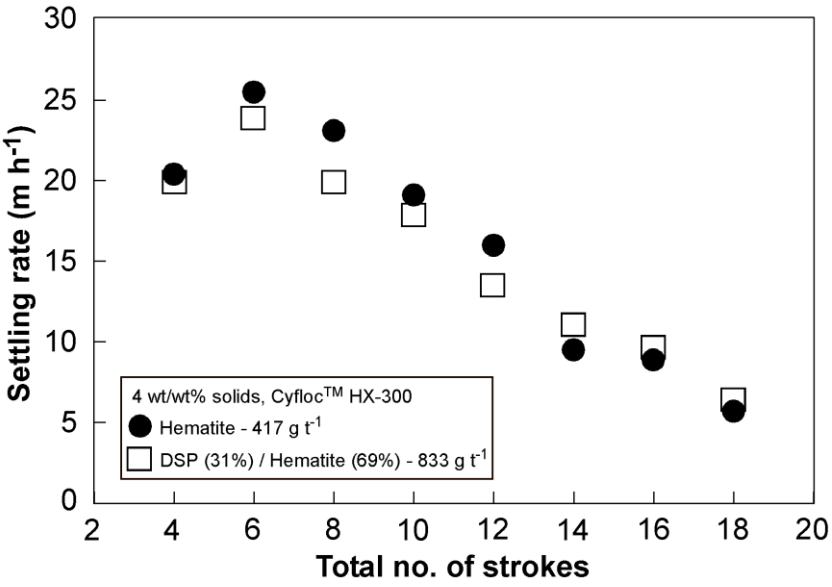


Figure 6.37. The effect of number of strokes on the settling rates of hematite and DSP/hematite slurries (HX-300 dosage: 417 g $t^{-1}$ for hematite and 833 g $t^{-1}$ for the DSP/hematite with 31 wt/wt% DSP; HX-300 was split dosed and the total number of strokes was recorded).

It can be seen from Figure 6.37 that the reduction in settling rates for the DSP/hematite mixture with the increasing number of strokes followed the same trend given by hematite slurries. Despite a different flocculant used in this settling test, the behaviour is very similar to that seen in the FBRM profiles (Figure 6.36), including the fact that DSP/hematite mixture required more flocculant to achieve the typical settling rate and the same degree of strength.

## *6.5 Summary*

This Chapter addressed a variety of aspects regarding the flocculation of DSP/hematite slurries in which the DSP was prepared *in-situ*. The increase of DSP content in its mixture with hematite had a detrimental effect on the extent of flocculation, with trends dependent to some degree on the flocculant chemistry. While a polyacrylate flocculant could generate relatively high settling rates at high

dosages, HX PAM flocculants gave an overall better resistance to the negative impacts from an increased DSP content. Nevertheless, the supernatant solids measurement gave readings that were almost an order of magnitude higher when the DSP content was high (31 wt/wt%) for both polyacrylate and HX PAM. High supernatant solids in the settling tests would correspond to poor overflow clarity in thickener operation and this would definitely create a problem in subsequent security filtration. Issues relevant to fines capture are discussed in more detail in Chapter 7.

The flocculation response to increased flocculant dosage was also poor when DSP was present. Reducing the solids concentration could improve bridging flocculation and be a partial remedy for treating DSP-rich bauxite residue, but settling fluxes will always be lower.

From FBRM monitoring of flocculation (M500 probe), the DSP/hematite slurries were shown to produce smaller aggregates than the pure hematite slurries. Smaller aggregates size was postulated as the main reason for reduced settling rates. The aggregate density data from FDA experiments did not provide any evidence that DSP (with a specific gravity lower than hematite) decreased the effective density of the aggregates. It is likely that the bigger DSP particles compensated for its lower specific gravity in the same aggregate structure, creating the same total mass per unit volume. This was indicated by an increase in effective solid volume fraction for the DSP/hematite aggregates.

Smaller aggregate sizes produced from the DSP/hematite slurries was initially thought to be a result of a lower collision efficiency, with DSP forming at the surface of hematite reduces the available active sites for flocculant adsorption. However, flocculant adsorption onto pure DSP was evident even at a very high dosage (3000 g $t^{-1}$). While flocculant was adsorbed by DSP, the size increments with increases in flocculant dosage were marginal for the DSP/hematite mixtures. This prompted the use of the G400 FBRM instrument that gives more representative aggregate size and better sensitivity to changes of chord length under continuous mixing (shear).

The G400 results showed that at the same flocculant dosage, DSP/hematite slurries still generated smaller aggregates although larger than those reported by the M500 instrument. At the same flocculant dosage, the larger aggregates formed from the pure hematite slurry seemed to break-up at a faster rate than the smaller DSP/hematite aggregates, this has to be viewed with caution, as larger aggregates are always more prone to breakage.

For a fair comparison of aggregate strength, the flocculated pure hematite and DSP/hematite slurries must have comparable maximum aggregate sizes. This was achieved by adjusting the flocculant dosages where twice the flocculant was required by the DSP/hematite slurries. Having comparable sizes, both type of aggregates showed similar breakage profiles. The DSP/hematite slurries required more flocculant, which in turn provides additional polymer bridges to preserve the structures formed. It can then be concluded that DSP/hematite aggregates exhibit a lower degree of strength. This was also confirmed in settling tests in which the number of strokes for flocculant mixing (representing the magnitude of shear) were varied.

# 7 The impact of silane-containing polymer

## *7.1 Introduction*

The impacts of DSP on the flocculation of hematite (as a model substrate for bauxite residue) were considered in Chapter 6. Although the HX PAM flocculant performs better than PAA, the former did not completely resolve the problems arising from the presence of DSP. Poor overflow clarity, for example, was still evident (Figure 6.21).

It is claimed that silane-containing polymer gives benefits in terms of decreasing supernatant solids and/or increasing settling rates when mixed with the DSP-rich bauxite residue slurry prior to the addition of HX PAM or PAA flocculant (Dai et al. 2008; 2010; Davis et al. 2010a, 2010b). These polymers may contain acrylate, amide or hydroxamate character with silicon-containing pendant groups (-$Si(OR)_3$) attached directly to the polymer backbone or through a suitable linking group (Dai et al. 2008). The linkages (referred to as X in Figure 7.1) can be $C_{1-6}$ alkyl chains (including those with ether or amide linkages) whereas R are possibly lower alkyl groups, $C_{1-6}$ alkyl groups, $C_{1-3}$ alkyl groups, phenyl, benzyl, $Na^+$, $K^+$ and $NH_4^+$.

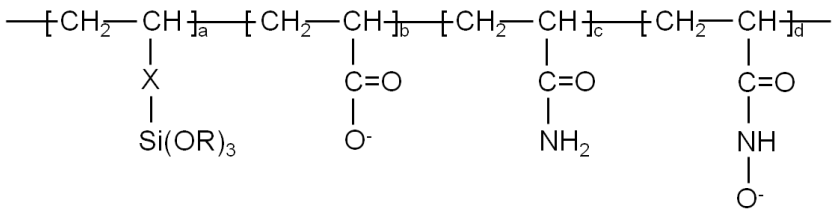


R = lower alkyl groups, $C_{1-6}$ alkyl groups, $C_{1-3}$ alkyl groups, phenyl, benzyl, $Na^+$, $K^+$, $NH_4^+$, etc.

X = $C_{1-6}$ alkyl chains, alkyl chains with ether linkages, alkyl chains with amide linkages, etc.

Figure 7.1. The chemical composition of silane-containing polymer. Adapted from Dai et al. (2008).

The same authors also stated that the concentration of $Si(OR)_3$ group in the silane-containing polymer is at least 1 wt/wt%, with the polymer's molecular weight between 1,000 and 15 million. Details of the silane-containing polymers, including

its chemical composition, concentration of $Si(OR)_3$ group and molecular weight, vary depending on the application and remain proprietary information for Cytec.

As the application of silane-containing polymer to bauxite residue flocculation is relatively recent, only a very limited number of studies have been published in this area. Table 7.1 summarises all the experimental conditions considered to test the effects of silane-containing polymers. It is important to note that in some studies, DSP originated from the reactive silica in the ores, while in the remainder, pre-made DSP was mixed with bauxite residue to produce mixtures of various DSP contents. The latter does not necessarily reflect actual refinery conditions where DSP is formed concurrently with bauxite residue. As was shown in Chapter 5, the physical mixtures of DSP and iron oxide (or residue) would give different flocculation behaviour when compared to that where DSP is made *in-situ*. Consequently, the effect given by silane-containing polymer could possibly be miss-represented.

It is of interest that the dosage range for the use of such polymers spanned to very high levels, with up to 5000 g $t^{-1}$ stated in the original patent (Set A in Table 7.1; Dai et al. 2008). However, in more recent studies carried out with the commercial product (S-10292), a more moderate dosage range (0-500 g $t^{-1}$) still displayed some improvements (Set B-D; Dai et al. 2010).

Table 7.1. Experimental conditions in the flocculation studies of bauxite residue and DSP.

| Set* | Solid | DSP content** | | Solid conc. ($g\ L^{-1}$) | PAA or HX PAM Dosage ($g\ t^{-1}$) | Silane polymer type | Silane polymer dosage ($g\ t^{-1}$) | Liquor*** |
|---|---|---|---|---|---|---|---|---|
| | | As R-$SiO_2$ | As DSP in Residue | | | | | |
| A | Residue + synthetic DSP | - | 0-100 | 40 | 0-125 (PAA)<br>0-500 (HX PAM) | Referred to as A-U | 0-5000 | A/C = 0.60<br>C/S = 0.85<br>C = 235 g/L |
| B | Diasporic bauxite | 13 | - | 98 | 522 (PAA) | S-10292 | 0-450 | Primary thickener |
| C | Diasporic bauxite (with 10% gibbsitic) | < 13 | - | 98 | 154 (PAA) | S-10292 | 0-500 | Primary thickener |
| D | Diasporic bauxite | Undisclosed | - | 98 | 120 (PAA) | S-10292 | 0-150 | 2nd washer |
| E | Residue + synthetic DSP | - | 20 | 40 | 375 (HX PAM) | Referred to as A-F | 750 | Undisclosed |
| F | Bauxite | 9 | - | 40 | 337 (HX PAM) | Undisclosed | 1000 | Undisclosed |
| G | Bauxite | 5.5 | - | 40 | 300 (HX PAM) | Undisclosed | 0-1375 | Primary thickener |
| H | Bauxite | 4.5 | - | 40 | 920 (HX PAM) | Undisclosed | 0-1375 | Plant slurry |
| I | Residue + Ca-aluminosilicate | - | 0-100 | 40 | 0-100 (PAA)<br>0-250 (HX PAM) | Referred to as A-E | 0-500 | A/C = 0.69<br>C/S = 0.87<br>C = 277 g/L |

Note: (*) Set A: Dai et al. (2008); Set B to D: Dai et al. (2010), Set E to H: Davis et al. (2010a), Set I: Davis et al. (2010b)
(**) as R-$SiO_2$ refers to reactive silica content in the ore and as DSP in residue refers to the physical mixture of pre-made DSP and bauxite residue
(***) A, C and S concentration in the primary thickener, 2nd washer and plant slurry were not given

The actual extent of improvement from silane-containing polymer addition is still inconclusive due to the different trends seen in measured settling rates and supernatant solids. Rationalisation is very difficult, given that non-identical solid substrates were employed with different polymeric flocculant combinations. For instance, selected results in Figure 7.2 show the settling rate and supernatant solids response to increasing silane-containing polymer dosage (with the same primary flocculant dosage constant within in each set). It can be seen that:

(i) when diasporic bauxite was used (Set B, Table 7.1), both the settling rate and supernatant solid increased. The latter was clearly undesirable as it creates an extra burden for security filtration of the overflow stream (Section 2.4.4);

(ii) when diasporic bauxite was mixed with the gibbsitic bauxite (Set C), the settling rate increased while supernatant solid decreased – this is the ideal outcome from feedwell processes in thickening;

(iii) when bauxite residue was mixed with synthetic DSP (Set G), the settling rate remained constant but improvement was seen in the measured supernatant solids.

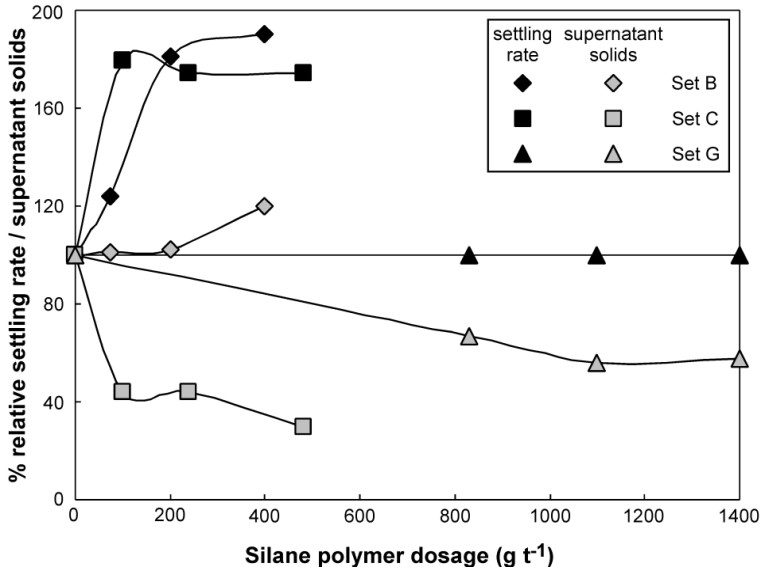


Figure 7.2. The effect of silane-containing polymer dosage on settling rate and supernatant solids with different bauxite residues containing DSP. Conditions given in Table 7.1.

Mixing (shear) intensity did not receive particular attention in these previous studies, although it is a variable that can shed light on fines capture (Sections 2.4.4 and 4.4.3), an expected feature in silane-containing polymer performance. The

mechanism by which this polymer enhances flocculation on subsequent addition of PAA or HX PAM flocculants also remains poorly understood.

## *7.2 Objectives and approaches*

The work described in this Chapter sought insights into hematite flocculation by PAA and HX PAM when DSP is present with pre-dosing of silane-containing polymer. Settling test and FBRM results derived from varying the following experimental parameters were used to explain the possible mechanisms regarding to the role of the silane functionality:

(i) PAA and HX PAM dosage,
(ii) silane polymer dosage,
(iii) solution composition,
(iv) solids concentration,
(v) mixing, and
(vi) DSP synthesis method.

SEM and XRD analysis were also applied to the supernatant solids collected from settling tests, to understand if any mineral phase is preferentially aggregated by a specific polymer. The physical characteristics of the supernatant solids (i.e. size and morphology) were of particular interest to elucidate if they influence flocculation.

Sub-samples of the post-flocculated solids were further examined by infrared (IR) to establish the adsorption mode of the silane-containing polymer. The corresponding liquor was analysed by fluorometry to determine the extent of adsorption.

Additionally, zeta potential measurements at pH 11 were used to contrast the effects of primary flocculant (HX-300) and silane polymer addition. The reason behind this is that silane polymer might act as a coagulant, requiring primary flocculant such as HX PAM or PAA (Dai et al. 2008; 2010; Davis et al. 2010a, 2010b), or otherwise settling rates will not be as high as required. Should silane-containing polymer act as a coagulant, a greater reduction in the magnitude of the zeta potential would be expected. In theory, bridging flocculation results in little change to the zeta potential due to limited electrostatic attachment onto active surface sites (Section 2.1).

## *7.3 Experimental*

### 7.3.1 DSP synthesis

In Chapter 5 and 6, DSP was mostly made *in-situ* with the co-existence of iron oxide (hematite). DSP synthesis was done at low solids concentration (60 g $L^{-1}$ as a mixture of hematite and kaolin initially – see Section 5.3.1). This simple method was also used to some extent in this Chapter. In reality, the solids concentration in pre-desilication can be as high as 200-1000 g $L^{-1}$ (e.g. Mugnier and Leizour 2010). This creates the need to understand the flocculation behaviour of hematite slurries containing DSP made at high solids concentration.

To seek some correlation with previous studies (Davis et al. 2010a) in which pre-made DSP was physically mixed with bauxite residue, some experiments in this Chapter also involved preparing DSP and hematite as a physical mixture.

DSP synthesis in this Chapter therefore involves:

(i) DSP made *in-situ* at low solids concentration in a bench top oven,

(ii) DSP made *in-situ* at high solids concentration in a temperature controlled bottle roller,

(iii) DSP separately made at high solids concentration in a temperature controlled bottle roller, following the methods developed by Cytec Industries (Davis et al. 2010a).

While the first method was described in Section 5.3.1, the others are explained below.

#### *7.3.1.1 In-situ DSP synthesis at high solids concentration*

Synthesis at high solids concentration in a temperature controlled bottle roller differed from that done in a bench top oven. A solids concentration of 480 g $L^{-1}$ was chosen in bottle roller desilication. In 1 L of liquor, that 480 g was composed of kaolin and hematite to represent bauxite residue. Assuming that in the refinery there

is ~40 wt/wt% available alumina in addition to kaolin and bauxite residue, the calculated solids concentration would equate to 800 g $L^{-1}$ of bauxite.

In this work, gibbsite/alumina cannot be involved because no digestion reaction takes place after desilication. The available alumina was only involved in the calculation so that the mass of kaolin could be calculated based on the reactive silica (R-$SiO_2$) in the feed containing kaolin, hematite and available alumina.

An example of the calculation for 8 wt/wt% reactive silica is given in Table 7.2. It is important to note that reactive silica in the feed is not equivalent to the kaolin content. A conversion factor is required based on the stoichiometry that one mol of kaolin ($Al_2Si_2O_5(OH)_4$) contains two moles of $SiO_2$.

Table 7.2. Calculation for pre-desilication in bottle roller synthesis.

| | wt/wt% | Mass (g) based on 800 g $L^{-1}$ calculated solids conc. | |
|---|---|---|---|
| | | 1 L | 150 mL |
| R-$SiO_2$ | 8 | 64.0 | 9.6 |
| Kaolin (K) | - | 137.6 | 20.6 |
| Alumina (A) | 40 | 320.0 | 48.0 |
| Hematite (H) | - | 342.4 | 51.4 |
| Total K+A+H | - | 800.0 | 120.0 |

Notes: (1) Alumina was assumed to be 40 wt/wt% for calculation only and not involved in the pre-desilication experiment
(2) R-$SiO_2$ to kaolin conversion factor = MR $Al_2Si_2O_5(OH)_4$ / (2×MR $SiO_2$)
(3) Synthetic bauxite residue was assumed to contain only hematite and DSP
(4) A 150 mL liquor is used due to the reactor size

A mixture of kaolin and hematite was then transferred into a stainless steel reactor containing 150 mL of digestion liquor (see Section 5.3.1 for the liquor composition). The same hematite (Sigma Aldrich) and kaolin (Eckalite, Imerys Minerals) samples described in Section 5.3.1 were also used here. The reactor was 5.3 cm in diameter and 10.5 cm in height (Figure 7.3a).

(a) (b)

Figure 7.3. Bottle roller desilication set-up: (a) stainless steel reactor and (b) bottle rolling equipment with a temperature controlled oil bath.

The reactor that contained kaolin and hematite slurry was hand-stirred for 15 s with a plastic rod, tightly closed and then fitted into a holder within the temperature controlled oil bath inside the bottle roller (Figure 7.3b). The reactor was kept in a continuous rolling motion for 24 h at 90°C. Several stainless steel reactors can be fitted into the bottle roller, producing the desired amount of solids for further tests.

The desilication reaction was stopped after 24 h and the reactor was quenched by cooling with tap water for subsequent safe handling. The slurry inside was further treated prior to any measurement, as described in Section 7.3.2.

When the kaolin concentration in desilication was increased to 137.6 g $L^{-1}$ (Table 7.2), it was important to know whether the mass conversion factor of kaolin to DSP would remain the same as when the kaolin concentration was far lower. This information was also crucial towards calculating the liquor volume that must be added to achieve the desired total solids concentration for flocculation tests.

A series of experiments were then conducted by varying the mass of kaolin fed to the desilication process. The mass was adjusted to emulate 2, 4, 6 and 8 wt/wt% reactive silica (see Table 7.2 for an example of the calculation). This was done without

alumina/gibbsite. The experiments were also extended in the absence of hematite, to see if DSP production was affected by hematite seed particles. The mass of DSP produced was measured and calculated gravimetrically, assuming hematite is inert in the highly alkaline solution.

From the results summarised in Table 7.3 and Figure 7.4, the mass conversion factor of kaolin to DSP was equal to 1.33. This value was consistent, regardless of the absence or presence of the iron oxide phase, and not dissimilar to the conversion factor derived at a low solids concentration (60 g $L^{-1}$, without stirring) in Section 5.3.1. Note that when kaolin was digested with hematite, the DSP mass produced was less by ~1 g. This was due to some hematite sticking to the wall of the stainless steel reactor (Figure 7.3a), making it unrecoverable and accounting for less total DSP.

Table 7.3. Mass of DSP produced from different masses of kaolin feed in desilication.

| | Unit | Reactive silica (wt/wt%) | | | |
|---|---|---|---|---|---|
| | | 2 | 4 | 6 | 8 |
| Kaolin feed | g | 5.16 | 10.33 | 15.49 | 20.65 |
| DSP (no iron oxide) | g | 6.69 | 13.72 | 21.46 | 28.24 |
| DSP (with iron oxide) | g | 5.75 | 12.40 | 19.21 | 27.91 |

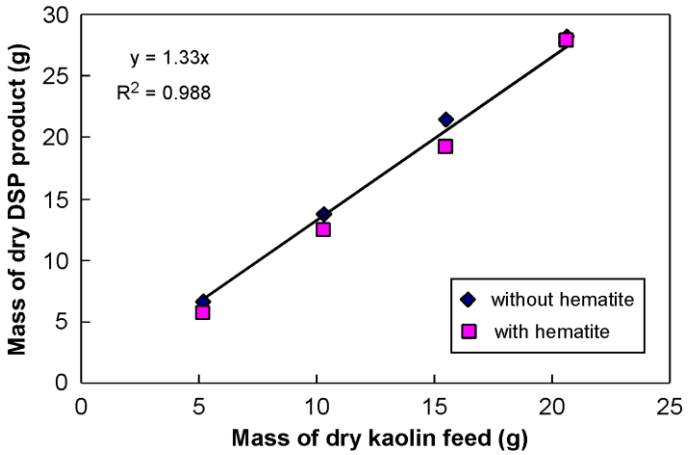


Figure 7.4. Plot of mass of DSP product vs. kaolin feed in high solids concentration desilication (in the absence vs. presence of hematite).

The same conversion factor irrespective of the presence of hematite agrees well with results in Figure 5.16, where the % conversion of soluble silica to DSP with or

without hematite particle seeds reached the same extent. The role of hematite particle seeds was limited to providing an initial rate acceleration. Theoretically, the mass conversion factor of kaolin to DSP is between 1.22-1.42, depending on "X" and "n" in the chemical formula of DSP: $Na_6(Al_6Si_6O_{24}).Na_2X.nH_2O$, where X is 2Cl, 2OH, $CO_3$, $SO_4$ or $2(Al(OH)_4)$ and n is between 1-6 (Smith 2014). The mass conversion factor of kaolin to DSP in this work is therefore within the theoretical range, confirming that experiments were done correctly.

#### *7.3.1.2 DSP made with Cytec's method*

Davis et al. (2010a) from Cytec Industries showed that DSP particle size was very much affected by the desilication conditions, in particular the solids (kaolin) concentration. The proportion of submicron particles (< 1 μm) increased from 4 to 18 and to 30 v/v% when the solids concentration in desilication was raised from 30 to 100 to 200 g $L^{-1}$, respectively, in the same synthetic liquor. This increase in submicron particles was postulated to adversely affect the supernatant clarity results.

Results discussed in Section 6.5.1.1 show that $d_{80}$ and $d_{90}$ of hematite slurries containing 0-31 wt/wt% DSP (prepared *in-situ*) increased with higher DSP content, whereas their $d_{10}$ and $d_{50}$ values remained unchanged. Considering that the PSD analysis was done in deionised water after sonication and addition of sodium hexametaphosphate dispersant (Section 4.3), it can be assumed that the extent of coagulation was minimal. Hence, it is very likely that a higher solids concentration of kaolin in the desilication process did not significantly alter the population of fines produced. This is in contrast to the results of Davis et al. (2010a), but it should be noted they synthesized DSP in liquor of a different composition, and without bauxite residue or any other (iron) oxide phase present.

It was therefore considered important to repeat the experiments based on the method developed by Cytec, to see if the DSP size distribution was different from the slurries prepared by the methods previously explained in Section 7.3.1.1. For this purpose; 4.5, 15 and 30 g of kaolin were added into a stainless reactor containing 150 mL of synthetic liquor (C = 126 g $L^{-1}$ $Na_2CO_3$, A/C = 0, C/S = 0.84, 20 g $L^{-1}$ $NaSO_4$) comparable to that used by Davis et al. (2010a). Those amounts were equivalent to

solids concentrations of 30, 100 and 200 g $L^{-1}$, respectively. After being hand-stirred for 15 s and tightly closed, the reactor was fitted into one of the holders inside the bottle roller. The contents were then predesilicated under standard conditions (90°C, 24 h) before hematite was added into the quenched slurry. This slurry was then further pre-treated for various tests.

### 7.3.2 Slurry preparation

In this Chapter, there were four main experimental methods employed to characterise the response of the solids to the silane-containing polymer. They were: cylinder settling tests, FBRM measurements with the G400 probe, quantification of polymer adsorption and zeta potential determination. Note that to study adsorption and zeta potentials, pure DSP slurry was prepared by the procedure in Section 5.3.1 (where DSP was made *in-situ* at low solids in a bench top oven). The hematite phase was not added to simplify interpretation.

Slurry preparation needed to be optimised for each method of performance characterisation. Digested slurry was initially filtered and washed, following the steps given in Section 5.3.2. The wet cake was re-slurried by using a replenishing solution, with all subsequent steps outlined in the chart given in Figure 7.5.

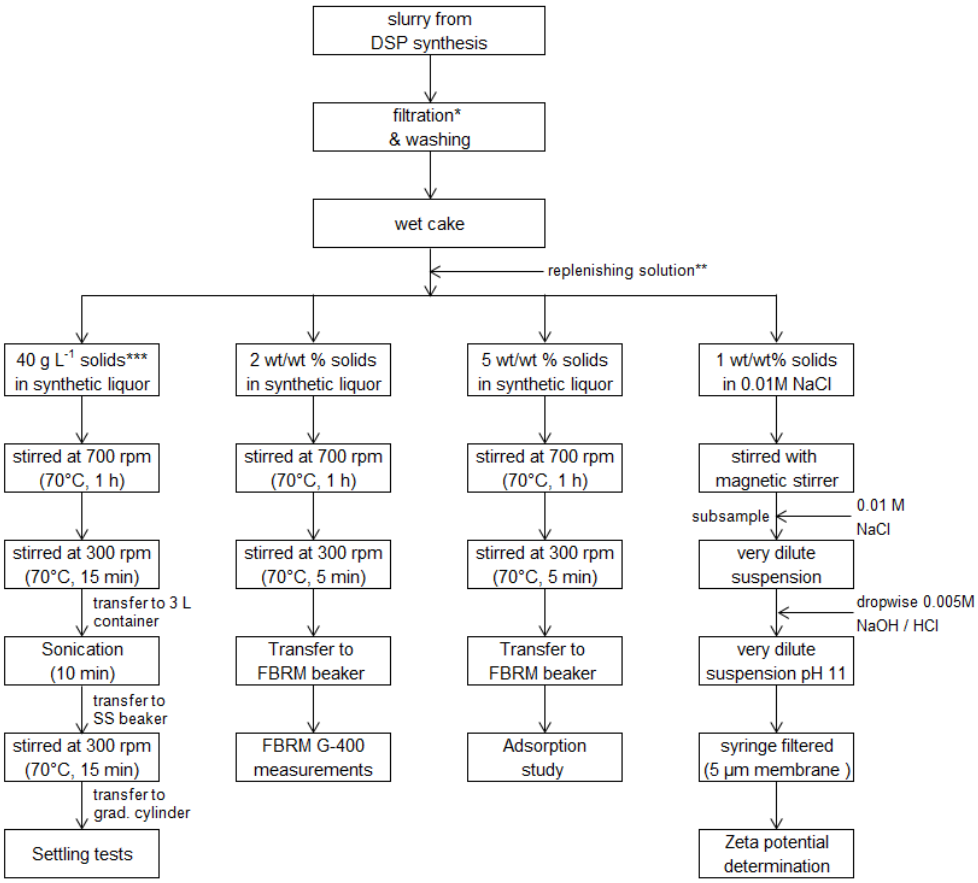


Note:(*) Filtration with 0.45 µm Supor® R-450 and washing with 5×200 mL of deionised water.

(**) Replenishing solutions mostly synthetic liquor (A/C = 0.55, C/S = 0.99, C = 230 g $L^{-1}$) except in the case of zeta potential determination (0.01M NaCl) or when A/C ratio was varied in synthetic Bayer liquor for settling tests.

(***) Unless stated otherwise, the solids concentration was 40 g $L^{-1}$.

Figure 7.5. Slurry preparation for different performance characterisation tests.

Redispersion of replenished slurry was carried out as explained in Section 5.3.2, except when preparing slurry for zeta potential determination where 0.01M NaCl was used. For settling tests, high mixing intensity (700 rpm for 1 h and 300 rpm for 15 min) and sonication (10 min) were still applied to ensure a stable dispersion before the slurry was stirred again (300 rpm) while being transferred into graduated cylinders. For FBRM and adsorption studies, sonication was not required as the continuous stirring provided during tests was sufficient to improve dispersion.

The majority of tests were done in synthetic liquor with a relatively high A/C ratio (A/C = 0.55, C/S = 0.99, C = 230 g $L^{-1}$). This A/C ratio was higher than that used in Chapter 4-6 (0.35) to be more representative of plant conditions, where primary thickeners often treat slurries with A/C ratios of 0.7 to 0.8. The A/C ratio used here

was limited to 0.55 because the sodium aluminate concentrate available for liquor preparation had a value of ~0.58 and dissolving additional high purity alumina/gibbsite in such a viscous liquor was impractical. In addition, a limited number of experiments were conducted where A/C was varied to see the effect of liquor composition.

Experiments at a relatively high A/C ratio need to be completed quickly to minimise the occurrence of gibbsite reversion (Equation 2.15). Therefore, overnight soaking of the slurry could not be applied, not even for zeta potential determinations done in a dilute salt background.

In zeta potential determinations, wet DSP cake from filtration and washing of digested slurry was re-dispersed in 0.01 M NaCl solutions (details of washing and filtration protocols can be found in Section 5.3.1). The slurry was vigorously stirred by a magnetic stirrer at room temperature for approximately 15 minutes. A few millilitres of slurry was sampled with a 20 mL syringe (Terumo® 20 mL DVR-5174) and transferred to a 100 mL plastic vial containing ~80 mL of 0.01 M NaCl. The suspension pH was adjusted to 11 by dropwise addition of 0.005 M NaOH/HCl following the method in Section 5.3.3. Suspension (25 mL) was then syringe-filtered (PALL® Acrodisc® with 5 μm membrane). The filtrate, containing only sub-5 μm particulates, was then ready for zeta potential determination (also see Section 5.3.3 for methods and equipment set-up in details).

### 7.3.3 Flocculant make-up and preparation

In addition to Alclar 665 and Cyfloc HX-200/300 flocculants, the silane-containing polymer S-10292 (Cytec Industries) was also applied for the work in this Chapter. The flocculant make-up and preparation for Alclar powder flocculant and Cyfloc HX emulsion flocculants were as described in Section 6.3.2. In contrast, S-10292 was received in a water-continuous form and did not require inversion or dissolution, but was simply diluted to 2 wt/wt% stock solutions with 20 g $L^{-1}$ NaOH and gently hand-shaken for 10 s. This stock was further diluted to 0.2 wt/wt% solutions and placed on a tabletop shaker (~120 rpm) for one hour prior to use.

All polymer reagents, including S-10292, were added at a temperature of 45°C. Similar to the dosing regime outlined in Chapter 6, Cyfloc$^{TM}$ HX flocculant was added in split (50:50) doses and the Alclar flocculant in single addition. Unless stated otherwise, S-10292 was added in single addition prior to the addition of Alclar or Cyfloc HX flocculants, following the standard procedures for its use (Dai et al. 2008; 2010; Davis et al. 2010a, 2010b).

### 7.3.4 Settling tests

Settling test procedures were described in Section 5.3.2. In Chapter 5 the number of strokes accompanying every flocculant addition was fixed at five, but in this Chapter was varied between three and eight. The different number of strokes was used to represent different applied shear conditions. Other than when the effect of solids concentration was studied, a fixed value of 40 g $L^{-1}$ was used, consistent with previous studies (Dai et al. 2008; Davis et al. 2010a, 2010b).

While cylinder settling tests are the most practical option to study flocculation, they suffer from high standard errors, up to 12% and 23% for settling rate and supernatant solids, respectively (Farrow and Swift 1996b). However, such errors are still smaller than the benefits reported from utilisation of silane-containing polymer, with 80 and 60% improvements claimed for settling rate and supernatant solids, respectively (Figure 7.1). Therefore, the initial sets of experiments were done to estimate the settling test error for flocculation of the *in-situ* prepared DSP/hematite slurries (31 wt/wt% DSP) made from low solids concentration desilication (60 g $L^{-1}$).

The settling rate and supernatant solids measured from cylinder settling tests of the same and different synthesis batches were presented in Figure 7.6. The dosage of 150 g $t^{-1}$ Alclar 665 was initially selected to give a ~20 m $h^{-1}$ settling rate (values higher than that are not required in most thickening operations). From the results in Figure 7.7, it is clear that there were unavoidable variations seen in the measured settling rates and supernatant solids, even for slurries produced from the same batch.

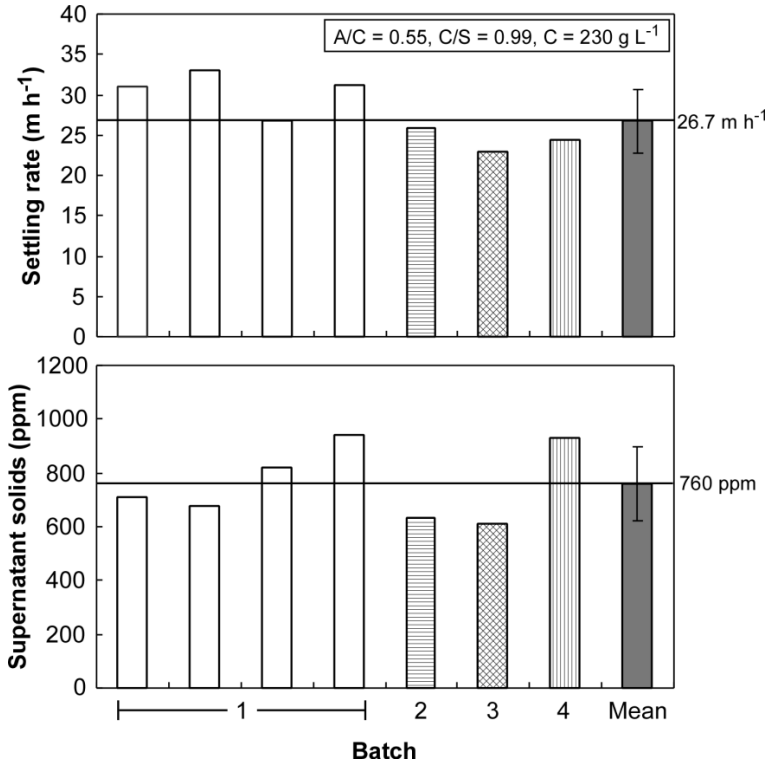


Figure 7.6. Reproducibility of the setting tests applied to the *in-situ* prepared DSP/hematite slurries (31 wt/wt% DSP) flocculated by 150 g $t^{-1}$ Alclar 665. Solids concentration in desilication = 60 g $L^{-1}$, solids concentration during flocculation = 40 g $L^{-1}$.

When settling tests were repeated seven times with the samples generated from four different batches, they gave standard deviations of 3.9 m $h^{-1}$ and 137 ppm for settling rate and supernatant solids, respectively. Any improvement given by silane-containing polymer less than those numbers can be assumed to be within experimental error.

Since one of the main objectives in this Chapter is to study the beneficial effect of silane-containing polymer in combination with both PAA and HX PAM flocculants, the reproducibility of settling tests with HX-300 flocculant was also assessed. The flocculation conditions were similar to that mentioned earlier in this section and in Figure 7.6, with the only exception that 300 g $t^{-1}$ HX-300 added. The settling rates and supernatant solids measured are presented in Figure 7.7.

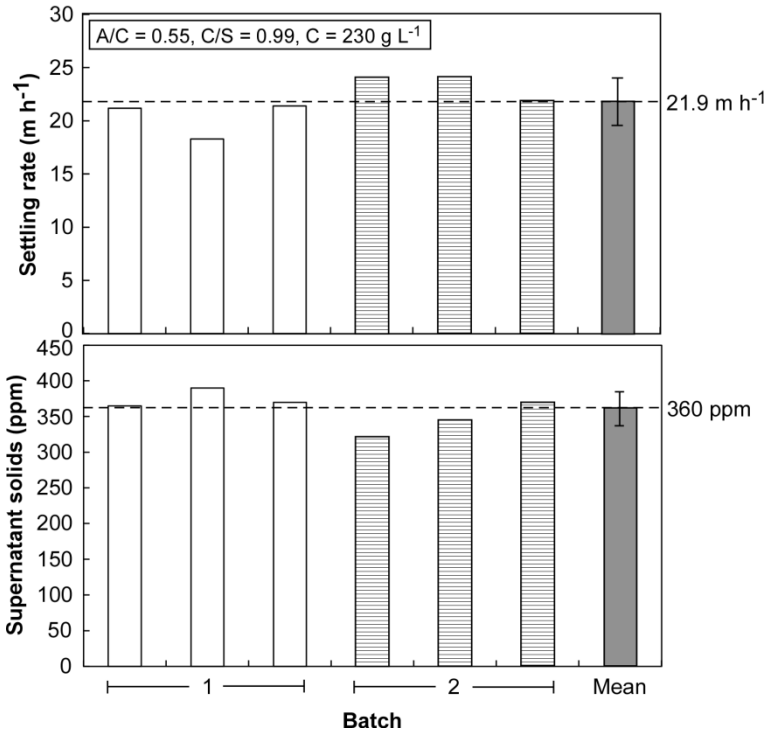


Figure 7.7. Reproducibility of setting tests from different synthesis batches for DSP-containing hematite slurry flocculated by 300 g $t^{-1}$ HX-300. Solids concentration in desilication = 60 g $L^{-1}$, solids concentration during flocculation = 40 g $L^{-1}$.

The error bars in Figure 7.7 are the standard deviations calculated from six nominally identical slurries prepared in different batches. With HX-300, the standard deviations for settling rate and supernatant solids were 2.2 m $h^{-1}$ and 25 ppm, respectively. These values were lower than those derived from Alclar 665, even when the standard deviation was converted to % relative to the mean values, which was 18% for Alclar 665 and 7% for HX-300 in the case of supernatant solids measured.

### *7.3.4.1 XRD and SEM of supernatant solids*

As at least three different polymers were employed in this Chapter, the affinity of each to the DSP or hematite solids can only be known by contrasting the mineralogy of supernatant solids which were poorly or not flocculated. Hence, it is also of importance that the supernatant solids recovered were also analysed by XRD, SEM and laser light scattering (for PSD).

After 60 s of flocculation, supernatant solutions were sampled at a given height (~4.5 cm below solution level, as described in Section 5.3.2). The sample was filtered

through a 0.45 μm membrane (Supor® R-450), washed with hot deionized water (2×100 mL) and the membrane (see Figure 7.8a) dried to constant weight to estimate the supernatant solids concentration. For XRD analysis, the thin layer of solids on the membrane was carefully rinsed off with ethanol. The suspension containing ethanol and particulates was then drawn into a pipette and dispensed on the top of a special holder (Figure 7.8b). This holder was fitted onto the Phillips X'pert diffractometer (see Section 5.3.1 for the details of diffractogram generation).

(a) (b)

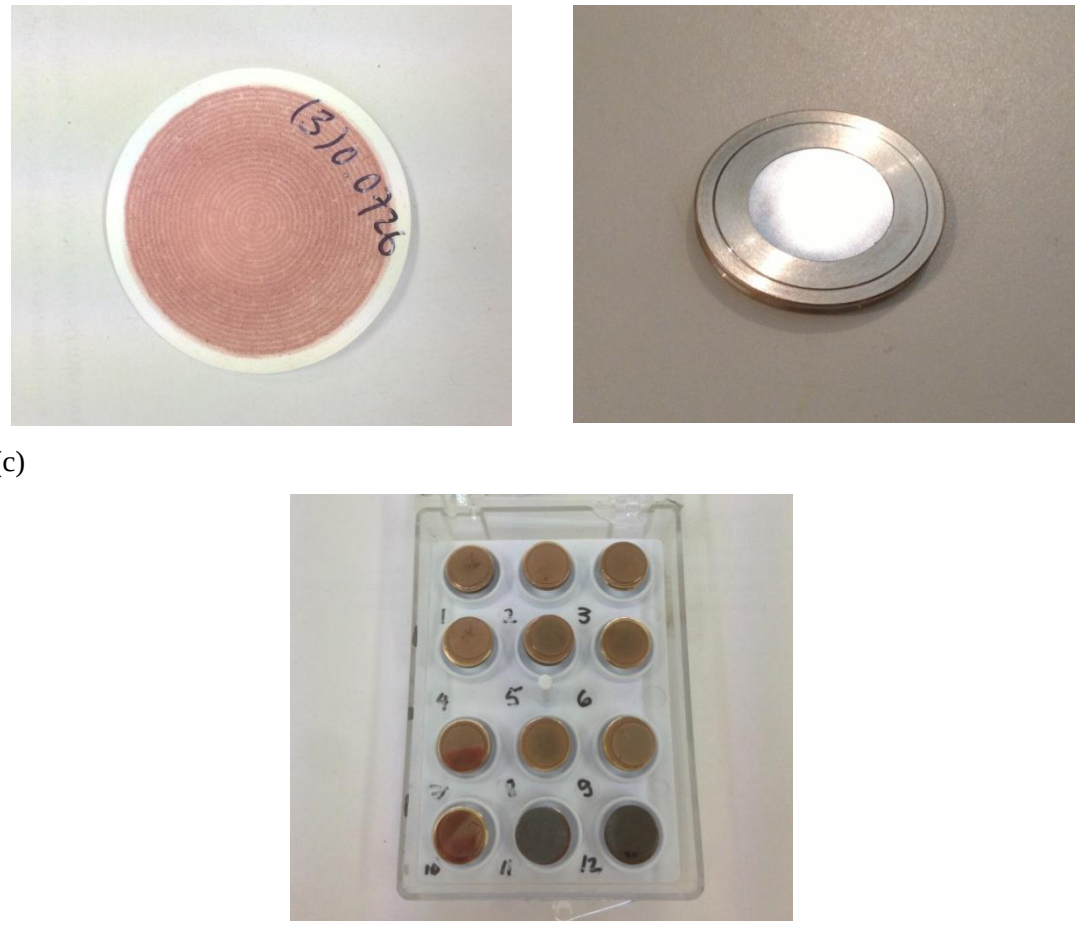


(c)




Figure 7.8. Pictures of: (a) supernatant solids at the membrane filter, (b) special XRD holder for limited amount of solids and (c) SEM holder.

For SEM analysis, a screw-like conductive holder (top view in Figure 7.8c) was prepared. Double-sided carbon tape was attached on the top of the holder. The membrane with a thin layer of recovered solids facing downwards was placed on that carbon tape. The membrane was then carefully taken off, leaving supernatant solids attached to the carbon tape. The top part of the holder was carbon coated prior to

SEM examination. Complete details about coating protocols and the SEM set-up can be found in Section 5.3.5.

#### *7.3.4.2 PSD analysis of supernatant solids*

For PSD analysis, the thin layer of supernatant solids was carefully rinsed off from the membrane by using a minimum amount of deionised water. Suspension samples were subjected to PSD analysis by laser light scattering (Section 4.3).

#### *7.3.4.3 Filtration of supernatant solutions*

For a limited number of tests, the filtration rate of supernatant solutions was measured to give an indication of the effect of flocculation conditions and polymer reagent choice on the liquor properties (e.g. is there any impact of reagent carry-over). This was not dissimilar to plant operation where thickener overflow is filtered prior to product precipitation (Section 1.2 and 2.4.4). A 50 mL aliquot of supernatant solution from the cylinder was sampled at a depth of ~4.5 cm. It was then immediately vacuum-filtered as described in Section 6.3.6.

### 7.3.5 FBRM tests

FBRM monitoring was applied during the flocculation of slurry prepared following the procedure given in Section 7.3.2. Unless stated otherwise, the slurry solids concentration was fixed at 2 wt/wt% due to its sensitivity to changes in process variables (Section 4.4.3). The FBRM G400 probe was used exclusively due to its enhanced sensitivity in the lower chord length region. The experimental set-up for measurements by the G400 probe is similar to that given in Section 4.3.

The flocculants and silane-containing polymer were added at room temperature. Alclar 665 was dosed 5 minutes after slurry stirring commenced in the FBRM beaker. As HX-300 was split dosed, dosing times were 5 and 8 minutes after stirring commenced. S-10292 itself was added 45 s before the addition of Alclar 665 or the first addition of HX-300 (i.e. 4.25 minutes after stirring commenced). Discussions in Section 7.4.1.8 will reveal why this was considered an optimised selection.

A concern in interpreting G400 FBRM results was whether different synthesis batches gave substantially different results. This aspect is important when considering that the G400 instrument is very sensitive at lower chord lengths. Small changes in feed characteristic (i.e. more fines) could potentially impact on flocculation efficiency and mask the effect of silane-containing polymer.

Figure 7.9 shows the unweighted chord length distribution measured 30 s after dosing 104 g $t^{-1}$ Alclar 665 to *in-situ* prepared DSP/hematite slurries (31 wt/wt% DSP). Despite the DSP/hematite slurries representing different batches, the unweighted chord length distributions were very similar. This implies that the samples prepared in different batches should not differ greatly in their response to polymer addition. The impact of silane-containing polymer is further discussed in Section 7.4.1.8.

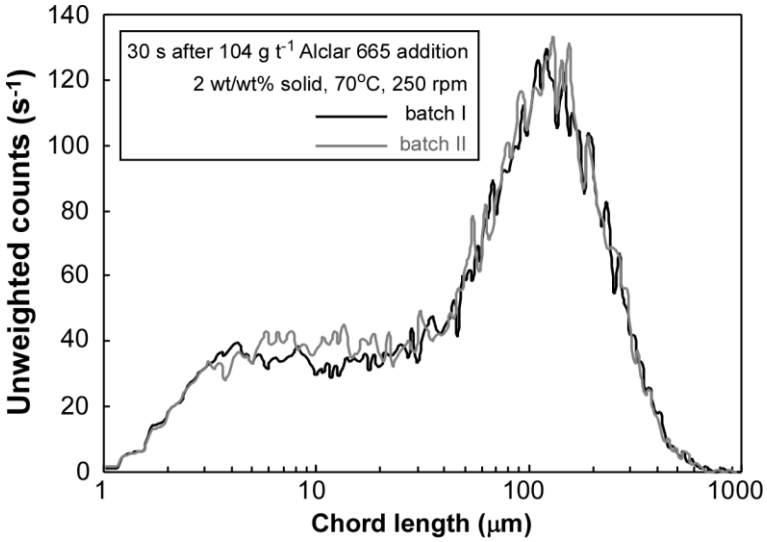


Figure 7.9. Effect of different synthesis batches on unweighted counts for *in-situ* prepared DSP/hematite slurries (31 wt/wt% DSP) measured 30 s after the addition of 104 g $t^{-1}$ Alclar 665 (G400 FBRM probe, macro mode, DSP synthesized at 40 g $L^{-1}$ solids concentration).

### 7.3.6 Adsorption study

To provide information comparable to the adsorption isotherm in Section 6.5.4, adsorption tests in this Chapter were conducted at a solids concentration of 5 wt/wt% in relatively low A/C ratio solutions (A/C = 0.35, C/S = 0.99, C = 230 g $L^{-1}$). The adsorption protocols remained unchanged from those in Section 6.3.6, which

involved pre-stirring slurry in an FBRM beaker for 5 minutes before reagent dosing. If added in combination, Alclar 665 was added 45 s after S-10292.

Slurry was mixed with polymer solutions for 15 minutes before it was allowed to settle. Flocculated solids were sampled and dried (with or without washing) before they were analysed by infrared. Meanwhile, supernatant solutions were sampled and centrifuged following the steps described in Section 6.3.6 to produce solids-free liquor for fluorometry. The details of both techniques are explained below.

#### *7.3.6.1 Fourier Transform Infrared (FTIR) of flocculated solids*

When a chemical compound absorbs infrared (IR) radiation (with frequency (ν) between 20 to 14300 $cm^{-1}$), its dipole moment changes during molecular vibrations (Putzig et al. 1994). The absorption peak is proportional to the change of dipole moment when sample molecules are excited to higher vibrational energy states. Meanwhile, the frequency where the absorption peak is detected is case-specific and dependent upon the chemical compound(s) that absorb IR radiation.

Fourier transform infrared (FTIR) has been previously used to study the conformation of PAA adsorbed onto hematite surfaces (Jones 1998), distinguishing carboxylate attachment via monodentate and asymmetric bidentate configurations. In this study, FTIR was employed to establish the configuration of silane-containing polymer adsorption onto DSP. This required solid samples post-flocculation, with sample preparation involving filtration, washing, drying and grinding as described in Section 5.3.2. The wet cake was dried at 105°C overnight (~15 h) before it was ground by hand in a pestle and mortar. The effect of washing was also studied by comparing results from non-washed samples.

The ground sample was diluted with analytical grade KBr (BDH Product No. 140182B) to make a mixture with 1 wt/wt% sample. This was placed in a specimen holder that goes into a static press to make a 13 mm diameter disk, which was subjected to IR transmittance measurements in a Bruker IFS 66 instrument (deuterated triglycine sulphite detector, 4 $cm^{-1}$ resolution, 12 mm aperture and 32

scans). The measured transmittance was converted to absorbance by the following equation:

$$\text{Absorbance} = - \log (\% \text{ transmittance} / 100) \quad 7.1$$

#### *7.3.6.2 Fluorometry of supernatant solutions*

**The details regarding to this method are unable to be shown here due to the proprietary reasons claimed by its inventor(s).**

### 7.3.7 Zeta potential determination

Changes in the DSP zeta potential as a result of S-10292 and HX-300 additions were measured in 0.01 M NaCl at pH ~11 and ambient temperature. Details on slurry preparation and equipment set-up for zeta potential determination can be read in Sections 7.3.2 and 5.3.3, respectively.

## *7.4 Results and discussion*

### 7.4.1 Low solids concentration in desilication reactions

Aggregation is improved by increasing polymer dosages up to an optimum value, beyond which efficiency can decrease (Section 2.1.4). In practice, flocculation is often acceptable at dosages well below such optimums. For dosing of S-10292 before a flocculant, it is necessary to establish appropriate dosage ranges for both reagents.

#### *7.4.1.1 The effect of S-10292 at various PAA dosages*

The appropriate dosage for S-10292 with DSP/hematite was an unknown, but published work on bauxite residue gave a practical starting point. Cylinder tests were conducted over a range of Alclar 665 dosages with and without pre-addition of 600 g $t^{-1}$ S-10292. Settling rates and supernatant solids measured for hematite and *in-situ* prepared DSP/hematite slurries (31 wt/wt%) are shown in Figure 7.12.

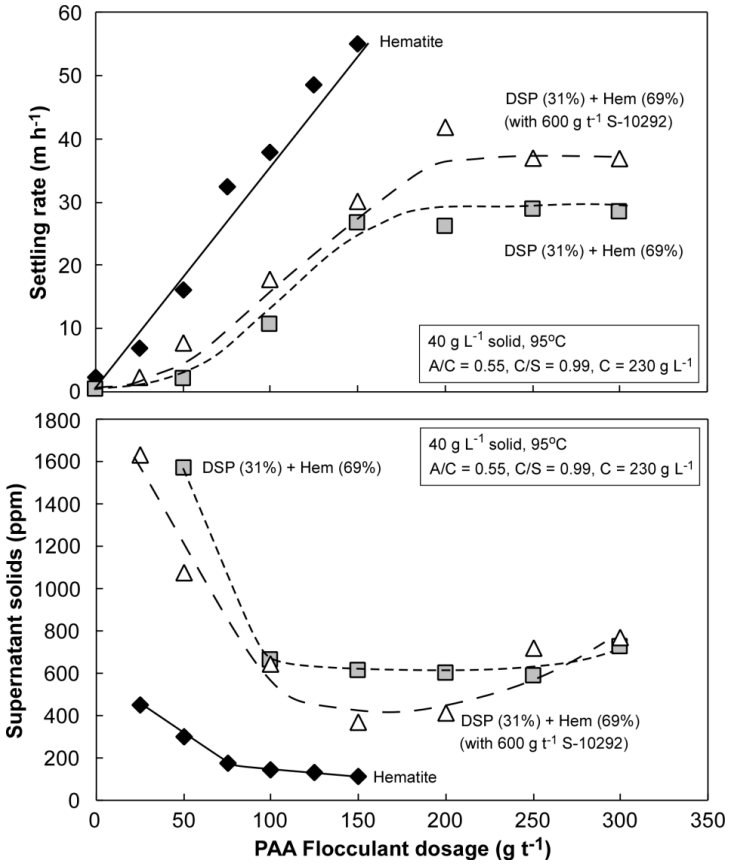


Figure 7.12. The effect of Alclar 665 dosage on the settling rates and supernatant solids of the hematite and the *in-situ* prepared DSP/hematite (31 wt/wt% DSP) slurries.

Interestingly, the settling rates of *in-situ* prepared DSP/hematite slurries were not greatly affected by pre-addition of 600 g $t^{-1}$ S-10292, other than at high Alclar 665 dosages (≥ 200 g $t^{-1}$). Given that the standard deviation in settling rates with Alclar 665 at 40 g $L^{-1}$ (Section 7.4.2) was as high as ~4 m $h^{-1}$, the benefit of S-10292 to settling may be marginal. However, the supernatant solids were consistently higher without S-10292 pre-addition, again except at very high Alclar 665 dosages.

The improvements seen in supernatant solids at settling rates ≤ 30 m $h^{-1}$ were quite distinct. Settling tests with 150 g $t^{-1}$ Alclar 665 were therefore repeated multiple times to better quantify this effect. From the average values and calculated standard deviations given in Table 7.4, 600 g $t^{-1}$ S-10292 gave on average ~40% improvement in supernatant solids (760 vs. 456 ppm).

Table 7.4. Comparison of supernatant solids measured with or without S-10292 addition for *in-situ* prepared DSP/hematite (31 wt/wt% DSP) slurries.

| | Supernatant solids (ppm) | | | | | | | | |
|---|---|---|---|---|---|---|---|---|---|
| | 1 | 2 | 3 | 4 | 5 | 6 | 7 | Mean | SD |
| Without S-10292 | 710 | 675 | 820 | 940 | 635 | 610 | 930 | 760 | 137 |
| With S-10292 | 370 | 450 | 665 | 590 | 415 | 330 | 370 | 456 | 125 |

Conditions: 40 g $L^{-1}$ solid, 600 g $t^{-1}$ S-10292, 150 g $t^{-1}$ Alclar 665.

Referring back to Table 7.1 which gives various trends for previous studies in Figure 7.1, the improvement in supernatants solids with little change in settling rates from the combination of silane-containing polymer and PAA was consistent with the Set G results for the flocculation of bauxite residue with synthetic DSP.

### *7.4.1.2 The effect of S-10292 dosage at fixed PAA dosage*

The next step was to identify the optimum dosage range for the silane-containing polymer S-10292. By fixing the Alclar 665 dosage, the settling rate and supernatant solids responses as a result of increasing silane polymer dosage were compared for both pure hematite and the *in-situ* prepared DSP/hematite (31 wt/wt% DSP) slurries.

The Alclar 665 dosage was maintained at 50 g $t^{-1}$ for the pure hematite slurry and 150 g $t^{-1}$ for the *in-situ* prepared DSP/hematite slurry. Average values from duplicate measurements are presented as a percentage of the base case (without S-10292 addition) in Figure 7.13. The fixed flocculant dosages were chosen from Figure 7.12, reproducing settling rates in the region of ~15-25 m $h^{-1}$. At 50 g $t^{-1}$ Alclar 665, the hematite slurry generated a settling rate of 17.8 m $h^{-1}$ and supernatants solids of 270 ppm, while addition of 150 g $t^{-1}$ Alclar 665 to the *in-situ* prepared DSP/hematite slurry gave a settling rate of 25.8 m $h^{-1}$ and supernatant solids of 673 ppm.

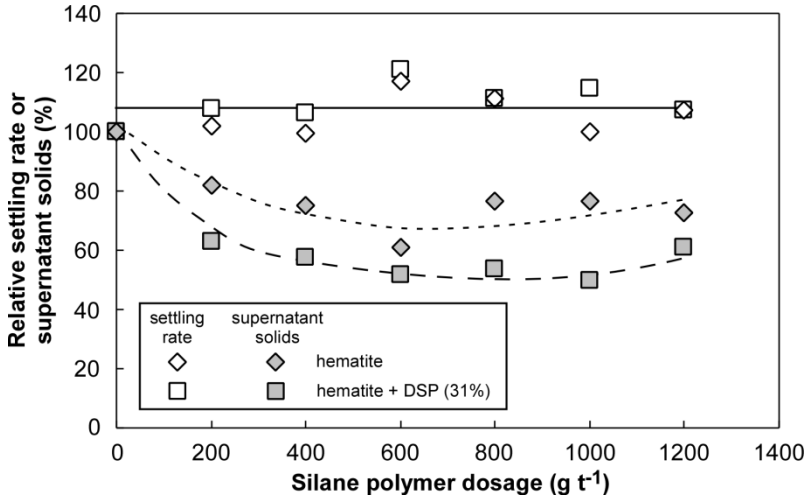


Figure 7.13. Relative settling rates and supernatant solids as a result of silane polymer addition to hematite and *in-situ* prepared DSP/hematite (31 wt/wt% DSP) slurries. Conditions: 40 g $L^{-1}$ solid, Alclar 665 = 50 g $t^{-1}$ (hematite) or 150 g $t^{-1}$ (DSP/hematite).

The settling rates on flocculation of both hematite and *in-situ* prepared DSP/hematite slurry were slightly higher with S-10292 pre-addition, whereas increasing S-10292 dosages up to 600 g $t^{-1}$ helped in decreasing supernatant solids. S-10292 dosages above 600 g $t^{-1}$ did not seem to give further improvement in supernatant clarity.

Hematite slurries gave a positive response to S-10292, despite the absence of DSP. However, the clarity improvement was limited to ~25%, while ~45% was achieved for *in-situ* prepared DSP/hematite slurry. This implies that the silane-containing polymer could interact with hematite surfaces to a degree. From a practical point of view, it is neither crucial nor necessary to add S-10292 to hematite slurries, as the same improvement can also be derived from increasing primary flocculant dosage, a response not achieved with significant DSP present (Figure 7.12).

### *7.4.1.3 Silane-containing polymer: coagulant or flocculant?*

With only slightly higher settling rates derived from the pre-addition of S-10292, it was expected that the silane-containing polymer behaved as a coagulant rather than a flocculant. The actual role of this polymer could be better established when FBRM was utilised to monitor the changes in the mean square-weighted chord length and unweighted counts as a result of pre-addition dosages and applied shear (mixing).

It is important that data collection is done with minimal interference from natural aggregation, which could mask the extent of coagulation. In this case, the steady-state mean square-weighted chord length and total unweighted counts values were achieved after stirring the slurry at a higher rate (300 rpm) for 5 minutes before returning to the mild stirring rate (200 rpm). The time of this reduction was defined at t = 0 and stirring was then maintained for another 5 minutes prior to S-10292 addition, ensuring that any natural aggregation was at a baseline level.

Figure 7.14 highlights the change in the primary mean square-weighted chord length and unweighted counts for hematite and the *in-situ* prepared DSP/hematite (31 wt/wt% DSP) slurries aggregated with S-10292. The primary measurement mode was chosen as it has better sensitivity to the lower chord length region, although it may undersize larger aggregates (Section 4.3). For comparison, the effect of Alclar 665 addition alone at higher stirring rate (300 rpm) was also shown on the same graph (Alclar 665 addition at 200 rpm is not presented due to the formation of excessively large aggregates). A solids concentration of 40 g $L^{-1}$ was chosen to correspond to conditions in the settling tests.

From the changes in mean square-weighted chord lengths alone, one can conclude that the *in-situ* prepared DSP/hematite slurry was aggregated by S-10292 to a greater extent than the pure hematite slurry. This was also confirmed by the changes in unweighted counts, indicating that more particles in the *in-situ* prepared DSP/hematite slurry were aggregated. These observations suggest that the silane-containing polymer was more selective towards DSP surfaces than those of hematite. Higher affinity of silane-containing polymer to the DSP particles explains the less significant impact on the pure hematite slurry in Figure 7.13.

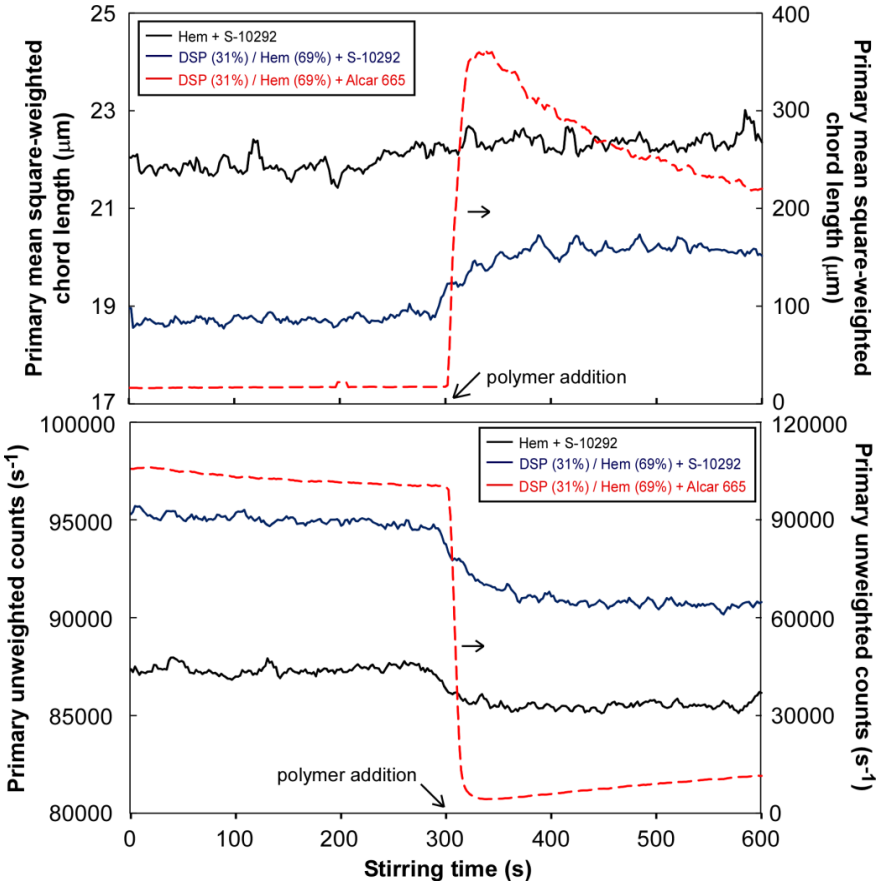


Figure 7.14. Plot of primary mean-square weighted chord length and unweighted counts as a function of stirring time. Conditions: 40 g $L^{-1}$ solids concentration; S-10292 = 600 g $t^{-1}$ – 200 rpm; PAA = 150 g $t^{-1}$ – 300 rpm, A/C = 0.55, C/S = 0.99, C = 230 g $L^{-1}$.

It is also worth noting that the degree of aggregation by S-10292 was still far lower than that derived from the addition of Alclar 665. The PAA flocculant was, in fact, able to produce aggregates that were almost twenty-fold larger. This is another hint that silane-containing polymer played a role as a coagulant, rather than a flocculant, although it was named so in some publications (e.g. Davis et al. 2010a).

The unweighted chord lengths distribution of the *in-situ* prepared DSP/hematite slurry (31 wt/wt% DSP) before and 60 s after the addition of S-10292 are presented in Figure 7.15. Addition of S-10292 slightly shifted the chord length distribution to the right-hand side with a small decrease in counts – both were a sign that aggregation did occur. Meanwhile, changing the measurement mode from primary to macro changed the peak into a broader one with lower counts, as expected (Section 4.4.1).

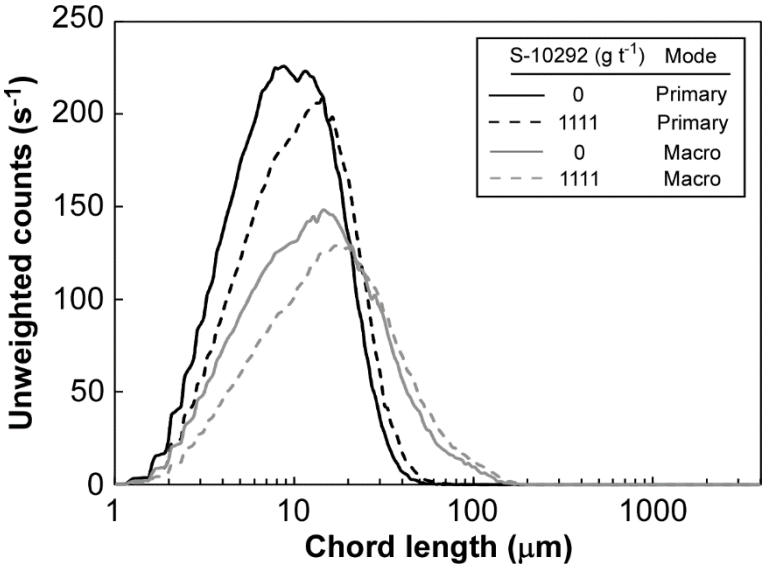


Figure 7.15. The unweighted chord length distribution of *in-situ* prepared DSP/hematite slurry (31 wt/wt% DSP, 2 wt/wt% solid) before and 60 s after addition of S-10292.

As discussed in Section 2.1 and 5.2.1, the reduction of the particle surface charge magnitude minimises the repulsive force that exists as a consequence of particle-particle interaction and therefore induces coagulation. In theory, the reduction of surface charge magnitude by coagulants will be more substantial than that by flocculants. In bridging flocculation, high molecular weight polymer is attached onto a particle at only a few points, and if that attachment was due to an electrostatic mechanism, the reduction of surface charge will be limited. Zeta potential can therefore be measured to reflect the change in surface charge as a result of S-10292 (coagulant) or HX-300 (flocculant) addition.

Zeta potential measurements applied to DSP samples (< 5 μm) suspended in 0.01 M NaCl at pH 11.2-11.4 are presented in Figure 7.16. Experiments at each HX-300 or S-10292 dosage were replicated four times, using the samples prepared in two separate synthesis batches. This approach introduced a little variation in the zeta potentials measured. However, such variance did not change the trend where S-10292 addition led to a higher reduction of surface charge magnitude. There was only a slight decrease in the surface charge magnitude when HX-300 was added at dosages comparable to S-10292.

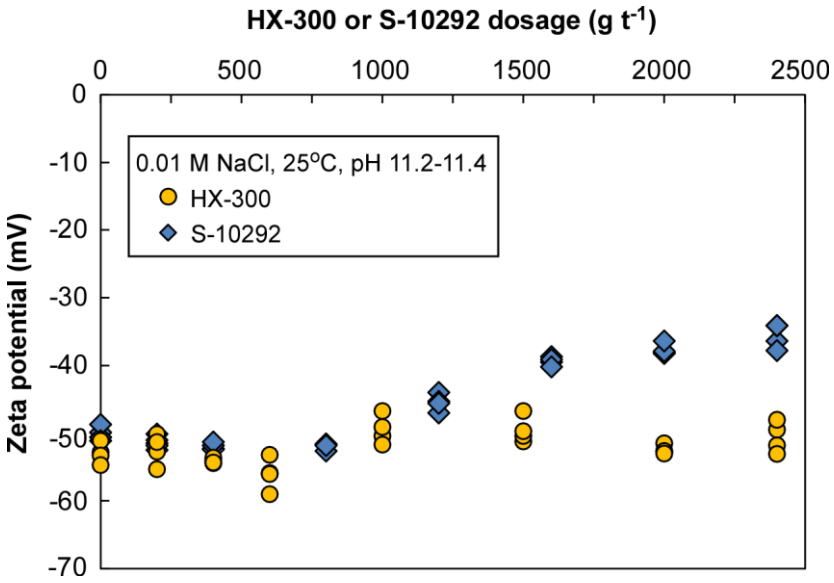


Figure 7.16. The effect of HX-300 and S-10292 dosages on the zeta potential of DSP (< 5 μm) measured at pH 11.2-11.4 in 0.01 M NaCl solutions.

The zeta potential of DSP with HX-300 addition was in the band of -55 to -45 mV and with the addition of 2400 g $t^{-1}$ S-10292 it increased to -35 mV. This was still far from 0 ± 5 mV, the region where repulsive forces are minimal (Section 5.2.1). However, it was close to ±30 mV, the region where partial coagulation can occur (Malvern, 2004). Increasing ionic strength will also theoretically reduce the surface charge magnitude due to electrostatic adsorption of counter-ions.

In highly ionic solutions such as Bayer liquor, the magnitude of DSP surface charge may be much lower than that measured in 0.01 M NaCl (close to 0) and S-10292 addition may bring it to a point that promotes coagulation. However, electrophoretic mobility is difficult to measure in high ionic strength solutions. Increasing the salt background from 0.01 to only 0.03 M NaCl resulted in increased noise measured by the Malvern Zetasizer ZS, such that results were rejected by the internal acceptance criteria. Hence, the zeta potential values reported in Figure 7.16 and their changes with respect to the increasing S-10292 dosage are not a true reflection of what happens in typical Bayer liquor, however, they are sufficient to indicate the coagulation effect given by S-10292.

With regard to the coagulation effect of S-10292, mineral slurries normally contain solid particles of a wide size range. Adsorption of high molecular weight polymer

(flocculant) onto submicron particles suffers from low statistical probability (Section 2.1). In a primary thickener with inefficient flocculation, many submicron particles will report to the overflow. In this situation, silane-containing polymer may firstly coagulate the fines and act as an anchor when bridging flocculation takes place.

#### *7.4.1.4 The effect of silane-containing polymer on the optimum solids concentration*

The effect of solids concentration is often not considered in flocculation studies, despite being one of the key features of flocculation processes (Section 2.1.5). Hence, settling tests were carried out at 40, 50 and 60 g $L^{-1}$, to determine the optimum solids concentration, at which the effect of silane-containing polymer will then be investigated.

Results from flocculating with Alclar 665 at different solids concentrations without pre-addition of S-10292 were compared in Figure 7.17. The settling rates of flocculated *in-situ* prepared DSP/hematite slurries (31 wt/wt% DSP) were consistently higher when the solids concentration was increased from 40 to 50 g $L^{-1}$. It seemed that 50 g $L^{-1}$ was the optimum solids concentration for the PAA flocculant, as increasing the solids concentration to 60 g $L^{-1}$ led to reduced settling rates.

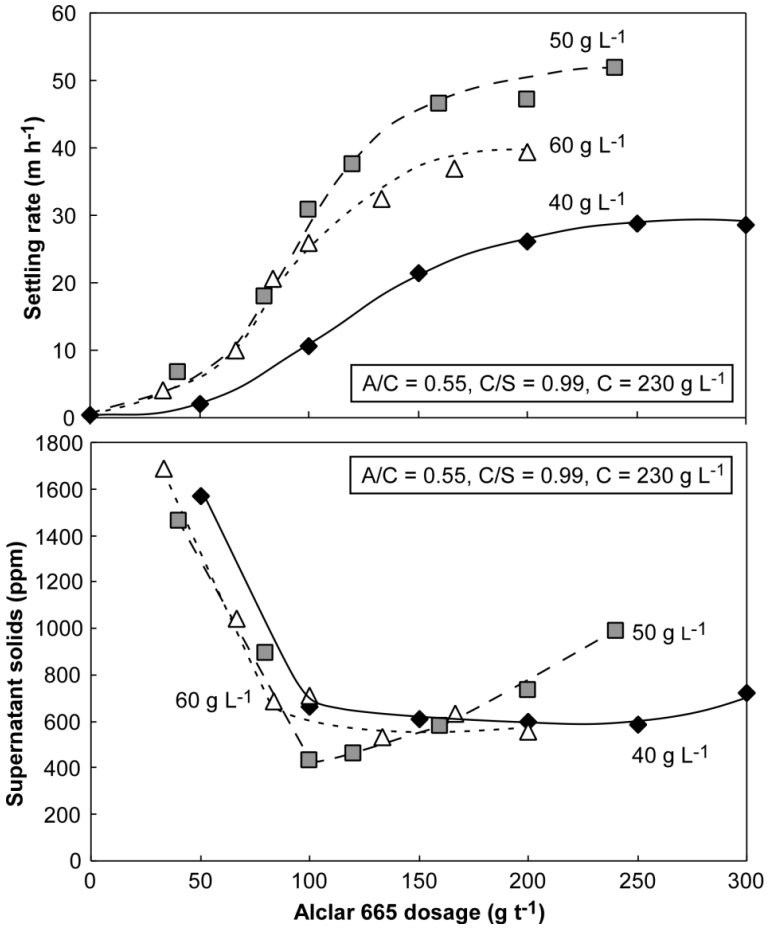


Figure 7.17. The effect of solids concentration on settling rate and supernatant solids of *in-situ* prepared DSP/hematite slurries (31 wt/wt% DSP) flocculated with Alclar 665.

In the case of supernatant solids, 40 and 60 g $L^{-1}$ solids gave similar trends with increasing dosage, where the supernatant solids levelled off at ~600 ppm. The lowest supernatant solids (~450 ppm) were measured when 100 g $t^{-1}$ Alclar 665 was added into a 50 g $L^{-1}$slurry. If a solids concentration of 50 g $L^{-1}$ and 100 g $t^{-1}$ Alclar 665 are considered as the optimum condition for both aggregate growth and fines capture, to prove the beneficial effect of the silane-containing polymer is real, it must also be tried under such conditions.

The supernatant solids measured at 50 g $L^{-1}$ and 100 g $t^{-1}$ Alclar 665 both with and without the pre-addition of S-10292 can be found in Figure 7.18. At 50 g $L^{-1}$, the presence of S-10292 (with 1200 g $t^{-1}$) clearly decreased the supernatant solids from ~500 to ~350 ppm. Regardless of this small difference, which was slightly higher than the standard deviation given by PAA flocculant (~120 ppm), the results still confirmed the beneficial effect of silane-containing polymer – especially when

looking at the trend of lower supernatant solids as a result of increasing silane polymer dosage in Figure 7.18.

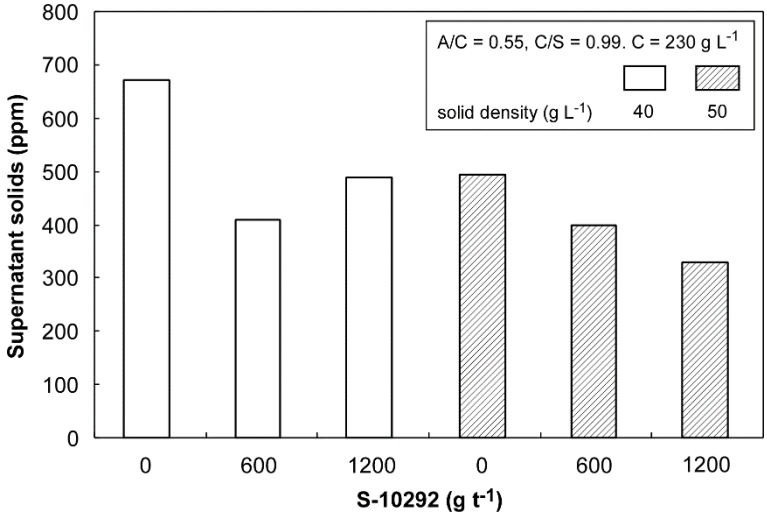


Figure 7.18. The effect of silane-containing polymer dosage on supernatant solids at 40 and 50 g $L^{-1}$ solids concentration with 100 g $t^{-1}$ Alclar 665 (averages of duplicate measurements).

When contrasted with supernatant solids measured at a solids concentration of 40 g $L^{-1}$, it is clear the silane-containing polymer gave a smaller effect at 50 g $L^{-1}$. This was hardly surprising, considering that at the higher solids concentration, the probability of collision and aggregation was also higher (Section 2.1.5). The biggest concern could really be the required S-10292 dosage, which was almost an order of magnitude higher than that of PAA. Furthermore; even with such a high dosage, the supernatant solids measured on flocculating *in-situ* prepared DSP/hematite slurries were not close to those of pure hematite (< 100 ppm, Figure 7.12).

### *7.4.1.5 The effect of alumina, caustic and A/C ratio*

Understanding the effect of alumina and caustic concentrations on flocculation is crucial from the point of view that Bayer refineries are not operated under uniform conditions. For instance, there are some refineries that operate with higher caustic concentration in order to enhance liquor productivity by its ability to dissolve more alumina at the same critical A/C ratio (Section 2.4.3).

Three sets of experiment were done in duplicate to investigate the following effects in the flocculation of *in-situ* prepared DSP/hematite slurries (31 wt/wt% DSP):

(a) alumina at the same caustic concentration (Set i vs. ii – Table 7.5), and
(b) caustic at the same alumina concentration (Set i vs. iii – Table 7.5)

The liquor compositions and their viscosities at 95°C (the temperature at which settling tests were done) are given in Table 7.5. None of those liquors had a composition similar to the primary thickener liquor with A/C ratio of 0.7-0.8, due to the available source of sodium aluminate concentrate, which had an A/C ratio of 0.58 (Section 7.3.2). However, only the trend regarding the increase of caustic or alumina concentration was of interest in this case.

Table 7.5. Experimental conditions for different alumina and caustic concentrations.

| Experimental Set | A ($g\ L^{-1}$) | C ($g\ L^{-1}$) | A/C ratio | C/S ratio | Viscosity at 95°C (cP) |
|---|---|---|---|---|---|
| i | 127 | 230 | 0.55 | 0.99 | 0.58 |
| ii | 81 | 230 | 0.35 | 0.99 | 0.60 |
| iii | 127 | 270 | 0.47 | 0.99 | 0.64 |

Note: viscosity was calculated based on the Ikkatai's equation (Appendix D)

The settling rates and supernatant solids resulting from varying alumina, caustic and S-10292 dosage at a fixed Alclar 665 dosage (150 $g\ t^{-1}$) are shown in Figure 7.19a and b, respectively. The settling rates for *in-situ* prepared DSP/hematite slurries did not vary greatly with or without S-10292 addition. Achieving similar settling rates at higher A/C ratios confirms that all the tests done at a relatively low A/C ratio liquor in Chapter 6 are still relevant in explaining the conditions in primary thickening.

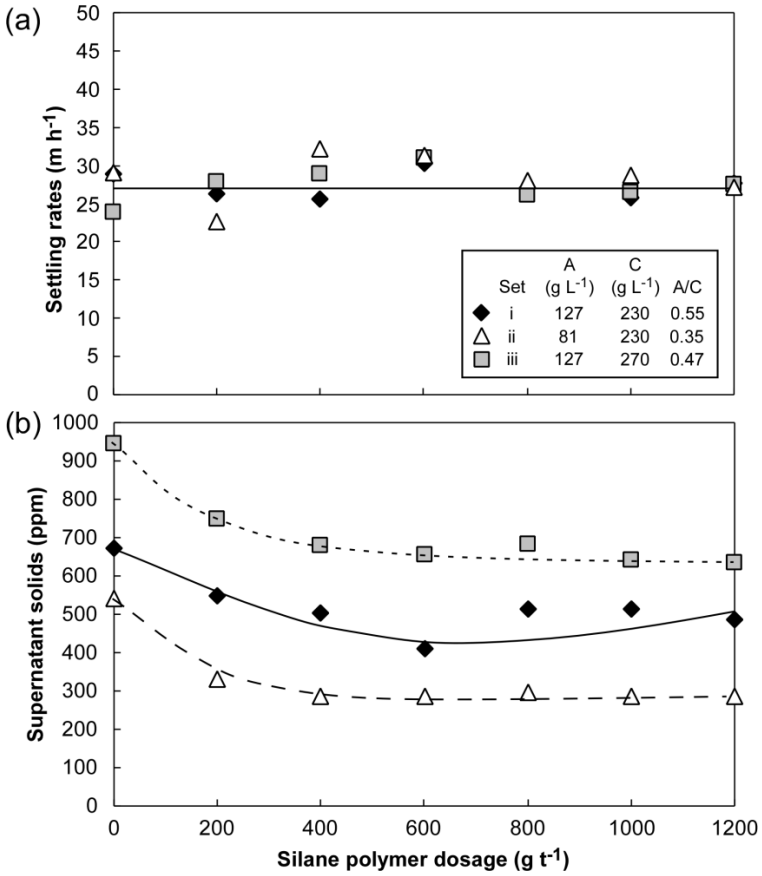


Figure 7.19. The effect of S-10292 dosage at various alumina and caustic concentrations on the: (a) settling rates and (b) supernatant solids of the *in-situ* prepared DSP/hematite slurries (31 wt/wt% DSP). Conditions: 40 g $L^{-1}$ solids concentration, 150 g $t^{-1}$ Alclar 665.

The disadvantage of operating at higher alumina or caustic concentration was most apparent in the higher supernatant solids measured after flocculation (diamond and square symbols in Figure 7.19b). Adding silane-containing polymer helped decrease the supernatant solids, although it did not alter the trend towards increased supernatant solids at higher alumina/caustic concentrations.

Possible explanations for the higher supernatant solids are:

(i) the influence of increasing ionic strength on the polymer conformation,

(ii) the effect of alumina/caustic concentration on solution viscosity, and

(iii) the influence of ionic species on the surface chemistry of solid substrates.

Flocculant conformation is influenced by the solution ionic strength. Higher concentrations of ions provide a greater shielding effect to charged flocculants, leading to a more coiled conformation (Jones 1998; Rogan 1995; Yu and Somasundaran 1993). Jones (1998) observed that the coiling effect tends to diminish

at very high salt concentrations, and that a sodium ion ($Na^+$) concentration between 2-6 M from NaCl, $Na_2CO_3$, NaOH or synthetic Bayer solutions resulted in comparable values of the radius of gyration of a polyacrylate flocculant (~140 nm). Considering that the liquor used here already has a high sodium ion concentration ($\geq$ 4.3 M NaOH), it is less likely that slightly higher caustic or alumina concentration leads to an additional reduction in flocculant dimensions. Thus, conformational effects can be ruled out from the possible reasons for sub-optimal fines capture.

Higher viscosity from varying alumina/caustic liquor concentrations may cause sub-optimal polymer dispersion in the slurry and fewer collisions between polymer and substrates during mixing. The poorest fines capture efficiency was seen in liquor that had the highest relative viscosity (C = 270 g $L^{-1}$, A/C = 0.47). Nevertheless, liquor which had the lowest relative viscosity (C = 230 g $L^{-1}$, A/C = 0.55) still suffered from high supernatant solids when compared to the liquor with slightly higher viscosity (C = 230 g $L^{-1}$, A/C = 0.35). There must therefore be additional factors aside from solution viscosity responsible for the reduced fines capture.

The adsorption of sodium aluminate as a neutral species may change the surface chemistry. Sodium ions are known to adsorb on hematite surface at pH 13, changing the effective surface charge from negative to positive and facilitating the adsorption of anionic flocculant (Section 2.1.1). Should the sodium ions form sodium aluminate neutral species at the surface of particles, the active sites for flocculant adsorption may be fewer and this may affect fines capture efficiency. The effect of other inorganic ions should be relatively minimal due to their very low concentrations in the liquors used for the settling tests (no sodium sulphate or chloride was added and carbonate was present as an impurity at a level of ~2 g $L^{-1}$).

#### *7.4.1.6 Methods of addition*

In previous studies (Dai et al. 2008; 2010; Davis et al. 2010a, 2010b); the silane-containing polymers were always added prior to the addition of primary flocculants (PAA or HX PAM), without any explanation why, although this is more apparent if the polymer does act as a coagulant (Section 7.4.1.3). The experimental work was

then extended to the addition method, trying to answer what is the effect of silane-containing polymer if added simultaneously with or after the primary flocculant.

How different S-10292 addition methods affect settling rates and supernatant solids on flocculation of *in-situ* prepared DSP/hematite slurries (31 wt/wt% DSP) is displayed in Figure 7.20a and b, respectively. The simultaneous addition of S-10292 and Alclar 665 (150 g $t^{-1}$) did not contribute to any change in settling rate. It still gave a beneficial effect in terms of decreasing supernatant solids, however, the improvement was not as significant as when S-10292 was added prior to Alclar 665. Competitive adsorption between S-10292 and Alclar 665 could explain this.

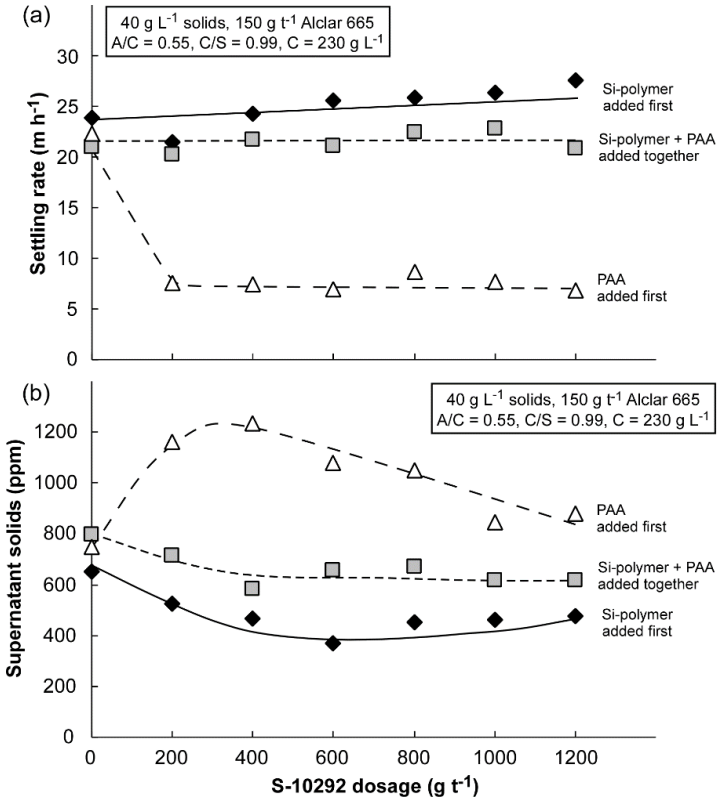


Figure 7.20. The effect of S-10292 addition method on (a) settling rate and (b) supernatant solids of *in-situ* prepared DSP/hematite slurries (31 wt/wt% DSP). Five strokes following each reagent addition.

When the sequence was reversed and S-10292 was added after Alclar 665, settling rates declined from ~20 to 5-10 m $h^{-1}$. When S-10292 was added after PAA, the slurry was mixed again with five additional strokes, but this was initially not done for 0 g $t^{-1}$ S-10292. The sharp decline in settling rate was therefore due to aggregate break-up from the extended shear. This is not unexpected; unlike flocculant,

coagulant would not offer any bridging capacity that helps preserve aggregate structures (see Section 4.4.3 and 6.5.5 for the effect of flocculant on aggregate strength).

Applying ten consecutive strokes without S-10292 addition resulted in the settling rate of ~5 m $h^{-1}$ with supernatant solids of ~1500 ppm, confirming that extra strokes caused aggregate rupture and released some fines or small fragments that reported to the supernatant solids. A decrease in supernatant solids (from 1200 to 800 ppm) was evident when S-10292 dosages were increased (Figure 7.20b), implying that such fines/fragments can still be aggregated by S-10292. Considering that the maximum hematite surface coverage by Alclar 665 was limited to only ~18% even at very high dosages (≈ 2000 g $t^{-1}$), it is likely that DSP/hematite fragments produced from aggregate break-up still provide active sites to adsorb S-10292 and allow some aggregation.

#### *7.4.1.7 The effect of flocculant chemistry*

The study of the silane-containing polymer was not complete without knowing its effect on HX PAM performance. Figure 7.21 plots settling rates and supernatant solids measured from *in-situ* prepared DSP/hematite slurries flocculated with HX-300 at various solids concentrations (40, 50 and 60 g $L^{-1}$). In comparison to the relevant results produced with PAA (Figure 7.17), HX PAM performance was more resistant to increases in solids concentration. Settling rates measured at 40 g $L^{-1}$ could reach very high values (~40 m $h^{-1}$). Increasing the solids concentration to 50 g $L^{-1}$ resulted in the identical response to dosage, with the exception that settling rates were limited at 25 m $h^{-1}$. The same response was achieved at 60 g $L^{-1}$ with slightly higher required dosages.

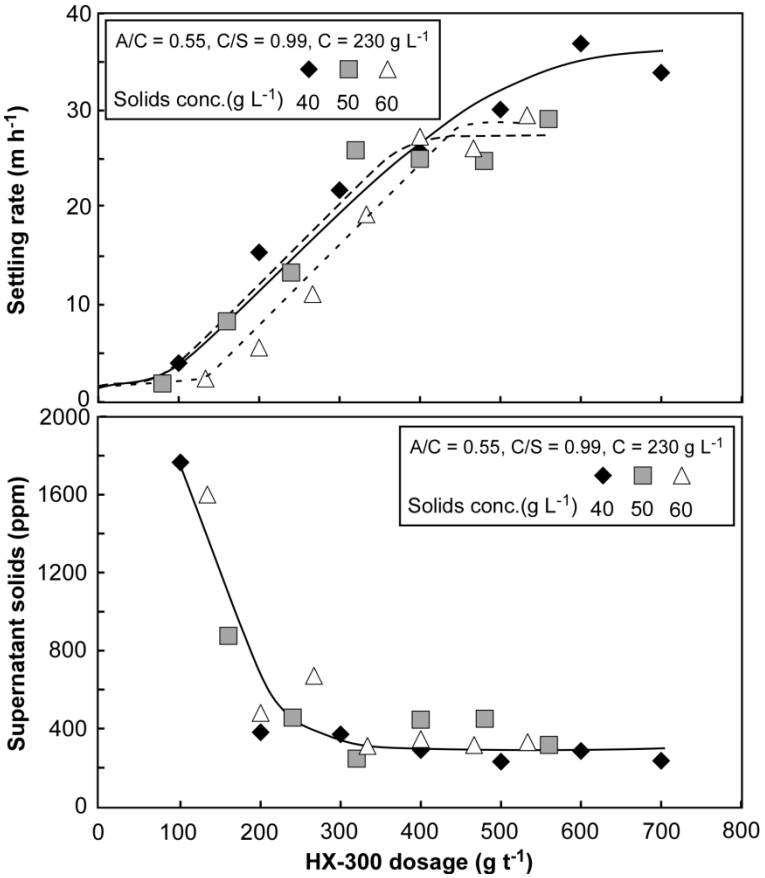


Figure 7.21. The effect of solids concentration and HX-300 dosage on the flocculation of *in-situ* prepared DSP/hematite slurry (31 wt/wt% DSP).

With respect to fines capture, higher HX-300 dosages decreased the supernatant solids to ~ 200-300 mg $L^{-1}$, regardless of solids concentration. HX-300 was clearly superior to Alclar 665, which could not improve the supernatant solids measured to a level less than 400 mg $L^{-1}$. The better fines capture efficiency given by HX PAM when compared to PAA was also seen in Section 6.5.1.

The effect of S-10292 dosage was then studied at 40 g $L^{-1}$ with different HX-300 dosages. From Figure 7.21, 150 and 300 g $t^{-1}$ of HX-300 gave settling rates of ~10 and ~20 m $h^{-1}$, respectively. Such settling rates were well within the practical range sought in primary thickening. The effect of S-10292 dosage on the settling rate and supernatant solids of *in-situ* prepared DSP/hematite slurry flocculated with 150 and 300 g $t^{-1}$ HX-300 is presented in Figure 7.22.

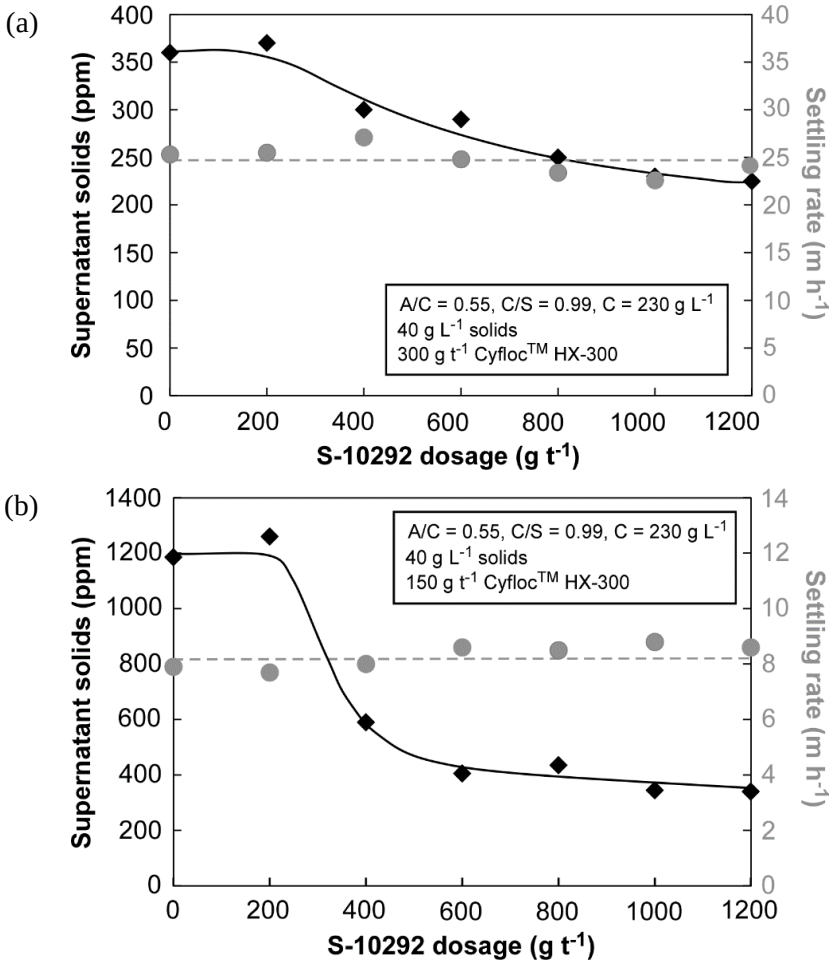


Figure 7.22. The effect of S-10292 dosage on settling rate and supernatant solids for *in-situ* prepared DSP/hematite slurry (31 wt/wt% DSP) flocculated with: (a) 300 g $t^{-1}$ and (b) 150 g $t^{-1}$ HX-300.

At 300 g $t^{-1}$ HX-300 (~25 m $h^{-1}$ settling rate), the improvement in supernatant solids was marginal, due to the value already being low without pre-addition of S-10292. Increasing the S-10292 dosage from 0 to 1200 g $t^{-1}$ only decreased the supernatant solids from ~350 to ~200 ppm (Figure 7.22a). The effect of silane-containing polymer was more pronounced at 150 g $t^{-1}$ HX-300 (~8 m $h^{-1}$ settling rate), where supernatant solids decreased from ~1200 to ~300 ppm on dosing ≥ 600 g $t^{-1}$ S-10292.

The effect of silane-containing polymer appeared to be greatest when the flocculant dosage was relatively low. This aspect is further discussed in Section 7.5.2.3. It is also of importance to stress that there was a critical S-10292 dosage (~200 g $t^{-1}$) required before its effect could be clearly seen in combination with HX-300. Unlike with PAA, where the pre-addition of S-10292 slightly increased the resultant settling rates (Figure 7.13), increasing S-10292 dosage at a fixed HX-300 dosage did not

change the settling rate of the *in-situ* DSP/hematite slurry. This is in accordance with results from Davis et al. (2010a), where settling rates were reported to remain unaffected when the combination of S-10292 and HX-400 was used to treat the DSP-containing residue.

#### *7.4.1.8 FBRM study*

If silane-containing polymer improved fines capture, then the enhanced sensitivity in the lower chord length region for the G400 FBRM instrument should be well suited to detect this. The most important characteristic sought from FBRM data was the unweighted chord length distribution after the addition of PAA or HX PAM flocculant. The unweighted counts in the chord length region between 1-10 or 1-20 μm may correspond to the fines capture efficiency which was indirectly measured as supernatant solids (ppm) in settling test. The difficulty in using G400 FBRM was determining when silane-containing polymer should be added to give optimum improvement.

Figure 7.23 contains the unweighted chord length distributions for *in-situ* prepared DSP/hematite slurry (31 wt/wt% DSP), measured 30 s after Alclar 665 was added at a fixed dosage of 104 g $t^{-1}$. The time delay between S-10292 and subsequent Alclar 665 additions was varied from 45, 60 and 90 s, trying to seek the optimised time lag that could clearly show the beneficial effect of silane-containing polymer. Generally, the size enhancement had reached its maximum 30 s after Alclar 665 (or HX-300) addition and so did fines capture.

The results derived from the Macro mode (Figure 7.23a) show that the biggest difference in the unweighted counts at lower chord length region (1-20 μm) was seen when the time delay was 45 s. A 60 s time delay between S-10292 and Alclar 665 addition still showed an improvement from S-10292, although it was not as discernible as that given by the shorter delay. The improvement in fines capture was no longer apparent when Alclar 665 was added 90 s after S-10292.

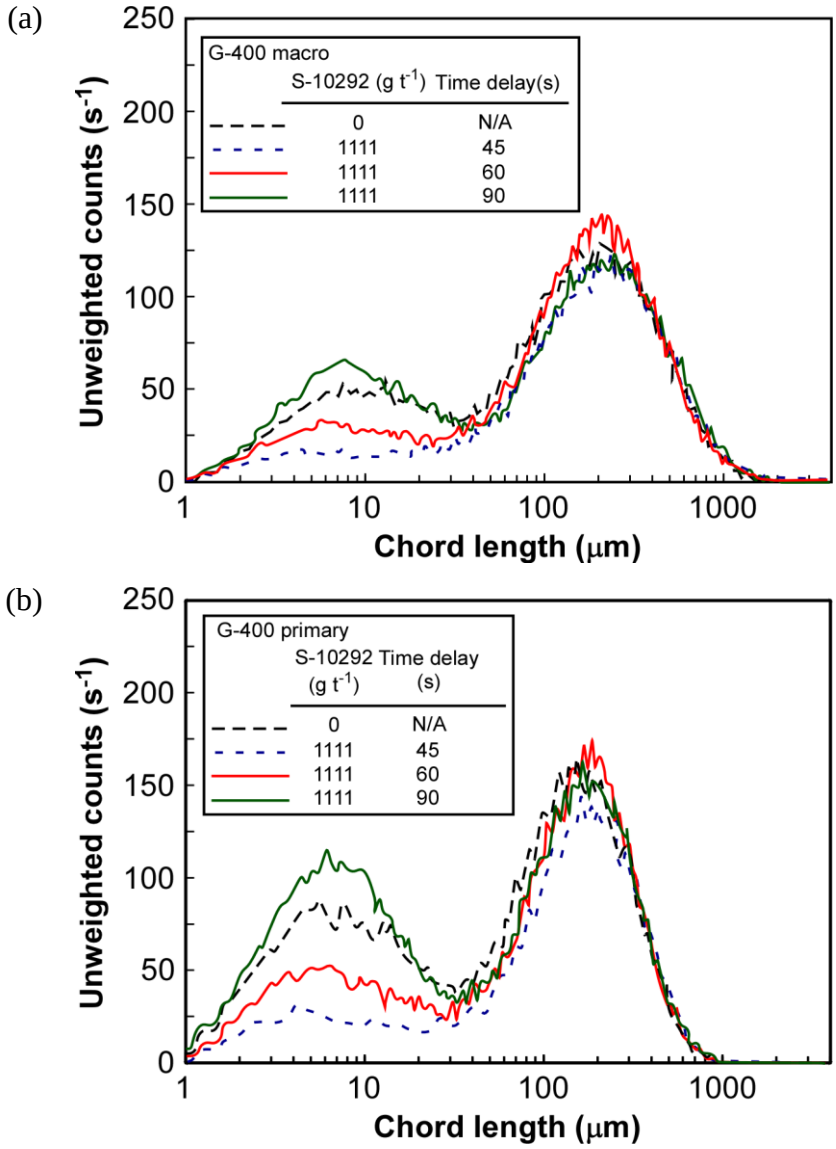


Figure 7.23. The unweighted chord length distributions of *in-situ* prepared DSP/hematite slurry (31 wt/wt% DSP) measured at 30 s after addition of 104 g $t^{-1}$ Alclar 665 with or without 1111 g $t^{-1}$ S-10292: (a) macro and (b) primary mode. G400 probe, A/C = 0.35, C/S = 0.99, C = 230 g $L^{-1}$.

When the coagulation effect of S-10292 was measured without the addition of Alclar 665, the aggregate size was maintained for a long period time (~5 minutes) and aggregate break-up was not detected (Figure 7.14). Thus, the diminishing effect of S-10292 given by the increasing time delay between S-10292 and Alclar 665 additions was not likely to be due to aggregate break-up. This issue, however, should also not be overlooked as in a thickener feedwell, optimum flocculation is achieved very fast, within the order of seconds (e.g. 10 s in Nguyen et al. 2012).

When the primary mode was used to treat the FBRM data, the relative improvement in fines capture was even clearer (Figure 7.23b), but did not change the fact that a 45 s time delay between S-10292 and Alclar 665 additions was optimal for fines capture. Hence, the primary mode was preferable when monitoring fines capture efficiency. A time delay less than 45 s was not practical because there was not sufficient time to operate data acquisition software, monitor the stopwatch while at the same time prepare to inject the polymer solutions. All further experiments were carried out with a 45 s time delay between silane-containing polymer and flocculant addition.

FBRM tests were extended to study the effect of S-10292 dosage. Figure 7.24 compares the effect of S-10292 dosages on unweighted chord length distributions for *in-situ* prepared DSP/hematite slurry (31 wt/wt% DSP) measured 30 s after the addition of 104 g $t^{-1}$ Alclar 665. A S-10292 dosage of 833 or 1388 g $t^{-1}$ led to slightly lower counts in the 1-20 μm chord length region when compared to baseline (0 g $t^{-1}$ S-10292) conditions (black dashed lines in Figure 7.24). The biggest improvement in fines capture was for 1111 g $t^{-1}$ S-10292. This dosage was therefore used to study the effect of S-10292 when HX-300, instead of Alclar 665, was the primary flocculant.

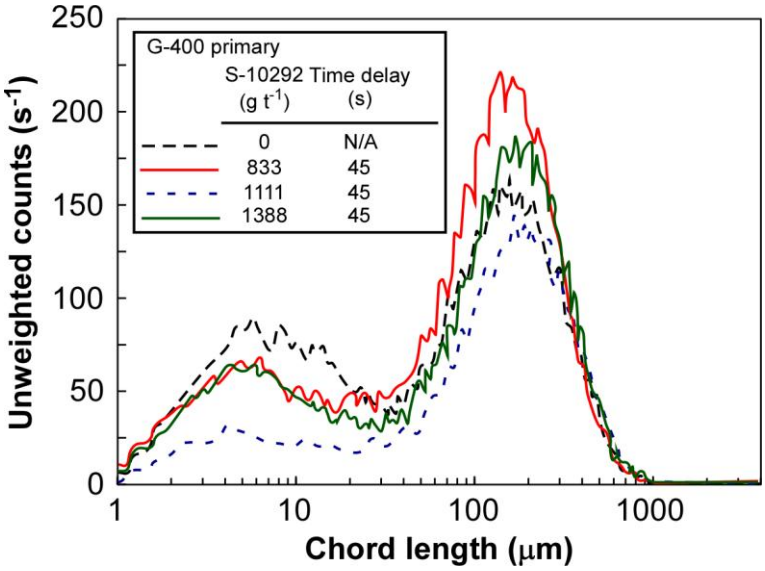


Figure 7.24. The effect of S-10292 dosage on unweighted chord length distribution for *in-situ* prepared DSP/hematite slurry (31 wt/wt% DSP) measured 30 s after addition of 104 g $t^{-1}$ Alclar 665. G400 probe, A/C = 0.35, C/S = 0.99, C = 230 g $L^{-1}$.

Figure 7.25 displays the effect of S-10292 on unweighted chord length distributions for *in-situ* prepared DSP/hematite slurry (31 wt/wt% DSP) flocculated with 208 g $t^{-1}$ HX-300. Since split addition (50:50 by volume) was practised for HX flocculants, the unweighted chord length distributions were measured at 30 s after the first and the second doses of HX-300 (referred to as 1st and 2nd dose in the Figure). Despite slightly less counts in the 1-7 μm chord length region after the first dose of HX-300, the benefit of S-10292 to fines capture was more apparent after the second HX-300 dose. In summary, besides confirming the role of silane-containing polymer as a coagulant, the G400 FBRM probe had successfully provided supporting evidence of improved fines capture from combining the polymer with a primary flocculant.

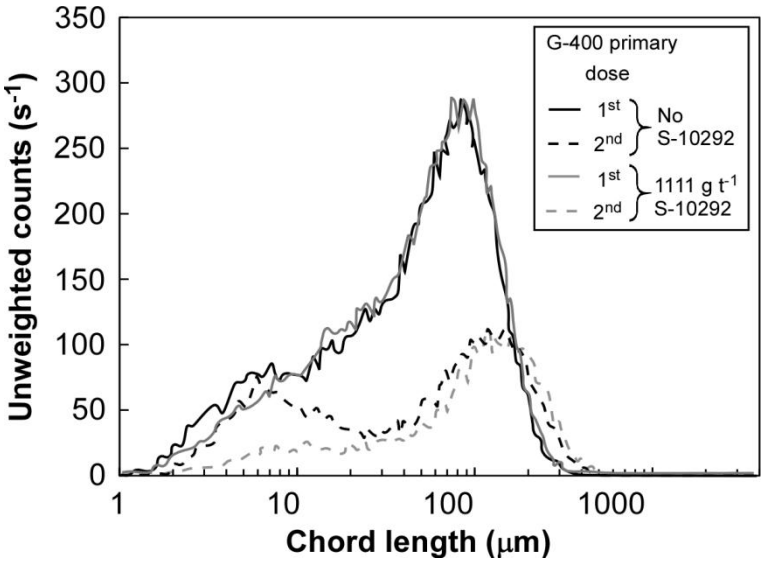


Figure 7.25. The effect of S-10292 on unweighted chord length distributions of *in-situ* prepared DSP/hematite slurry (31 wt/wt% DSP) measured at 30 s after the 1st and 2nd additions of HX-300. G400 probe, A/C = 0.35, C/S = 0.99, C = 230 g $L^{-1}$, HX-300 dosage = 208 g $t^{-1}$ (dosed in split addition – 50:50 by volume).

### *7.4.1.9 Adsorption of silane-containing polymer onto DSP – FTIR*

The IR spectra of S-10292 and DSP feed are presented in Figure 7.26. Since S-10292 was supplied in a water-continuous form, it had to be dried and carefully ground prior to IR reflectance measurements. Peaks were visible in the S-10292 spectrum at 862, 970, 1385, 1440, 1560, 1626 and 3423 $cm^{-1}$ (Figure 7.26a). The peaks at 1626 and 3423 $cm^{-1}$ could be H-O-H and OH bands (Freda et al. 2005), and were probably due to moisture adsorbed during sample preparation. The peak at 1440 $cm^{-1}$ may represent carbonate which was transferred from the $CO_2$ in the atmosphere to the S-

10292 polymer solutions; ~1400 $cm^{-1}$ is known as the fingerprint frequency for carbonate-containing minerals (Huang and Kerr 1960).

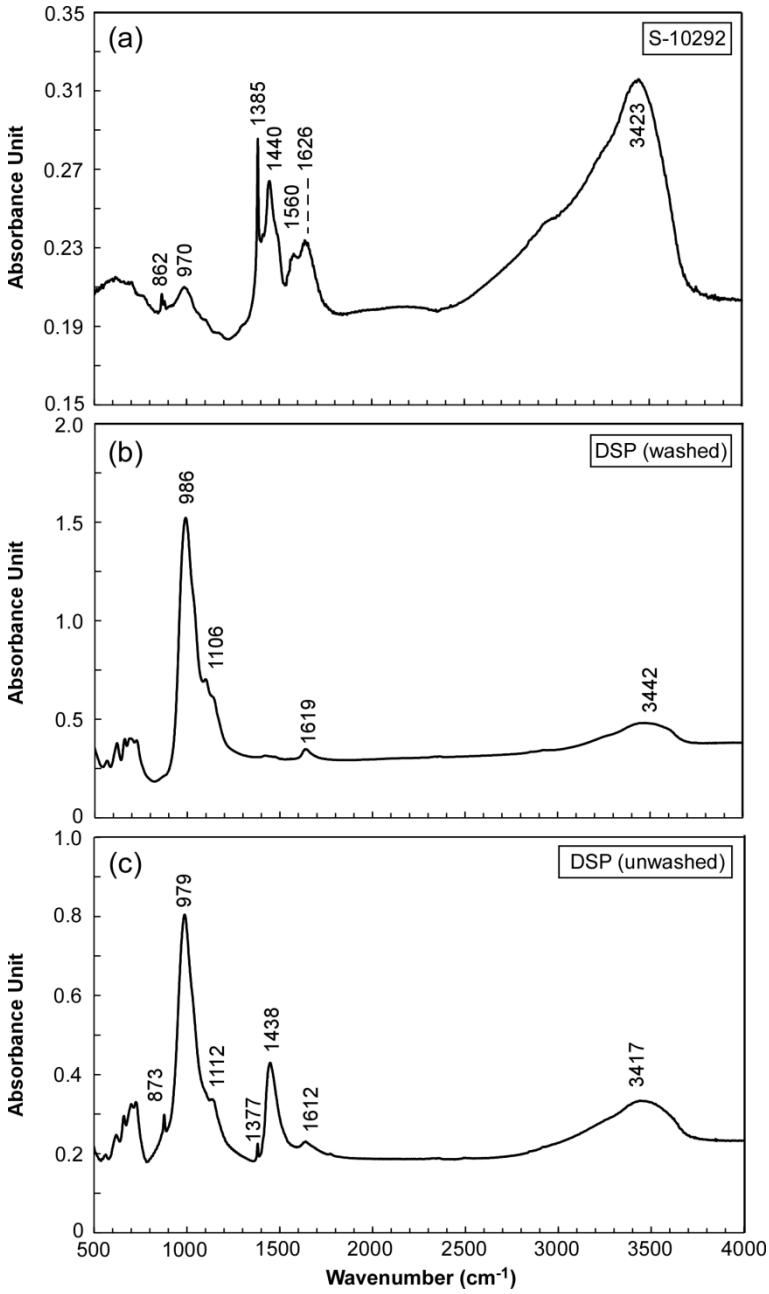


Figure 7.26. IR spectra for (a) dried S-10292, (b) washed DSP and (c) unwashed DSP.

The polymeric components of S-10292 are likely to be associated with the peaks at 862, 970, 1385 and 1560 $cm^{-1}$. The last two peaks are characteristic of $COO^-$ symmetric/asymmetric stretch of carboxylate reported by Jones (1998). This suggests that S-10292 contained some acrylate character. The peak at 862 $cm^{-1}$ matched the description of Si-OH that is often marked by a single band at 810-950 $cm^{-1}$ (Launer

1987). The peak at 970 $cm^{-1}$ did not match any known frequency reported for organosilicon groups (Launer 1987).

The spectrum of washed DSP (Figure 7.26b) contained a strong peak at 984 $cm^{-1}$ with smaller peaks in the region 600-800 $cm^{-1}$ and at 1076, 1619 and 3442 $cm^{-1}$. The small peaks at 1619 and 3442 $cm^{-1}$ were the H-O-H and O-H bands, as mentioned previously. From published literature, a series of small peaks at 600-800 $cm^{-1}$ were already known as the symmetric stretches of $\nu_{Al-O}$ for the Si-O-Al framework in sodalite, whereas the strong peak at ~980 $cm^{-1}$ and its shoulder (1076 $cm^{-1}$) were reported as the asymmetric stretches of $\nu_{Al-O}$ also for the Si-O-Al framework (Barnes et al. 1999b; Farmer 1974; Flanigen et al. 1971; Hermeler et al. 1991).

To study the effect of washing on post-aggregated solids, DSP slurry that had been prepared by the methods given in Section 7.3.2 and resuspended in sodium aluminate liquor was sampled prior to the addition of S-10292 or Alclar 665. It was oven-dried without being washed and subjected to IR reflectance measurement. The IR spectrum of unwashed DSP (Figure 7.26c) differed from the washed samples due to the existence of several extra peaks at 876, 1377 and 1438 $cm^{-1}$. The peak at 1438 $cm^{-1}$ was much stronger than the other two very minor peaks. It seemed that carbonate, as a contaminant in sodium aluminate liquor (A/C = 0.35, C/S = 0.99, C = 230 g $L^{-1}$), was adsorbed onto DSP and detected at ~1400 $cm^{-1}$.

Figure 7.27a compares the IR spectrum of DSP that had been mixed with 1200 g $t^{-1}$ S-10292 and washed. The IR spectrum of washed DSP was the same as that in Figure 7.26 and is therefore not shown. From the vis-à-vis comparison between the washed DSP (Figure 7.26b) and DSP that have been mixed with S-10292 and washed (Figure 7.27a), it seemed that there was no difference between the two, with no trace of the S-10292 fingerprint peaks at 862, 1385 and 1560 $cm^{-1}$.

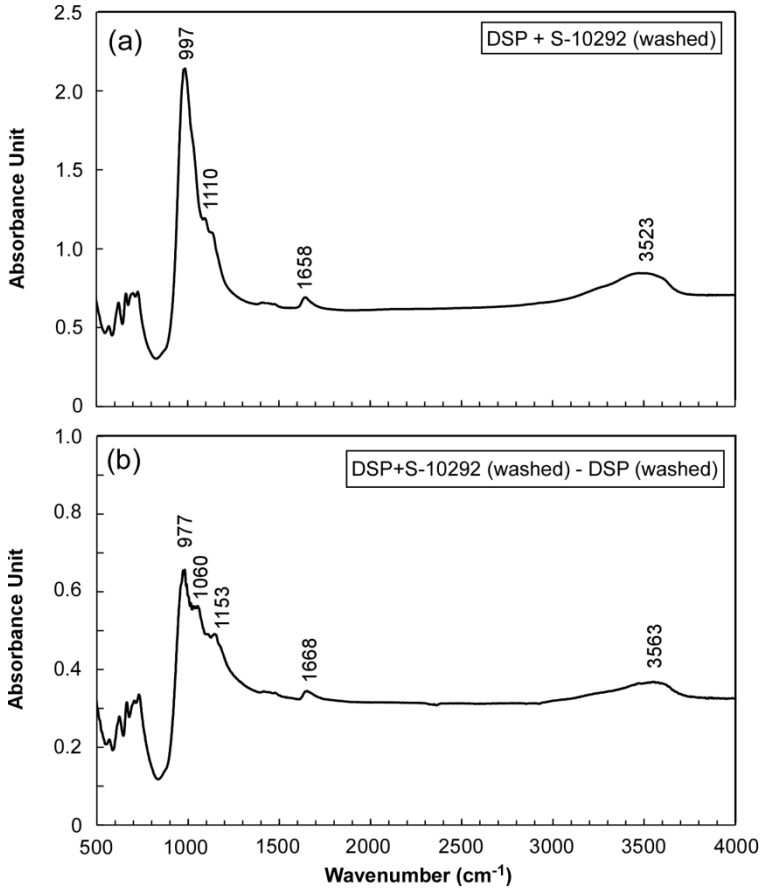


Figure 7.27. The IR spectra of (a) washed DSP + S-10292 and (b) normalisation of this spectrum with that of washed DSP (Figure 7.26b). 1200 g $t^{-1}$ S-10292.

A similar situation is found when the IR spectrum of DSP mixed with S-10292 and washed was contrasted with that of washed DSP (the latter was subtracted from the former). The subtraction result is given in Figure 7.27b and the pattern matches to DSP, not S-10292.

Examining the methodology, dried samples were mixed with KBr (to make mixtures with ~1 wt/wt% sample) and pressed into a disk prior to measurement. It was possible there was slightly higher amount of DSP sample in the disks containing DSP mixed with S-10292 and hence only a DSP pattern was still seen after subtraction. Since washed samples did not give any trace of S-10292, then it was thought that this may also be a consequence of the washing process. The effect of washing and Alclar addition after S-10292 was therefore examined.

The IR spectra of unwashed DSP and DSP mixed with S-10292 (600 g $t^{-1}$) and dried without washing are shown in Figure 7.26c and Figure 7.28a, respectively. Again,

DSP mixed with S-10292 showed a similar pattern to pure DSP. Regardless of pre-treatment (washing or non-washing), the fingerprint peaks of S-10292 were not detected, even on magnifying certain regions (800-900 and 1300-1600 $cm^{-1}$). Thus, there is no evidence that washing promoted desorption of S-10292 from the surface.

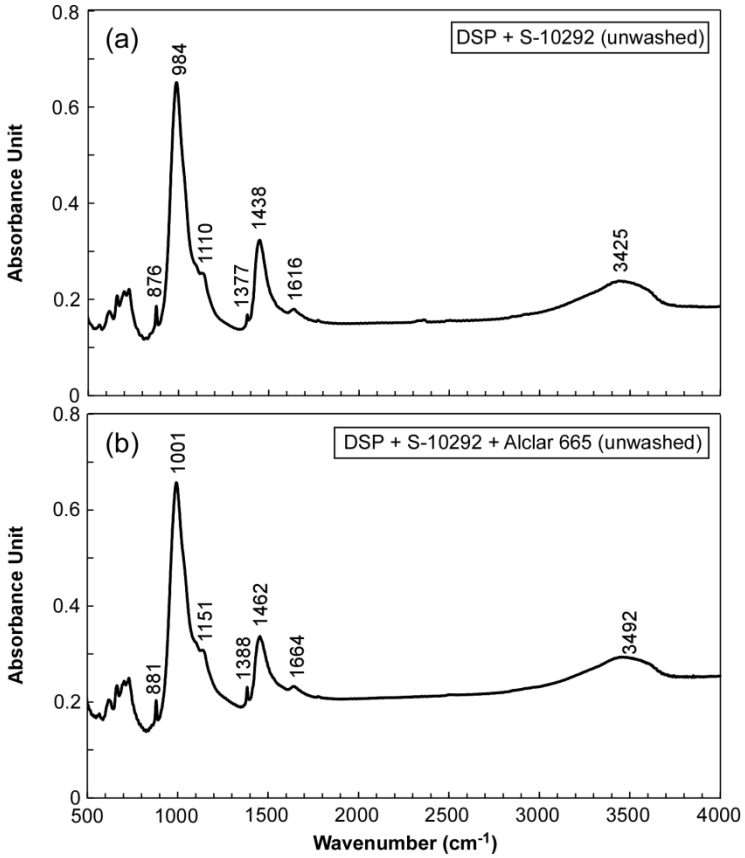


Figure 7.28. IR spectra of: (a) unwashed DSP + S-10292 and (b) unwashed DSP + S-10292 + Alclar 665 (1200 g $t^{-1}$ S-10292, 150 g $t^{-1}$ Alclar 665).

Alclar 665 was then added after the DSP slurry was mixed with S-10292, to find evidence whether S-10292 was retained at the surface when the primary flocculant was involved. Figure 7.28b displays the IR spectrum of unwashed DSP that had been mixed with 600 g $t^{-1}$ S-10292 and 150 g $t^{-1}$ Alclar 665 (S-10292 was added 45 s before Alclar 665). The combination of S-10292 and Alclar 665 did not change the IR spectrum of washed DSP.

The absorbance of S-10292 in Figure 7.26a was already low when it was compared to that from DSP samples. Note that this was the absorbance derived from drying S-10292 solutions. When it was added at a dosage of 1200 g $t^{-1}$ adsorbent, the relative

percentage of S-10292 in DSP became very small. This may decrease the absorbance proportionally, to a level below the detection limit.

FTIR-Attenuated Total Reflectance (FTIR-ATR) was used for a limited number of analyses as it did not require sample dilution by KBr. However, the results were still not able to show the presence of S-10292, making it unnecessary to include such results here. Therefore, an analytical method that was more sensitive than infrared was required to study the adsorption of S-10292 onto the DSP surface.

### *7.4.1.10 Adsorption of silane-containing polymer onto DSP – Fluorimetry*

The extent of S-10292 adsorption onto DSP was studied with fluorimetry, where the fluorescence intensity of supernatant liquor was measured and converted to the residual S-10292 concentration using the calibration graph in Figure 7.11. The plot of S-10292 adsorbed per unit mass of DSP vs. residual S-10292 concentration in the liquor is shown in Figure 7.29. The plot of percentage adsorption vs. residual S-10292 concentration is also presented in the same graph.

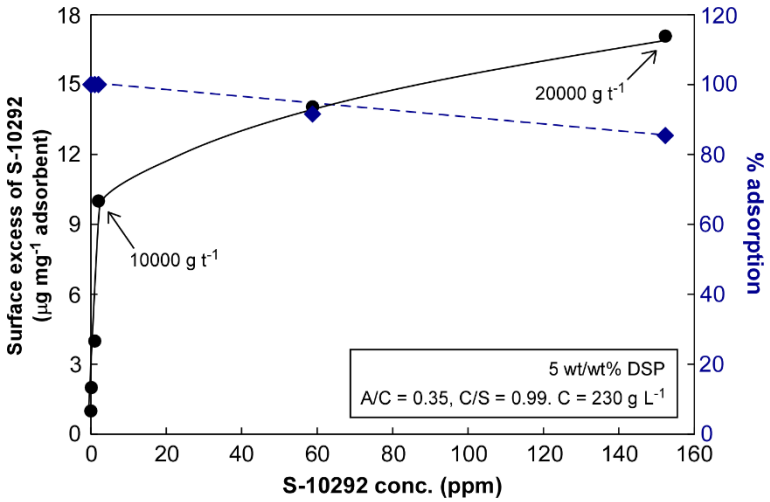


Figure 7.29. S-10292 adsorption onto DSP (μg $mg^{-1}$) vs. S-10292 concentration (ppm) (conditions: 70°C, 15 minutes stirring at 300 rpm).

The adsorption density of S-10292 onto DSP was very high. For example, complete adsorption of S-10292 was achieved when its dosage was 10000 g $t^{-1}$. In fact; when 20000 g $t^{-1}$ S-10292 was added into the DSP slurry, ~85% of it still adsorbed without any sign of surface saturation despite such an extremely high reagent dosage. The

advantage of its high affinity onto DSP particles was that at operational dosage (0-1000 g $t^{-1}$), S-10292 will be completely adsorbed and not remain in the liquor as a contaminant that may adversely affect downstream processes.

The dimension (radius of gyration) of S-10292 in synthetic Bayer liquor was not measured. Consequently, it is not known if S-10292 was smaller or bigger than the average pore size in DSP (~19 nm – Table 6.7), or whether it was adsorbed by the pores. If adsorption by the pores did occur, controlling the silane-containing polymer molecular weight and its effective dimension in Bayer-type liquor could be a partial solution to prevent S-10292 accessing the pores, thereby maximising the S-10292 concentration that adsorbs onto the surfaces.

## 7.4.2 High solids concentration in the desilication reaction

### *7.4.2.1 The PSD of DSP produced*

The question as to whether or not higher DSP content produces more sub-micron particles has to be answered, as it may help explain the sharp increase in supernatant solids measured after flocculation of DSP-containing slurry. The conflicting trends from the results in Section 6.5.1.1 compared to those in Davis et al. (2010a) could be because of the difference in solids concentration during desilication. In Davis et al. (2010a), the kaolin concentration reaches 200 g $L^{-1}$ and this may produce finer DSP.

The desilication process was therefore repeated at a solids concentration of 480 g $L^{-1}$ in a temperature-controlled bottle roller (Section 7.3.1.1). The solids concentration was the sum of hematite and kaolin, which were both varied to mimic 1-8 wt/wt% reactive silica. The effect of increasing kaolin solids concentration on the size distribution of solids produced was thereby examined.

Figure 7.30 contrasts PSDs produced from 1 and 8 wt/wt% reactive silica mixtures, representing 4.7 and 34.9 wt/wt% DSP, respectively. The 8 wt/wt% reactive silica mixture was chosen as an upper limit because it is considered the current economic

limit of high silica bauxite processing (Smith, 2009). On first inspection, it seems that high DSP content increased the fraction of 5-20 μm particles.

(a)

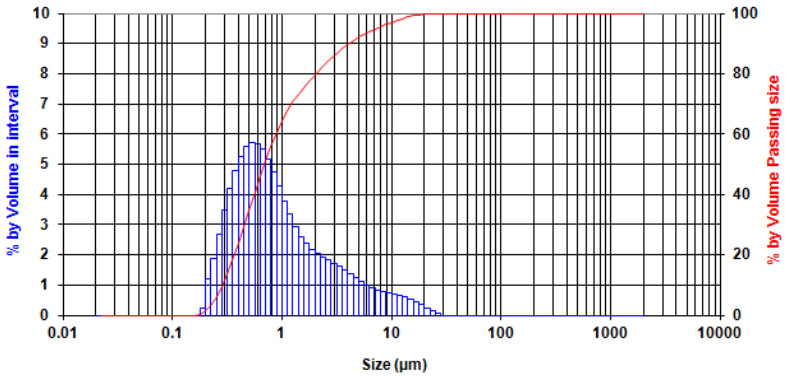


(b)

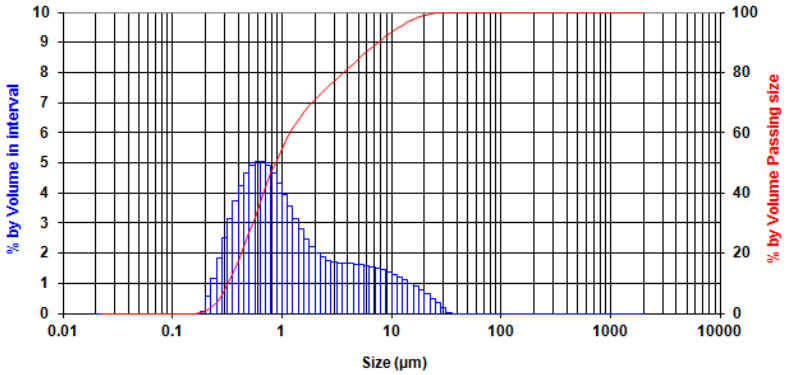


Figure 7.30. PSD of *in-situ* prepared DSP/hematite slurries made at high solids concentration in desilication: (a) 4.7 wt/wt % DSP (R-$SiO_2$ = 1 wt/wt%) and (b) 34.9 wt/wt% DSP (R-$SiO_2$ = 8 wt/wt%).

A better comparison is provided in Figure 7.31, where $d_{10}$, $d_{50}$, $d_{80}$ and $d_{90}$ are plotted vs. DSP content. The $d_{10}$ and $d_{50}$ values were both below 1 μm and remained unaffected by increased DSP content, therefore giving no evidence of a higher DSP content increasing the proportion of sub-micron particles. The $d_{80}$ and $d_{90}$ values were larger when the DSP content was increased. This was due to the increased coarse fraction (~5-20 μm) mentioned previously. That the presence of DSP increased the coarse fraction of particles in the slurry was evident in low and high solids concentrations, 60 and 480 g $L^{-1}$, respectively.

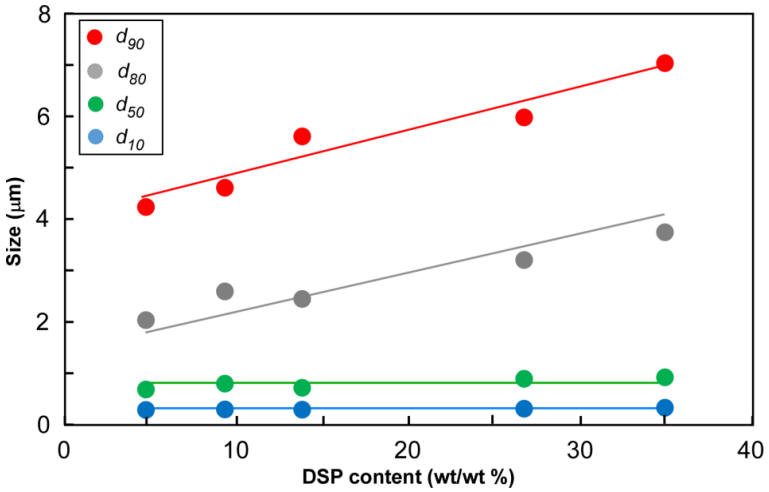


Figure 7.31. The effect of DSP content on the size characteristics of *in-situ* prepared DSP/hematite slurries made at high solids concentration during desilication.

It is also of interest that desilication done at 60 g $L^{-1}$ produced different PSD characteristics from that done at 480 g $L^{-1}$. A Hematite:kaolin ratio = 3:1 at lower solids concentration represented 15 g $L^{-1}$ of kaolin and on reaction produced a mixture with 31 wt/wt% DSP and a $d_{90}$ of ~9 μm. At higher solids concentration, a slightly lower ratio (2.5:1) represented 138 g $L^{-1}$ of kaolin and the mixture formed on reaction contained 34.9 wt/wt% DSP and a $d_{90}$ of ~7 μm. The concentration of hematite seed particles seemed to also affect the size distribution of DSP formed. The effects of solids concentration in desilication (60 vs. 480 g $L^{-1}$) on settling rates and supernatant solids on flocculation of the *in-situ* prepared DSP/hematite slurries (31 wt/wt% DSP) were examined and the results are shown in Figure 7.32a and b, respectively. All other experimental variables were fixed and at this stage, silane-containing polymer was not involved.

Although the settling rates and supernatant solids measured were quite similar at high flocculant dosages (≥ 300 g $t^{-1}$ HX-300), at a moderate dosage (200 g $t^{-1}$), the supernatant solids measured from the DSP/hematite slurries synthesized at a high solids concentration was twice that for slurries synthesized at a low concentration. For the slurry synthesized at high solids concentration, the settling rate and supernatant solids at a low dosage (100 g $t^{-1}$) could not be measured due to a very poor clarity preventing mudline detection. This observation clearly indicates that the generally smaller particles from desilication at 480 g $L^{-1}$ solids did lead to poor flocculation. The effect given by the smaller particles diminished at high flocculant

dosages, which provided a higher probability of collision and adsorption of flocculant onto the smaller particles (Section 2.1).

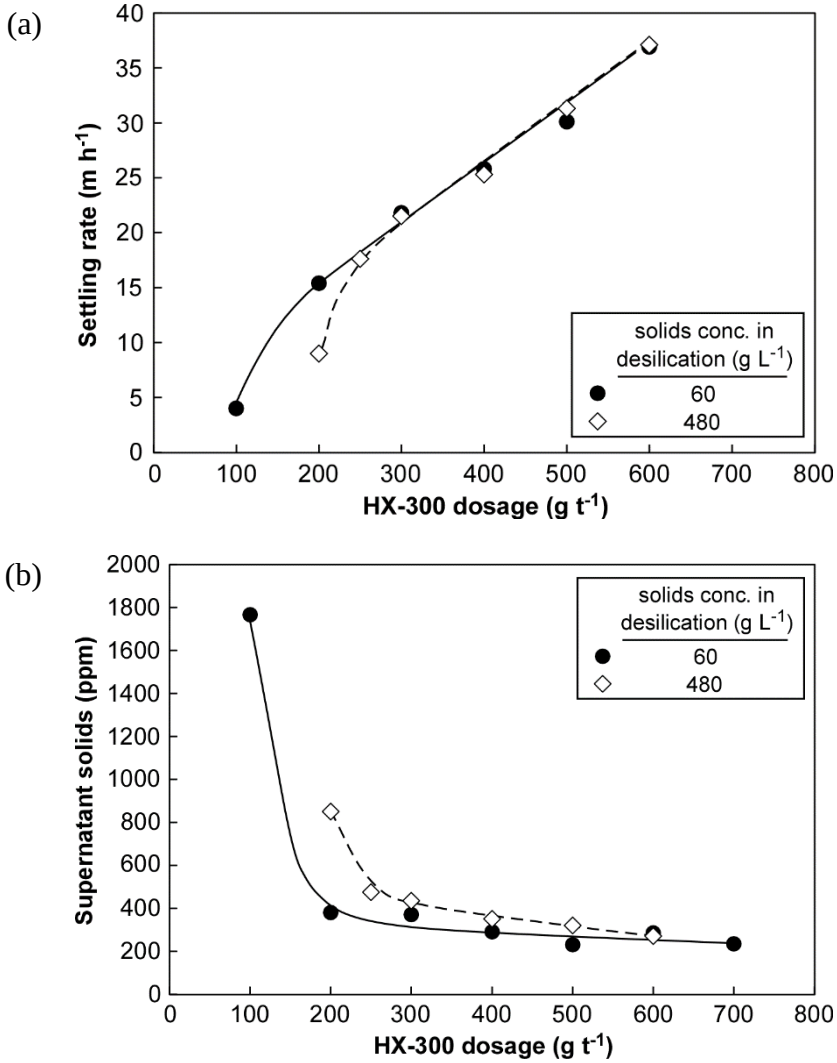


Figure 7.32. The effect of different solids concentration during desilication on (a) settling rate and (b) supernatant solids after flocculation of *in-situ* prepared DSP/hematite slurry (31 wt/wt% DSP). A/C = 0.55, C/S = 0.99, C = 230 g $L^{-1}$.

### *7.4.2.2 Effect of silane-containing polymer on different shear regimes*

In a feedwell, the shear rate distribution can be non-uniform and quite broad, depending on its design (Section 2.3). Many feedwells used in mineral processing still suffer from poor hydrodynamics that result in shear rates that are too low or too high for optimum flocculation. Experiments that vary the applied shear conditions could provide insights into the flocculation process, especially in the case of shear-sensitive DSP/hematite aggregates (Section 6.5.5).

In a cylinder settling test, the number of strokes following coagulant/flocculant addition can be varied to create a difference in the relative applied shear. For the work discussed in this section, the number of strokes accompanying the second addition of HX-300 flocculant was varied between two, five or eight strokes (with a single stroke consisting of both down and up plunger movements). Since the relative applied shear will be lowest for two strokes and highest for eight strokes, the variation in strokes following the second addition of HX-300 is referred to as "low", "moderate" and "high" shear. The strokes following the S-10292 addition or the first addition of HX-300 remained the same (five strokes).

Figure 7.33a compares the settling rates measured when the different relative shear conditions were applied to *in-situ* prepared DSP/hematite slurries flocculated with HX-300. The DSP content was fixed at 34.9 wt/wt% (from 8 wt/wt% reactive silica). The effect of silane-containing polymer (600 g $t^{-1}$ S-10292) for each relative shear condition is also presented in the same graph. The pre-addition of S-10292 did not appear to influence the settling rates of the slurries. This is in agreement with the results in Section 7.4.1.7 where a combination of S-10292 and HX-300 also did not change the settling rates of DSP/hematite slurries made at low solids concentration during desilication.

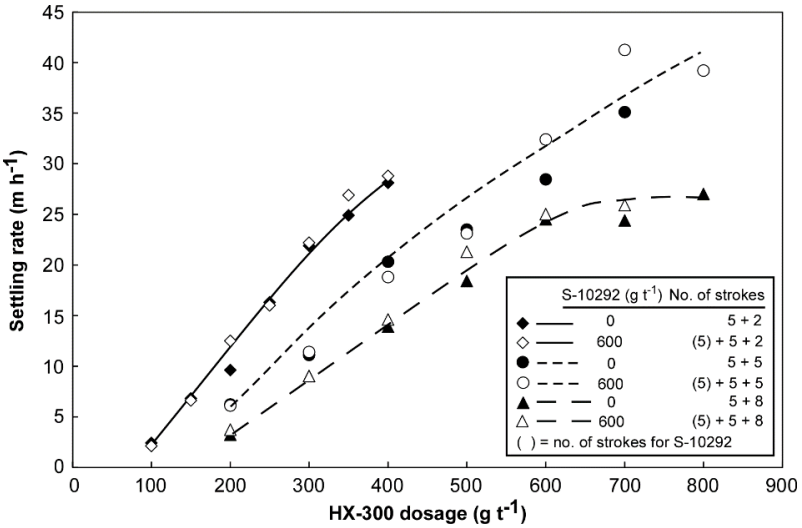


Figure 7.33. The effect of relative shear on settling rates on the flocculation of *in-situ* prepared DSP/hematite slurries (40 g $L^{-1}$, DSP 34.9 wt/wt%) made at high solids concentration during desilication. A/C = 0.55, C/S = 0.99. C = 230 g $L^{-1}$.

Higher relative shear shifted the settling rate response to dosage curves to the right, indicating higher flocculant consumption. The higher relative shear induces aggregate break-up and thereby lower settling rates, which can be compensated for to some extent with the addition of more flocculant.

The supernatant solids corresponding to the settling rates given in Figure 7.33 can be found in Figure 7.34a, b and c for the low, moderate and high shear conditions, respectively. They demonstrate a trend of great interest. For the low applied shear, the pre-addition of S-10292 gave a reduction of supernatant solids even at high flocculant consumption ($\geq$ 300 g $t^{-1}$ HX-300). In fact, a 20-30% reduction in supernatant solids was found from adding 600 g $t^{-1}$ S-10292 under conditions where increasing HX-300 dosage alone was not able to decrease the supernatant solids from a limiting value of ~600 ppm (Figure 7.34a).

Increasing the relative shear (from low to moderate) decreased the overall supernatant solids (Figure 7.34b), which was not unexpected. In hematite flocculation, FBRM data showed that the unweighted counts for 1-20 μm particles decreased as a result of increasing stirring rate (Figure 4.13). The combination of higher relative shear and high HX-300 dosage ($\geq$ 400 g $t^{-1}$) was able to improve the fines capture efficiency, with the measured supernatant solids very close to that achieved by pre-addition of 600 g $t^{-1}$ S-10292.

High shear conditions also gave flocculation performance where the beneficial effect of S-10292 was diminished (Figure 7.34c). In general, fines capture efficiency was actually at its best when moderate shear was applied, suggesting an optimal shear regime for fines capture (considering that supernatant solids reached a limiting value at the low shear condition). A negative effect (i.e. a marginal increase in supernatant solids) was observed when the relative shear changed from moderate to high. Since this happened with or without pre-addition of S-10292, it was most likely due to the aggregate break-up process releasing fragments/fines that reported to the supernatant.

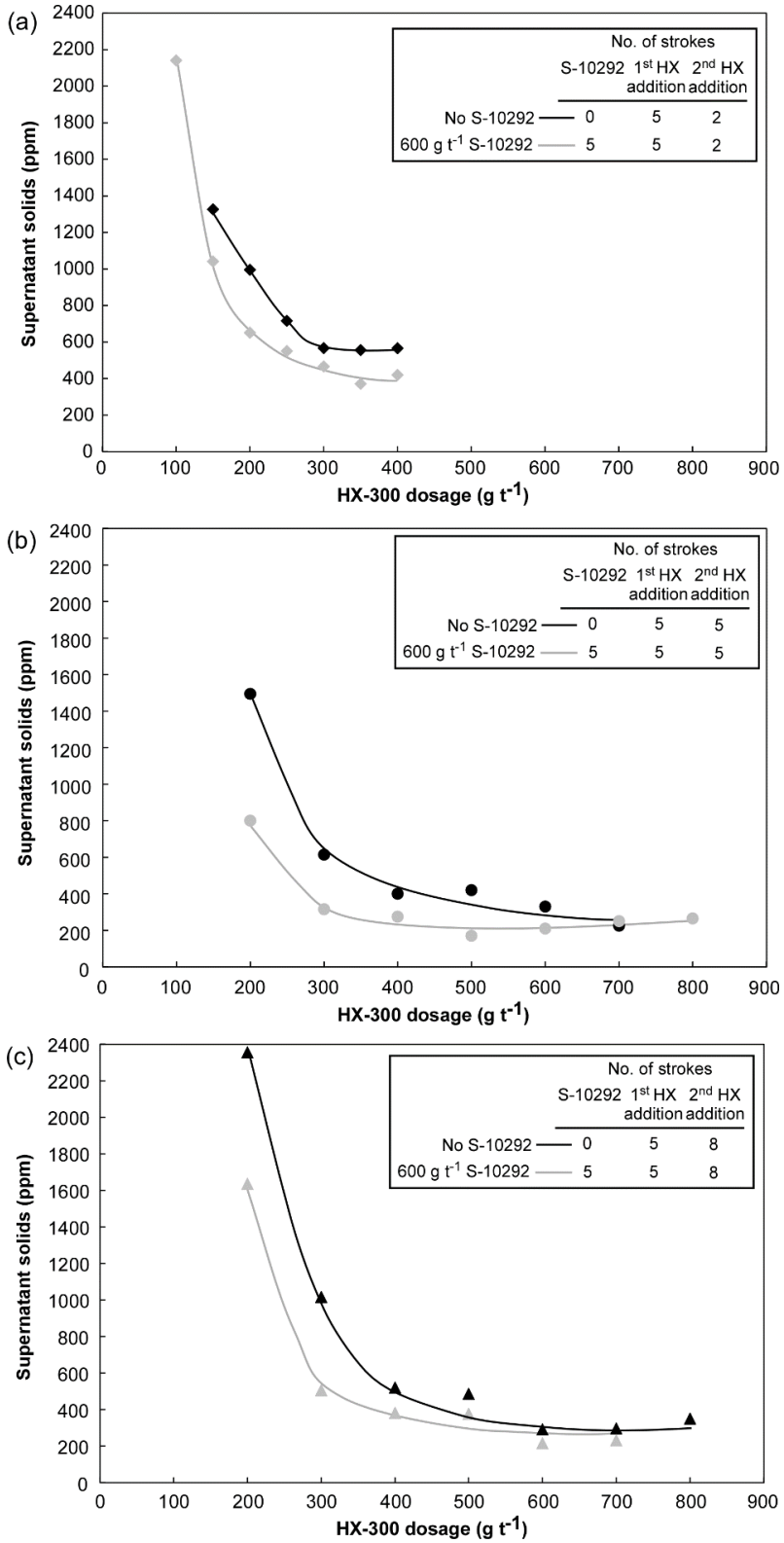


Figure 7.34. The effect of relative shear on the supernatant solids after flocculation of *in-situ* prepared DSP/hematite slurries (40 g $L^{-1}$, DSP 34.9 wt/wt%) made at high solids concentration during desilication: (a) low, (b) moderate and (c) high applied shear. A/C = 0.55, C/S = 0.99. C = 230 g $L^{-1}$, corresponding settling rates in Figure 7.33.

Given that the best fines capture efficiency was found under moderate shear, the experiments were extended to include the effect of a different flocculant on such conditions. A variant of the HX PAM range of flocculants, HX-200, was tested under the moderate shear condition with five strokes following S-10292 or HX-200 addition. The settling rates and supernatant solids measured from *in-situ* prepared DSP/hematite slurries (34.9 wt/wt% DSP) flocculated with HX-200, with or without the pre-addition of S-10292, are shown in Figure 7.35a and b, respectively. For comparison, the settling rates generated from the same conditions but with HX-300 flocculant are also presented.

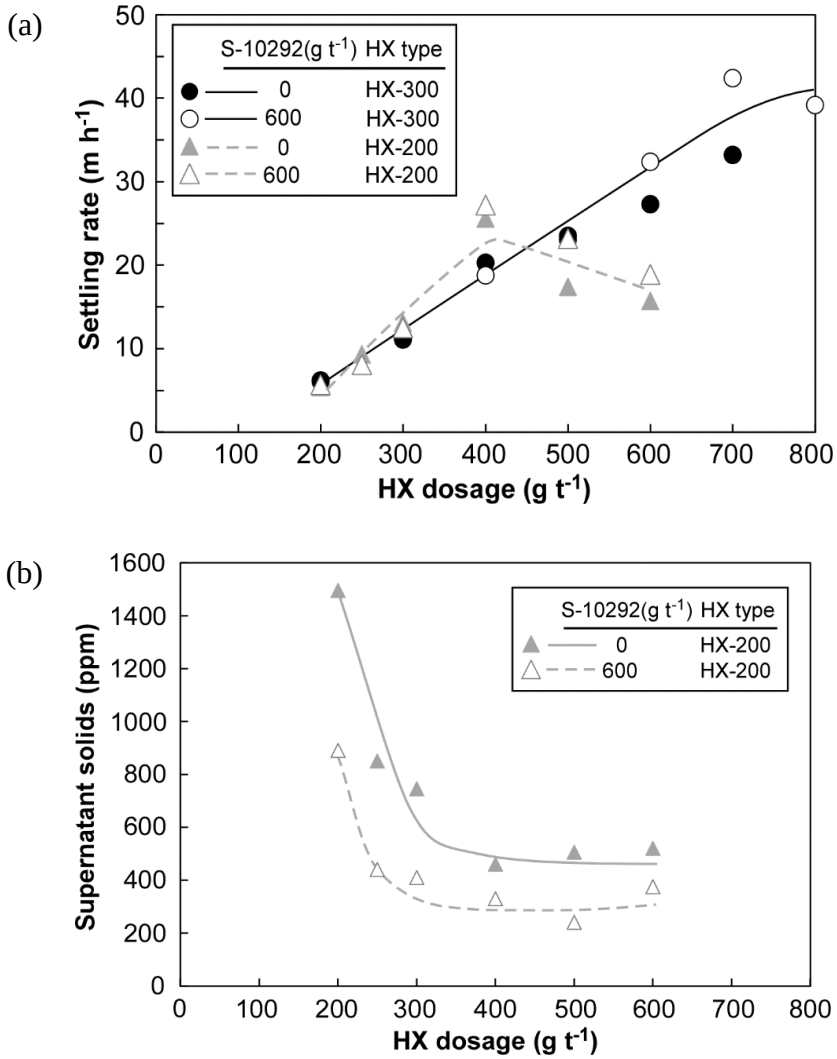


Figure 7.35. The effect of HX-200 dosage on the: (a) settling rates and (b) supernatant solids on flocculation of *in-situ* prepared DSP/hematite (40 g $L^{-1}$, 34.9 wt/wt% DSP) made at high solids concentration during desilication. A/C = 0.55, C/S = 0.99. C = 230 g $L^{-1}$, settling rates from HX-300 are shown for comparison.

Note that increasing the HX-200 dosage beyond 400 g $t^{-1}$ did not bring any further increase in settling rates. The number in the Cyfloc$^{TM}$ HX flocculant code is an indication of the relative hydroxamate functionality content of the polymer, with a lower number meaning less hydroxamate and presumably a greater proportion of carboxylate groups. However, it is still questionable if a higher proportion of acrylate monomer groups in the polymer would result in limiting settling rates to a level of ~20 m $h^{-1}$. In fact, higher settling rates (up to 30-35 m $h^{-1}$) were evident from the addition of polyacrylate to the *in-situ* prepared DSP/hematite slurries (Figure 7.12).

The most important performance measure was actually the supernatant solids measured in the absence and presence of S-10292. When only HX-200 was added as flocculant, the supernatant solids reached a plateau of ~500 ppm, a higher level than seen from the application of HX-300 (Figure 7.34b). The pre-addition of S-10292 (600 g $t^{-1}$) successfully reduced the supernatant solids to a level of ~300 ppm, comparable to the level given by the combination of S-10292 and HX-300.

Therefore, it can be surmised that fines capture efficiency is governed by many factors that include the applied shear during aggregation, liquor composition, flocculant type and their applied dosage. Pre-addition of the silane-containing polymer decreased the supernatant solids to a level that was better than the addition of primary flocculant alone under all conditions other than when flocculant dosages or applied shear were very high. The risk from using excessive flocculant or shear in the bridging flocculation process is discussed further in Section 7.5.2.5.

#### *7.4.2.3 Analysis of supernatant solids*

The supernatant solids measured in settling tests often reach a plateau value, beyond which further addition of primary flocculant can provide no further reduction. The pre-addition of S-10292 was found to provide a partial remedy to this problem. The question whether such plateau values were observed due to the presence of solid particles with a particular morphology, mineralogy or size distribution remained unanswered. Analysis of the supernatant solids collected from settling tests may present some evidence towards resolving this question.

Table 7.6 summarises information regarding the experiments in Section 7.5.2.2 that provided supernatant solids for further analysis. The initial feed for all experimental sets in Table 7.6 was *in-situ* prepared DSP/hematite samples (34.9 wt/wt% DSP) made at high solids concentration during desilication (Set 1). Set 2 refers to the supernatant solids samples recovered from settling tests using HX-200 with or without the pre-addition of S-10292 (Figure 7.35a and b). Comparing the Set 1 and 2 samples under SEM may reveal the evolution of supernatant solid morphology as a result of aggregation by silane-containing polymer and HX PAM.

Table 7.6. Analysis of supernatant solids from *in-situ* prepared DSP/hematite (35 wt/wt% DSP) flocculated with different flocculants.

| Set* | Sub-set | S-10292 (g $t^{-1}$) | Primary flocculant | | No. of strokes** | Supernatant solids (ppm) | Settling rate (m $h^{-1}$) |
|---|---|---|---|---|---|---|---|
| | | | Type | Dosage (g $t^{-1}$) | | | |
| 1*** | - | 0 | 0 | 0 | 0 | N/A | N/A |
| 2 | A | 0 | HX-200 | 300 | 5+5 | 745 | 13.1 |
| | B | 600 | HX-200 | 300 | (5)+5+5 | 410 | 12.5 |
| 3 | A | 600 | HX-300 | 100 | (5)+5+2 | 2140 | 2.1 |
| | B | 600 | HX-300 | 250 | (5)+5+2 | 570 | 16.0 |
| | C | 600 | HX-300 | 400 | (5)+5+2 | 440 | 28.8 |
| 4 | A | 600 | HX-200 | 200 | (5)+5+5 | 890 | 5.7 |
| | B | 600 | HX-200 | 300 | (5)+5+5 | 410 | 12.5 |
| | C | 600 | HX-200 | 600 | (5)+5+5 | 370 | 18.9 |

Note: (*) flocculation conditions for Set 2-4: 40 g $L^{-1}$ solids, liquor: A/C = 0.55, C/S = 0.99, C = 230 g $L^{-1}$; (**) (5) = no. of strokes accompanying S-10292 addition; (***) initial feed for Set 2-4.

Before making such comparisons, it was important to first know the morphology of the pure hematite and DSP phases. The SEM images of pure hematite and pure DSP (made with 137.6 g $L^{-1}$ kaolin in the absence of hematite – see also Table 7.2) are shown in Figure 7.36a and b, respectively. The image of the hematite sample was dominated by the presence of very fine spherically-shaped particles, while DSP formed woolball-like particles that can give large agglomerates. Figure 7.36b captures an image of DSP particle with this woolball morphology, which has been reported in previous studies (e.g. Duncan et al. 1995; Ho et al. 1992; Lowe et al. 2005; Radomirovic et al. 2013).

(a)

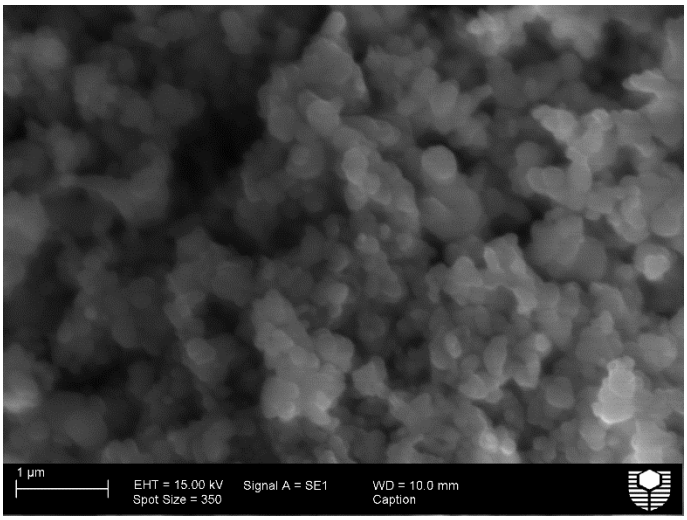


(b)

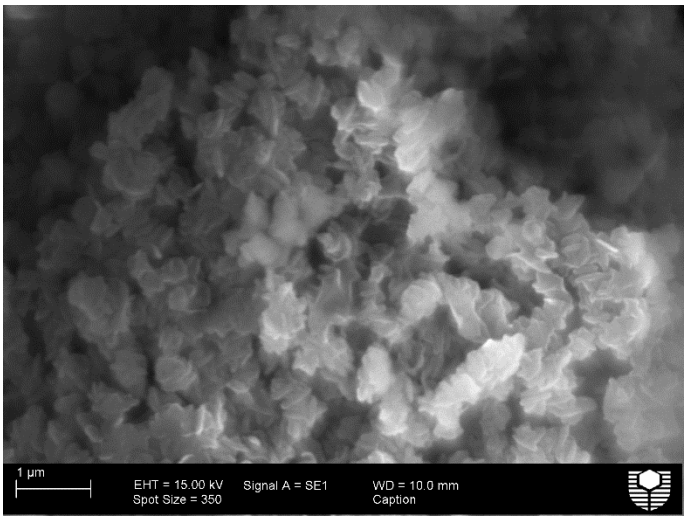


Figure 7.36. SEM images of (a) pure hematite and (b) pure DSP.

Figure 7.37 displays the SEM images of samples in Set 1 and 2 (Table 7.6) at two different magnifications (~3000 and ~11000×). Higher magnification on the initial feeds (Set 1 – Table 7.6) in Figure 7.37a shows the co-presence of fine hematite particles and DSP with woolball morphology. After flocculation with HX-200, the supernatant solids were dominated by the presence of DSP (Figure 7.37b) and the pre-addition of S-10292 did not appear to change this morphology (Figure 7.37c). It was still unclear if the high supernatant solids measured on flocculation of DSP-containing samples were due to the presence of DSP or hematite particles, or both. There may be a chance that hematite particles, partly or completely covered by DSP, were poorly aggregated and reported to the supernatant. SEM could not give clarification on this issue, simply because it is a surface analysis tool. This provided scope for methods focusing on the bulk sample rather than the surface, such as XRD.

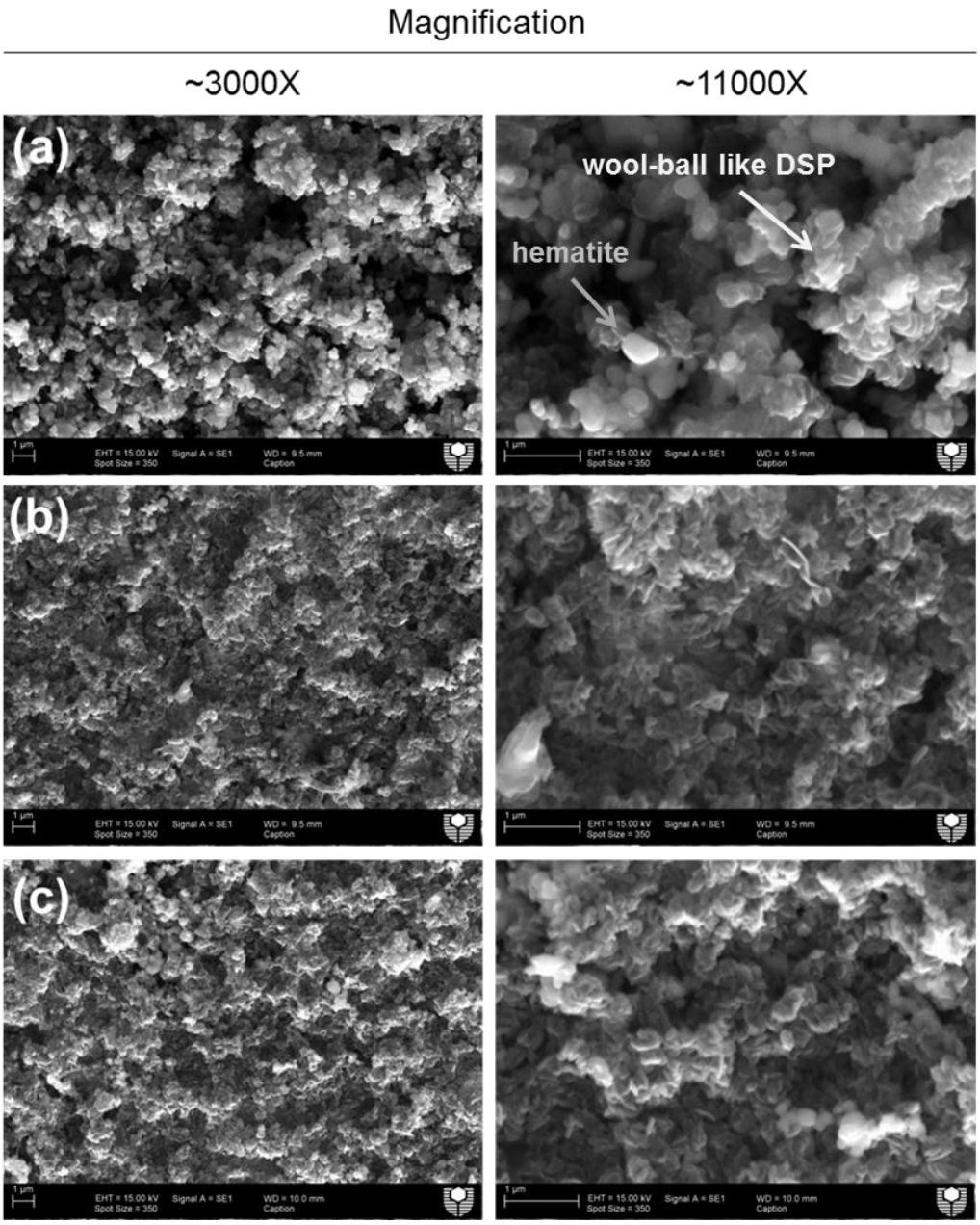


Figure 7.37. SEM images of *in-situ* prepared DSP/hematite (34.9 wt/wt% DSP) made at high solids concentration during desilication: (a) unflocculated feed and supernatant solids after flocculation with: (b) 300 g $t^{-1}$ HX-200 and (c) 600 g $t^{-1}$ S-10292 and 300 g $t^{-1}$ HX-200.

XRD patterns of the supernatant solids collected from flocculation of *in-situ* prepared DSP/hematite slurries with 300 g $t^{-1}$ HX-200 (Set 2 in Table 7.6) are shown in Figure 7.38. Figure 7.38a and b give the XRD patterns without and with the addition of silane-containing polymer (600 g $t^{-1}$ S-10292), respectively. Hematite peaks were still found in both samples, suggesting that the surface coverage of hematite by DSP may contribute to the high supernatant solids measured after flocculation.

Note that the three strongest peaks in the diffractograms represent hematite (2θ = 38°), DSP (2θ = 16°) and both DSP and hematite (2θ = 28°), which together can be used quantitatively as a measure of what had been aggregated and what remained in the supernatant. For simplicity, the hematite, DSP and DSP + hematite peaks are referred to H, D and HD in the text. The relatively low H:D and H:HD ratios in the sample without S-10292 addition (Figure 7.38a) were due to the strong presence of DSP in such samples. In other words, there is less DSP in the sample with S-10292 (Figure 7.38b), confirming that silane-containing polymer had a higher affinity for the DSP particles than for hematite.

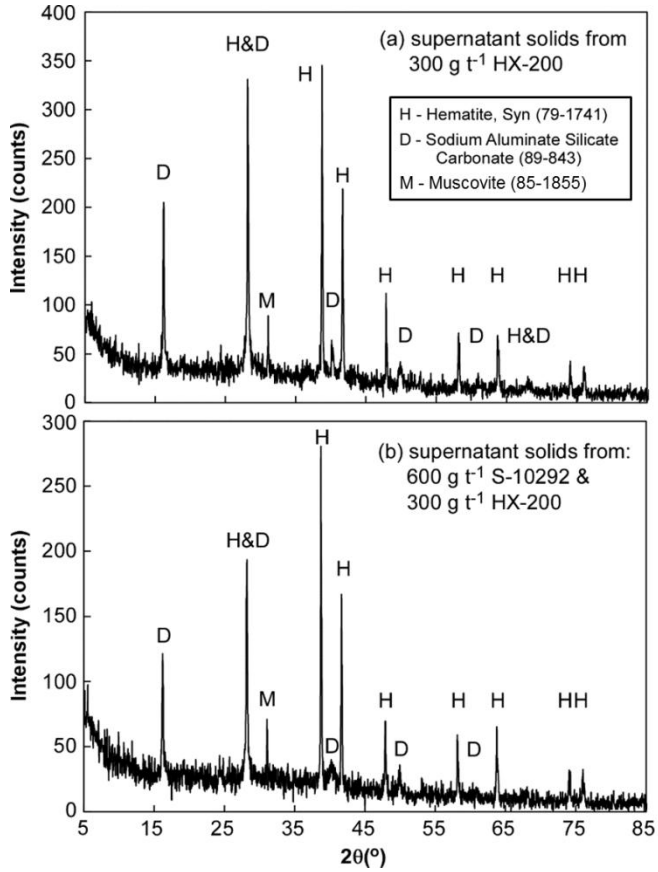


Figure 7.38. XRD patterns of the supernatant solids collected after flocculation of *in-situ* prepared DSP/hematite slurries with 300 g $t^{-1}$ HX-200: (a) without and (b) with pre-addition of 600 g $t^{-1}$ S 10292. Detail conditions for flocculation refer to Set 2 in Table 7.6.

XRD studies were extended to the supernatants solids derived from varying HX PAM dosage. In Set 3 (Table 7.6), the HX-300 dosage was varied between 100, 250 and 400 g $t^{-1}$, all with the pre-addition of 600 g $t^{-1}$ S-10292. The XRD patterns for the corresponding supernatant solids can be seen in Figure 7.39, together with the pattern for the supernatant solids collected after 10 minutes of natural gravity settling

(without addition of polymer/flocculant). This was intended to provide useful information of which phases could potentially 'float' when unflocculated.

By comparing XRD patterns of the original feed (Figure 7.39a) and its supernatant solids collected 10 minutes after natural settling (Figure 7.39b), it can be inferred that hematite particles settle slightly faster than DSP, i.e. the supernatant solids after natural settling had a slightly higher DSP content, apparent from the marginal decrease of H:D and H:HD peak ratios. As sufficient masses (> 3 g) were available from both samples, it was less likely that the differences seen in H:D and H:HD ratios were due to experimental error caused by (for example) different conditions during pattern acquisition.

Addition of 100 g $t^{-1}$ HX-300 also resulted in decreasing H:D and H:HD ratios (Figure 7.39c). Moreover, the peak intensity of D or HD was much higher than that of H. This was a strong indication that DSP particles dominated the supernatant solids, as the majority of hematite particles had been flocculated by HX-300.

Increasing the HX-300 dosage to 250 g $t^{-1}$ actually reversed the situation, with the hematite fraction now dominating the supernatant solids (Figure 7.39d). From gravimetry, it was known that increasing the HX-300 dosage from 100 to 250 g $t^{-1}$ decreased the supernatant solids substantially from 2140 to 570 ppm. It seemed that hematite was initially flocculated and further addition of HX-300 targeted distinct DSP particle and hematite whose surface was partially or completely covered by DSP. The presence of muscovite was also detected in the supernatant solids; its concentration was too low to be detected in the non-flocculated samples where there was a significant amount of hematite.

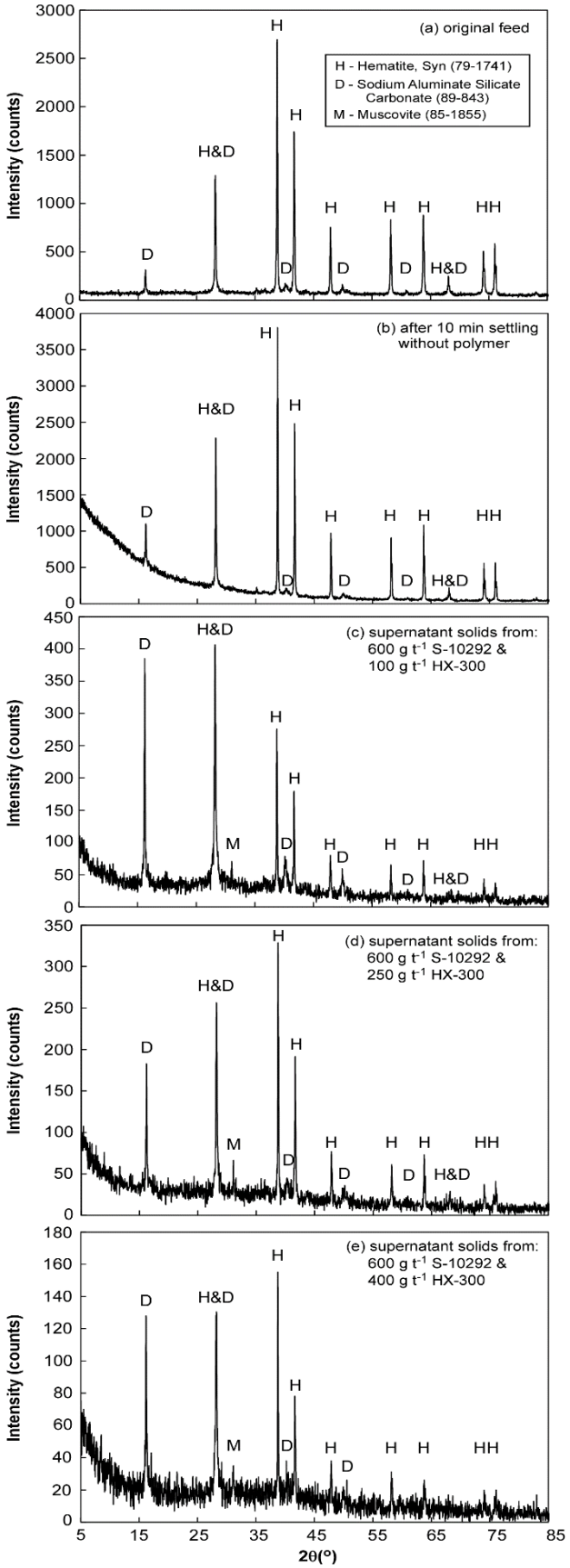


Figure 7.39. XRD patterns of (a) initial feed and supernatant solids collected: (b) 10 minutes after natural settling or after flocculation with (c) 100, (d) 250 and (e) 400 g $t^{-1}$ HX-300. Detail conditions for flocculation refer to Set 1 and 3 – Table 7.6.

Addition of HX-300 at 400 g $t^{-1}$ did not dramatically decrease the supernatant solids when compared to a dosage of 250 g $t^{-1}$ (440 vs. 570 ppm). The changes in H:D and H:HD ratios were also quite subtle when comparing the XRD patterns of solids from 250 and 400 g $t^{-1}$ HX-300 (Figure 7.39 d and e). It should be noted that at the higher clarities for both dosages, less than < 25 mg of supernatant solid was supplied for XRD analysis, and acquiring patterns on small samples may make such subtle changes fall within experimental error.

XRD analysis did confirm the beneficial effect of silane-containing polymer and revealed what was flocculated when the dosage of primary flocculant was increased. The limit in supernatant clarity improvement may be a consequence of the fine particle size, which requires detailed characterisation of the supernatant solids PSD. Full PSDs of the original feed and the supernatant solids from flocculation of *in-situ* prepared DSP/hematite slurry (34.9 wt/wt% DSP) made at high solids concentration are given in Figure 7.40. The HX-300 dosage was varied from 200 to 600 g $t^{-1}$ while the S-10292 dosage was kept constant (600 g $t^{-1}$).

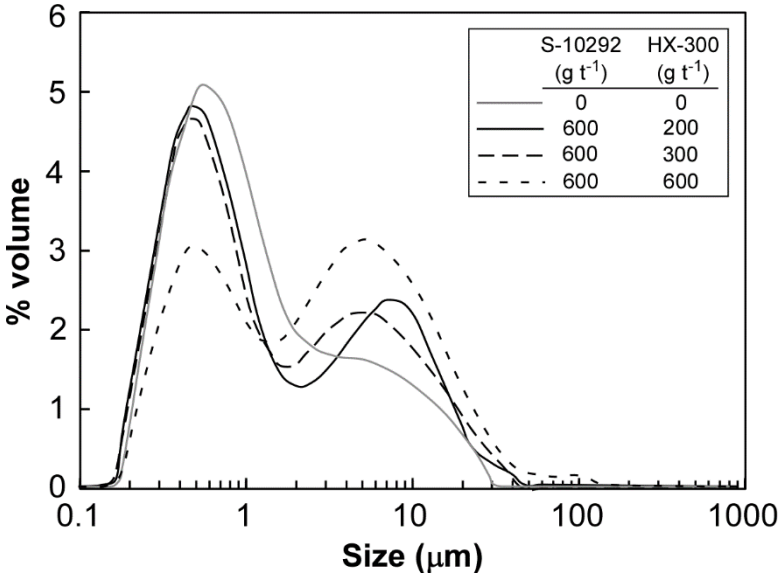


Figure 7.40. PSD of the original feed and supernatant solids from flocculation of *in-situ* prepared DSP/hematite slurry (34.9 wt/wt% DSP). Detail conditions for flocculation refer to Set 4 – Table 7.6.

The bimodal character of the PSDs for the original feed and the supernatant is readily apparent. It has to be kept in mind that the PSDs in Figure 7.40 are volume-based and it does not reflect the actual numbers of particles. In order to have the same %

volume, the number of spherical particles of 1 μm diameter must be 1000 times higher than those of 10 μm diameter. The bimodal distribution in Figure 7.40 means that there were larger particles (3-30 μm), which were not flocculated and settled. Nonetheless, their numbers have to be much smaller than the 0.1-1 μm particles.

Increasing the flocculant dosage decreased the population of 0.1-1 μm particles. It is of interest that the supernatant solids only decreased from 410 to 370 ppm when the HX-300 dosage was increased from 300 to 600 g $t^{-1}$. It was only a minimal improvement when taking into account that twice the amount of flocculant was added. However, there was a significant drop in the submicron fraction accompanying this small mass-based improvement, indicating that the submicron particles consumed high amounts of flocculant to aggregate.

Although the hematite sample used in this thesis contained a sub-micron fraction (Section 4.4.1), it was less likely that sub-micron hematite particles required extremely high flocculant dosages for aggregation. As a matter of fact, supernatant solids measured from pure hematite flocculation was low (≤ 100 ppm) with a small amount of flocculant added (Figure 7.12). Thus, the sub-micron particles that required significant amount of flocculant could likely be the DSP or hematite (partly or completely) covered by DSP.

#### *7.4.2.4 Effect of S-10292 dosage*

It was shown in Section 7.4.1.7 that S-10292 had the greatest effect at relatively low flocculant dosages and moderate settling rate (~10 m $h^{-1}$). The effect of S-10292 was then re-assessed under different shear conditions while maintaining settling rates in the range 10-15 m $h^{-1}$. The conditions that gave low and moderate shear in Section 7.5.2.2 were reproduced. The flocculant (HX-300) dosage was set to 250 and 300 g $t^{-1}$ for low and moderate shear, respectively. Note that higher applied shear required more flocculant to produce comparable settling rates.

The effect of S-10292 dosage on the settling rates and supernatant solids for *in-situ* prepared DSP/hematite slurries (34.9 wt/wt% DSP) flocculated under low and moderate shear are shown in Figure 7.41a and b, respectively. The settling rates

achieved with 250 g $t^{-1}$ HX-300 for low applied shear and with 300 g $t^{-1}$ HX-300 for moderate shear remained in the range of 15 to 17 m $h^{-1}$, despite the increasing S-10292 dosages. In contrast, the effect of S-10292 dosage on supernatant solids was quite distinct under the different shear conditions.

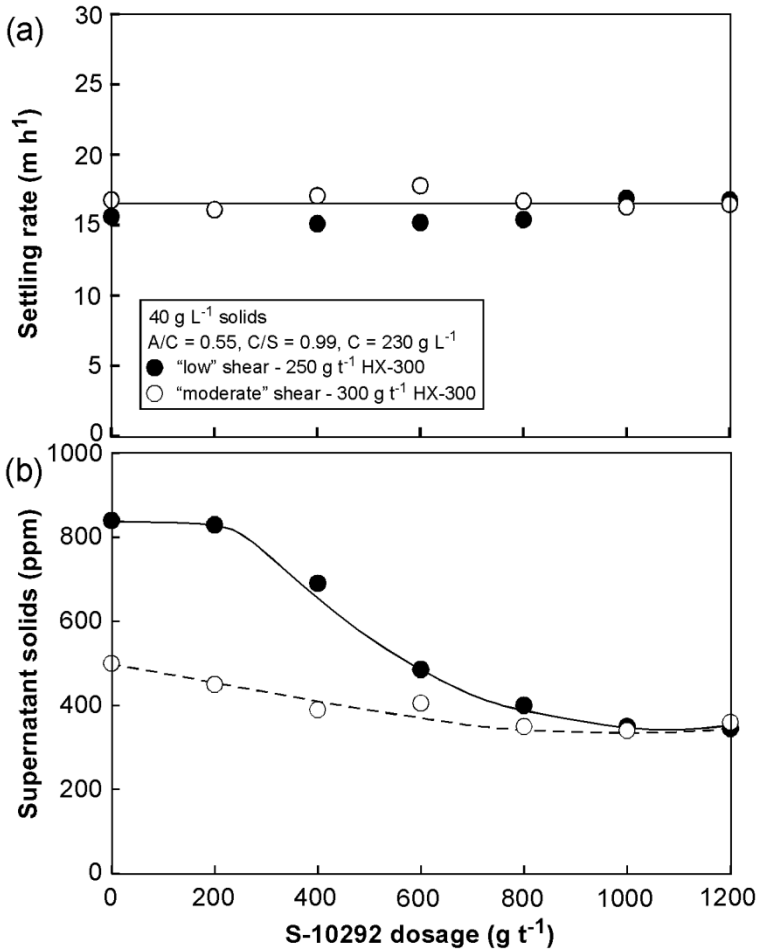


Figure 7.41. The effect of S-10292 dosage on (a) settling rate and (b) supernatant solids of *in-situ* prepared DSP/hematite slurries (34.9 wt/wt% DSP) made at high solids concentration during desilication and flocculated under low and moderate shear.

The low shear regime required relatively low flocculant dosages (250 g $t^{-1}$ HX-300) to target a decent settling rate of ~16 m $h^{-1}$. Low dosage had an adverse impact on fines capture efficiency, with high supernatant solids observed without the pre-addition of S-10292. Increasing the S-10292 dosage from 200 to 1000 g $t^{-1}$ substantially decreased the supernatant solids from 800 to 400 ppm. Under low shear, if the supernatant clarity only relied upon increasing HX-300 dosage, it would be limited to ~600 ppm (Figure 7.34a).

In direct contrast to the situation under low shear, the combination of moderate shear and higher flocculant dosage led to a decent settling rate (also in the range of 16 m $h^{-1}$) with better fines capture efficiency, even without S-10292. The effect of S-10292 was not that significant, given that the fines capture efficiency was already quite good. In fact, the supernatant solids just decreased from ~500 ppm (without S-10292) to ~400 ppm (with 1000 g $t^{-1}$ S-10292); this small difference could also be due to experimental error (see Section 5.3.2). To sum up, increasing S-10292 dosage under low shear conditions could give a remarkable effect in improving the overflow clarity to a level which can otherwise only be achieved with higher shear.

#### *7.4.2.5 Strategy for low supernatant solids*

In Bayer process solid/liquid separation circuits, primary thickener performance is measured by a balance of sedimentation rate, overflow clarity and underflow density (Section 2.4.4). From experiments under different relative shear with and without the S-10292 polymer (Section 7.5.2.2), there are different scenarios that lead to lower supernatant solids. The experimental details relevant to each scenario are summarised in Table 7.7.

Table 7.7. The relationship between number of strokes and polymer dosage with supernatant solids and settling rates of *in-situ* prepared DSP/hematite slurries (34.9 wt/wt% DSP).

| Set | Conditions | S-10292 | HX-300 | Supernatant solids* (ppm) | Settling rate* (m $h^{-1}$) |
|---|---|---|---|---|---|
| I | Dosage (g $t^{-1}$) | 0 | 400 | ~600 | ~30 |
| | No. of strokes | 0 | 5 + 2 | | |
| II | Dosage (g $t^{-1}$) | 600 | 400 | ~400 | ~30 |
| | No. of strokes | 5 | 5 + 2 | | |
| III | Dosage (g $t^{-1}$) | 0 | 400 | ~400 | ~20 |
| | No. of strokes | 0 | 5 + 5 | | |
| IV | Dosage (g $t^{-1}$) | 0 | 600 | ~400 | ~30 |
| | No. of strokes | 0 | 5 + 5 | | |

Note: (*) based on the results in Table 7.6

If a supernatant solids value of 400 ppm was set as a goal, it could be realistically achieved under low shear condition with the addition of S-10292 (Set II – Table 7.7)

or under moderate shear condition without the addition of S-10292 (Set III – Table 7.7). The consequence of increasing the applied shear to aim for lower supernatant solids is aggregate break-up and accordingly a decrease in settling rate. The settling rate of the flocculated slurry was reduced from 30 to 20 m $h^{-1}$ if five strokes were applied instead of two after the second dose of HX-300 (Set II vs. III – Table 7.7). A schematic illustration of how shear affects aggregate size and fines capture in the absence and presence of silane-containing polymer is given in Figure 7.42.

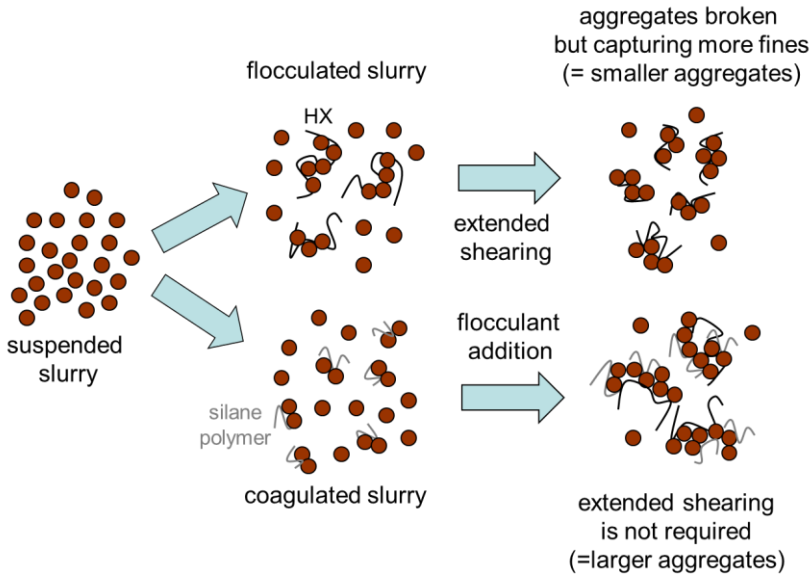


Figure 7.42. Schematic illustration of scenarios for better fines capture (i.e. lower supernatant solids).

If a high settling rate (~30 m $h^{-1}$) had to be maintained while still producing low supernatant solids (~400 ppm), the HX-300 dosage in moderate shear condition must be increased (Set III vs. IV in Table 7.7). The problem associated with increasing the dosage of high molecular weight polymers is the risk of incomplete adsorption (Section 2.4.4). In the Bayer process, primary thickener overflow is filtered prior to product precipitation and any residual flocculant in the overflow liquor exposes the risk of deteriorating filtration performance (Section 2.4.4).

A simple filtration test was therefore applied to 50 mL of supernatant liquor from Set (II) and (IV) in Table 7.7. HX-300 dosage in Set (IV) was higher than that in Set (II) but the latter involved the pre-addition of 600 g $t^{-1}$ S-10292. Previous experiments

showed that applying different relative shear in both sets resulted in comparable settling rates and supernatant solids (Section 7.5.2.2).

The measurements were replicated three times and filtration time results are shown in Figure 7.43. It is obvious that the supernatant liquor from the higher HX-300 dosage required a higher filtration time per unit volume. The average filtration time for 50 mL of supernatant liquor from 600 g $t^{-1}$ HX-300 was 22 s, whereas the same volume of supernatant liquor from 600 g $t^{-1}$ S-10292 and 400 g $t^{-1}$ HX-300 was filtered within 17.5 s.

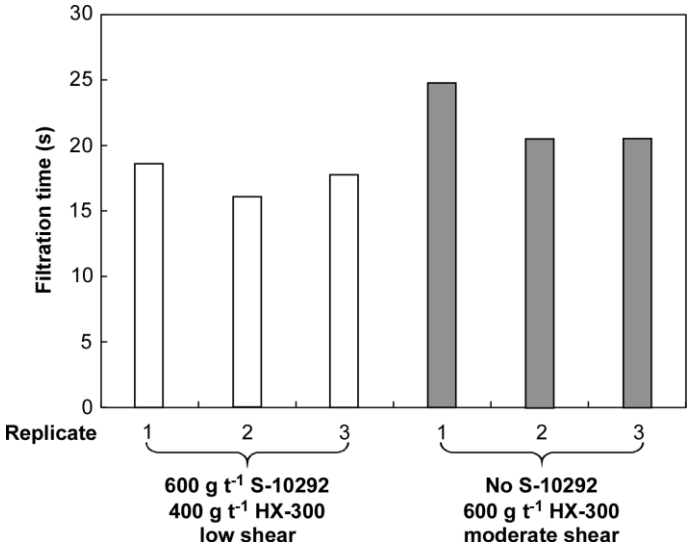


Figure 7.43. The filtration time of 50 mL of supernatant liquors derived from different HX-300 dosages and relative shear conditions with and without pre-addition of S-10292.

It has to be stressed that the pre-mixing of slurry and polymer(s) was achieved through simple plunging action. While useful, this claim still needs validation in a larger scale experiment with better controlled shear and under conditions where flocculant is injected at a concentration and velocity that are relevant to a refinery. For example, dilute flocculant provides better dispersion and higher probability of collisions (adsorption onto solid particles – Section 2.1.6). However, the concentration of HX-300 product used in this Chapter was quite high (0.05 wt/wt%) due to the constraint mentioned previously (Section 6.4.6).

### 7.4.3 High solids concentration in desilication reaction – Cytec Method

#### *7.4.3.1 What makes finer DSP?*

As discussed in Section 6.5.1.1 and 7.5.2.1, increasing the kaolin:hematite ratio in the desilication process did not generate a higher fraction of sub-micron particles at either low or high solids concentration (60 or 480 g $L^{-1}$). This creates the need to reproduce the method used by Cytec Industries (Section 7.3.1.2), to establish if their claim of increasing kaolin concentration in desilication producing sub-micron particles is correct.

A desilication reaction was performed in the bottle roller equipment with kaolin solids concentrations of either 30 or 200 g $L^{-1}$. The liquor composition used was the same as that in Davis et al. (2010a) and it is given in Table 7.8. The PSD results obtained from starting solids concentrations of 30 and 200 g $L^{-1}$ are contrasted in Figure 7.44, as well as the size distribution of kaolin feed.

When compared to the PSD of kaolin feed depicted in Figure 7.44a, the DSP made from 30 g $L^{-1}$ kaolin concentration in the desilication reaction had a narrower size distribution with reduced sub-micron and > 10 μm fractions (Figure 7.44b). However, increasing the kaolin concentration from 30 to 200 g $L^{-1}$ did increase the presence of sub-micron particles, as was previously stated by Davis et al. (2010a). This is hardly surprising since increasing kaolin concentration also increases the supersaturation of soluble silica (represented by the peak maxima of silica concentration in Figure 5.5), resulting in higher driving force for precipitation and therefore higher number of nuclei. These nuclei may start growing, depending on their growth rates and the time given some of them may be measured as fine particles. This effect was not seen when hematite was present in the desilication reactions, consistent with the premise that DSP may preferably form at the surface of hematite seeds particles.

When 200 g $L^{-1}$ kaolin was digested at a similar temperature but in a liquor composition that was different from that in Davis et al. (2010a) and used throughout this thesis (see Table 7.8), the DSP produced was larger overall and had fewer sub-micron particles (Figure 7.44c).

Table 7.8. Composition of digestion liquors used in Davis et al. (2010a) and in this thesis

| | A/C | C/S | C ($g\ L^{-1}\ Na_2CO_3$) | $SO_4^{2-}$ ($g\ L^{-1}$) | $Cl^-$ ($g\ L^{-1}$) |
|---|---|---|---|---|---|
| Davis et al. (2010a) | 0 | 0.84 | 126 | 13.5 | 0 |
| This thesis | 0.35 | 0.85 | 230 | 20 | 10 |

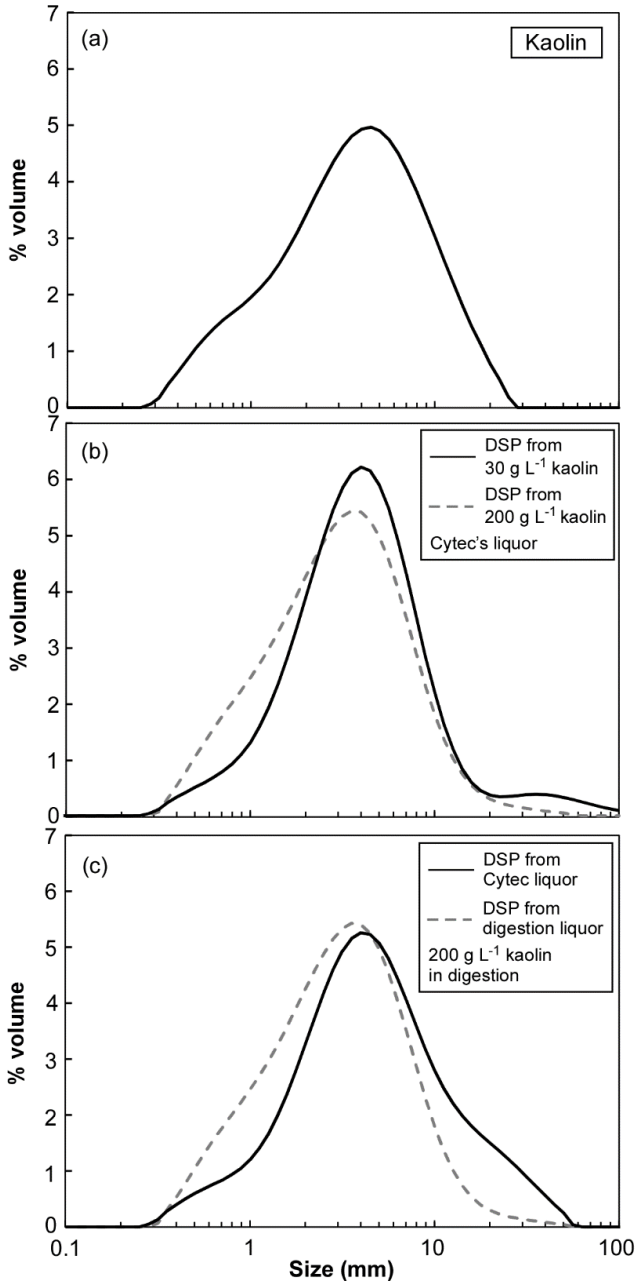


Figure 7.44. Particle size distribution of (a) kaolin feed, (b) DSP made at 30 and 200 g $L^{-1}$ with Cytec liquor and (c) DSP made at 200 g $L^{-1}$ solids concentration with different liquor used throughout this thesis. Details for liquor composition refer to Table 7.8.

It is the liquor composition that also dictated the size distribution of DSP produced. The liquor used to digest kaolin in Davis et al. (2010a) differed from that used in this thesis in terms of the alumina, caustic, carbonate, sulfate and chloride concentrations (see Table 7.8). Each of them can possibly contribute to the generation of finer DSP. However, the most notable aspect is that the alumina and caustic concentrations in their liquor did not closely represent the spent liquor used for digestion in refineries (A/C ≈ 0.3-0.4 and C ≈ 200-300 g $L^{-1}$). Further studies are then required to investigate the effect of each anion and cation, especially the aluminate and sodium, and to know which ones have a bigger effect on the size distribution.

#### *7.4.3.2 The effect of silane-containing polymer*

To be comparable with previous results (Section 7.5.2.2), the DSP made by Cytec's method at 300 g $L^{-1}$ kaolin was mixed with hematite to make a mixture with 34.9 wt/wt% DSP. While the ultimate goal was to study the effect of silane-containing polymer dosage applied on the physical mixture of hematite with DSP made from Cytec's method, the full dosage response curve must first be known to select conditions where the effect of the polymer was not masked by HX-300. Figure 7.45a highlights the change in settling rate and supernatant solids as a result of increasing HX-300 dosage on the physical hematite and DSP mixture. The settling test was performed with five strokes following S-10292/HX-300 addition, nominally the same as that referred to as moderate shear in Section 7.5.2.2.

Although DSP made by Cytec's method at 300 g $L^{-1}$ kaolin had a higher fraction of sub-micron particles (Figure 7.44c), the settling rates of the DSP/hematite physical mixtures were quite high at relatively low dosage. For example, a settling rate of 30 m $h^{-1}$ could be achieved with the addition of 300 g $t^{-1}$ HX-300. The same settling rate was produced with 600 g $t^{-1}$ HX-300 when the feed was *in-situ* prepared DSP/hematite with the same DSP content (Figure 7.33). This is not unexpected, as higher settling rates for physical mixtures were seen before (Figure 5.13).

The effect of a higher fraction of sub-micron particles was apparent in the supernatant solids measured. When the DSP was made at 300 g $L^{-1}$ by Cytec's method, the supernatant solids measured after flocculation reached a plateau level of

~500 ppm, higher than the 300-400 ppm measured for *in-situ* prepared DSP/hematite slurry flocculated under the same shear intensity (Figure 7.34b).

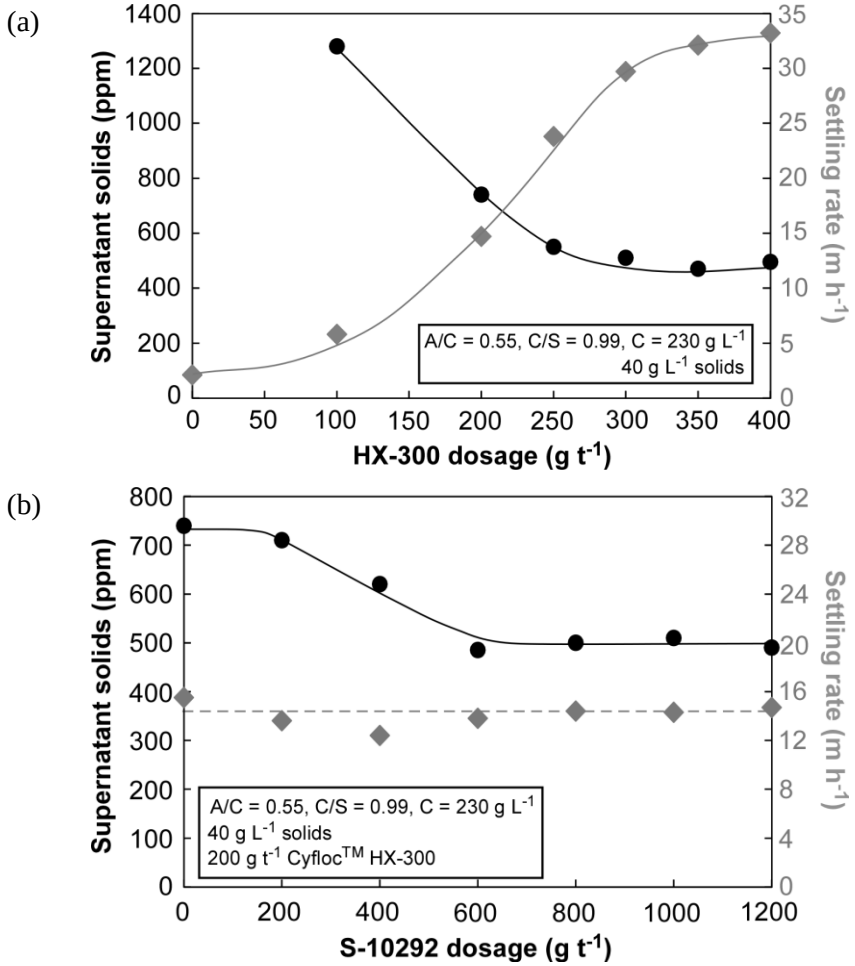


Figure 7.45. The effect of (a) HX-300 and (b) S-10292 dosages on supernatant solids and settling rate of hematite and DSP physical mixtures (34.9 wt/wt% DSP). DSP made by Cytec's method. No. of strokes following S-10292/HX-300 addition = 5.

The effect of S-10292 dosage was studied at fixed HX-300 dosage of 200 g $t^{-1}$, giving a moderately high settling rate (~15 m $h^{-1}$). At that HX-300 dosage, increasing the S-10292 dosage decreased the supernatant solids measured from ~750 to ~500 ppm without affecting the settling rate (Figure 7.45b). That ~30% improvement was achieved with 600 g $t^{-1}$ S-10292; further increasing the S-10292 dosage gave no improvement in clarity. Several other tests in this Chapter also similarly found that 600 g $t^{-1}$ S-10292 gave the biggest improvement in terms of fines capture efficiency.

## *7.5 Summary*

The effect of silane-containing polymer (represented by S-10292 from Cytec Industries) on flocculation of DSP-containing hematite slurries was studied by various methods. The effect on the settling rate was consistently minimal. A combination of S-10292 and a polyacrylate flocculant (Alclar 665) gave slightly higher settling rates but they remained unaffected if the primary flocculant was HX PAM (HX-300).

The effect of silane-containing polymer on measured supernatant solids was more significant. The extent of improvement was dependent on several factors, such as primary flocculant dosage, applied shear, primary flocculant type and liquor composition. The major advantage of silane-containing polymer was seen under low shear during flocculation or when the primary flocculant dosage was low. There are conditions where low supernatant solids could be achieved without S-10292 while maintaining the settling rate, such as applying higher shear rate and increasing primary flocculant dosage. However, increasing the primary flocculant dosage did have the potential to lower the filterability of the supernatant liquor.

The silane-containing polymer itself behaved as a coagulant that had a higher affinity for DSP than for hematite particles. This higher affinity was evident from multiple tests; cylinder settling, FBRM and XRD applied to the supernatant solids. The coagulation effect of silane-containing polymer was also confirmed by the results derived from the zeta potential measurement and FBRM. Moreover, the G400 FBRM instrument was able to confirm the benefit of silane-containing polymer in enhancing fines capture efficiency through the lower counts measured in the chord length region of 1-20 μm on flocculation.

Finally, liquor composition in digestion influenced the size distribution of DSP produced. This answered why different particle size distribution trends were seen when results from this thesis were compared to those from Davis et al. (2010a). If controlling the digestion liquor composition is possible, it may possibly be a key to improving bauxite residue dewatering characteristics.

# 8 Plant implications

The results from the systematic studies outlined in the previous chapters have revealed how the formation of DSP at the surface of iron oxide affects the interaction with polymeric flocculant and the resultant aggregate properties under different process variables. Optimised conditions for the application of silane-containing polymer have also been identified by considering a wide range of factors (e.g. the method of addition, the polymer and flocculant dosages in combination, the relative applied shear). However, such knowledge is incomplete without attempting to extrapolate the insights from laboratory tests to improved plant practice. This chapter is therefore dedicated to expressing how the findings reported in Chapters 4 to 7 may have implications for Bayer process primary thickener operation.

## *8.1 FBRM as a control sensor*

As was noted in Section 2.3, feedwell flocculation is expected to produce large aggregates to achieve the required settling rate while still providing good fines capture. In modern thickeners it is also necessary to maintain good control of underflow density, bed level, bed pressure and rake torque for steady operation. Dramatic change in any of these may burden the thickener itself and possibly subsequent unit operations. For example, too high a bed level increases the risk of undesirably high overflow solids concentrations reporting to the following processes (e.g. filtration, precipitation, solvent extraction or electrowinning).

Table 8.1 lists the different parameters measured in thickening and classifies them as inputs, controlled variables and outputs. Feedback control is normally used, where one or more process output dictates how far the underflow pumping, flocculant addition or rake height has to be adjusted to maintain the required outputs (e.g. Brougham et al. 2003; Johnson et al. 1990; Karageorgos et al. 2009). For example, more flocculant may be added to bring the settling rate closer to the targeted value.

Table 8.1. Variables measured in a thickener.

| | Input | Controlled Variable | Output |
|---|---|---|---|
| Torque | | | ✓ |
| Rake height | | ✓ | |
| Bed level | | | ✓ |
| Bed pressure | | | ✓ |
| Feed rate | ✓ | | |
| Feed density | ✓ | | |
| U/F pumping rate | | ✓ | |
| U/F density | | | ✓ |
| Settling rate | | | ✓ |
| O/F clarity | | | ✓ |
| Flocculant addition rate | | ✓ | |

Note: U/F = underflow, O/F = overflow

Sensors can be located at different points within a thickener to measure the variables in Table 8.1. The schematic illustration of different sensors used to monitor the thickener performance is given in Figure 8.1. However, measuring settling rates from feedwells is rather difficult. Devices such as the Clarometer® can be used to withdraw flocculated slurry and measure the settling rate in an isolated column (e.g. Brougham et al. 2003).

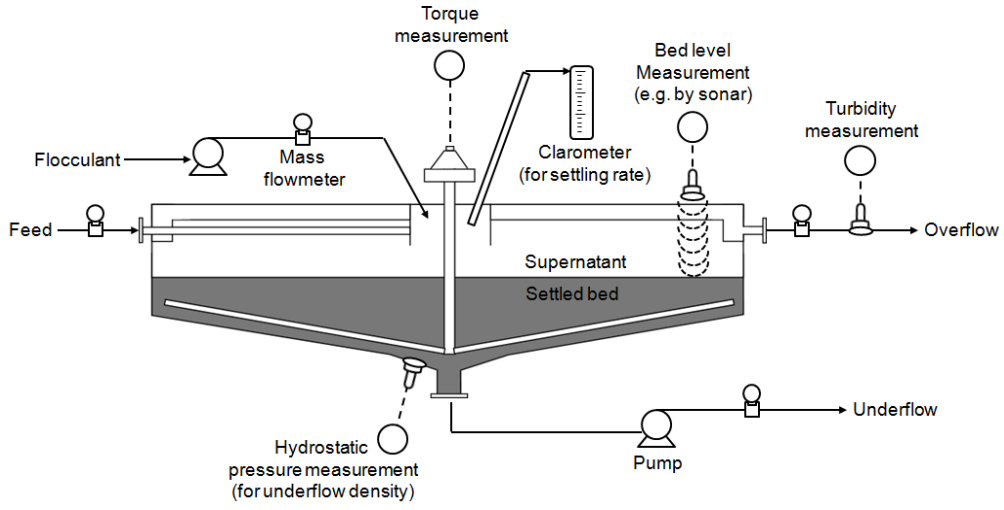


Figure 8.1. Schematic illustration of different sensors used in thickener. Adapted from Johnson et al. (1990).

A problem with such sampling is the variance in solids concentration due to the uneven and changing turbulence inside a feedwell (Brougham et al. 2003). The measured settling rate would then also fluctuate in response to the solids concentration, possibly giving non-representative feedback in the control loop. Direct measurement of the aggregate size is potentially of greater value for control of flocculation. FBRM could therefore be used to monitor aggregation *in-situ* within feedwells, giving a more representative and, perhaps even more important, a continuous real-time response to flocculation conditions.

The challenges in using FBRM as a sensor relate to the potential for scaling on the probe's window and ensuring representative presentation. In a well mixed environment, window scaling has not been an issue, even in high A/C Bayer liquors, but this may not be the case if positioned in lower shear regions within a feedwell.

When FBRM is monitoring flocculation in a stirred beaker, the probe is placed just above the impeller so that the slurry is directed towards the tip's window for representative measurements (Section 4.3). How an FBRM probe should best be located inside a feedwell for representative measurements is still an open question, one that needs to be considered for each feedwell under its specific operating conditions. It should also be noted that sampling for a Clarometer® faces the same issue, but the greater range of statistics measured by FBRM does provide more scope to identify periods of non-representative flows.

The potential for using FBRM as a sensor in thickeners is not only complicated by the issues mentioned above, but also its price and the need for operator training on the interpretation of chord length statistics. However, its robustness for monitoring both aggregation extent and fines capture, plus its flexibility for installation in different parts of feedwell, cannot be discounted.

Of possibly even greater significance is the potential to use FBRM to instead monitor feed properties in advance of the flocculation process. Given that flocculation is actually more affected by the proportion of fines than the larger particles within a feed, FBRM unweighted chord length statistics may offer more useful information

than conventional particle volume-sensitive sensors. The FBRM response to solids concentration is not linear (Heath et al. 2002), but still may provide useful information at thickener feed solids concentrations. This offers the scope for feed-forward control, with a much faster response than can ever be achieved with feedback from process outputs, and in sensitive applications (like primary thickening of bauxite residue) this may justify the costs associated with FBRM instruments.

## *8.2 Solids dilution inside the feedwell and feedwell design*

Settling tests for varying proportions of DSP in slurries with hematite and at different total solids concentrations strongly indicated that the presence of DSP increased the requirement for solids dilution prior to flocculation (Section 6.5.1.2). Poor flocculation was suffered at high solids concentrations (> 5 wt/wt%), even with excessive flocculant dosages (> 1000 g $t^{-1}$ HX-300). This emphasizes the importance of utilising any natural dilution provided by the feedwell when the bauxite residue contains significant amounts of DSP. Flocculant selection and efficient flocculation can offer incremental benefits to the solids dilution requirements, but the majority of any dilution needs to be achieved from within the feedwell or prior to it with added liquor, the latter not being favoured in primary residue thickening.

Using computational fluid dynamics, Nguyen et al. (2012) predicted that the dilution factors for feedwells at standard flows decreased in the order: open (1.87) > open with shelf (1.13) > closed (0.03). However, these numbers do not tell the full story. The strong dilution streams in the open design are a consequence of the feed stream sinking with a short feedwell residence time, the extreme example of this problem can be seen in the historical case of Worsley Alumina primary thickener (Figure 2.19 – Kahane et al. 1997), and therefore the dilution cannot be effectively utilised.

The open feedwell with shelf design is therefore the most simple and practical option for Bayer process primary thickeners. It retains solids for an appropriate residence time, provides a tapered shear regime for flocculation (high above the shelf, lower below) and is able to utilise liquor flows from below to give ~1:1 dilution of the feed (e.g. Arbuthnot and Jagger, 1999; Fawell et al. 2009b; Nguyen et al. 2006, 2012).

With regards to the last point, that the feedwell can give such dilution does not mean that it always will, and this is a problem that often contributes to the failure of laboratory tests to extend to plant performance. For natural feedwell dilution to be utilised, the flocculant then needs to be dosed sufficiently far downstream of the feed entry for solids dilution to be effective. However, at this point, aggregate growth may have progressed too far, depending on how shear is distributed inside the feedwell in addition to the flow direction and velocity. The role of shear is especially important when it is found out that the DSP decreases the aggregate strength when compared to hematite (Section 6.4.5).

In a well mixed feedwell, such as an open feedwell with shelf (Fawell et al. 2009b), if flocculant is dosed at the feed entry (or earlier within the feedpipe), then some portion of the solids dilution may take place after aggregate breakage becomes significant, reducing any benefit to flocculation. Conversely, in an under-mixed feedwell as in the case of a feedwell with less than optimum volumetric flow rate (e.g. Echeverri et al. 2012, Nguyen et al. 2006), solids will not be retained for suitable residence times even in the presence of a shelf, and therefore natural solids dilution will not be effective. The situation is even more complicated when considering the fact that HX PAM should be added in split addition (Section 6.1.5) while silane-containing polymer is preferably added prior to the HX PAM or PAA primary flocculant (Section 7.4.1.6).

Fitch feedwells (e.g. Fitch and Lutz 1960, Foster et al. 1999), still well known for bauxite residue flocculation, present an interesting variation on open feedwell designs. The twin opposed feeds at different levels that enter through the races formed by three (sometimes four) shelves allows high throughputs and fairly symmetrical discharge. However, fluid dynamics modelling for such feedwells has shown their flows to be highly unstable, with the zone between the races intended for flocculant sparging actually giving quite variable shear. Effective utilisation of flocculant is therefore hard to achieve within a Fitch feedwell, although HX PAM flocculants may better cope with this variability than PAA products (Section 7.3.4).

## *8.3 Flocculant selection for DSP-containing residue*

Statistical analysis also showed that HX PAM gave smaller standard deviations in settling rate and supernatant solids relative to PAA (Section 7.4.2). PAA solutions are known to have higher viscosity than HX PAM solutions when both were diluted with the same liquor to same concentration (0.02-0.5 wt/wt%), even when PAA is supplied in an emulsion form (Kirwan 2009a). Higher flocculant solution viscosity can cause non-uniform distribution through a slurry. On the other hand, although the conventional cylinder settling tests were performed by the same operator with the number of strokes kept constant, the magnitude of applied shear cannot be exactly the same from one experiment to another. The combination of non-uniform flocculant distribution and slight shear variation between experiments may then lead to differences in adsorption and aggregation. This may in part explain why cylinder settling tests with PAA undesirably suffered from a high degree of variability.

A lower degree of variability in output variables (Table 8.1), including settling rates, is sought in thickeners because it provides more stable performance. The previous section gave a good example of how fluctuation in settling rates may exacerbate the instability of feedback control loop. Thus, regarding to their application in Bayer process primary thickening, combining HX PAM and PAA flocculants may be cost effective and give the best features of both products (Section 2.4.4). The actual optimum ratio of HX PAM to PAA will likely be influenced by the residue's DSP content and the consistency of the settling rate, overflow clarity and underflow density produced.

Use of the silane-containing polymer S-10292 in conjunction with a flocculant is proposed for enhanced flocculation of DSP containing bauxite residue. The results summarised in Chapter 7 clarified the role of S-10292 as a coagulant that is best dosed prior to the primary flocculant (PAA or HX PAM). Addition of S-10292 must therefore be done either in the feedpipe or soon after slurry is fed into the feedwell, although the latter would only be practical when the primary flocculant is dosed well downstream of the feed inlet.

The main benefit observed from pre-dosing with the silane-containing polymer was improved fines capture, i.e. reduced solids in supernatant liquors from cylinder settling tests, usually taken as representing the potential for better overflow clarity from thickening. However, the flocculation results in Sections 2.4.4 and 7.5.2.2 suggest that higher shear after dosing with a flocculant alone can, to some extent, also give similar effects on supernatant solids.

Ideally, the applied shear during flocculation must be sufficient to provide collisions that give optimum aggregate size and fines capture while avoiding excessive breakage that will release fines to the overflow (Section 2.1.3). Depending on the feedwell design and operational conditions, often the shear rates generated inside a feedwell are too high (e.g. Echeverri et al. 2012, Triglavcanin 2008), giving extra collisions to incorporate fines, but with the trade-off of a smaller average aggregate size due to breakage or (often more likely) a higher flocculant dosage being applied to compensate for such breakage. Under such conditions, the benefit of pre-dosing with the silane-containing polymer may be minimal, as fines capture in its absence may already be as good as can be achieved due to the extra collisions occurring in the system.

When the shear inside a feedwell is too low (i.e. the volumetric flow of the feed is lower than ideal for the feedwell's diameter or the linear velocity of the incoming stream is too low to promote good swirling flow – Nguyen et al. 2006), then the average aggregate size formed on flocculation may be larger, however, this is likely to reflect local over-dosing and there will also be a higher population of particles left unflocculated through poor contact with the flocculant. It is under these conditions where the silane-containing polymer will give optimum benefit, by aggregating fines at an early stage. In this case, the subsequently added flocculant only needs to attach to these small aggregates, not to every particle in the system (Section 2.1.6). A description of a feedwell under conditions that produces a low shear rate can be found in the discussion on open feedwells (Section 2.3.3).

The above discussion considers two extremes for feedwell flocculation, in reality most operating feedwells will lie somewhere in between, although not in a fixed position but varying depending on volumetric flows and, to some extent, solids

concentration. It is also important to recognise the broadness of the shear rate distribution within feedwells – even a feedwell considered well mixed is likely to have regions of low shear (Echeverri et al. 2012, Nguyen et al. 2012, Probst 1999). It is therefore not surprising that reagents such as the silane-containing polymer can exhibit good performance in laboratory testing that is in some instances not reproduced in full-scale operation. This may not be due to any failure of the reagent, but rather a reflection of a feedwell shear regime that masks or prevents any benefit from being observed in final performance measures.

# 9 Conclusions

The presence of DSP during Bayer process primary thickening of bauxite residue has been identified as problematic for flocculation for at least two decades. However, the advancement of residue flocculation studies involving DSP over that time has been limited. Most of the work using DSP-containing slurry focused on finding or developing flocculants that can improve the post-aggregation conditions, such as increasing settling rate and/or decreasing supernatant solids. Understanding the impacts of DSP on the resultant aggregate characteristics (e.g. size, density) was never the main focus of such studies, nor were the effects of the main operational parameters affecting the flocculation process (e.g. shear, solids concentration, solution composition).

This study therefore sought fundamental understanding of the impacts of DSP formation on flocculant adsorption and on the characteristics of aggregate subsequently formed, considering different conditions that may be encountered during primary bauxite residue thickening at Bayer refineries. Hematite was used as a model phase to represent bauxite residue, while various protocols for DSP synthesis were employed to help elucidate how the physical state of the DSP formed may affect the subsequent flocculation process.

It was recognised that a limitation of almost all previous flocculation studies in the area was the limited range of conditions considered, in particular the critical aspects of applied shear and solids concentration. A more systematic approach has been taken in this study, seeking detailed quantification of how the main commercially-available flocculants (individually and in combination) respond over a range of conditions. In addition, clarification was sought as to the mode of action of a new generation silane-containing polymer (S-10292, Cytec Industries) specifically developed to enhance the flocculation of DSP-containing bauxite residue.

It is important to highlight that aggregate characterisation is complicated by the fragile nature of the structures formed. While conventional cylinder testing provides valuable indirect information on the aggregation process, FBRM offers the ability to

directly measure large aggregates *in-situ* and at solids concentrations of relevance to full-scale operation. Chord length distributions are obtained in real time and are updated every few seconds, allowing the kinetics of the flocculation process to be monitored. The new generation G-series FBRM became available during this study, with enhanced sensitivity to lower chord lengths (1-10 μm). This proved important, giving crucial supporting evidence of the improved fines capture efficiency from addition of the silane-containing polymer.

## *9.1 FBRM for studying flocculation*

While this study only sought to use FBRM as a tool to study flocculation of the specific substrate systems of interest, the fortuitous access to the G400 instrument soon after its commercial release meant that this was the first application of the G-series FBRM in the field of flocculation. The refinements made with the G-series were aimed at addressing issues with FBRM use for general particle characterisation in relation to the discrimination of fines and providing a more linear response to variations in solids concentration. However, this study produced the first evidence that the refinements made to the measurement principle in the G-series may have unintentionally enhanced the power of the FBRM for monitoring and characterising flocculation. This was demonstrated in a synthetic bauxite residue system, but the observations and insights should be applicable to flocculation for any system in which the particles (or coagulated particles) are mostly > 1 μm in size.

The key for better sensitivity in chord length measurements is how the FBRM backscattered intensity is treated differently in the G-series instrument, with the threshold intensity for measured intensity effectively reduced to zero, as explained in Figure 2.27. In some cases, the measured mean square-weighted chord lengths for flocculated aggregates exceeded 1 mm, more than double that seen with the older generation M-series instruments (M500), indicating that the lower reflection threshold for the G400 instrument was more likely to detect a low density, open aggregate structure as a single chord. The G400 measurements were also confirmed by *in-situ* imaging to be more representative of the actual aggregate size.

The G400 probe was used to study the flocculation of a model hematite phase in synthetic Bayer liquor for the following process variables: flocculant dosage, stirring rate and solids concentration. Excessive flocculant dosages initially led to bimodal character in the unweighted chord length distributions, an indication of local overdosing that leaves a high fraction of unflocculated fines. Increasing the stirring rate helped the incorporation of those fines into the relatively larger aggregates by raising the collision rate and promoting bridging. However, the aggregate size achieved diminished as the trade-off from increasing the applied shear.

With respect to the solids concentration, increases up to the optimum range (4-6 wt/wt%) resulted in larger aggregate sizes. On the other hand, higher viscosity as a result of increasing solids concentration also increased the aggregate breakage rate. A solids concentration of 2 wt/wt% provided more sensitive responses to the change in process variables, and was therefore chosen to study the effect of different polymers used to improve aggregation.

It is important to note that the increased ability of the G400 FBRM probe to give distinctly bimodal unweighted chord length distributions, clearly discriminating between fines/coagulated fines and flocculated aggregates, represents a major advantage over older FBRM instruments, for which bimodal character was rarely more than a shoulder seen on the main peak. This capability provided by the G400 probe is valuable for most flocculation studies, but is absolutely essential towards the detailed study of bauxite residue flocculants applied under primary thickener conditions. It enabled insights to be gained into the action of silane-containing polymer in promoting fines capture that would otherwise have not been possible.

## *9.2 DSP formation at the surface of iron oxide*

Before this study, it was not known whether or not DSP was formed at the surface of iron oxides that make up most of the bauxite residue solids. Understanding of that particular aspect was considered critical, given that partial or complete coverage of the iron oxide surface by DSP may reduce the fraction of active sites available for flocculant adsorption, depending on the affinity of the flocculant for DSP. On the other hand, the formation of DSP particles as a distinct phase would lead to a greater

increase in the effective solids volume fraction, and certainly the total surface area exposed to any flocculant. Both pathways will decrease the extent and efficiency of flocculation, but for different reasons.

By contrasting the settling properties of slurries where DSP was either made *in-situ* (in the presence of hematite) or added to the hematite slurry as a distinct phase, it was found that the latter behaved more like a pure hematite slurry while the former (*in-situ* prepared DSP/hematite) was more poorly flocculated. Zeta potential measurements on the *in-situ* prepared DSP/hematite and DSP suspensions were similar, with their iep (or the pH where zeta potential equals to 0) measured at pH ≈ 8. This characteristic implied that DSP probably covers the surface of hematite and changes its physicochemical properties.

Desilication experiments also proved that hematite seed particles could host DSP nuclei and promote the DSP precipitation rate. To understand the surface behaviour towards imaging by electron microscopy, a natural hematite rock was cut to give a flat surface and mounted in a high temperature resistant resin, with 4 $cm^2$ then exposed to the desilication environment. The images obtained by electron microscopy confirmed a thin layer of DSP was formed, completely covering the surface. In a real desilication process, the total exposed surface area presented to the liquor by an equivalent particle suspension is very much higher than 4 $cm^2$. Hence, it cannot be simply concluded that every hematite particle will be completely covered by DSP.

Whether or not there is a distinct DSP phase in the real desilication process also remained questionable. This study was not designed to be able to isolate one DSP-containing particle and did depth profiling with conventional electron beam method such as SEM. However, that both unseeded and (hematite) seeded DSP precipitation experiments produced particles with similar top size (≤ 30 μm) could be a hint of distinct DSP that was formed in both conditions. In other words, we cannot rule out the possibility of distinct DSP formed in seeded precipitation, such as the real desilication process. What cannot be questioned is that there will be some fraction of the hematite solids which is at least partially covered by DSP. This affects the aggregate characteristics, as is discussed in the following section.

## *9.3 The flocculation of in-situ prepared DSP/hematite slurry*

Slurry stability and the reproducibility of flocculant handling are both important factors that must be well understood prior to any flocculation study. While different synthesis batches of DSP did not contribute significant sample variance, the hematite slurries did age over time, even without DSP present. This may be due to a gradual natural aggregation process within the synthetic liquor. An elevated stirring rate during stock slurry preparation resolved this issue, giving a stable starting size distribution throughout the flocculation tests.

The activity of the flocculant used could be more sensitive than the slurry itself, depending on the polymer functionality and the physical form of the supplied flocculant product. HX PAM flocculants were supplied as emulsions that had to be inverted to 1 wt/wt% solutions before dosing at much lower concentrations (0.025-0.1 wt/wt%). The dilution liquor used affected the flocculant activity. Dilution with synthetic Bayer liquor containing sodium aluminate led to a rapid deterioration in flocculant activity. The use of 0.5 M NaOH solutions for dilution was found to be the best option.

The 1 wt/wt% HX PAM solutions were also susceptible to air degradation over time, presumably from reaction between one of the HX PAM functionalities with oxygen. As a consequence, fresh batches of 1 wt/wt% HX PAM solutions must be regularly prepared.

In the case of PAA flocculant, it was supplied in the powder form that must be initially dissolved in deionised water to give 0.5 wt/wt% solutions, using a small amount of ethanol as an initial wetting agent. The 0.5 wt/wt% solutions were further diluted to 0.025-0.05 wt/wt% solutions prior to dosing. Unlike with HX PAM, the dilution liquor did not affect the activity of 0.025-0.05 wt/wt% flocculant solutions. The 0.5 wt/wt% solutions also did not suffer from air degradation over time. Such knowledge on flocculant handling was critical for comparing the performance of two or more flocculants as discussed below.

Despite the fact that the presence of DSP actually increasing the proportion of larger particles, increasing DSP content in *in-situ* prepared DSP/hematite slurries was detrimental to the resultant settling rates, supernatant solids and bed height after flocculation. Interestingly, flocculation with HX PAM was more resistant than PAA to increases in DSP content. At a fixed HX PAM dosage, settling rates decreased almost linearly with increasing DSP content. In contrast, with PAA the settling rates decreased sharply with the introduction of DSP and reached a low plateau at higher DSP contents. The aggregate size response as measured by FBRM gave remarkably similar trends.

The flocculation of *in-situ* prepared DSP/hematite slurries with high DSP content was very sensitive to solids concentration, with dilution from 7 to 3 wt/wt% greatly improving settling rates at a fixed flocculant dosage. The benefit from solids dilution prior to flocculation was still evident but less pronounced in the case of pure hematite slurries. A feedwell that provides a significant degree of natural solids dilution is often desirable in the flocculation of bauxite residue, but is likely to be a major requirement when DSP is present.

The fear that DSP formation at the hematite surface may inhibit flocculant adsorption was proved to be unfounded. In fact, adsorption isotherms determined from solution depletion measurements on the pure phases indicated the extent of PAA flocculant adsorbed per unit mass of DSP was higher than per unit mass of hematite. The nature of DSP as a zeolite-type material leads to a high porosity. However, there was no evidence supporting flocculant being adsorbed within the pores, as the average pore size was actually smaller than the flocculant's expected solution dimensions.

The primary reason for low settling rates in *in-situ* prepared DSP/hematite slurries with high DSP content can be attributed to limitations on the aggregate size attainable. The flocculated aggregate sizes reported by FBRM were consistently smaller for DSP-containing slurries when compared to those of pure hematite under the same flocculant dosage or shear regime. However, when the post-flocculated aggregates were sampled and the settling rates of free settling individual aggregates measured as a function of size using the FDA, it seemed that the effective aggregate densities were not affected by the presence of DSP.

Larger DSP-containing particles are therefore assumed to replace smaller hematite particles in the same aggregate structure, with the larger size of the former possibly compensating for its lower specific gravity in maintaining the effective density of the aggregates formed. It is almost impossible to know whether such DSP-containing particles were distinct DSP or DSP-coated hematite as there was no proof that DSP completely coated every hematite particle.

Substantially increasing flocculant dosages applied to *in-situ* prepared DSP/hematite slurries with high DSP content could, to some extent, achieve aggregate sizes comparable to those readily achieved from hematite slurries. It was therefore clear that DSP-containing aggregates displayed a lower degree of aggregate strength, with extra flocculant crucially required to achieve or preserve aggregate sizes under the identical shear regime.

If a reasonably high settling rate accompanied by low flocculant dosage is set as the operational requirement in primary thickening of bauxite residue, then a feedwell that provides a moderate shear regime will be preferable for feeds with a high DSP content. However, it may come at the price of poor fines capture, as lower shear conditions at quite short feedwell residence times may not provide the collisions required for effective incorporation of the fines into larger aggregates. This is an important consideration in regards to the use of silane-containing polymer.

## *9.4 The role of silane-containing polymer*

Understanding the role of dosing silane-containing polymer prior to primary flocculant in improving the flocculation of DSP-containing slurry is complicated by the distinct and sometimes conflicting trends seen under different experimental conditions (see Table 7.1 and Figure 7.1). By closely controlling the DSP synthesis process, differences in the physicochemical properties of the feeds can be minimised.

As a consequence, the repeatability of settling tests conducted in this study for silane-containing pre-dosing was quite good with PAA as the flocculant and even better with HX PAM. The improvement given by silane-containing polymer was

higher than the standard deviation in the baseline conditions (without pre-dosing), underlining that the beneficial effect of silane-containing polymer use is real.

While the improvement in fines capture was significant, the pre-addition of silane-containing polymer to DSP/hematite slurry then treated with PAA or HX PAM flocculants gave little, if any, improvement in settling rates. Taking into account that silane-containing polymer did not itself flocculate DSP/hematite slurries when added alone (without flocculant co-dosing), it was apparent that the silane-containing polymer acted as a coagulant that enhanced flocculation by providing pre-aggregation of fines.

Analysis of supernatant solids recovered from settling tests disclosed a key difference between the behaviours of silane-containing polymer and the primary flocculant, represented by HX PAM. The silane-containing polymer had a higher affinity than the flocculant to DSP surfaces. This was evident from contrasting the XRD patterns of supernatant solids collected after the flocculation of *in-situ* prepared DSP/hematite slurries with the same primary flocculant dosage, with and without the pre-addition of silane-containing polymer. Meanwhile, primary flocculant alone at least initially preferentially aggregated hematite particles.

Increasing primary flocculant dosages then captured the DSP-coated hematite particles or lightly aggregated DSP. Excessive amounts of primary flocculant were required to fully flocculate such particles in the 1-10 μm size region. Statistical analysis has previously shown that prohibitively high dosages of high molecular weight polymers are required to ensure sufficient polymer is adsorbed onto fine particles to give efficient bridging aggregation (Section 2.1).

The magnitude of clarity improvement resulting from the pre-addition of silane-containing polymer was influenced by two main factors: the primary flocculant dosage that is then added and the shear applied during flocculation. Increasing the primary flocculant dosage improved both settling rates and supernatant clarities of the flocculated DSP/hematite slurry, even without the addition of silane-containing polymer. Increasing the relative shear, achieved by applying extra strokes in cylinder tests, improved supernatant clarities while adversely affecting the corresponding

settling rates. In other words, increasing primary flocculant dosages could emulate the effect given by silane-containing polymer without decreasing the settling rates. However, the filtration rates of supernatant suspensions were found to be slower when flocculant was applied at such high dosages. This was almost certainly due to residual (unadsorbed) flocculant in the liquor. In contrast, complete adsorption of silane-containing polymer by DSP was still achieved at 10000 g $t^{-1}$, whereas its operational dosages hardly exceeded 600 g $t^{-1}$. This high affinity of silane-containing polymer for DSP minimises any prospect of unadsorbed polymer being discharged and potentially affecting downstream processes, while at the same time reducing the subsequently required dosages of primary flocculant, which is known to have a greater risk of being discharged to the overflow.

## *9.5 Further work*

This study has produced some results with practical implications that deserve further attention. Some of the conclusions need validation at larger scales. For example, utilisation of high flocculant dosages under more tightly controlled shear conditions (such as within a turbulent pipe flow reactor) would help clarify if there is still a significant fraction of unadsorbed flocculant left after flocculation. Such experiments could readily be done under high and low shear for different residence times, and the results could then more easily be correlated to full-scale feedwell conditions.

In terms of the flocculation of the *in-situ* prepared DSP/hematite slurry, while knowledge about aggregate characteristics and the fines capture mechanism has advanced to a level that gives new insights, consolidation aspects were very lightly considered in this study. Further studies are therefore required to investigate the rheology of the settled slurries. This may provide extra information towards producing higher underflow densities in primary thickening, which can be expected to be lower for high DSP feeds.

Characterisation of the properties of silane-containing polymer is also required. A measurement of the polymer solution dimension will help to estimate its size (radius of gyration). This information is vital, since the pores within the DSP phase may act as an adsorbent for the silane-containing polymer if the polymer's solution

dimensions are smaller than the average pore size. An implication of such losses within pores would be a decrease in the effective concentration of silane-containing polymer available for coagulation. Manipulating the intrinsic properties of silane-containing polymer (e.g. molecular weight, molecular structure, functionalities) may therefore decrease its required dosages (which were quite high with the present product, S-10292), whilst magnifying its impact.

Further in-depth studies focusing on the pre-desilication conditions are also considered important. The desilication (precipitation) experiments done in different liquor compositions led to DSP with different size characteristics. Therefore, adjusting the pre-desilication conditions can potentially control the size distribution of the precipitated DSP. However, the above-mentioned desilication experiments were carried out in the absence of hematite, as the main objective was to reproduce and confirm the result from other researchers. Thus, the effect of hematite seed particles on the size distribution of DSP-containing solids produced in various liquors is still not known, nor is the effect of each anion/cation in the liquor. Study into the effect of these factors is then a priority when focusing on desilication conditions.

# References


Addai-Mensah, J., A.R. Gerson, R. Jones, and M. Zbik. 2001. "Reduction of sodium aluminosilicate scale in Bayer plant heat exchangers." *Light Metals*: 13-18.

Alfano, J.C., P.W. Carter, and A. Gerli. 1998. "Characterization of the flocculation dynamics in a papermaking system by non-imaging reflectance scanning laser microscopy (SLM)." *Nordic Pulp and Paper Research Journal* 13 (2): 159-165.

Allison, J.D., J.W. Wimberly, and T.L. Ely. 1987. "Automated and manual methods for the determination of polyacrylamide and other anionic polymers." *SPE Reservoir Engineering* 2 (2): 184-188.

Andermann, L.J., Jr., and G.J. Pollet. 2003. "The manufacture of tricalcium aluminate." *Light Metals*: 11-17.

Arbuthnot, I., and N. Jagger. 1999. "Advances in thickener technology" In *Mineral Processing and Hydrometallurgy Plant Design,*edited by N. Jackson, G. Dunlop and P. Cameron, Perth, Australia: Australian Mineral Foundation. 149-168.

Arbuthnot, I.M., and N.D. Jagger. 1992. "Economics of the treatment of gold plant tailings in high rate thickeners." *Minerals & Metallurgical Processing* 9 (2): 80-84.

Arslan, S., G.K. Demir, B. Celikel, M. Baygul, and C.E. Suarez. 2012. "ETI Aluminum red mud characterization and processing." *Light Metals*: 81-85.

Authier-Martin, M., G. Forte, S. Ostap, and J. See. 2001. "The mineralogy of bauxite for producing smelter-grade alumina." *Journal of Metals* 53 (12): 36-40.

Avotins, P.V., L.L. Laviolette, E.F. Repetto, and A.M. Eli. 1999. "The effect of flocculant on thickener scaling." In *The 5th International Alumina Quality Workshop (AQW)*, Bunbury, Australia: AQW Inc. 448-455.

Ayyala, S., R.J. Pugh, and E.J. Forssberg. 1993. "Aggregate characteristics in coagulation and flocculation." *Mineral Processing and Extractive Metallurgy Review* 12 (2-4): 165-184.

Azevedo, E., L.H. Laviolette, and E. Repetto. 1995. "Evaluation of new technology flocculant in Alumar." *Light Metals*: 89-94.

Bagatto, P.F., B.P. Dancose, P.C. Harrington, G.M. Jean, and M.A. Lepage. 1992. Process for decantation of suspensions. US Patent 5080803 A.

Ballentine, F., M.E. Lewellyn, and S.A. Moffatt. 2011. "Red mud flocculants used in the Bayer process." *Light Metals*: 107-112.

Baran, A.A., N.S. Mitina, and A.A. Baichenko. 1983. "Adsorption of water-soluble polymers and its effect on flocculation of muds from coal beneficiation." *Khimiya i Tekhnoliya Vody* 5 (3): 215-19.

Bárány, S., R. Meszaros, L. Marcinova, and J. Skvarla. 2011. "Effect of polyelectrolyte mixtures on the electrokinetic potential and kinetics of flocculation of clay mineral particles." *Colloids and Surfaces A: Physicochemical and Engineering Aspects* 383 (1–3): 48-55.

Barham, S.L., S.U. Khan, J.T. Malito, and W.J. Rennick. 2000. "Optimization of tricalcium aluminate for enhanced Bayer liquor filtration." *Light Metals*: 111-116.

Barnes, M.C., J. Addai-Mensah, and A.R. Gerson. 1999a. "The solubility of sodalite and cancrinite in synthetic spent Bayer liquor." *Colloids and Surfaces A: Physicochemical and Engineering Aspects* 157 (1–3): 101-116.

Barnes, M.C., J. Addai-Mensah, and A.R. Gerson. 1999b. "A methodology for quantifying sodalite and cancrinite phase mixtures and the kinetics of the sodalite to cancrinite phase transformation." *Microporous and Mesoporous Materials* 31 (3): 303-319.

Barrett, E.P., L.G. Joyner, and P.P. Halenda. 1951. "The Determination of Pore Volume and Area Distributions in Porous Substances. I. Computations from Nitrogen Isotherms." *Journal of the American Chemical Society* 73 (1): 373-380.

Basu, P. 1983. "Reactions of iron minerals in sodium aluminate solutions." *Light Metals*: 83-97.

Basu, P., G.A. Nitowski, and P.J. The. 1986. "Chemical interactions of iron minerals during Bayer digest and clarification" In *Iron Control in Hydrometallurgy*,edited by J.E. Dutrizac and A.J. Monhemius, Toronto, Canada: Ellis Horwood Limited. 223-244.

Benn, F.A. 2013. "Internal Report - The CSIRO Floc Density Analyser: Principles and Procedures for Operation for Model FDA-96 with Digital Software", Perth, Australia: CSIRO.

Blanco, A., E. Fuente, C. Negro, and J. Tijero. 2002. "Flocculation monitoring: focused beam reflectance measurement as a measurement tool." *Canadian Journal of Chemical Engineering* 80 (4): 734-740.

Bott, R., T. Langeloh, and J. Hahn. 2008. "Advanced filtration methods for pregnant liquor purification." *Light Metals*: 39-43.

Bremmell, K.E., and P.J. Scales. 2004. "Adhesive forces between adsorbed anionic polyelectrolyte layers in high ionic strength solutions." *Colloids and Surfaces A: Physicochemical and Engineering Aspects* 247 (1-3): 19-25.

Bronswijk, W.v., L.J. Kirwan, and P.D. Fawell. 2006. "In situ adsorption densities of polyacrylates on hematite nano-particle films as determined by ATR-FTIR spectroscopy." *Vibrational Spectroscopy* 41 (2): 176-181.

Brougham, R., A.M. Supomo, and M. Simanjuntak. 2003. "Process control and flocculant optimisation of tailings thickeners at PT Freeport Indonesia." In *The 8th Mill Operators' Conference*, Townsville, Australia: AusIMM. 245-249.

Brunauer, S., P.H. Emmett, and E. Teller. 1938. "Adsorption of Gases in Multimolecular Layers." *Journal of the American Chemical Society* 60 (2): 309-319.

BS. 1963. *Doc. No. 3406 Part 2 - Liquid sedimentation methods*. British Standard.

Bublik, E.P., C. Happs, G. Odor, L. Revesz, and Z. Sartowski. 1986. "The Use of Synthetic Polymers in Alumina Production" In *The 5th Yugoslav International Symposium on Aluminium*,edited by A. Paulin and A. Smolej, Ljublana, Slovenia: University of Ljubljana. 505-517.

Buscall, R., and L.R. White. 1987. "The consolidation of concentrated suspensions. Part 1. The theory of sedimentation." *Journal of the Chemical Society, Faraday Transactions 1: Physical Chemistry in Condensed Phases* 83 (3): 873-891.

Buscall, R., and L.R. White. 1988. "Reply to comment on "The continuous-flow gravity thickener: steady-state behavior"." *AIChE Journal* 34 (11): 1933-1934.

Bushell, G.C., Y.D. Yan, D. Woodfield, J. Raper, and R. Amal. 2002. "On techniques for the measurement of the mass fractal dimension of aggregates." *Advances in Colloid and Interface Science* 95 (1): 1-50.

Bustos, M.C., F. Concha, R. Burger, and E.M. Tory. 1999. *Sedimentation and Thickening. Phenomenological Foundation and Mathematical Theory, Mathematical Modelling: Theory and Application*. Netherlands: Kluwer Academic Publishers.

Caron-Charles, M., and J.P. Gozlan. 1996. "Improvement of the floc resistance to a centrifugal shear field by polymer adjunction." *Chemical Engineering Science* 51 (20): 4649-4659.

Chakraborti, R.K., K.H. Gardner, J.F. Atkinson, and J.E. Van Benschoten. 2003. "Changes in fractal dimension during aggregation." *Water Research* 37 (4): 873-883.

Chandler, J.L. 1976. "Advances in the use of synthetic flocculants." *Light Metals* 2: 163-171.

Chandler, J.L. 1986. *Thickening, Advances in Solid-Liquid Separation*. Columbus, USA: Battelle Press.

Chen, H.T., S.A. Ravishankar, and R.S. Farinato. 2003. "Rational polymer design for solid–liquid separations in mineral processing applications." *International Journal of Mineral Processing* 72 (1–4): 75-86.

Chen, W., R.R. Fischer, and J.C. Berg. 1990. "Simulation of particle size distribution in an aggregation-breakup process." *Chemical Engineering Science* 45 (9): 3003-3006.

Chung, C.-B., S.-H. Park, I.-S. Han, Y.-H. Seo, and B.-T. Yang. 1998. "Modeling of ABS latex coagulation processes." *AIChE Journal* 44 (6): 1256-1265.

Chvedov, D., S. Ostap, and T. Le. 2001. "Surface properties of red mud particles from potentiometric titration." *Colloids and Surfaces A: Physicochemical and Engineering Aspects* 182 (1–3): 131-141.

Connelly, L.J., D.O. Owen, and P.F. Richardson. 1986. "Synthetic flocculant technology in the Bayer process." *Light Metals*: 61-68.

Costine, A., D. Lester, P. Fawell, and A. Chryss. 2014. "Shear isn't mixing: how to build larger aggregates using chaotic advection for accelerated dewatering " In *Paste 2014,*edited by D. Van Zyl, R.J. Jewell and A.B. Fourie, Vancouver, Canada: Australian Centre of Geomechanics. (in CD form).

Cousineau, P.G., and G.D. Fulford. 1987. "Aspects of the desilication of Bayer liquors." *Light Metals*: 11-17.

Cresswell, P.J. 1983. "Factors affecting desilication of Bayer process liquors." In *Chemeca 84* Melbourne, Australia: Institution of Engineers, Australia. 285-292.

Croker, D., M. Loan, and B.K. Hodnett. 2008. "Desilication reactions at digestion conditions: an in situ X-ray diffraction study." *Crystal Growth & Design* 8 (12): 4499-4505.

Crummett, W.B., and R.A. Hummel. 1963. "The determination of traces of polyacrylamides in water." *Journal of American Water Works Association* 55 (2): 209-219.

Curtis, A.S.G., and L.M. Hocking. 1970. "Collision efficiency of equal spherical particles in a shear flow. Influence of London-Van der Waals forces." *Transactions of the Faraday Society* 66 (Pt. 6): 1381-1390.

Cytec. 2011. "Technology note: Preparation of CYFLOC™ HX flocculants." Cytec Industries.

Dahlstrom, D.A., R.C. Bennett, R.C. Emmett, P. Harriott, T. Laros, W. Leung, C. McCleary et al. 1998. "Liquid-solid operations and equipment." In *Perry's*

*Chemical Engineers' Handbook, Eighth Edition*, eds D.W. Green and R.H. Perry, 18(1)-18(134). New York: McGraw-Hill.

Dai, Q., D.P. Spitzer, H.I. Heitner, and H.L.T. Chen. 2008. Use of silicon-containing polymers to improve red mud flocculation in the bayer process. US Patent 20080257827 A1.

Dai, Q., M.J. Davis, and R. Zhang. 2010. "New flocculants for improved processing of high silica bauxites." *Travaux* 25 (39): 200-204.

Danko, M., P. Hrdlovič, E. Borsig, 2003. "Characterization of interpenetrating polymer-like network based on polyethylene/poly(styrene-co-butylmethacrylate) (PE/P(S-co-BMA)) by non-radiative energy transfer." *Journal of Photochemistry and Photobiology* 154: 279-288.

Dash, M., R.K. Dwari, S.K. Biswal, P.S.R. Reddy, P. Chattopadhyay, and B.K. Mishra. 2011. "Studies on the effect of flocculant adsorption on the dewatering of iron ore tailings." *Chemical Engineering Journal* 173 (2): 318-325.

Davis, M.J., Q. Dai, H.L.T. Chen, and M. Taylor. 2010a. "New polymers for improved flocculation of high DSP-containing muds." *Light Metals*: 57-61.

Davis, M.J., Q. Dai, H.L.T. Chen, and M. Taylor. 2010b. Use of silicon-containing polymers for improved flocculation of solids in processes for the production of alumina from bauxite. CA Patent 2740842 A1.

De Clercq, B., P.A. Lant, and P.A. Vanrolleghem. 2004. "Focused Beam Reflectance Technique for in situ particle sizing in wastewater treatment settling tanks." *Journal of Chemical Technology and Biotechnology* 79 (6): 610-618.

Den Hond, R., I. Hiralal, and A. Rijkeboer. 2007. "Alumina yield in the bayer process past, present and prospects." *Light Metals*: 37-42.

Derjaguin, B.V., and L.D. Landau. 1941. "Theory of the stability of strongly charged lyophobic sols and of the adhesion of strongly charged particles in solutions of electrolytes." *Acta Physicochimica* 14: 633-662.

Dickey, G.D., and C.L. Bryden. 1946 *Theory and Practice of Filtration*. New York: Reinhold Pub. Corp.

Dickey, G.D. 1961. *Filtration*. New York: Reinhold Pub. Corp.

Dihang, D., P. Aimar, J. Kayem, and S.N. Koungou. 2008. "Coagulation and flocculation of laterite suspensions with low levels of aluminium chloride and polyacrylamids." *Chemical Engineering and Processing: Process Intensification* 47 (9–10): 1509-1519.

Dippenaar, A. 1985. *Mintek Report M230: Shear Flocculation of Fines for Improved Flotation*. Randburg, South Africa.

Dollimore, D., and G.B. McBride. 1968. "Alternative methods of calculating particle size from hindered settling measurements." *Journal of Applied Chemistry* 18 (5): 136-140.

Drzymala, J., and D.W. Fuerstenau. 1987. "Adsorption of polyacrylamide, partially hydrolyzed polyacrylamide and polyacrylic acid on ferric oxide and silica." In *Flocculation in Biotechnology and Separation Systems*, ed. Y.A. Attia, 45-60. New York: Elsevier.

Du, J., G. Morris, R.A. Pushkarova, and R.S.C. Smart. 2010. "Effect of surface structure of kaolinite on aggregation, settling rate, and bed density." *Langmuir* 26 (16): 13227-13235.

Duncan, A., H. Muller-Steinhagen, B. Verity, and B. Welch. 1995. "An investigation of desilication kinetics in spent Bayer liquor." *Light Metals*: 37-44.

Echeverri, L., F. Schoenbrunn, M.B. Hansen, and B. Ranganathan. 2012. "Title Optimization Of The Hydraulic Design Of Thickener Feedwells Applying Computational Fluid Dynamics And Experimental Techniques." In *SME Annual Meeting* Seattle, Washington: Society for Mining, Metallurgy and Exploration, Inc. Preprint 12-106, 1-7.

Eckart, D., J. Kildea, D. Nicholson, and P. Prinsloo. 2010. "Improved performance of red mud settlers at Worsley Alumina." *Light Metals*: 107-112.

Emmett, R.C. 1986. "Thickening and filtration techniques for dewatering iron-bearing minerals and precipitates" In *Iron Control in Hydrometallurgy*,edited by J.E. Dutrizac and A.J. Monhemius, Toronto, Canada: Ellis Horwood Limited. 593-602.

Emmett, R.C., and R.P. Klepper. 1991. "High density red mud thickeners." *Light Metals*: 229-233.

Fan, A., N.J. Turro, and P. Somasundaran. 2000. "A study of dual polymer flocculation." *Colloids and Surfaces A: Physicochemical and Engineering Aspects* 162 (1-3): 141-148.

Faneitte, M., A. Galarraga, and T. Foster. 1994. "Utilization of new polymer in Interalumina." *Light Metals*: 129-131.

Farmer, V.C. 1974. *The infrared spectra of minerals, Mineralogical Society Monograph Vol. 4*. London, U.K.: Mineralogical Society.

Farrow, J., and L. Warren. 1993. "Measurement of the size of aggregates in suspension." In *Coagulation and Flocculation*, ed. B. Dobias, 391-426. New York, USA: Marcel Dekker Inc.

Farrow, J.B., and J.D. Swift. 1996a. "Agitation and residence time effects during the flocculation of mineral suspensions." In *The 4th International Alumina Quality Workshop (AQW)*, Darwin, Australia: AQW Inc. 355-363.

Farrow, J.B., and J.D. Swift. 1996b. "A new procedure for assessing the performance of flocculants." *International Journal of Mineral Processing* 46 (3–4): 263-275.

Fawell, P., W. Richmond, L. Jones, and M. Collisson. 1997. "Focused beam reflectance measurement in the study of mineral suspensions." *Chemistry in Australia* 64 (2): 4-6.

Fawell, P. 2013. "Solid-liquid separation of clay tailings." In *Report No. 300 - Clays in the Mineral Resources Value Chain: A Literature Survey*, eds M. Grafe, C. Klauber and A. McFarlane, 377-431. Perth, Australia: Minerals and Energy Research Institute of Western Australia (MERIWA).

Fawell, P.D., L.J. Kirwan, and W. van Bronswijk. 2002. "Adsorption of polyacrylates on hematite: *in-situ* examination by FTIR-ATR at high and low pH." In *The 6th International Alumina Quality Workshop*, Brisbane, Australia: AQW Inc. 301-308.

Fawell, P.D., A.T. Owen, A.F. Grabsch, F.A. Benn, D.M. Labbett, and J.D. Swift. 2009a. "Factors affecting flocculation within gravity thickeners." In *Water in Mining 2009*, Perth, Western Australia: AusIMM. 71-76.

Fawell, P.D., J.B. Farrow, A.R. Heath, T.V. Nguyen, A.T. Owen, D. Paterson, M. Rudman et al. 2009b. "20 years of AMIRA P266 'Improving Thickener Technology' - how has it changed the understanding of thickener performance?" In *Paste 2009*,edited by R. Jewel, A. Fourie, S. Barrera and J. Wiertz, Viña del Mar, Chile, Nedlands, Australia: Australian Centre of Geomechanics. 59-68.

Fellows, C.M., and W.O.S. Doherty. 2006. "Insights into bridging flocculation." *Macromolecular Symposia* 231: 1-10.

Ferland, P., J.T. Malito, and E.C. Phillips. 2003. "Effects of temperature and method of solution preparation on the performance of a typical red mud flocculant." *Light Metals*: 35-42.

Filho, J., T. Santos, H. Lima, A. Borges, J. Borges, F. Giust, and A. Rabaca. 2012. "Tests with new flocculant for red mud decanting in Alunorte." *Light Metals*: 67-70.

Fitch, E.B., and W.A. Lutz. 1960. "Feedwells for density stabilization." *Journal of Water Pollution Control Federation* 32: 147-56.

Flanigen, E.M., H. Khatami, and H.A. Szymanski. 1971. "Infrared structural studies of zeolite frameworks." *Advances in Chemistry Series* 101 (Molecular Sieve Zeolites-I): 201-29.

Fleer, J.G., and J.M.H.M. Scheutjens. 1993. "Modelling polymer adsorption, steric stabilization." In *Coagulation and Flocculation*, ed. B. Dobias, 209-263. New York, USA: Marcel Dekker Inc.

Flesch, J.C., P.T. Spicer, and S.E. Pratsinis. 1999. "Laminar and turbulent shear-induced flocculation of fractal aggregates." *AIChE Journal* 45 (5): 1114-1124.

Foster, T., S.A. Moffatt, and V.T. Sinha. 1996. "Selecting the optimum addition points for flocculants in decanter feedwells " In *SME Annual Meeting*, Phoenix, Arizona: Society for Mining, Metallurgy and Exploration, Inc. Preprint 96-140, 1-13.

Freda, M., A. Piluso, A. Santucci, and P. Sassi. 2005. "Transmittance Fourier transform infrared spectra of liquid water in the whole mid-infrared region: temperature dependence and structural analysis " *Applied Spectroscopy* 59 (9): 1155-1159.

Gagnon, M.J., G. Simard, A. Charette, M. Brassard, R. Veillette, and G. Peloquin. 2001. "Shear-induced flocculation and break up of red mud aggregates." *Light Metals*: 59-63.

Gagnon, M.J., G. Simard, M. Normandin, and G. Peloquin. 2002. "Behavior of red mud agglomerated with various flocculants under shear conditions." *Light Metals*: 107-114.

Gagnon, M.J., A. Leclerc, G. Simard, and G. Peloquin. 2003. "A fractal model for the aggregate size distributions generated during red mud flocculation." *Light Metals*: 105-111.

Gardner, G.R., and K.B. Ray. 1939. "Flocculation and Clarification of Slimes with Organic Flocculants." *AIME Transactions*: 146-168.

Giles, C.H., T.H. MacEwan, S.N. Nakhwa, and D. Smith. 1960. "786. Studies in adsorption. Part XI. A system of classification of solution adsorption isotherms, and its use in diagnosis of adsorption mechanisms and in measurement of specific surface areas of solids." *Journal of the Chemical Society*: 3973-3993.

Giles, C.H., D. Smith, and A. Huitson. 1974. "A general treatment and classification of the solute adsorption isotherm. I. Theoretical." *Journal of Colloid and Interface Science* 47 (3): 755-765.

Gill, R.I.S., and T.M. Herrington. 1987a. "The flocculation of kaolin suspensions with cationic polyacrylamides of varying molar mass but the same cationic character." *Colloids and Surfaces* 22 (1): 51-76.

Gill, R.I.S., and T.M. Herrington. 1987b. "The effect of surface charge on the flocculation of kaolin suspensions with cationic polyacrylamides of varying molar mass but similar cationic character." *Colloids and Surfaces* 25 (2-4): 297-310.

Gill, R.I.S., and T.M. Herrington. 1987c. "The flocculation of kaolin suspensions using polyethylenimine and cationic polyacrylamides of the same molar mass but different charge density." *Colloids and Surfaces* 28: 41-52.

Gill, R.I.S., and T.M. Herrington. 1988. "Floc size studies on kaolin suspensions flocculated with cationic polyacrylamides." *Colloids and Surfaces* 32: 331-344.

Gill, R.I.S., and T.M. Herrington. 1989. "The effect of colloid concentration and pH on kaolin suspensions flocculated with cationic polyacrylamides of high molar mass." *Colloids and Surfaces* 42 (1): 23-37.

Gladman, B.R., R.G. de Kretser, M. Rudman, and P.J. Scales. 2005. "Effect of shear on particulate suspension dewatering." *Chemical Engineering Research and Design* 83 (7): 933-936.

Gladman, B.R., S.P. Usher, and P.J. Scales. 2006. "Understanding the thickening process" In *Paste 2006*,edited by R.J. Jewell, S. Lawson and P. Newman, Limerick, Ireland, Nedlands, Australia: Australian Centre for Geomechanics 5-23.

Gladman, B.R., M. Rudman, and P.J. Scales. 2010. "Experimental validation of a 1-D continuous thickening model using a pilot column." *Chemical Engineering Science* 65 (13): 3937-3946.

Govier, G.W., and K. Aziz. 1972. *The flow of complex mixtures in pipes*. New York-London: Van Nostrand Reinhold Comp.

Grabsch, A.F., P.D. Fawell, S.J. Adkins, and A. Beveridge. 2013. "The impact of achieving a higher aggregate density on polymer-bridging flocculation." *International Journal of Mineral Processing* 124: 83-94.

Greaves, D., J. Boxall, J. Mulligan, A. Montesi, J. Creek, E.D. Sloan, and C.A. Koh. 2008. "Measuring the particle size of a known distribution using the focused beam reflectance measurement technique." *Chemical Engineering Science* 63 (22): 5410-5419.

Gregory, J., and D.W. Nelson. 1986. "Monitoring of aggregates in flowing suspensions." *Colloids and Surfaces* 18 (2-4): 175-88.

Gregory, J. 1989. "Fundamentals of flocculation." *Critical Reviews in Environmental Control* 19 (3): 185-230.

Gregory, J. 1997. "The density of particle aggregates." *Water Science and Technology* 36 (4, Role of Particle Characteristics in Separation Processes): 1-13.

Gregory, J. 2009. "Optical monitoring of particle aggregates." *Journal of Environmental Science* 21 (1): 2-7.

Gregory, J., and S. Barany. 2011. "Adsorption and flocculation by polymers and polymer mixtures." *Advances in Colloid and Interface Science* 169 (1): 1-12.

Guibai, L., and J. Gregory. 1991. "Flocculation and sedimentation of high-turbidity waters." *Water Research* 25 (9): 1137-1143.

Guibault, G.G. 1990. *Practical Flourescence*. 2nd ed. New York, USA: Marcel Dekker Inc.

Happel, J., and H. Brenner. 1973. *Low Reynolds Number Hydrodynamics: With Special Applications to Particulate Media*. Leiden: Noordhoff International Publishing.

Harato, T., T. Ishida, Y. Kumagae, M. Inami, K. Ishibashi, and M. Murakami. 1996a. Process for production of aluminum hydroxide from ore containing alumina. US Patent 5545384 A.

Harato, T., T. Ishida, H. Kato, M. Inami, K. Ishibashi, Y. Kumagae, and M. Murakami. 1996b. "The development of a new Bayer process that reduces the desilication loss of soda by 50 % compared to the conventional process." In *The 4th International Alumina Quality Workshop (AQW)*, Darwin, Australia: AQW Inc. 311-320.

Harif, T., M. Khai, and A. Adin. 2012. "Electrocoagulation versus chemical coagulation: Coagulation/flocculation mechanisms and resulting floc characteristics." *Water Research* 46 (10): 3177-3188.

Hassan, I. 1982. "The Crystal Structure and Crystal Chemistry of Sodalite and Cancrinite." PhD Thesis, McMaster University, Ontario, Canada.

Heath, A.R., P.D. Fawell, P.A. Bahri, and J.D. Swift. 2002. "Estimating Average Particle Size by Focused Beam Reflectance Measurement (FBRM)." *Particle & Particle Systems Characterization* 19 (2): 84-95.

Heath, A.R., P.A. Bahri, P.D. Fawell, and J.B. Farrow. 2006a. "Polymer flocculation of calcite: Experimental results from turbulent pipe flow." *AIChE Journal* 52 (4): 1284-1293.

Heath, A.R., P.A. Bahri, P.D. Fawell, and J.B. Farrow. 2006b. "Polymer flocculation of calcite: Population balance model." *AIChE Journal* 52 (5): 1641-1653.

Heath, A.R., P.A. Bahri, P.D. Fawell, and J.B. Farrow. 2006c. "Polymer flocculation of calcite: Relating the aggregate size to the settling rate." *AIChE Journal* 52 (6): 1987-1994.

Heath, A.R., and R.A. Triglavcanin. 2010. "Advances in thickener feedwell design via computational fluid dynamics modelling." In *The 25th International Mineral Processing Congress (IMPC) 2010*, Brisbane, Australia: AusIMM. 3229-3235.

Heath, A.R., and I. Arbuthnot. 2013. "Advances in Thickener Flocculant Delivery." In *MetPlant 2013 Metallurgical Plant Design and Operating Strategies - World's Best Practices*, Perth, Australia: AusIMM. 86-92.

Hecker, R., L. Kirwan, A. Jefferson, P.D. Fawell, J.B. Farrow, and J.D. Swift. 1999. "Focused beam reflectance measurement for the continuous assessment of flocculant performance" In *Polymers in Mineral Processing,*edited by J.S. Laskowski, Quebec, Canada: Canadian Institute of Mining, Metallurgy and Petroleum. 91-105.

Heffels, C., R. Polke, M. Raedle, B. Sachweh, M. Schaefer, and N. Scholz. 1998. "Control of particulate processes by optical measurement techniques." *Particle & Particle Systems Characterization* 15 (5): 211-218.

Henriksson, B., A. Scarsella, and M. Misalla. 2011. "Feedwell design for alumina thickeners and clarifiers - Where to next?" In *ICSOBA-2011 Bauxite Residue Seminar* Goa, India: ICSOBA. 94-100.

Hermeler, G., J.C. Buhl, and W. Hoffmann. 1991. "The influence of carbonate on the synthesis of an intermediate phase between sodalite and cancrinite." *Catalysis Today* 8 (4): 415-426.

Hirosue, H., E. Abe, N. Yamada, and H. Ihara. 1980. "Coagulation and dispersion of red mud suspensions." *Powder Technology* 27 (2): 197-202.

Ho, G.E., W.A. Robertson, G.I.D. Roach, and A. Antonovsky. 1992. "Morphological study of Bayer process desilication product and its application to laboratory

and plant digests." *Industrial & Engineering Chemistry Research* 31 (3): 982-986.

Hocking, M.B., K.A. Klimchuk, and S. Lowen. 1999. "Polymeric flocculants and flocculation." *Journal of Macromolecular Science - Reviews in Macromolecular Chemistry and Physics* 39 C (2): 177-203.

Hogg, R. 1984. "Collision efficiency factors for polymer flocculation." *Journal of Colloid and Interface Science* 102 (1): 232-236.

Hogg, R. 1999. "The role of polymer adsorption kinetics in flocculation." *Colloids and Surfaces A: Physicochemical and Engineering Aspects* 146 (1-3): 253-263.

Holt, P.K., G.W. Barton, M. Wark, and C.A. Mitchell. 2002. "A quantitative comparison between chemical dosing and electrocoagulation." *Colloids and Surfaces A: Physicochemical and Engineering Aspects* 211 (2–3): 233-248.

Honaker, R.Q., G.H. Lutrell, and R.-H. Yoon. 1994. "*In-situ* measurements of coagula size using an on-line particle size analyzer." In *SME Annual Meeting*, New Mexico, USA: Society for Mining, Metallurgy and Exploration, Inc. Preprint 94-258, 1-7.

Hongting, Z., D. Youjun, J.B. Harsh, M. Flurry, and J.S. Boyle. 2004. "Alteration of kaolinite to cancrinite and sodalite by simulated Hanford tank waste and its impact on cesium retention." *Clay and Clay Minerals* 52 (1): 1-13.

Huang, C.K., and P.F. Kerr. 1960. "Infrared study of the carbonate minerals." *American Mineralogist* 45: 311-324.

Hukkanen, E.J., and R.D. Braatz. 2003. "Measurement of particle size distribution in suspension polymerization using *in situ* laser backscattering." *Sensors and Actuators B: Chemical* 96 (1-2): 451-459.

Hulston, J. 2005. "Effect of Flocculation Conditions on the Dewaterability of Hematite and Red Mud Suspensions." PhD Thesis, Dept. of Chemical and Biomolecular Engineering, University of Melbourne, Melbourne, Australia.

Hunter, R.J. 1981. *Zeta Potential in Colloid Science. Principles and Applications*. Edited by R.H. Ottewill and R.L. Rowell, *Colloid Science - A Series of Monograph*. New York, USA: Academic Press Inc.

Hunter, R.J. 1993. *Introduction to Modern Colloid Science*. 1st ed. New York, USA: Oxford University Press.

Hunter, T.K., G.M. Moody, S.E. Sankey, and C.A. Tran. 1991. "Advances with chemical additives for the alumina industry." *Light Metals*: 159-165.

Hurd, M.D., L.H. Laviolette, and M.E. Lewellyn. 1994. "Making emulsion polymers work better in the Bayer process." *Light Metals*: 117-20.

Ikkatai, T., N. Okada, and K.K. Showa. 1963. "Viscosity, specific gravity and equilibrium concentration of sodium aluminate solutions " In *Extractive Metallurgy of Alumunium* eds G. Gerard and P.T. Stroup, 133-158. New York, USA: Interscience

ISO. 2009. *13320:2009(E): Particle size analysis - Laser diffraction methods*. ISO.

Jagger, N.D., and I.M. Arbuthnot. 1991. "Flocculant usage in high rate and conventional thickeners." In *The 4th Mill Operators' Conference*, Tasmania, Australia: AusIMM. 5-8.

Jamialahmadi, M., and H. Müller-Steinhagen. 1998. "Determining silica solubility in bayer process liquor." *Journal of Metals* 50 (11): 44-49.

Jarabo, R., E. Fuente, A. Moral, A. Blanco, L. Izquierdo, and C. Negro. 2010. "Effect of sepiolite on the flocculation of suspensions of fibre-reinforced cement." *Cement and Concrete Research* 40 (10): 1524-1530.

Johnson, G., S. Jackson, and I. Arbuthnot. 1990. "Control of a high rate thickener on gold plant tailings." In *The AusIMM Annual Conference*, Rotorua, New Zealand: AusIMM. 115-121.

Johnson, S.B., G.V. Franks, P.J. Scales, D.V. Boger, and T.W. Healy. 2000. "Surface chemistry-rheology relationships in concentrated mineral suspensions." *International Journal of Mineral Processing* 58 (1-4): 267-304.

Jones, F. 1998. "The Mechanism of Bayer Residue Flocculation." PhD Thesis, Dept. of Chemistry, Curtin University, Perth, Australia.

Jones, F., J.B. Farrow, and W. Van Bronswijk. 1998a. "Flocculation of hematite in synthetic Bayer liquors." *Colloids and Surfaces A: Physicochemical and Engineering Aspects* 135 (1-3): 183-192.

Jones, F., J.B. Farrow, and W. Van Bronswijk. 1998b. "Effect of caustic and carbonate on the flocculation of haematite in synthetic Bayer liquors." *Colloids and Surfaces A: Physicochemical and Engineering Aspects* 142 (1): 65-73.

Jones, F., J.B. Farrow, and W. Van Bronswijk. 1998c. "An infrared study of a polyacrylate flocculant adsorbed on hematite." *Langmuir* 14 (22): 6512-6517.

Jungreis, E. 1981. "A Simple Microdetermination Of Polymer Flocculants (Polyacrylamides And Guar) In Mine Water." *Analytical Letters* 14 (14): 1177-1183.

Kahane, R., T. Nguyen, and M.P. Schwarz. 2002. "CFD modelling of thickeners at Worsley Alumina Pty Ltd." *Applied Mathematical Modelling* 26 (2): 281-296.

Kahane, R.B., R.J. Schwarz, and R.M. Johnston. 1997. "Residue thickener modelling at Worsley Alumina." In *The 1st International Conference on CFD in Mineral & Metal Processing and Power Generation*, Melbourne, Australia: CSIRO. 109-117.

Kang, Y., S. Moon, S. Park, J. Kim, S.S. Lee, K. Park, 2007. "Synthesis, complexation and fluorescence properties of N-anthracenylmethyl dipodal ligand with quinoline end-group." *Bulletin of Korean Chemical Society* 28 (5): 873-876.

Kang, J., T.D. Sowers, O.W. Duckworth, A. Amoozegar, J.L. Heitman, and R.A. McLaughlin. 2013. "Turbidimetric determination of anionic polyacrylamide in low carbon soil extracts." *Journal of Environmental Quality* 42 (6): 1902-1907.

Karageorgos, J., S. Davies, E. Broers, and J. Goh. 2009. "Current trends in countercurrent decantation and thickener circuit operability and control." In *The 10th Mill Operators' Conference 2009*, Adelaide, Australia: AusIMM. 255-260.

Karakyriakos, E., and V. Patrick. 2005. "Report No. 253 - Industrial applications using improved measurements of particle surface charge", Perth, Australia: Minerals and Energy Research Institute of Western Australia (MERIWA).

Kim, M.J., and S.O. Lee. 2003. "Overview of the behavior of sodium oxalate in Bayer liquor and its effect of the process." *Light Metals*: 19-24.

Kirwan, L.J. 2002. "An Investigation of Polyacrylate Adsorption onto Hematite." PhD Thesis, Dept. of Chemistry, Curtin University, Perth, Australia.

Kirwan, L.J., P.D. Fawell, and W. Van Bronswijk. 2003. "In situ FTIR-ATR examination of poly(acrylic acid) adsorbed onto hematite at low pH." *Langmuir* 19 (14): 5802-5807.

Kirwan, L.J., P.D. Fawell, and W. Van Bronswijk. 2004. "An in situ FTIR-ATR study of polyacrylate adsorbed onto hematite at high pH and high ionic strength." *Langmuir* 20 (10): 4093-4100.

Kirwan, L.J. 2009a. "Investigating bauxite residue flocculation by hydroxamate and polyacrylate flocculants utilising the focussed beam reflectance measurement probe." *International Journal of Mineral Processing* 90 (1-4): 74-80.

Kirwan, L.J. 2009b. "A study of polyacrylate and hydroxamate co-dosing flocculation of stabilised bauxite residue material." *International Journal of Mineral Processing* 91 (1-2): 28-33.

Klimpel, R.C., and R. Hogg. 1986. "Effects of flocculation conditions on agglomerate structure." *Journal of Colloid and Interface Science* 113 (1): 121-131.

Klimpel, R.R. 1998. *Introduction to solid-liquid separation*. Edited by R. Rajagopalan, *Instructional Module Series*. Florida, USA: University of Florida

Kosmulski, M. 2002. "The pH-dependent surface charging and the points of zero charge." *Journal of Colloid and Interface Science* 253 (1): 77-87.

Kosmulski, M., and J.B. Rosenholm. 2004. "High ionic strength electrokinetics." *Advances in Colloid and Interface Science* 112 (1-3): 93-107.

Kosmulski, M. 2004. "pH-dependent surface charging and points of zero charge II. Update." *Journal of Colloid and Interface Science* 275 (1): 214-224.

Kosmulski, M. 2006. "pH-dependent surface charging and points of zero charge. III. Update." *Journal of Colloid and Interface Science* 298 (2): 730-741.

Kosmulski, M. 2009. "pH-dependent surface charging and points of zero charge. IV. Update and new approach." *Journal of Colloid and Interface Science* 337 (2): 439-448.

Kosmulski, M. 2011. "The pH-dependent surface charging and points of zero charge. V. Update." *Journal of Colloid and Interface Science* 353 (1): 1-15.

Kotte, J.J. 1981. "Bayer digestion and predigestion desilication reactor design." *Light Metals*: 45-81.

Kusters, K.A., J.G. Wijers, and D. Thoenes. 1996. "Aggregation kinetics of small particles in agitated vessels." *Chemical Engineering Science* 52 (1): 107-121.

Kynch, G.J. 1952. "A theory of sedimentation." *Transactions of the Faraday Society* 48: 166-176.

La Mer, V.K., and T.W. Healy. 1963. "Adsorption-flocculation reactions of macromolecules at the solid-liquid interface." *Reviews of Pure and Applied Chemistry* 13: 112-33.

Lakowicz, J.R. 1983. *Principles of Flourescence Spectroscopy*. 1st ed. New York, USA: Springer.

Landman, K.A., L.R. White, and R. Buscall. 1988. "The continuous-flow gravity thickener: steady-state behavior." *AIChE Journal* 34 (2): 239-252.

Langmuir, I. 1918. "The adsorption of gases on plance surfaces of glass, mica and platinum." *Journal of the American Chemical Society* 40 (9): 1361-1403.

Laros, T.J., and F.A. Baczek. 2009. "Selection of sedimentation equipment for the Bayer Process an overview of past and present technology." *Light Metals*: 107-110.

Launer, P.J. 1987. "Infrared analysis of organosilicon compounds: Spectra-structure correlations." In *Silicon Compounds Register and Review*, eds B.C. Arkles, W.R. Peterson and R. Anderson. Bristol, U.K.: Petrarch Systems.

Li, L.Y., and G.K. Rutherford. 1996. "Effect of bauxite properties on the settling of red mud." *International Journal of Mineral Processing* 48 (3-4): 169-182.

Li, L.Y. 1998. "Properties of red mud tailings produced under varying process conditions." *Journal of Environmental Engineering* 124 (3): 254-264.

Li, L.Y. 2001. "A study of iron mineral transformation to reduce red mud tailings." *Waste Management* 21 (6): 525-534.

Liu, P., Z. Lu, Y. Li, H. Chou, F. Wang, and H. Wang. 1994. "The influence of the predesilication temperature of bauxite slurry on the sedimentation of red mud and the utilization of which in alumina production." *Light Metals* 133-136.

Liu, S., and J.H. Masliyah. 1996. "Flow of suspensions in pipelines." In *Suspensions: Fundamentals and Applications to the Petroleum Industry* ed. L.L. Schram, 107-176. Washington: American Chemical Society.

Liu, Y., R. Naidu, and H. Ming. 2013. "Surface electrochemical properties of red mud (bauxite residue): Zeta potential and surface charge density." *Journal of Colloid and Interface Science* 394: 451-457.

Loan, C. 1999. "The Adsorption and Solution Properties of High Molecular Weight of Polymeric Flocculant." Honours Thesis, Dept. of Chemisty Curtin University Perth, Australia.

Loan, C., G. Showers, and R. Triglavcanin. 2009. "Operational results from the vane feedwell – cutting-edge modelling turned into reality." In *The 10th Mill Operators' Conference 2009*, Adelaide, Australia: AusIMM. 261-266.

Loan, C., and I. Arbuthnot. 2010. "Innovative technology for optimised thickening sedimentation." In *The 25th International Mineral Processing Congress (IMPC) 2010*, Brisbane, Australia: AusIMM. 3663-3674.

Lowe, J.L., R.D. Hart, P.G. Smith, A.L. Rohl, and G.M. Parkinson. 2005. "Understanding growth of DSP in the presence of inorganic ions." In *The 7th International Alumina Quality Workshop*, Perth, Australia: AQW Inc. 168-173.

Lowe, J.L. 2007. "DSP in the Bayer Process: A Fundamental Study of its Precipitation and Role in Impurity Removal." PhD Thesis, Dept. of Chemistry, Curtin University, Perth, Australia.

Lynch, J. 2003. *Physico-chemical analysis of industrial catalysts: a practical guide to characterisation*. Paris, France: Editions Technip.

Ma, X. 2011. "Effect of a low-molecular-weight polyacrylic acid on the coagulation of kaolinite particles." *International Journal of Mineral Processing* 99 (1–4): 17-20.

Malito, J.T. 1996. "Improving the operation of red mud pressure filters." *Light Metals*: 81-86.

Malvern. 2004. *Zetasizer Nano Series User Manual*. Worchestershire, U.K.: Malvern Instruments Ltd.

Maude, A.D., and R.L. Whitmore. 1958. "A generalized theory of sedimentation." *British Journal of Applied Physics* 9: 477-482.

McGuire, M.J., J. Addai-Mensah, and K.E. Bremmell. 2006. "The effect of polymer structure type, pH and shear on the interfacial chemistry, rheology and dewaterability of model iron oxide dispersions." *Colloids and Surfaces A: Physicochemical and Engineering Aspects* 275 (1–3): 153-160.

McGuire, M.J. 2008. "Improved Dewaterability of Iron Oxide Dispersions." PhD Thesis, University of South Australia, Adelaide, Australia.

Meakin, P. 1987. "Fractal aggregates." *Advances in Colloid and Interface Science* 28: 249-331.

Michaels, A.S., and O. Morelos. 1955. "Polyelectrolyte Adsorption by Kaolinite." *Industrial & Engineering Chemistry Research* 47 (9): 1801-1809.

Mills, P.D.A., J.W. Goodwin, and B.W. Grover. 1991. "Shear field modification of strongly flocculated suspensions - aggregate morphology." *Colloid and Polymer Science* 269 (9): 949-63.

Moody, G. 1992. "The use of polyacrylamides in mineral processing." *Minerals Engineering* 5 (3–5): 479-492.

Morris, G.E., D. Fornasiero, and J. Ralston. 2002. "Polymer depressants at the talc–water interface: adsorption isotherm, microflotation and electrokinetic studies." *International Journal of Mineral Processing* 67 (1–4): 211-227.

Moss, N. 1978. "Theory of flocculation." *Mine and Quarry* 7: 57-61.

Moudgil, B.M., and A. McCombs. 1987. "Physical simulation of the flocculation process." *Minerals & Metallurgical Processing* 4 (3): 151-155.

Moudgil, B.M., B.D. Shah, and H. Soto. 1987. "Collision efficiency factors in polymer flocculation of fine particles." *Journal of Colloid and Interface Science* 119 (2): 466-473.

Mpofu, P., J. Addai-Mensah, and J. Ralston. 2003. "Investigation of the effect of polymer structure type on flocculation, rheology and dewatering behaviour of kaolinite dispersions." *International Journal of Mineral Processing* 71 (1–4): 247-268.

Mpofu, P., J. Addai-Mensah, and J. Ralston. 2004. "Flocculation and dewatering behaviour of smectite dispersions: effect of polymer structure type." *Minerals Engineering* 17 (3): 411-423.

Mugnier, N., P. Clerin, and J. Sinquin. 2001. "Industrial experience of polishing filtration performance improvement and interpretation." *Light Metals*: 33-39.

Mugnier, N., and P. Leizour. 2010. Method for attacking bauxite enhancing filterability of sludge in attack output. US Patent 7658896 B2.

Murphy, D.D., M.G. Bakker, and D.R. Spears. 1994. "New insights into the mechanism of shear-flocculation of silica with fatty acids." *Minerals & Metallurgical Processing* 11 (1): 26-30.

Murray, J.P., and S.A. Millington. 2002. "Revised application of synthetic flocculants in red mud separation." *Light Metals*: 121-124.

Nakagaki, M., T. Handa, and S. Shimabayashi. 1973. "S-shaped adsorption isotherms of surface active electrolytes from aqueous solutions." *Journal of Colloid and Interface Science* 43 (2): 521-529.

Nasser, M.S., and A.E. James. 2006. "The effect of polyacrylamide charge density and molecular weight on the flocculation and sedimentation behaviour of kaolinite suspensions." *Separation and Purification Technology* 52 (2): 241-252.

Negro, C., A. Blanco, I. San Pio, and J. Tijero. 2005. "Methodology for flocculant selection in fibre-cement manufacture." *Cemenet and Concrete Composite* 28 (1): 90-96.

Nguyen, T., A. Heath, and P. Witt. 2006. "Population balance–CFD modelling of fluid flow, solids distribution and flocculation in thickener feedwells." In *The 5th International Conference on CFD in the Process Industries*, Melbourne, Australia: CSIRO. (Proceedings in CD form only)

Nguyen, T.V., J.B. Farrow, J. Smith, and P.D. Fawell. 2012. "Design and development of a novel thickener feedwell using computational fluid dynamics." *Journal of the Southern African Institute of Mining and Metallurgy* 112 (11): 939-948.

Nguyen, T.V. 2013. Personal communication,
Normandin, M., M.J. Gagnon, A. Leclerc, G. Simard, R. Verreault, and G. Péloquin. 2006. "Study on the clarification of a red mud slurry during flocculation." *Light Metals*: 23-26.
Nunn, R.F. 1998. "Advances in red mud dewatering and disposal technologies." *Light Metals*: 107-113.
Oku, T., and K. Yamada. 1971. "Dissolution rate of quartz and the rate of desilication in the Bayer liquor." *Light Metals*: 31-45.
Oku, T., A. Suzuki, N. Tawara, and K. Niwa. 1973. Process for producing alumina. US Patent 3716617 A.
Oles, V. 1992. "Shear-induced aggregation and breakup of polystyrene latex particles." *Journal of Colloid and Interface Science* 154 (2): 351-358.
Olsen, A., G. Franks, S. Biggs, and G.J. Jameson. 2006. "An improved collision efficiency model for particle aggregation." *Journal of Chemical Physics* 125 (18): 184906/1-184906/9.
Ostap, S. 1985. "Control of silica in the Bayer process used for alumina production." In *Impurity Control Disposal, The 15th CIM Annual Hydrometallurgical Meeting*: Canadian Institute of Mining, Metallurgy and Petroleum. 14/1-14/14.
Owen, A.T., P.D. Fawell, J.D. Swift, and J.B. Farrow. 2002. "The impact of polyacrylamide flocculant solution age on flocculation performance." *International Journal of Mineral Processing* 67 (1–4): 123-144.
Owen, A.T., P.D. Fawell, and J.D. Swift. 2007. "The preparation and ageing of acrylamide/acrylate copolymer flocculant solutions." *International Journal of Mineral Processing* 84 (1-4): 3-14.
Owen, A.T., P.D. Fawell, J.D. Swift, D.M. Labbett, F.A. Benn, and J.B. Farrow. 2008. "Using turbulent pipe flow to study the factors affecting polymer-bridging flocculation of mineral systems." *International Journal of Mineral Processing* 87 (3-4): 90-99.
Owen, A.T., T.V. Nguyen, and P.D. Fawell. 2009. "The effect of flocculant solution transport and addition conditions on feedwell performance in gravity thickeners." *International Journal of Mineral Processing* 93 (2): 115-127.
Owen, D.O., L.J. Connelly, P.A. Dimas, A.E. Gross, and N.L. Passantino. 1991. "Evaluation of downstream effects of specialty chemicals in the Bayer process." *Light Metals*: 173-176.
Pan, Z., P. Somasundaran, N.J. Turro, and S. Jockusch. 2004. "Interactions of cationic dendrimers with hematite mineral." *Colloids and Surfaces A: Physicochemical and Engineering Aspects* 238 (1–3): 123-126.
Pearse, M.J., and Z. Sartowski. 1984. "Application of special chemicals (flocculants and dewatering aids) for red mud separation and hydrate filtration." *Light Metals*: 788-810.
Pearse, M.J. 2003. "Historical use and future development of chemicals for solid-liquid separation in the mineral processing industry." *Minerals Engineering* 16 (2): 103-108.
Pearse, M.J. 2005. "An overview of the use of chemical reagents in mineral processing." *Minerals Engineering* 18 (2 SPEC. ISS.): 139-149.
Peloquin, G., H. Baxter, G. Simard, D. Kocaefe, and R.T. Bui. 2002. "Improved red mud flocculation at Aughinish Alumina Limited." In *The 6th International Alumina Quality Workshop*, Brisbane, Australia: AQW Inc. 288-293.

Peloquin, G., and G. Simard. 2002. "Improved thickener for red mud." In *The 6th International Alumina Quality Workshop (AQW)*, Brisbane, Australia: AQW Inc. 40-45.

Peloquin, G., G. Simard, A. Boivin, R. Dufour, R. Lemyre, and A. Carruthers. 2005. Apparatus for and method of settling of mineral slurries. US Patent 6936178 B2.

Peng, S.J., and R.A. Williams. 1993. "Control and optimisation of mineral flocculation and transport using on-line particle size analysis." *Minerals Engineering* 6: 133-153.

Peng, S.J., and R.A. Williams. 1994. "Direct measurement of floc breakage in flowing suspensions." *Journal of Colloid and Interface Science* 166 (2): 321-32.

Perrier, X., B. Cristol, A. Cuneo-Raffaelli, and P. Dountsis. 1999. "Settler throughput increase at Aluminium de Grece refinery." *Light Metals*: 63-69.

Phillips, E.C. 1999. "New water-continuous red mud flocculants for the Bayer process." *Light Metals*: 39-43.

Phillips, E.C. 2003. "New salicylic acid containing red mud flocculants." *Light Metals*: 137-143.

Phillips, E.C. 2004. "Continued efforts on the development of salicylic acid containing red mud flocculants." *Light Metals*: 21-26.

Phillips, E.C., and K.L. O'Brien. 2006. "Development of new polyacrylate flocculants for red mud clarification." *Light Metals*: 5-9.

Potanin, A.A., and N.B. Uriev. 1991. "Microrheological models of aggregated suspensions in shear flow." *Journal of Colloid and Interface Science* 142 (2): 385-395.

Power, G., J.S.C. Loh, and K. Niemelae. 2011. "Organic compounds in the processing of lateritic bauxites to alumina." *Hydrometallurgy* 108 (1-2): 149-151.

Power, G.P., and W. Tichbon. 1990. "Sodium oxalate in the Bayer process: Its origin and effects." In *The 2nd International Alumina Quality Workshop (AQW)*, Perth, Australia: AQW Inc. 99-115.

Probst, A. 1999. "Next generation sedimentation equipment for ultimate thickening" In *The COPPER 99-COBRE 99 International Conference,*edited by B. Hancock and M. Pon, Phoenix, USA: Minerals, Metals & Materials Society. 217-232.

Putzig, C.L., M.A. Leugers, M.L. McKelvy, G.E. Mitchell, R.A. Nyquist, R.R. Papenfuss, and L. Yurga. 1994. "Infrared Spectroscopy." *Analytical Chemistry* 66 (12): 26R-66R.

Radomirovic, T., P. Smith, D. Southam, S. Tashi, and F. Jones. 2013. "Crystallization of sodalite particles under Bayer-type conditions." *Hydrometallurgy* 137: 84-91.

Ravi Shankar, S.A., Pradip, M.G. Deo, R.A. Kulkarni, and S. Gundiah. 1988. "Selective flocculation of iron oxide-kaolin mixtures using a modified polyacrylamide flocculant." *Bulletin of Materials Science* 10 (5): 423-433.

Richardson, J.F., and W.N. Zaki. 1954. "The sedimentation of a suspension of uniform spheres under conditions of viscous flow." *Chemical Engineering Science* 3 (2): 65-73.

Riley, J. 2005. "Charge in colloidal systems." In *Colloid Science*, ed. T. Cosgrove, 14-35. Oxfod, U.K.: Blackwell Publishing Ltd.

Roach, G.I.D., and A.J. White. 1988. "Dissolution kinetics of kaolin in caustic liquors." *Light Metals*: 41-47.

Roach, G.I.D., M.G. Aylemore, R.J. Gilkes, and R.R. Anand. 1989. "Mineralogy and the grinding and settling properties of Western Australian bauxite." *Light Metals*: 43-48.

Roach, G.I.D., E. Jamieson, N. Pearson, and A.B. Yu. 2001. "Effect of particle characteristics on the solids density of Bayer mud slurries." *Light Metals*: 51-58.

Rogan, K.R. 1995. "The variations of the configurational and solvency properties of low molecular weight sodium polyacrylate with ionic strength." *Colloid and Polymer Science* 273 (4): 364-369.

Rosenberg S.P., D.J. Wilson, C.A. Heath, 2001. "Some aspects of calcium chemistry in the Bayer process." *Light Metals*: 19-25.

Rothenberg, A.S., D.P. Spitzer, M.E. Lewellyn, and H.I. Heitner. 1989. "New reagents for alumina processing." *Light Metals*: 91-96.

Rousseaux, J.-M., B. Cristol, and S. Torsiello. 2004. "Combination of hydroxamate and polyacrylamide based flocculants for settler performance improvement in ADG alumina refinery." *Light Metals*: 15-20.

Rousseaux, J.-M., and P. Ferland. 2009. "Impact of excess synthetic flocculant on security filtration." *Light Metals*: 157-161.

Rudman, M., K. Simic, D.A. Paterson, P. Strode, A. Brent, and I.D. Šutalo. 2008. "Raking in gravity thickeners." *International Journal of Mineral Processing* 86 (1–4): 114-130.

Ryles, R.G., and P.V. Avotins. 1996. "Superfloc HX, a new technology for the alumina industry." In *The 4th International Alumina Quality Workshop (AQW)*, Darwin, Australia: AQW Inc. 205-216.

Sabah, E., H. Yüzer, and M.S. Çelik. 2004. "Characterization and dewatering of fine coal tailings by dual-flocculant systems." *International Journal of Mineral Processing* 74 (1–4): 303-315.

Saffman, P.G., and J.S. Turner. 1956. "On the collision of drops in turbulent clouds." *Journal of Fluid Mechanics* 1 (1): 16-30.

Sankey, S.E., and R.J. Schwarz. 1984. "The use of synthetic flocculant polymers in settling red muds derived from high-goethite bauxite ores." *Light Metals*: 1653-1667.

Sato, C., Y. Shibue, N. Arakawa, and Y. Kawai. 1984. "Flocculation and thickening of red mud." *Light Metals*: 197-210.

Schoenbrunn, F. 2011. "Dewatering to higher densities — an industry review " In *Paste 2011,*edited by R.J. Jewell and A.B. Fourie, Perth, Australia, Nedlands, Australia: Australian Centre for Geomechanics 19-23.

Schram, L.L. 1996. "Suspensions: Basic principles." In *Suspensions: Fundamentals and Applications in the Petroleum Industry* ed. L.L. Schram, 3-44. Washington: American Chemical Society.

Schwarz, F.P., S.P. Wasik, 1976. "Fluorescence measurements of benzene, naphthalene, anthracene, pyrene, flouroanthene and benzo[e]pyrene in water." *Analytical Chemistry* 48 (3): 524:528.

Schwertmann, U., and R.M. Cornell. 1991. *Iron Oxides in the Laboratory: Preparation and Characterization*. New York - Weinheim: Wiley-VCH Verlag GmbH.

Sengupta, D.K., J. Kan, A.M. Al Taweel, and H.A. Hamza. 1997. "Dependence of separation properties on flocculation dynamics of kaolinite suspension." *International Journal of Mineral Processing* 49 (1–2): 73-85.

Serra, T., and X. Casamitjana. 1998. "Effect of the shear and volume fraction on the aggregation and breakup of particles." *AIChE Journal* 44 (8): 1724-1730.

Shammas, N., and L. Wang. 2007. "Gravity thickening." In *Biosolids Treatment Processes*, eds L. Wang, N. Shammas and Y.-T. Hung, 45-69. Humana Press.

Shaw, D.J. 1992. *Introduction to Colloid and Surface Chemistry*. 4th ed. Oxford, U.K.: Butterworth-Heinemann.

Siebentritt, M., P. Volovitch, K. Ogle, and G. Lefèvre. 2014. "Adsorption and electroreduction of hematite particles on steel in strong alkaline media." *Colloids and Surfaces A: Physicochemical and Engineering Aspects* 440: 197-201.

Sivamohan, R., and J.M. Cases. 1990. "Dependence of shear-flocculation on surface coverage and zeta potential." *International Journal of Mineral Processing* 28 (3–4): 161-172.

Smith, B. 2013. The Next Generation FBRMVR (Focused Beam Reflectance Measurement). http://tinyurl.com/d9ounu6. (accessed March 19, 2013)

Smith, P., J.L. Lowe, A.L. Rohl, R. Pennifold, and G.M. Parkinson. 2002. "Understanding growth of DSP in the presence of inorganics ions." In *The 6th International Alumina Quality Worksop (AQW)*, Brisbane, Australia: AQW Inc. 191-194.

Smith, P. 2009. "The processing of high silica bauxites — Review of existing and potential processes." *Hydrometallurgy* 98 (1–2): 162-176.

Smith, P. 2014. Personal communication,

Smoluchowski, M.v. 1916. "Theoretische bemerkungen über die viskosität der kolloide." *Kolloid-Zeitschrift* 18 (5): 190-195.

Smoluchowski, M.v. 1917. "Grundriß der koagulationskinetik kolloider lösungen." *Kolloid-Zeitschrift* 21 (3): 98-104.

Soliz, L., R. Vinhas, E. Repetto, P. Prado, H.L.T. Chen, R.S. Junior, A. Arantes, R. Santos, and R. Moreno. 2012. "Performance evaluation of CYFLOC™ HX-5300 - A new HXPAM red mud flocculant applied in CBA (Companhia Brasileira de Aluminio)." In *ICSOBA-2012 The 19th Symposium of ICSOBA*, Belem, Brazil: ICSOBA. 1-11.

Solymar, K., I. Sajo, J. Steiner, and J. Zoldi. 1992. "Characteristics and separability of red mud." *Light Metals*: 209-23.

Sparks, T. 2012. *Solid-liquid filtration : a user's guide to minimizing cost & environmental impact, maximizing quality & productivity*. Boston, USA: Butterworth-Heinemann.

Spears, D.R., and D.A. Stanley. 1994. "Study of shear-flocculation of silica." *Minerals & Metallurgical Processing* 11 (1): 5-11.

Spicer, P.T., and S.E. Pratsinis. 1996. "Shear-induced flocculation: The evolution of floc structure and the shape of the size distribution at steady state." *Water Research* 30 (5): 1049-1056.

Spicer, P.T., S.E. Pratsinis, J. Raper, R. Amal, G. Bushell, and G. Meesters. 1998. "Effect of shear schedule on particle size, density, and structure during flocculation in stirred tanks." *Powder Technology* 97 (1): 26-34.

Spitzer, D.P., A.S. Rothenberg, H.I. Heitner, M.E. Lewellyn, L.H. Laviolette, T. Foster, and P.V. Avotins. 1991. "Development of new Bayer process flocculants." *Light Metals*: 167-171.

Spitzer, D.P., and P.V. Avotins. 1994. "Effect of polymers on flow properties of Bayer process underflow muds." *Light Metals*: 1225-1230.
Steinour, H.H. 1944a. "Rate of sedimentation." *Industrial & Engineering Chemistry Research* 36: 901-907.
Steinour, H.H. 1944b. "Rate of sedimentation. Nonflocculated suspensions of uniform spheres." *Industrial & Engineering Chemistry Research* 36: 618-624.
Steinour, H.H. 1944c. "Rate of sedimentation." *Industrial & Engineering Chemistry Research* 36: 840-847.
Stokes, G.G. 1843. "On some cases of fluid motion." *Transactions of the Cambridge Philosophical Society* 8: 105-137.
Suharyono, H., and R. Hogg. 1996. "Flocculation in flow through pipes and in-line mixers." *Minerals and Metallurgical Processing* 13: 501-505.
Suttill, K.R. 1991. "The ubiquitous thickener." *Engineering and Mining Journal* 192 (2): 20-26.
Suttle, H.K. 1969. *Filtration, Process engineering technique evaluation series* West Wickham, U.K.: Morgan-Grampian
Svarovsky, L. 2000. *Solid-liquid separation* 4th ed. Boston, USA: Butterworth-Heinemann.
Swerin, A., L. Ödberg, and L. Wågberg. 1996. "An extended model for the estimation of flocculation efficiency factors in multicomponent flocculant systems." *Colloids and Surfaces A: Physicochemical and Engineering Aspects* 113 (1–2): 25-38.
Swift, J.D., K. Simic, R.R.M. Johnston, P.D. Fawell, and J.B. Farrow. 2004. "A study of the polymer flocculation reaction in a linear pipe with a focused beam reflectance measurement probe." *International Journal of Mineral Processing* 73 (2–4): 103-118.
Taylor, K.C., and H.A. Nasr-El-Din. 1994. "Acrylamide copolymers: A review of methods for the determination of concentration and degree of hydrolysis." *Journal of Petroleum Science and Engineering* 12 (1): 9-23.
Taylor, M.L., G.E. Morris, P.G. Self, and R.S.C. Smart. 2002. "Kinetics of adsorption of high molecular weight anionic polyacrylamide onto kaolinite: The flocculation process." *Journal of Colloid and Interface Science* 250 (1): 28-36.
Thapa, K.B., Y. Qi, and A.F.A. Hoadley. 2009. "Interaction of polyelectrolyte with digested sewage sludge and lignite in sludge dewatering." *Colloids and Surfaces A: Physicochemical and Engineering Aspects* 334 (1-3): 66-73.
The, P.J., and J.F. Bush. 1987. "Solubility of sodium oxalate in Bayer liquor and a method of control." *Light Metals*: 5-10.
The, P.J. and T.J. Sivakumar, 1985. "The effect of impurities on calcium in Bayer liquor." *Light Metals*: 209-222.
Thomas, D., and B. Pei. 2007. "Chemical reaction engineering in the Bayer process." *Light Metals*: 118-123.
Triglavcanin, R.A. 2008. "Designing feedwells for the 21st century." In *MetPlant 2008 Metallurgical Plant Design and Operating Strategies*, Perth, Australia: AusIMM. 559-573.
Tscharnuter, W. 2001. "Mobility measurements by phase analysis." *Applied Optics* 40: 3995-4003.
USGS. 2012. Mineral commodity summaries 2012. http://minerals.usgs.gov/minerals/pubs/mcs/2012/mcs2012.pdf. (accessed 14 March 2014)

Vay, K., W. Friess, and S. Scheler. 2012. "Understanding reflection behavior as a key for interpreting complex signals in FBRM monitoring of microparticle preparation processes." *International Journal of Pharmaceutical* 437 (1-2): 1-10.

Vergouw, J.M., A. Difeo, Z. Xu, and J.A. Finch. 1998. "An agglomeration study of sulphide minerals using zeta-potential and settling rate. Part 1: Pyrite and galena." *Minerals Engineering* 11 (2): 159-169.

Verwey, E.J.W., and J.T.G. Overbeek. 1948. *Theory of the stability of lyophobic colloids*. Amsterdam, Netherlands: Elsevier/Academic Press.

Vidyasagar, P. 1996. "Red mud separation in alumina industry for cleaner environment" In *Solid Liquid Separation in Mineral and Metallurgical Industries, Selected Papers contributed for the National Seminar on Solid Liquid Separation in Mineral and Metallurgical Industries,*edited by R. Bhima Rao and M.I. Ansari, Bhubaneswar, India: Indian Institute of Mineral Engineers, Bhubaneswar Chapter. 30-56.

Webster, N.A.S., M.J. Loan, I.C. Madsen, R.B. Knott, and J.A. Kimpton. 2011. "An investigation of the mechanisms of goethite, hematite and magnetite-seeded $Al(OH)_3$ precipitation from synthetic Bayer liquor." *Hydrometallurgy* 109 (1–2): 72-79.

White, R.B., K. Simic, and P.R. Strode. 2001. "The combined use of flow visualisation, electrical resistance tomography and computational fluid dynamics modelling to study mixing in a pipe." In *The 2nd World Congress on Industrial Process Tomography*, Hannover, Germany: Virtual Centre for Industrial & Process Tomography. 610-617.

Whittington, B.I., B.L. Fletcher, and C. Talbot. 1998. "The effect of reaction conditions on the composition of desilication product (DSP) formed under simulated Bayer conditions." *Hydrometallurgy* 49 (1–2): 1-22.

Wickramanayake, G.B., B.W. Vigon, and R. Clark. 1987. "Analytical techniques for polyelectrolytes in wastewater: a review." *Flocculation and Biotechnology Separation Systems* 4: 125-47.

Williams, R.A., S.J. Peng, and A. Naylor. 1992. "*In situ* measurement of particle aggregation and breakage kinetics in a concentrated suspension." *Powder Technology* 73 (1): 75-83.

Wu, F. 2012. "Aluminous Goethite in the Bayer Process and its Impact on Alumina Recovery and Settling." PhD Thesis, Dept. of Chemistry, Curtin University, Perth, Australia.

Xu, B., C. Wingate, and P. Smith. 2009. "Transformation of sodalite to cancrinite under high temperature Bayer digestion conditions." *Light Metals*: 51-56.

Xu, B., P. Smith, C. Wingate, and L. De Silva. 2010. "The effect of calcium and temperature on the transformation of sodalite to cancrinite in Bayer digestion." *Hydrometallurgy* 105 (1-2): 75-81.

Yamada, K., T. Hashimoto, and K. Nakano. 1973. "Behavior of organic substances in the Bayer process." *Light Metals* 2: 745-54.

Yamada, K., T. Harato, and Y. Shiozaki. 1980. "Flocculation and sedimentation of red mud." *Light Metals*: 39-50.

Yu, X., and P. Somasundaran. 1993. "Enhanced flocculation with double flocculants." *Colloids and Surfaces A: Physicochemical and Engineering Aspects* 81: 17-23.

Zbik, M.S., R.S.C. Smart, and G.E. Morris. 2008. "Kaolin flocculation structure." *Journal of Colloid and Interface Science* 328 (1): 73-80.

Zhang, K.-Y., H.-P. Hu, L.-J. Zhang, and Q.-Y. Chen. 2008. "Effects of polymeric flocculants on settlement of Bayer red mud generated from Chinese diaspore bauxite." *The Chinese Journal of Process Engineering* 8 (2): 267-273.

Zheng, K., A.R. Gerson, J. Addai-Mensah, and R.S.C. Smart. 1997. "The influence of sodium carbonate on sodium aluminosilicate crystallisation and solubility in sodium aluminate solutions." *Journal of Crystal Growth* 171 (1–2): 197-208.

# Abbreviations, nomenclature and liquor terminology

## Abbreviations

| | |
|---|---|
| BET | - Brunauer, Emmet and Taylor |
| BJH | - Barrett, Joyner and Halenda |
| CFD | - computational fluid dynamics |
| DCT | - deep cone thickeners |
| DSP | - desilication product |
| DMAEA | - dimethyl-aminoethyl acrylate |
| EDX | - energy dispersive X-ray |
| FBRM | - focused beam reflectance measurement |
| FDA | - floc density analyser |
| FTIR | - Fourier transform infrared spectroscopy |
| HX PAM | - hydroxamate/polyacrylate/acrylamide |
| ICP-AES | - inductively coupled plasma atomic emission spectrometer |
| iep | - isoelectric point |
| IHP | - inner Helmholtz plane |
| IR | - infrared |
| LDV | - laser Doppler velocimetry |
| NTU | - nephelometric turbidity unit |
| OHP | - outer Helmholtz plane |
| PAA | - polyacrylate/acrylamide |
| PALS | - phase analysis light scattering |
| PB | - population balance |
| ppb | - part per billion |
| ppm | - part per million |
| PSD | - particle size distribution |
| PVM | - particle vision and measurement |
| SD | - standard deviation |
| SEM | - scanning electron microscopy |
| TCA | - tricalcium aluminate |
| XRD | - X-ray diffraction |
| XRF | - X-ray fluorescence |

## Nomenclature

| | |
|---|---|
| *1/Tb* | = rate of aggregate decay due to stirring |
| *A* | = filtration area ($m^2$) |
| *a* | = particle diameter of the ellipse (μm) |
| $a_i$ | = particle radius of i sized particle |
| $a_j$ | = particle radius of j sized particle |
| *b* | = horizontal diameter of the ellipse (μm) |
| *c* | = total suspended solids concentration (kg $m^{-3}$) |
| $C_o$ | = steady-state mean square-weighted chord length (μm) |
| $d_a$ | = aggregate's calculated size (μm) |
| $d_{st}$ | = diameter of sphere with settling velocity equivalent to the ellipse with certain dimension (μm) |
| $d_1$ | = density of the particle (kg $m^{-3}$) |

$d_2$ = density of the media (kg $m^{-3}$)
$\bar{d}_{agg}$ = average size of aggregates (m)
$\bar{d}_p$ = average size of primary particles (m)
$dt/dV$ = filtration rate ($m^3$ $s^{-1}$)
$dX/dt$ = rate of reactive silica conversion to DSP
$D_f$ = mass-length fractal dimension
$f(ka)$ = Henry function
$g$ = gravitational constant (cm $s^{-2}$ or m $s^{-2}$)
$G$ = mean shear rate ($s^{-1}$)
$L$ = diameter or radius of the aggregate (μm)
$m$ = mass of aggregate (μg)
$M_i$ = midpoint of a channel (μm)
$MOH$ = neutral hydroxyl sites of metallic oxides
$MOH_2^+$ = positively charged sites of metallic oxides
$MO^-$ = negatively charged sites of metallic oxides
$N$ = caustic concentration in g $L^{-1}$ NaOH
$n_i$ = counts in a chord channel ($s^{-1}$)
$n_{i,2}$ = square-weighted counts in a chord channel ($s^{-1}$)
$\Delta P$ = differential pressure (Pa)
$R_m$ = filter medium resistance ($m^{-1}$)
$r$ = radius of the particle
SR = settling rate of individual aggregate (m $h^{-1}$)
svf = solid volume fraction
$T$ = temperature (°C)
$U$ = settling velocity (cm $s^{-1}$)
$U_E$ = electrophoretic mobility ($cm^2$ $V^{-1}$ $s^{-1}$)
$U_h$ = hindered settling rate (m $h^{-1}$)
$V$ = filtrate volume ($m^3$)
$V$ = settling velocity (m $s^{-1}$)
$V_{Al}$ = viscosity of the sodium aluminate solutions (cP)
$X$ = fraction of reactive silica that has been converted to DSP
$y$ = mean square-weighted chord length at time x (μm)
$\alpha$ = collision efficiency [0,1]
$\alpha$ = filter cake resistance (m $kg^{-1}$)
$\alpha$ = the amount of seed particles present in the desilication
$\beta_{ij}$ = rate of collision between i and j sized particles or aggregation kernel ($m^3$ $s^{-1}$)
$\theta$ = surface coverage
$\eta$ = fluid viscosity (N s $m^{-2}$)
$\eta_l$ = fluid viscosity (g s $cm^{-1}$)
$\eta$ = coefficient of viscosity of the media
$\varepsilon$ = energy dissipation rate ($m^2$ $s^{-3}$)
$\varepsilon$ = dielectric constant
$\mu$ = dynamic viscosity (N s $m^{-2}$)
$\mu_o$ = fluid viscosity in the absence of solid (N s $m^{-2}$)
$\mu_s$ = slurry viscosity (N s $m^{-2}$)
$\phi$ = fraction of active sites for flocculant adsorption
$\phi_m$ = maximum solids volume fraction
$\phi_{eff}$ = effective solids volume fraction
$\phi_s$ = solids volume fraction

$\rho_a$ = aggregate density (kg $m^{-3}$)
$\rho_l$ = liquid (fluid) density (g $cm^{-3}$ or kg $m^{-3}$)
$\rho_f$ = fluid density (kg $m^{-3}$)
$\rho_s$ = solid (particle) density (g $cm^{-3}$ or kg $m^{-3}$)
$\gamma$ = laminar shear ($s^{-1}$)
$\nu$ = kinematic viscosity ($m^2$ $s^{-3}$)
$\xi$ = zeta potential (mV)

**Liquor terminology**

This thesis uses specific Bayer industry terminologies and those related to the liquor composition are explained below:

A is aluminium in the solution (expressed as g $L^{-1}$ $Al_2O_3$),

C is sodium hydroxide plus sodium aluminate (expressed as g $L^{-1}$ $Na_2CO_3$), and

S is C plus sodium carbonate (expressed as g $L^{-1}$ $Na_2CO_3$).

# Appendix A – Settling Test Reproducibility

Conditions : 4 wt/wt% solids
HX-300 dosage = 583 g $t^{-1}$
concentration of dosed flocculant = 0.05%
temperature of dosed flocculant = 45°C
other experimental details provided in Sections 5.3.2 and 6.3.3

Table A.1. Reproducibility of hematite slurry settling tests.

| Ageing time at 300 rpm (min) | Settling rate ( m $h^{-1}$) | Supernatant solids (ppm) | Bed height (mL) |
|---|---|---|---|
| 15 | 27.4 | 6 | 45 |
| 30 | 28.0 | 12 | 46 |
| 45 | 24.5 | 16 | 45 |
| 60 | 25.8 | 24 | 46 |
| 75 | 25.9 | 16 | 46 |
| 130 | 22.8 | 46 | 48 |

Table A.2. Reproducibility of settlings tests for the *in-situ* DSP/hematite slurry.

| Batch | Settling rate (m $h^{-1}$) | Supernatant solids (ppm) | Bed height (mL) |
|---|---|---|---|
| 1 | 14.5 | 190 | 44 |
| 2 | 18.4 | 190 | 43 |
| 3 | 15.6 | 150 | 44 |
| 4 | 16 | 160 | 44 |
| 5 | 15.3 | 155 | 46 |
| Mean | 16.0 | 169 | 44 |
| SD | 1.5 | 20 | 1 |

# Appendix B – Floc Density Analyser

*Determining a Single Size Parameter for Measured Aggregates*

From visual observation, it is known that aggregates are non-spherical and size determinations from imaging are therefore normally done by assuming that individual aggregates have ellipsoidal forms (Farrow and Warren 1993; Gagnon et al. 2003; Owen et al. 2008). In such cases the third dimension of the aggregates, on the axis which is not seen in the two-dimensional image, is assumed to be equal to the horizontal dimension of the aggregates.

Since the objective of FDA is to provide the relationship between settling rate (and thereby effective density) and the aggregate size, a single size parameter must be used by translating the ellipsoidal aggregates to the size of the sphere which settles at the same velocity. A mathematical equation introduced by Happel and Brenner (1973) can be used to calculate the diameter of spheres that settles at the same velocity of ellipsoids which have vertical-to-horizontal dimension ratios of between 0.1 to 20 (Benn 2013; Farrow and Warren 1993; Owen et al. 2007). Happel and Brenner's expression is given below:

$$d_{st} = \left[0.8248 + 0.168\left(\frac{a}{b}\right) + 1.033 \times 10^{-2}\left(\frac{a}{b}\right)^2 - 1.264 \times 10^{-3}\left(\frac{a}{b}\right)^3 + 3.728 \times 10^{-5}\left(\frac{a}{b}\right)^4\right] b$$

where: $d_{st}$ = the diameter of the sphere with the equivalent settling velocity for ratio a : b from 0.1 to 20 (μm)

$a$ = vertical diameter of the ellipse (μm)

$b$ = horizontal diameter of the ellipse (μm)

*Calculating the Effective Aggregate Density*

Stokes' Law states that the particle size, the particle density and the velocity of the settling particle in a certain fluid media can be used to calculate the effective density of an aggregate when other parameters are known and measured. The settling rate of a rigid sphere under steady creeping flow conditions (i.e. Stokes' conditions) is given as follows:

$$U^2 = \frac{4\ d\ g\ (\rho_s - \rho_l)}{3\rho_l}\frac{R_e}{24}$$

and since

$$R_e = \frac{U\ d\ \rho_l}{\eta_l}$$

then the equation can be rewritten as:

$$U = \frac{d^2 g(\rho_s - \rho_l)}{18\eta_l}$$

where $U$ = terminal settling velocity (cm $s^{-1}$)

$d$ = particle diameter (cm) = $d_{st}$

$g$ = gravity constant (cm $s^{-2}$)

$\rho_s$ = particle's density (g $cm^{-3}$)

$\rho_l$ = fluid density (g $cm^{-3}$)

$R_e$ = Reynold number

$\eta_l$ = fluid viscosity (g $cm^{-1}$ $s^{-1}$, i.e. poise)

If a particle is seen as individual aggregates, the above equation can be rearranged to the following form:

$$\rho_a = \frac{18\ U\ \eta}{d_a^2 g} + \rho_l$$

With the standard value of gravity constant ($g$) = 9.8 m $s^{-2}$, it gives:

$$\rho_a = \frac{183.75\ U\ \eta}{d_a^2} + \rho_l$$

where $\rho_a$ = aggregate's effective density (g cm$^{-3}$)

$U$ = aggregate's settling velocity (μm s$^{-1}$)

$\eta$ = fluid viscosity (poise)

$d_a$ = aggregate's calculated size (μm)

$\rho_l$ = fluid density (g cm$^{-3}$)

This equation for aggregate's effective density is accurate for Re < 0.2 (BS 1963) or

$$\frac{U\ d_a\ \rho_l}{\eta_l} < 0.2$$

For Bayer liquor whose viscosity at ~60°C = 1.174 cp and density = 1.2 g cm$^{-3}$, this means $U\,d_a < 2\times10^{-3}$. When using units of μm s$^{-1}$ for $U$ and μm for $d_a$, this requires: $U(\mu m/s)\ d_a\ (\mu m) < 2\times10^{-5}$.

Measurements showed that very few aggregates had settling velocities > 800 μm s$^{-1}$ and single size parameters > 250 μm. Those aggregates were not presented in the subsequent plots of settling rate/effective density vs. size. It is also worth noting that the equations used to calculate the effective density of aggregates are based on the assumptions the aggregates are rigid, have no fluid flow through the aggregates and there are no aggregate – aggregate interactions (Farrow and Warren 1993).

# Appendix C – Flocculant adsorption calculation

A number of assumptions were required for estimating the extent of flocculant surface coverage. These were:

- Flocculant adsorption is a two-step process, where flocculant in the solution is first adsorbed at the solid surface and the polymer's conformation relaxes and flattens upon equilibration, as illustrated in the figure below (Fleer and Scheutjens, 1993).

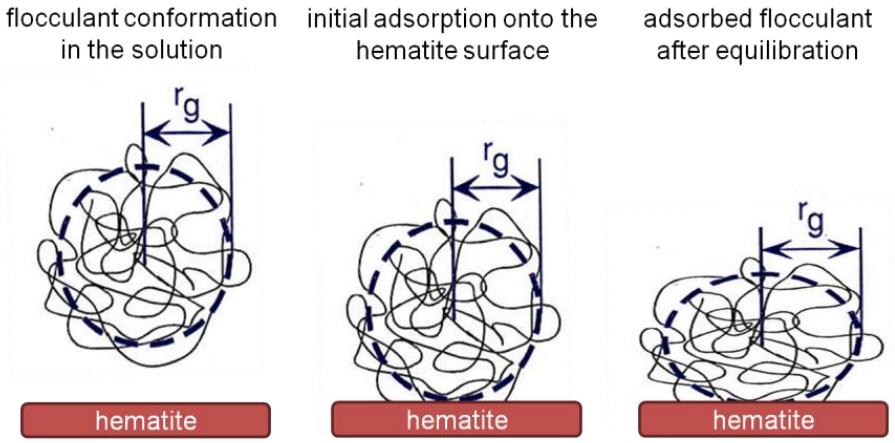


Figure B.1. Schematic illustration of the flocculant adsorption process based on the model proposed by Fleer and Scheutjens. Image adapted from Loan (1999).

- If the flocculant's molecular weight is known, then the number of flocculant molecules adsorbed can be calculated by relating the molecular weight to the surface saturation (maximum adsorption that gives a plateau in the plot of flocculant adsorbed vs. flocculant remaining in the liquor). Of course the molecular weight may have a broad distribution, but for the purpose of this simple estimate, a single mean molecular weight is used.

- Each flocculant molecule adsorbed will also cover a certain area depending on the flocculant dimension (the radius of gyration), assuming that the flocculant essentially maintains its dimensions during the initial stages of adsorption (Loan 1999).

- The total surface coverage by flocculant molecules can therefore be estimated by multiplying the number of flocculant molecule adsorbed with the area covered by each flocculant molecules.

- Flocculant solution dimensions are dependent on its conformation mode, or in other words, the ionic strength of the liquor. From previously published measurement, the radius of gyration was taken to be equal to 140 nm in synthetic Bayer liquor or 170 nm in 0.2 M NaCl (Jones 1998).

For Alclar 665 adsorption onto hematite particles in synthetic Bayer liquor:

- Optimum flocculant adsorption = 5.2 mg
- Hematite solids = 12 g
- Flocculant dimension = 140 nm
- Specific surface area of hematite (BET) = 5.08 $m^2\ g^{-1}$
- Molecular weight = $18 \times 10^6$ dalton

Calculations:

- No. of flocculant molecules adsorbed

  = [grams of flocculant adsorbed : MW] × Avogadro's number

  = $\left[\frac{5.2\times10^{-3}}{18\times10^{6}}\right] \times 6.022 \times 10^{23}$

  = $1.7397 \times 10^{14}$

- Surface coverage by flocculant

  = No. of flocculant adsorbed x Area covered by 1 flocculant ($m^2$)

  = $(1.7397 \times 10^{14}) \times \left[\frac{22}{7} \times (140 \times 10^{-9})^2\right]$

  = 10.7166 $m^2$

- % surface coverage

  = [surface coverage by flocculant ($m^2$) / total area provided by solid substrate ($m^2$)] × 100%

  = $[10.7166 \div (12 \times 5.08)] \times 100\%$

  = 17.58 % ≈ 18%

For the adsorption of Magnafloc 919 onto hematite in salt solutions (0.2 M NaCl at pH = 5), the calculation of % surface coverage is analogous to that mentioned above. The results are tabulated below.

Table B.1. Calculation of surface coverage by flocculant adsorption in the synthetic Bayer liquor and 0.2 M NaCl.

| | (unit) | Synthetic Bayer liquor | 0.2 M NaCl (pH ≈ 5) |
|---|---|---|---|
| Optimum adsorption | mg | 5.2 | 6.8 |
| Flocculant dimension | nm | 140 | 170 |
| No. of flocculant molecules adsorbed | --- | $1.74 \times 10^{14}$ | $2.27 \times 10^{14}$ |
| Surface coverage by flocculant | $m^2$ | 10.72 | 20.66 |
| | % | 18 | 34 |

Refer to Section 6.3.6 for conditions in adsorption tests

# Appendix D – Sodium Aluminate Viscosity

Viscosity of sodium aluminate solutions can be calculated from Ikkatai's equation (Ikkatai et al. 1963):

$$\log V_{Al} = (0.0857 - 0.00658\ T + 0.0000023\ T^2) + [(N/1000)\ \text{x}\ (3.56 - 0.0357\ T + 0.000184\ T^2)] + [(A/1000)\ \text{x}\ (3.23 - 0.0034\ N - 0.1246\ T + 0.00204\ T^2 - 0.00001107\ T^2)]$$

where:

$V_{Al}$ = viscosity of the sodium aluminate solutions (cP)

$T$ = temperature (°C)

$N$ = caustic concentration in g $L^{-1}$ NaOH

$A$ = alumina concentration in g $L^{-1}$ $Al_2O_3$

In Section 7.4.1.5, the composition of synthetic Bayer liquor was varied in order to assess the effect of higher alumina or caustic concentration. The calculated results based on Ikkatai's equation are given in Table C.1 below.

Table C.1. Viscosities of sodium aluminate solutions used in Section 7.4.1.5 at 95°C.

| Experimental Set | A (g $L^{-1}$ $Al_2O_3$) | C (g $L^{-1}$ $Na_2CO_3$) | A/C ratio | C/S ratio | N (g $L^{-1}$ NaOH) | Viscosity at 95°C (cP) |
|---|---|---|---|---|---|---|
| i | 127 | 230 | 0.55 | 0.99 | 174 | 0.580 |
| ii | 81 | 230 | 0.35 | 0.99 | 174 | 0.598 |
| iii | 127 | 270 | 0.47 | 0.99 | 204 | 0.640 |

Refer to Section 6.3.6 for conditions in adsorption tests